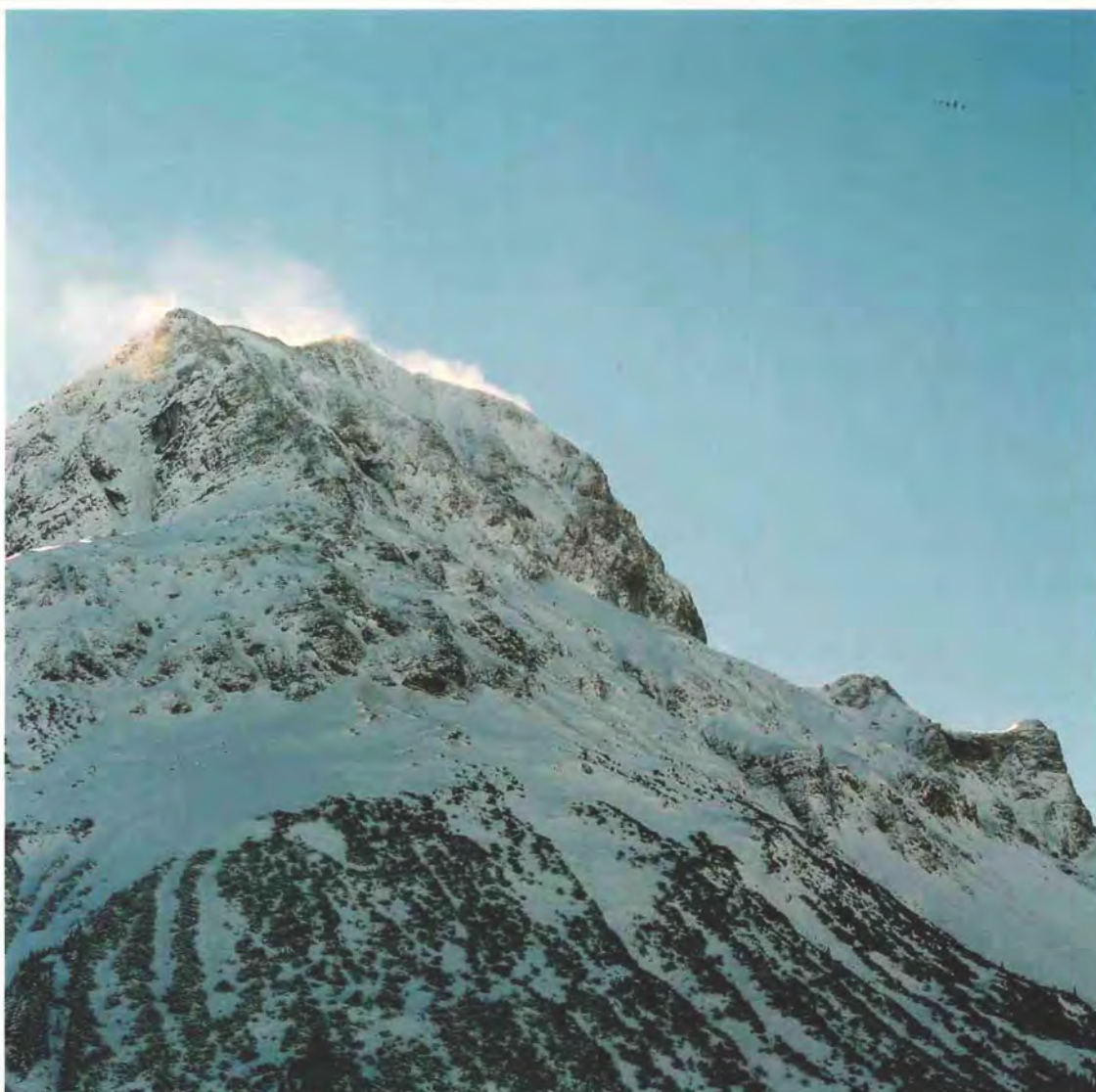




Nationalpark  
Berchtesgaden



# Proceedings Alpine\*Snow\*Workshop

Forschungsbericht 53

**Impressum:**

Nationalpark Berchtesgaden  
Forschungsbericht 53/2007

Herausgeber:

Nationalparkverwaltung Berchtesgaden, Doktorberg 6,  
D-83471 Berchtesgaden, Telefon 0 86 52/96 86-0, Telefax 0 86 52/96 86 40,  
e-Mail: poststelle@npv-bgd.bayern.de

Internet: <http://www.nationalpark-berchtesgaden.de>

im Auftrag des Bayerischen Staatsministeriums für Umwelt, Gesundheit und Verbraucherschutz

Alle Rechte vorbehalten!

ISSN 0172-0023

ISBN 13 978-3-922325-60-4

ISBN 10 3-922325-60-2

EAN-Code 9783922325604

Druck: Berchtesgadener Anzeiger, Berchtesgaden

Gedruckt auf chlorfrei gebleichtem Papier

Titelbild:

Blowing snow during blue skies in the winterly alps (Peter Neusser, München)

Bild letzte Umschlagseite:

Automatic meteorological station Kühroint (Peter Neusser, München)

Fotos:

Helmut Franz, Wilhelm Gaulhofer, Jan Greune, Lawinenwarnzentrale Bayern,  
Archiv Nationalparkverwaltung Berchtesgaden, Peter Neusser, Susanne Schmidt,  
Karen und Jan Skinner, Ulrich Strasser, Markus Weber, Max Wisshak

# Inhaltsverzeichnis

Proceedings Alpine\*Snow\*Workshop (Munich (Germany),  
October 5-6, 2006

Vorwort/Preface .....	6 - 7
1. <b>A distributed energy balance snowmelt model as a component of a flood forecasting system for the Inn river</b> .....	9 - 17
JUDIT ASZTALOS, ROBERT KIRNBAUER, HEIDI ESCHER-VETTER AND LUDWIG BRAUN	
2. <b>Provision of snow information from satellite data within Polar View and application example for a mesoscale Alpine catchment using PROMET</b> .....	18 - 23
HEIKE BACH, FLORIAN APPEL AND WOLFRAM MAUSER	
3. <b>High resolution modelling of snow transport in complex terrain using simulated wind fields</b> .....	24 - 33
MATTHIAS BERNHARDT, GLEN E. LISTON, GÜNTHER ZÄNGL, ULRICH STRASSER AND WOLFRAM MAUSER	
4. <b>Snow variability and change in Romania</b> .....	34 - 38
ROXANA BOJARIU AND MIHAELA DINU	
5. <b>Evaluation of snowmelt from MODIS images</b> .....	39 - 43
ANGELO COLOMBI, ANNA RAMPINI, FRANCESCO ROTA NODARI	
6. <b>Heavy Snowfalls and avalanche activity over eastern Pyrenees: a study of two extreme cases</b> .....	44 - 48
PERE ESTEBAN, GLORIA MARTÍ, CARLES GARCÍA, MONTSE ÀRAN, JORDI GAVALDÀ AND IVAN MONER	
7. <b>Weather and snow pack conditions of major avalanches in the Catalan Pyrenees</b> .....	49 - 56
CARLES GARCÍA, GLÒRIA MARTÍ, ALBERT GARCÍA, ELENA MUNTAN, PERE OLLER, PERE ESTEBAN	
8. <b>Mathematical modelling of metamorphic structural evolution in the snow cover and soil</b> .....	57 - 63
ELENA GUSEVA-LOZINSKI	
9. <b>Estimation of snow water equivalence using the polarimetric scanning radiometer from the Cold Land Processes Experiments (CLPX03)</b> .....	64 - 68
LINGMEI JIANG, JIANCHEN SHI, SAIBUN TJUAJUA, KUNSHAN CHEN AND LIXIN ZHANG	
10. <b>Comparison of several sets of modelled and analysed precipitation fields over the French Alps. Impact of different spatial resolutions</b> .....	69 - 77
LAURENT MERINDOL, YVES DURAND AND GILBERT GUYOMARC'H	
11. <b>Validation of a physically based snow model for the simulation of the accumulation and ablation of snow (ESCIMO)</b> .....	78 - 91
MONIKA PRASCH, ULRICH STRASSER AND WOLFRAM MAUSER	
12. <b>Snow cover area (SCA) estimation and analysis in the alpine range using moderate resolution satellites</b> .....	92 - 102
FRANCESCO ROTA NODARI, FRANCESCA SAPIO AND MICHELA BIAGGI	

13.	<b>The dilemma of resolution and seasonality of snow cover in alpine environments</b> .....	103 - 110
	SUSANNE SCHMIDT AND BERNHARD WEBER	
14.	<b>Computational fluid dynamics simulation of snow drift in alpine environments for operational avalanche warning</b> ....	111 - 116
	SIMON SCHNEIDERBAUER, WALTER HINTERBERGER AND PETER FISCHER	
15.	<b>Distributed modelling of snow processes in the Berchtesgaden National Park (Germany)</b> .....	117 - 130
	ULRICH STRASSER, HELMUT FRANZ AND WOLFRAM MAUSER	
16.	<b>Climate change and the competition among ski areas for day tourists</b> .....	131 - 137
	MONIKA TEPFENHART, WOLFRAM MAUSER AND FLORIAN SIEBEL	
17.	<b>A parameterization for the turbulent fluxes over melting surfaces derived from eddy correlation measurements</b> ....	138 - 149
	MARCUS WEBER	
18.	<b>Measurement network in the Berchtesgaden National Park: the example of Kühroint Measurement Station</b> .....	150 - 152
	BENNO WIESENBERGER AND WOLFRAM SOMMER	
19.	<b>Field trip to the "Ice Chapel"</b> .....	153 - 155
	HELMUT FRANZ, MATTHIAS BERNHARDT, MONIKA PRASCH, VOLKMAR KONNERT AND ULRICH STRASSER	
	<b>Glossary</b> .....	156 - 159
	<b>Appendix: List of participants</b> .....	161 - 162

## Vorwort

Zu den Aufgaben eines Nationalparks gehören auch die Arbeitsbereiche Langzeitbeobachtung und Forschung. Für den einzigen alpinen Nationalpark Deutschlands zählt hierzu auch die Beschäftigung und wissenschaftliche Auseinandersetzung mit dem Thema und Phänomen „Schnee“, am besten zusammen mit einem kompetenten Partner wie der LMU München. Ein erstes Zwischenergebnis dieser seit Jahren bestehenden, fruchtbaren Zusammenarbeit können wir Ihnen hiermit übergeben.



Von 5.-7. Oktober 2006 fand in München der Alpine\*Snow\*Workshop statt, der von der Ludwig-Maximilians-Universität, dem Nationalpark Berchtesgaden sowie der Fa. Sommer gemeinsam organisiert und gesponsert wurde. Etwa 100 Wissenschaftler aus insgesamt 19 Ländern der Welt nahmen teil. Die Vorträge und Poster der ersten beiden Tage behandelten aktuelle Themen der Schneehydrologie wie: Messmethoden, Monitoring, numerische Modellierung, Fernerkundung, Wechselwirkung von Schnee mit Vegetation, windinduzierter Schneetransport, Lawinenrisiko und Einfluss des Klimawandels. Die informelle Veranstaltung war geprägt von einer ungezwungenen, offenen Gesprächs- und Arbeitsatmosphäre, die von allen Teilnehmern als sehr angenehm empfunden wurde; dazu trug nicht zuletzt auch die hervorragende Verpflegung bei, großzügig unterstützt durch die Ludwig-Maximilians-Universität und den Nationalpark Berchtesgaden.

Am dritten Tag der Veranstaltung fand eine Exkursion in den Nationalpark Berchtesgaden statt. Nach der Schiffsfahrt über den Königssee und einem typisch bayerischen Weißwurst-Frühstück im Gasthaus St. Bartholomä machten sich die Tagungsteilnehmer auf den Weg zur Eiskapelle am Fuß der gewaltigen Watzmann-Ostwand. Trotz oder gerade wegen des schlechten Wetters war die Annäherung an die riesige, vor Schmelzwasser tiefende und mit einer mächtigen Eisdecke überspannte Höhle ein großes Erlebnis.

Nun, ein Jahr später, findet der positive Geist dieser Veranstaltung ihren Ausdruck im vorliegenden Tagungsband. Die Veröffentlichung der Beiträge war für die Autoren kostenfrei. Obwohl der Terminplan zur Drucklegung zeitlich sehr eng gesteckt war, beteiligten sich die Autoren rege am gegenseitigen Korrekturlesen. Die vorliegenden Artikel spiegeln einen repräsentativen Querschnitt der Beiträge des Workshops wider, einige dokumentieren darüber hinaus das im Nationalpark entstehende Messnetz an Klimastationen, welches sich für wissenschaftliches Arbeiten in idealer Weise eignet und laufend ausgebaut wird.

Der Erfolg des Alpine\*Snow\*Workshop wäre nicht möglich gewesen ohne die vielen freiwilligen und hilfsbereiten Hände der Teilnehmer, der Mitarbeiter, Kollegen und Studenten. Ihnen allen, die das Gelingen des Workshops, der Exkursion und der Erstellung des vorliegenden Tagungsbandes ermöglicht haben, sei an dieser Stelle herzlichst gedankt. Unser besonderer Dank gilt insbesondere auch den Sponsoren, die mit ihrer großzügigen Unterstützung den Workshop ermöglicht und damit einen wertvollen Beitrag für die Wissenschaft geleistet haben.

## Preface

One of the central tasks of a National Park is long time monitoring and research. Thus it follows that the only Alpine National Park in Germany is engaged in the scientific discussion on the issue and phenomenon of "snow", in partnership with the esteemed University of Munich (LMU). The initial report presented here is the outcome of this fruitful and long-term cooperation.

On October, 5-7 2006 the Alpine\*Snow\*Workshop took place in Munich, organized and sponsored jointly by the National Park Berchtesgaden, the University of Munich and the Sommer company. About 100 participants from 29 countries of the world were in attendance. The talks and posters presented on the first two days dealt with currently discussed topics of snow hydrology, such as: measurement techniques, monitoring, numerical modelling, remote sensing, snow-vegetation interaction, wind-induced snow transport, avalanche risk and the effects of climate change. The informal event was characterized by an open-minded atmosphere of discussion and collaboration, perceived by the participants as very enjoyable and rounded off by the most agreeable catering which was generously subsidized by the LMU and the National Park administration.

On the third day, an excursion to the National Park was organized. After the boat trip across the Königssee and a typical Bavarian Weißwurst breakfast in St. Bartholomä the group hiked up to the so-called ice chapel at the foot of the gigantic east face of Watzmann. In spite of, or perhaps due to the rainy weather, the approach to the spectacular snow and ice cave, dripping with meltwater and over-spanned by an impressive ice ceiling, was a great experience.

Now, a year later, the positive spirit of the meeting finds its expression in the research report presented here. The contributions were published at no cost to the authors. Even though the printing schedule was rather tight, each of the authors also contributed in the form of peer reviews. The submitted papers reflect a representative cross-section of the workshop contributions, and some also document the network of automatic weather stations which are installed in the National Park. This network is perfectly suited to the investigation of scientific questions, and it is continuously being expanded.

The success of the Alpine\*Snow\*Workshop would not have been possible without the many voluntary and helpful hands of the participants, assistants, colleagues and students. We gratefully acknowledge their many contributions, which guaranteed the success of the workshop, the field trip and the publishing of this research report. Our special thanks go to the sponsors who, through their most generous support, enabled the workshop to take place and to produce such a valuable contribution to scientific research.

**Dr. Ulrich Strasser**  
Organizer of  
Alpine\*Snow\*Workshop

**Dr. Michael Vogel**  
Head of Berchtesgaden  
National Park

# 1 A distributed energy balance snowmelt model as a component of a flood forecasting system for the Inn river

JUDIT ASZTALOS<sup>1</sup>, ROBERT KIRNBAUER<sup>1</sup>,  
HEIDI ESCHER-VETTER<sup>2</sup>, LUDWIG BRAUN<sup>2</sup>

<sup>1</sup> Institute for Hydraulic and Water Resources Engineering, Water Resources Engineering Department, Vienna University of Technology, Karlsplatz 13/222, A-1040 Vienna, Austria

<sup>2</sup> Commission for Glaciology of the Bavarian Academy of Sciences and Humanities, Munich, Alfons-Goppel-Str. 11, D-80539 Munich, Germany

## Abstract

Snowmelt is an important contribution to Alpine runoff and to the generation of floods in Alpine rivers. Thus, a snow (and glacier) melt model has been developed as a component of an operational flood forecasting system which is under development for the Inn river in Tyrol, Austria. The model is based on a fully distributed energy balance approach, and internal processes are parameterized. Because radiation energy input is the most important factor for snowmelt in Alpine regions special attention is paid to the temporal variability of albedo during snow melt. In contrast to many snowmelt models, the decrease of albedo during melt is not modelled as a function of time with the well known aging curve approach of the U.S. ARMY CORPS OF ENGINEERS (1956) but as a function of the total energy input the snowpack has received since the last snowfall. The point snowmelt model was calibrated and checked against data collected at the research plot of the Commission for Glaciology of the Bavarian Academy of Sciences and Humanities near the Vernagtferner (Ötztal, Tyrol, Austria). The model is then applied for fully distributed snowmelt simulations in

the headwater reaches of the great southern tributaries of the Inn river. A distributed model needs to be calibrated and evaluated with distributed data. Distributed measurements of data suitable for verifying such a model type, e.g. continuous measurements of snow water equivalent or of snowpack outflow, usually do not exist. The only distributed information on melt is the existence or non existence of snowcover on the ground. This information can be derived from a series of photographs taken from a definite point in the catchment and rectifying them to a map scale. These depletion patterns can then be compared to the results of the depletion simulations performed by the model. This procedure could be performed making use of photos taken from the Schwarzkögele above the Vernagtferner. They were rectified, and the depletion patterns were identified manually. Corresponding to the observations the model was upgraded to simulate the water balance of the firn as well. At the present state, the model is driven with parameters calibrated and evaluated with photos of the Vernagtferner and applied to other headwater catchments in the Ötztal region where no photos but runoff measurements of the streams exist. These runoff observations can be seen as an overall performance check of the melt model. On the whole, the model shows reasonable results. For better simulations of the runoff dynamics, however, it was necessary to implement routing algorithms based on cascades of linear reservoirs that allow the routing of meltwater through the snowpack and along the river reaches to the gauging stations.

## 1 Introduction

Snowmelt is an important contribution to alpine runoff and to the generation of floods in alpine rivers. Thus, a snow and glacier melt model has been developed as a component of an operational flood forecasting system for the Inn river in Tyrol, Austria (KIRNBAUER AND SCHÖNLAUB 2006). In the headwaters of the southern tributaries of the Inn there are large glaciated areas and therefore the runoff from these catchments is highly influenced by

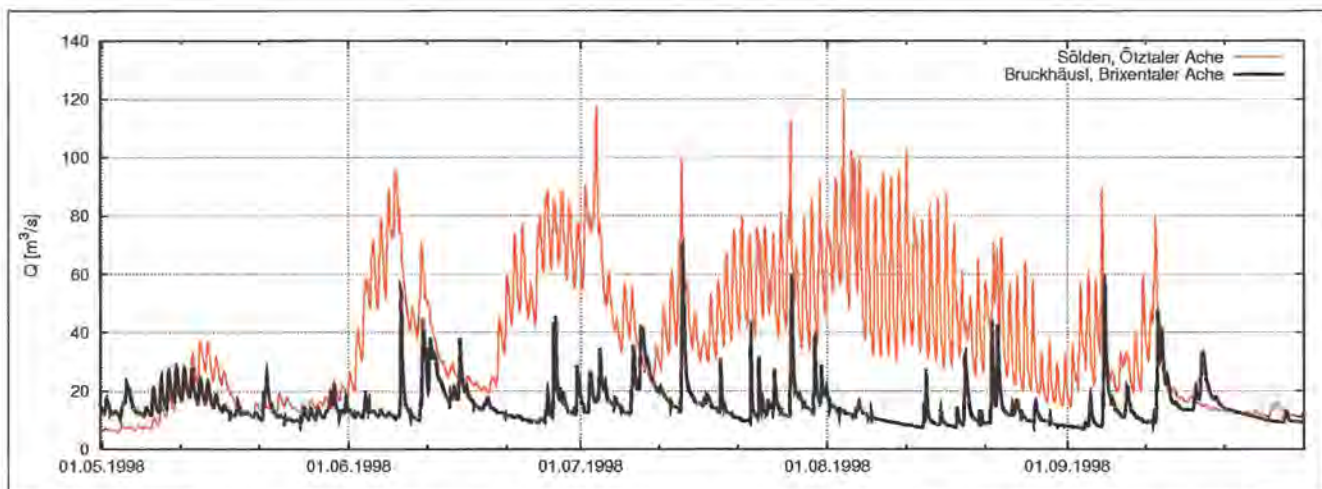
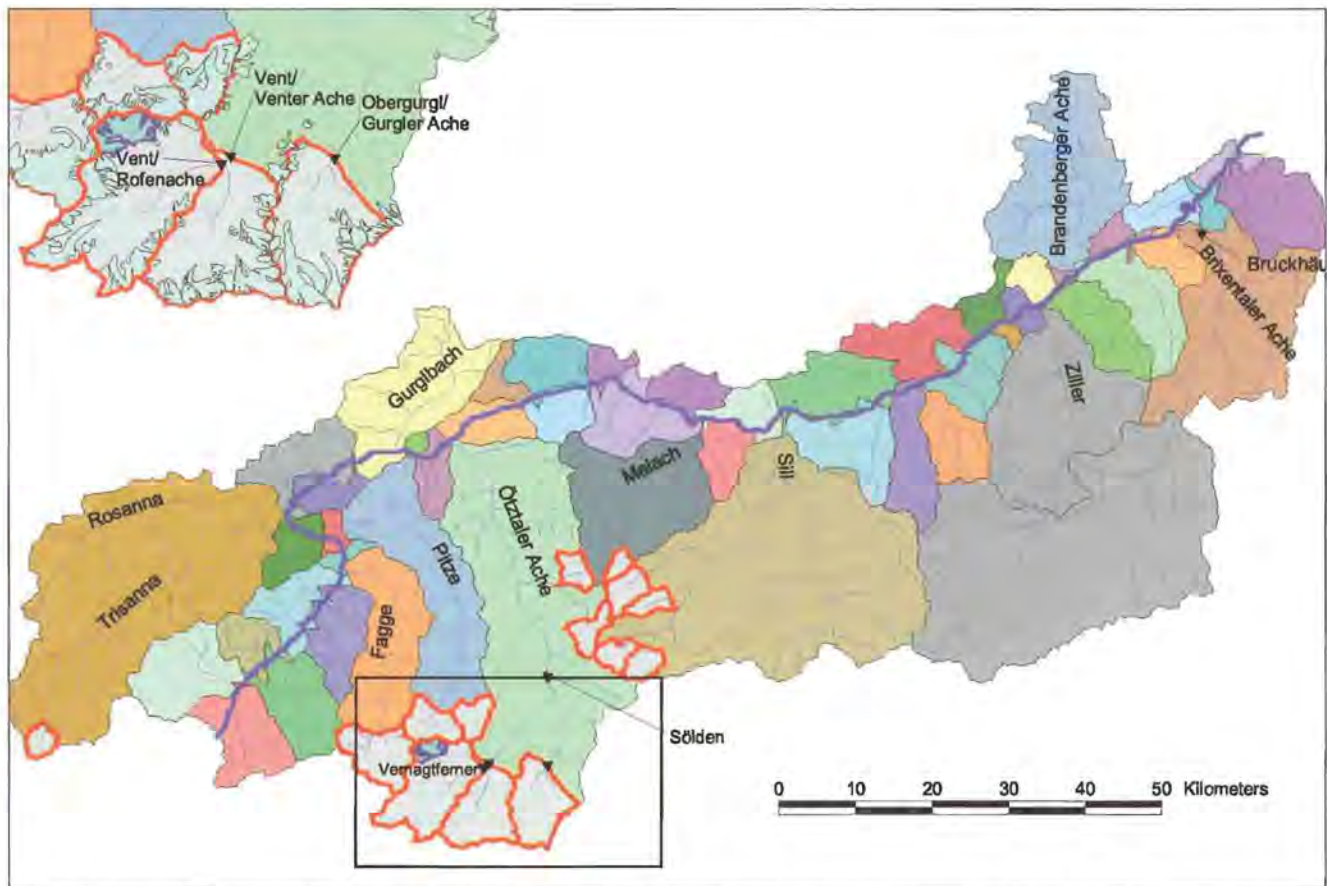


Figure 1: Hydrograph of a glaciated (Sölden/Ötztaler Ache, 375 km<sup>2</sup>) and a non-glaciated (Bruckhäusl/Brixentaler Ache, 320 km<sup>2</sup>) catchment for the summer 1998.



**Figure 2:** Inn catchment with tributaries, headwater catchments calculated by SES are outlined in red. The black framed area is shown more detailed in the upper left corner.

the runoff characteristics of glaciers. In spring when the glaciers are deeply covered with snow, they act as a reservoir for liquid and solid precipitation which leads to a retention effect. In summer, during rainfall, the glaciers – being snow free in large parts – react similar to impermeable areas and therefore contribute much to flood formation. Fig. 1 shows the hydrographs of two southern tributaries of the Inn river with similar catchment areas, for the locations of the gauges see fig. 2. The catchment of the Ötztaler Ache at Sölden is about 27% glaciated, the Brixentaler Ache has no glaciers within its catchment. At the beginning of May and at the end of September the two catchments have similar discharge levels. In the catchment of the Brixentaler Ache snowmelt ends in the middle of May, in summer peaks produced by rainfall events are characteristic. Whereas the high peaks in June at the Ötztaler Ache might be explained by snowmelt due to the higher altitude of the catchment, the continuously high discharge level with large diurnal variation in July and August is a typical result of glacier melt.

The Inn River Forecasting System is developed on behalf of the Tyrolean State Government and TIWAG (Tyrolean Hydropower Company) by alpS – Centre for Natural Hazard Management in cooperation with the Institute for Hydraulic and Water Resources Engineering, Vienna University of Technology, Austria and the Institu-

te of Geography, University of Innsbruck, Austria. The hybrid forecasting system consists of 4 modules: 1) data management and preprocessing, 2) meteorology, 3) hydrology, 4) hydraulics. It provides discharge rates and water level information at relevant cross sections of the Inn river for a lead time of 24 hours on an hourly basis. In order to better reproduce the runoff from the partially glaciated headwaters of the southern tributaries of the Inn river (fig. 2) the hydrology module includes the distributed energy balance snow and glacier melt model SES (Schnee- und Eisschmelzmodell) (ASZTALOS 2004).

In the following a short overview of the forecasting system is given: The input data for the forecasting system are derived from meteorological measurements as well as forecast data from the Central Institute for Meteorology and Geodynamics (ZAMG). They are stored in a database where quality checks are performed and missing data are interpolated. Temperature and precipitation are spatially interpolated to a 5 km grid.

The inflow from the non-glaciated areas of the tributaries to the Inn river is computed applying the semi-distributed model HQsim (KLEINDIENST 1996), which is a further development of the water balance model BROOK (FEDERER AND LASH 1978). HQsim is based on hydrological response units (hru), which were classified over topography (elevation, slope, aspect), soil and vegetation

maps. The model calculates snowmelt with a modified degree day approach. The degree day factor is corrected by the ratio of global radiation on the inclined surface (mean slope of the hru) to global radiation on a horizontal surface and a vegetation factor. Vegetation is incorporated by leaf and stem area indices (LAI and SAI). To determine surface flow the contributing area concept (HEWLETT 1961, HEWLETT AND NUTTER 1970, DICKINSON AND WHITELEY 1970) is used. Within the unsaturated zone hydraulic conductivity is calculated by the Mualem-Van GENUCHTEN (1980) relationship. The outflow from the unsaturated zone which depends on soil moisture content is divided into interflow and drainage into the groundwater. The saturated zone is represented by a simple linear reservoir.

For the calibration of the hydrological model five representative (gauged) catchments are selected (fig. 2): 1) Brandenberger Ache – limestone – non-glaciated – unaffected (by hydropower), 2) Brixentaler Ache – crystalline – non-glaciated – unaffected, 3) Ötztaler Ache – crystalline – glaciated – unaffected, 4) Ziller – crystalline – glaciated – affected, 5) Fagge – crystalline – glaciated – affected. The model parameters are transferred to the other tributaries of the Inn without further calibration.

The results of the hydrological module serve as input for the 1D-hydrodynamic model Flux<sup>DSS/DESIGNER/FLORIS<sup>2000</sup></sup> (REICHEL AND BAUMHACKL 2000, LEONHARDT et al. 2006). It calculates the flood wave propagation in the Inn river

channel. During a flood event the operation of run-of-river power plants substantially influences the downstream runoff (LEONHARDT et al. 2006). Therefore, it is essential for the hydraulic module to be able to represent the operation of these power stations.

## 2 The Snow and Glacier Melt Model

For the calculation of the partly glaciated headwaters of the Inn the snow and glacier melt model SES is used. It is a fully distributed energy balance model. Such models have been developed by e.g. RANZI AND ROSSO (1991), ESCHER-VETTER (2000), BROCK et al. (2000), STRASSER et al. (2004) or LISTON AND ELDER (2006). SES is based on a snowmelt model developed by BLÖSCHL et al. (1987, 1991). It calculates snow accumulation and snow, firn and ice ablation in an hourly time step. SES was calibrated on the well observed Vernagtferner catchment, Tyrol, Austria (fig. 3). Within the Inn River Forecasting System the Snow and Glacier Melt Model SES was applied to 13 headwater catchments (fig. 2).

### Topographic input

The topographic input data for SES is derived from a digital elevation model. It consists of: 1) elevation, 2) slope, 3) aspect, 4) curvature and 5) local horizon. The local horizon is used to incorporate shading effects from the

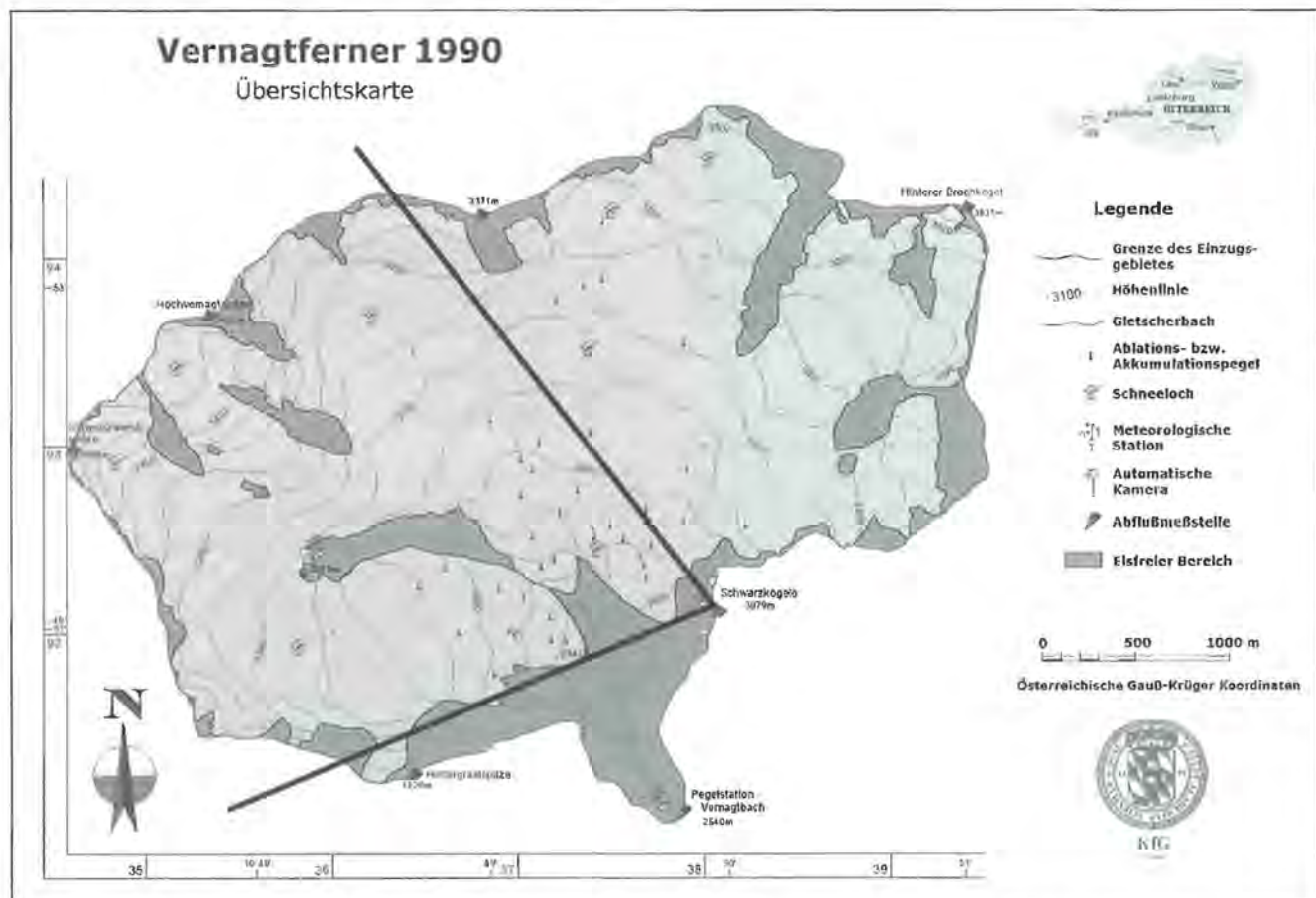


**Figure 3:** Vernagtferner catchment in Tyrol, Austria with gauging station "Pegelstation Vernagtbach" at basin outlet and automatic camera at Schwarzkögele (field of vision marked by solid line). Basin area: 11.4 km<sup>2</sup>. Source: <http://www.glaziologie.de> (with minor changes).

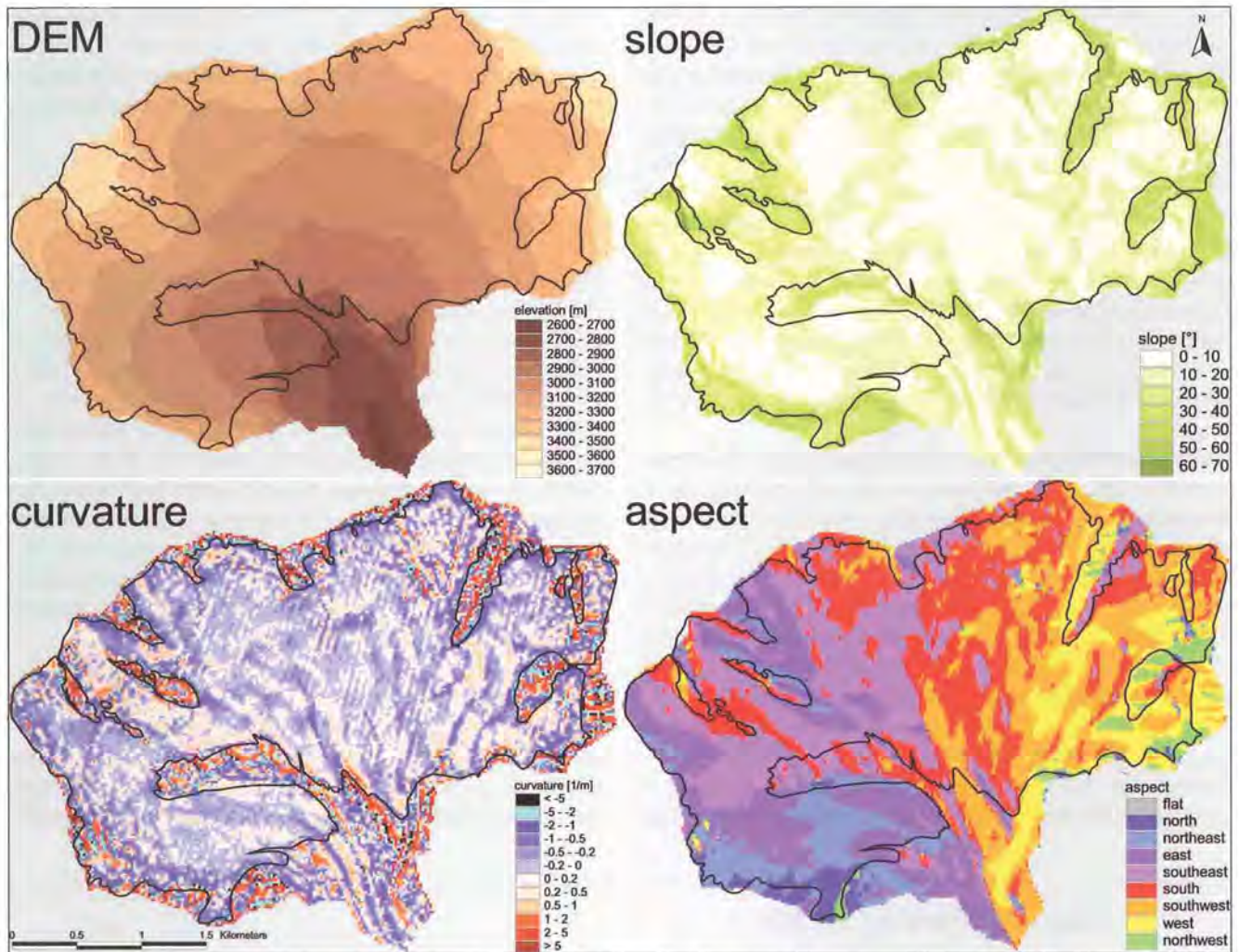


**Figure 4:** Topographic input data: DEM with a resolution of 20 m (ENDRES, 2001), slope, aspect and curvature for catchment Vernagtferner, Tyrol.

terrain and is specified in a certain number of directions for each grid element. Fig. 4 shows the 20 m DEM (ENDRES 2001) for the Vernagtferner catchment and the derived values slope, aspect and curvature.

### Meteorological input

Hourly meteorological input consists of air temperature, lapse rate, precipitation, relative humidity, wind speed, global radiation and – if available – cloudiness. At Vernagtferner catchment measured data of air temperature, relative humidity, wind speed and global radiation at the gauging station Vernagtbach were available. As precipitation data at the gauging station were daily sums, hourly data from the 8 km near automatic meteorological station Pitztaler Gletscher were used.

Cloudiness comes either from the ALADIN model – Local Area Model (LAM) nested in the circulation model of the European Centre for Medium Range Weather Forecasts (ECMWF) in Reading, GB – or is estimated from measured global radiation and astronomically possible radiation using the approach of KASTEN AND CZEPLAK (1980):

$$\frac{Q_G}{Q_{G_0}} = a - b \cdot B^c \quad (1)$$

$Q_G$  measured global radiation [W/m<sup>2</sup>]

$Q_{G_0}$  astronomically possible radiation [W/m<sup>2</sup>],  
calculated with HEINDL AND KOCH (1976)

$a, b, c$  coefficients [-]

$B$  cloudiness [-]

Meteorological data is expanded to the catchment area on the basis of the DEM. For calibration at Vernagtferner catchment during precipitation adiabatic lapse rates were calculated. During dry weather lapse rates based on measurements at Vernagtferner (ESCHER-VETTER 2000) were used. Within the Inn River Forecasting System lapse rates calculated by the meteorology module were used. The redistribution of deposited snow due to wind and gravity is parameterised by slope and curvature (BLÖSCHL et al. 1991). Measured global radiation is divided into direct and diffuse radiation depending on cloudiness. Diffuse radiation is constant over the catchment, whereas the direct component is calculated with consideration to slope, aspect and shading.

### Energy balance

Short wave radiation is the main energy input for snow

and ice melt, especially in high altitude catchments, where glaciers are situated. It depends on the albedo how much of the short wave radiation is effective for melt. Therefore in SES special attention was paid to the temporal variability of the albedo.

In contrast to many snowmelt models – e.g. BLÖSCHL (1990), ESCHER-VETTER (2000) or STRASSER et al. (2004) – the decrease of snow albedo during melt is not modelled as a function of time with the well known aging curve approach of the U.S. ARMY CORPS OF ENGINEERS (1956). Here, albedo is modelled using a function of the total energy input the snow pack has received since the last snowfall. This approach seems to meet the physical background of the process better than the aging curve: Alpine skiers know that even on the same day snow conditions (e.g. density or albedo) can be totally different on north or south facing slopes. This difference can be traced back to the different energy consumed by the snow on the two slopes.

TROFIMOVA (1970) parameterises albedo decrease against the energy balance  $Q$ :

$$\frac{da}{dt} = -c \cdot (a - b) \cdot Q \cdot H(Q) \quad (2a)$$

with

$$H(Q) = \begin{cases} 0 & \text{if } Q < 0 \\ 1 & \text{if } Q > 0 \end{cases} \quad (2b)$$

where  $a$  is the albedo (dimensionless),  $b$  the lower limit of snow albedo,  $c$  the decrease factor in  $m^2/(W \cdot h)$ ,  $Q$  the energy balance in  $W/m^2$ . The dimensionless Heaviside unit step function  $H$  (BERG, 1932) ensures that albedo decrease is only caused by a positive energy balance. The solution of equ. (2a) for time intervals  $\Delta t = t_1 - t_0$  in which  $Q$  can be considered constant yields:

$$a(t_1) = b + (a(t_0) - b) \cdot e^{-c \cdot Q \cdot H(Q) \cdot \Delta t} \quad (3)$$

This assumption is acceptable for daily but not for hourly time steps. In order to include the diurnal change of the albedo which can be observed (fig. 5), the original approach was revised (ASZTALTOS, 2004). Albedo decrease still is a function of the energy balance, but additionally of its derivative:

$$a(t_1) = b + (a(t_0) - b) \cdot e^{-c^* \cdot [Q(t_1) \cdot H(Q(t_1)) - Q(t_0) \cdot H(Q(t_0))] \cdot Q(t_1) \cdot H(Q(t_1)) \cdot \Delta t}$$

$c^*$  being the decrease factor in  $m^4/(W^2 \cdot h)$ . Since the albedo depends on the energy balance and in turn the energy balance is a function of the albedo, an iterative solution of equ. (4) is required. During calibration it was shown that the calculation of a preliminary energy balance with the albedo of the previous time step is adequate. In the model a grid element is either snow covered or snow-free and the snow cover is considered to be homogeneous. After snow fall albedo is increased to new snow albedo only if the sum of freshly fallen snow over six hours exceeds a certain threshold. This criterion is to ensure that new snow albedo is only reset if the entire grid element is completely snow covered.

During the ablation season a glacier becomes snow free, first at the glacier tongue, later also in the firn area. In order to incorporate ice and firn albedo and the transition from snow to ice and firn respectively, the following assumptions were made (fig. 6):

After snow fall the albedo follows the revised TROFIMOVA approach (equ. 4), until old snow albedo  $b$  is reached. If the examined point is located at the glacier in the firn area (dot-and-dash line), the albedo will remain at the value of old snow until all snow is melted. Then the albedo decreases to the firn albedo  $a_{firn}$ . At low snow depths the assumption of a homogeneous snow cover over a grid element with a few hundred square meters is unrea-

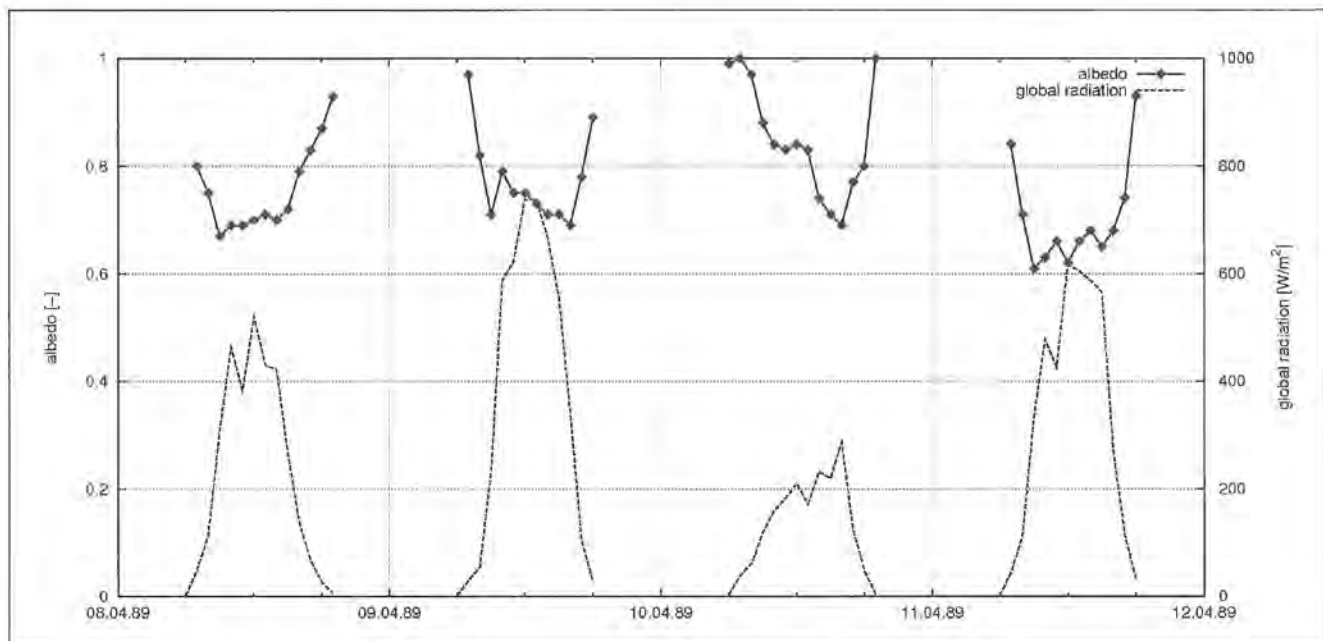


Figure 5: Diurnal change of albedo and global radiation at Kühtai, Tyrol.

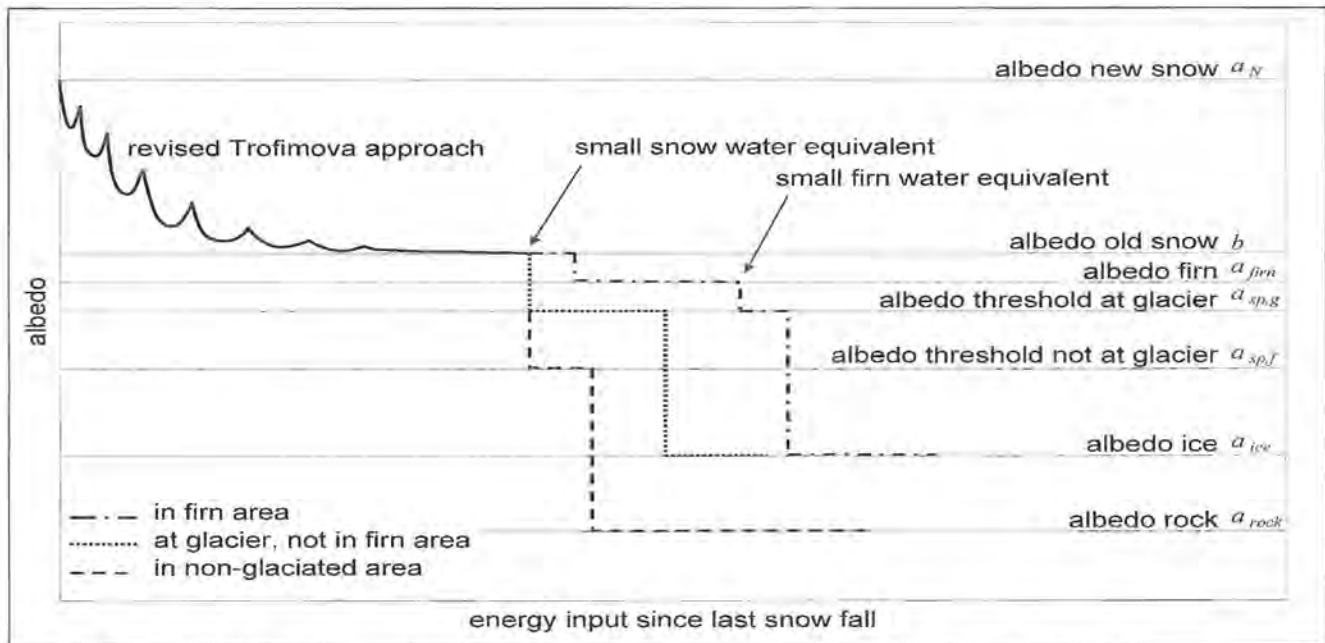


Figure 6: Schematic albedo evolution for different points at the glacier.

listic (BLÖSCHL et al., 1991). Hence at low snow water equivalents  $we_{crit}$  albedo is limited with a value  $a_{sp,g}$  smaller than old snow albedo  $b$ . An equal procedure is applied at low firn depths. Arrows in fig. 6 indicate small snow/firn water equivalents.

Incoming ( $Q_h$ ) and outgoing ( $Q_{lo}$ ) long wave radiation are calculated with the Stefan-Boltzmann equation;  $\sigma$  being the Stefan-Boltzmann constant ( $\sigma = 5.77 \cdot 10^{-8} \text{ W}/(\text{m}^2 \cdot \text{K}^4)$ ),  $T_A$  and  $T_S$  are air and snow surface temperature in K,  $\varepsilon_S$  is the dimensionless emission coefficient for snow ( $\varepsilon_S = 0.99$ ):

$$Q_h = \varepsilon_C \cdot \varepsilon_S \cdot \sigma \cdot T_A^4 \quad (5)$$

$$Q_{lo} = \varepsilon_S \cdot \sigma \cdot T_S^4 \quad (6)$$

For incoming long wave radiation  $Q_h$  the emission coefficient for cloudy sky  $\varepsilon_C$  (dimensionless) is determined using vapour pressure  $e_A$  (in mbar) and cloudiness  $C$  (dimensionless);  $k_G$  is a value for dependence of the emission coefficient on cloudiness (BLÖSCHL et al., 1987):

$$\varepsilon_C = \varepsilon + (1 - \varepsilon) \cdot k_G \cdot C \quad (7a)$$

$$\varepsilon = 0.887 - 0.26 \cdot 10^{-0.052 \cdot e_A} \quad (7b)$$

The turbulent fluxes are parameterised with  $\alpha$  wind function, where  $\cdot$  is the heat transfer coefficient in  $\text{W}/(\text{m}^2 \cdot \text{K})$  and  $w$  is the wind speed in  $\text{m}/\text{s}$ :

$$\alpha = 3.0 + 3.6 \cdot w^{0.7} \quad (8)$$

Ground heat flux is a calibration parameter, it is constant for non-glaciated areas, at glaciers it is zero.

### Internal processes

To calculate the internal processes (heat and mass fluxes) in the snow pack, an approach by BRAUN (1985) is used, based on the concepts of water retention and cold content. The numerical solution of the system of coupled differential equations for heat and mass balance of ice, water and water vapour in the snow cover is extremely CPU-intensive and its application in the forecasting system is not justified.

### Runoff concentration

Melt water from different areas of the (partly) glaciated catchment follows different flow paths on its way to the catchment outlet and is retained in different ways. The catchment area is divided into four regions with tempo-

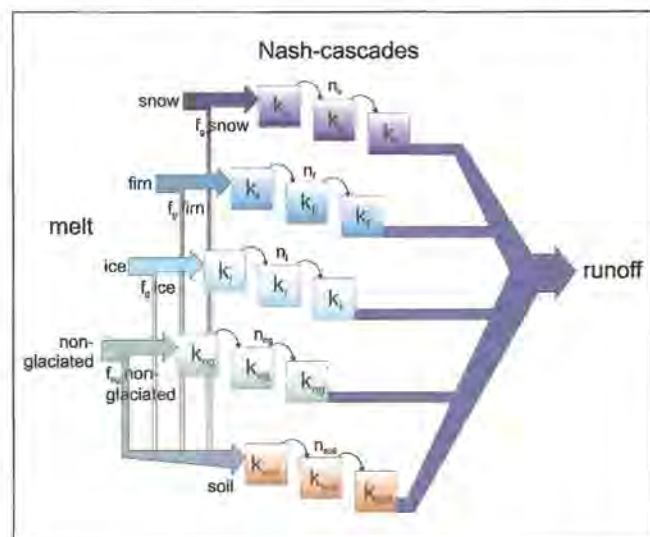


Figure 7: Runoff concentration concept with Nash-cascades. The numbers of reservoirs ( $n_s, n_f, n_i, n_{ng}, n_{soil}$ ) and the outflow rate constants ( $k_s, k_f, k_i, k_{ng}, k_{soil}$ ), as well as the factors  $f_s$  and  $f_{ng}$  to specify the ratio of melt to the soil reservoir, are calibration parameters.

rally changing extents: 1) non-glaciated area, 2) snow free glacier, 3) firn area and 4) snow on the glacier. Melt water emerging in a time step is summed up for these areas and routed through four parallel Nash-cascades (NASH 1958) (fig. 7). A Nash-cascade consists of  $n$  linear reservoirs of equal storage constant  $k$  connected in series. Part of the melt of the four zones can be by-passed through a slower soil reservoir, which is represented by a Nash-cascade, too. The parameters  $n$  and  $k$  of the five cascades are to be determined by calibration.

### 3 Calibration and Verification

Calibration and verification of SES is based on data from monitoring sites at Vernagtferner in Tyrol, Austria (ESCHER-VETTER et al. 2005) (fig. 3). The topographic input is derived from a 20 m DEM of Vernagtferner (ENDRES 2001) (fig. 4).

The calibration and verification was performed in several steps: a) checking the albedo module against measured values at "Pegelstation Vernagtbach" (1994 – 2000) (ASZTALOS 2004), b) checking simulated against observed depletion patterns (1999/2000 – 2000/2001), c) checking the melt model combined with the runoff concentration module against runoff data from "Pegelstation Vernagtbach" (1994/1995 – 2001/2002).

Depletion patterns were derived from photographs made by an automatic camera observing the western part of Vernagtferner (fig. 8). Due to data availability the period for calibration and verification (1999/2000 and 2000/2001) was rather short. Although photographs were taken every day from May to October, only a limited number of images were suitable, as a result of camera malfunction, snow fall, fog or cloudiness. Three characteristic photographs per year were selected and rectified using ORIENT/ORPHEUS (KAGER 1989). In the rectified photographs the depletion patterns were identified manually (fig. 9) and compared to the simulated spatial distribution of snow and firn water equivalent. Fig. 10 shows good the agreement of simulated and observed depletion patterns. In table 1 parameters of the albedo calculation as resulting from calibration are given.

Parameter	Unit	Value	Note
$a_N$	-	0.85	albedo new snow
$b$	-	0.60	lower limit snow albedo
$a_{sp,s}$	-	0.50	albedo shallow pack, glacier
$a_{sp,f}$	-	0.25	albedo shallow pack, non-glaciated
$a_{firn}$	-	0.55	firn albedo
$a_{ice}$	-	0.20	glacier ice albedo
$c^*$	$m^4/(W^2 \cdot h)$	$8 \cdot 10^{-5}$	snow albedo decrease factor
$w_{crit}$	mm	30	small snow water equivalent

**Table 1:** Parameters of SES for albedo calculation as resulting from calibration

Parameters of the runoff concentration module are calibrated manually on the basis of runoff data from the gauging station "Pegel Vernagtbach" at different depletion situations of the glacier. In fig. 11 measured (black) and simulated (red) runoff for August 1999 are shown. Within the Inn River Forecasting System SES was applied to 13 headwater catchments (fig. 2), from which five are located in the Ötztal and three are gauged. The calibration of snow melt was accomplished at the well-



**Figure 8:** Photograph taken by the automatic camera at Schwarzkögele on Aug. 15<sup>th</sup> 2000, showing the western part of Vernagtferner.



**Figure 9:** Rectified image of the western part of Vernagtferner on Aug. 15<sup>th</sup> 2000, manually identified snow line in red.

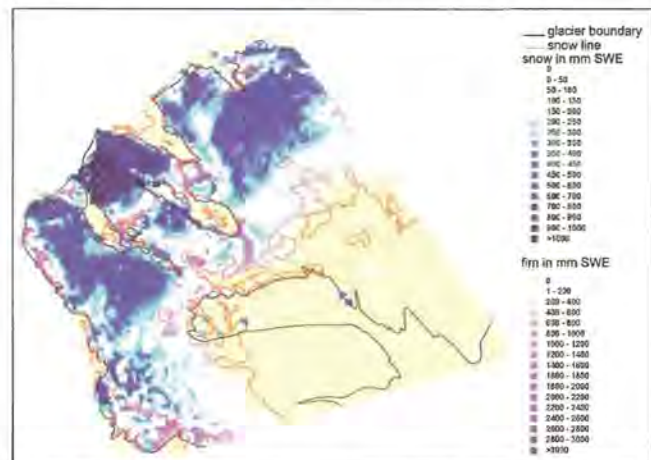


**Figure 10:** Spatial distribution of snow (blue) and firn (magenta) water equivalent simulated by the model and snow line (red) derived from photograph for Aug. 15<sup>th</sup> 2000.

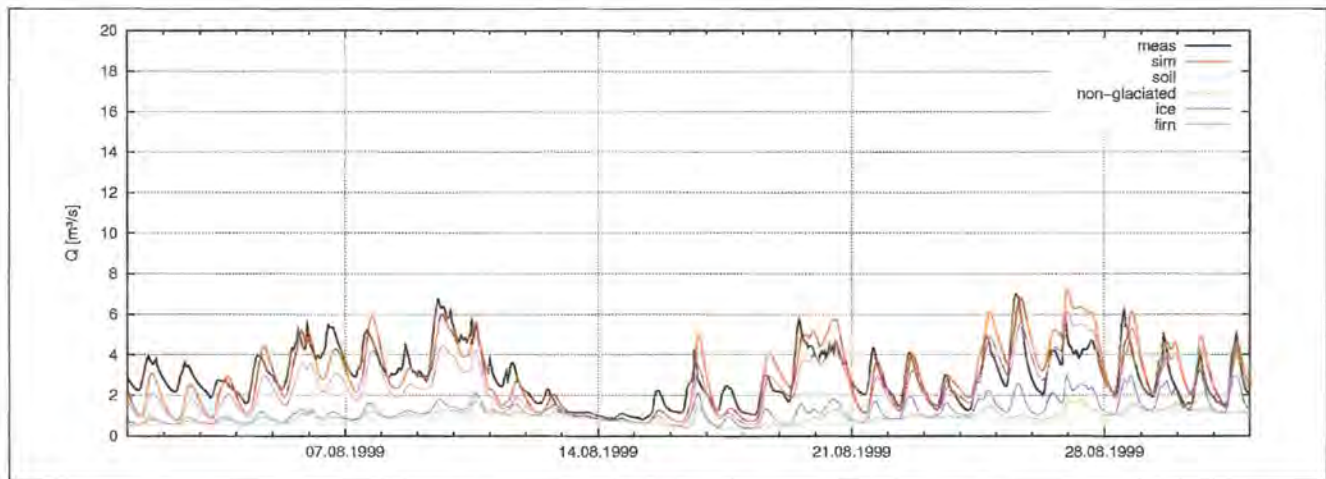


Figure 11: Measured and simulated runoff for August 1999 at „Pegel Vernagtbach“.

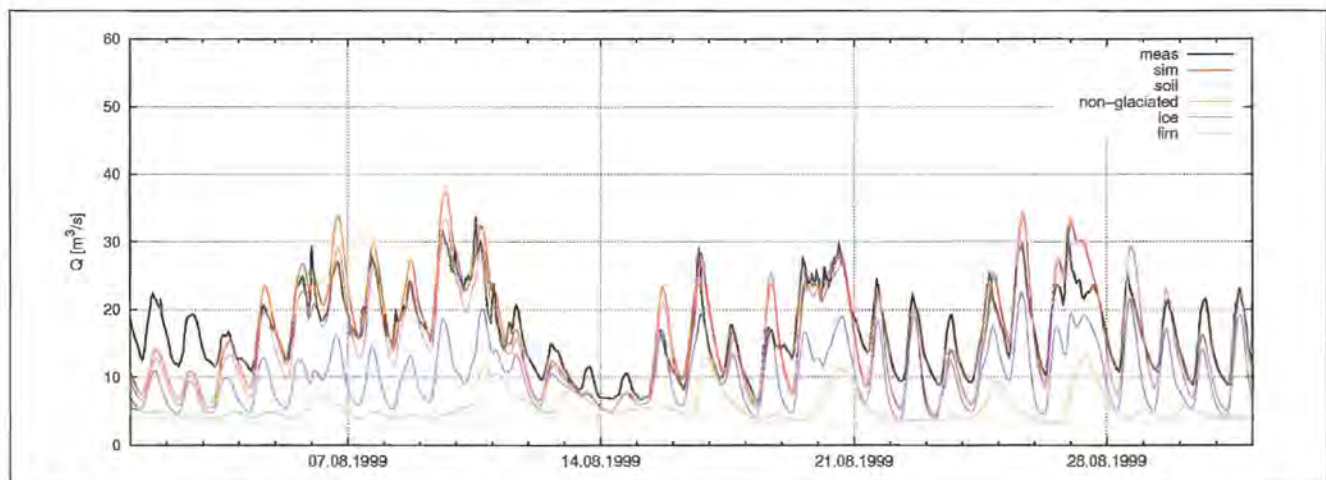


Figure 12: Measured and simulated runoff for August 1999 at Vent/Rofenache.

observed glacier Vernagtferner on the basis of depletion patterns derived from rectified photographs. In Tyrol area-wide orthophotographs with the required spatial resolution are only available infrequently (every 2 to 5 years). Therefore verification of snow melt and, if necessary, recalibration of parameters in other gauged catchments is only possible on the basis of runoff. The topographic input data for the 13 catchments was derived on basis of a DEM with 50 m resolution. No recalibration of the melt model was done, merely the parameters relating to snow redistribution (based on slope and curvature) were slightly adjusted due to the different resolution of topographic data. Runoff parameters were modified in order to improve routing delay correlation. Fig. 12 shows measured (black) and simulated (red) runoff at Vent/Rofenache. Comparing fig. 11 and 12 the good agreement of simulated and observed runoff in both catchments is recognisable.

#### 4 Summary

As part of the Inn River Forecasting System the fully distributed energy balance snow and glacier melt model SES calculates runoff from partly glaciated headwaters

of the southern tributaries of the Inn. The special feature of SES is the method of albedo calculation: A modified approach of TROFIMOVA (1970) is used, in which albedo decrease is a function of the (positive) energy balance and its derivative.

Calibration and verification of SES is done stepwise with data from Vernagtferner, Tyrol. Firstly, the albedo algorithm is verified, secondly, observed (from rectified photographs) and computed depletion patterns are compared and, thirdly, runoff is checked against data from „Pegel Vernagtbach“.

As area-wide orthophotographs in Tyrol are available infrequently, verification of the model in other catchments can only occur on the basis of runoff data. Within the Inn River Forecasting System the Snow and Glacier Melt Model SES was successfully applied to 13 headwater catchments.

#### Acknowledgements

We would like to thank Ass.Prof. Dipl.-Ing. Dr.techn. Helmut Kager of the Institute of Photogrammetry and Remote Sensing of the Vienna University of Technology for his assistance with the rectification of images to orthophotographs.

The fundings from various sources such as DFG, BMBF, the Thiernig Foundation, and the Academy Research Programme III.B.1 of the Federal Republic of Germany and the State of Bavaria are gratefully acknowledged.

## References

- ASZTALOS, J. (2004): Ein Schnee- und Eisschmelzmodell für vergletscherte Einzugsgebiete. Master's thesis, Technische Universität Wien.  
[http://www.hydro.tuwien.ac.at/fileadmin/mediapool-hydro/Diverse/Lehre/Diplomarbeiten/da\\_asztalos2004.pdf](http://www.hydro.tuwien.ac.at/fileadmin/mediapool-hydro/Diverse/Lehre/Diplomarbeiten/da_asztalos2004.pdf)
- BERG, E. J. (1932): Rechnung mit Operatoren. Oldenbourg, München.
- BLOESCHL, G. (1990): Snowmelt simulation in rugged terrain. PhD thesis, Vienna University of Technology.
- BLOESCHL, G., KIRNBAUER, R. AND GUTKNECHT, D. (1987): Zur Berechnung des Wärmeeintrags an einem Punkt der Schneedecke. Deutsche Gewässerkundliche Mitteilungen, 31(5):149–155.
- BLOESCHL, G., KIRNBAUER, R. AND GUTKNECHT, D. (1991): Distributed snowmelt simulations in an alpine catchment – 1. Model evaluation on the basis of snow cover patterns. Water Resources Research, 27(12):3171–3179.
- BRAUN, L. N. (1985): Simulation of snowmelt-runoff in lowland and lower alpine regions of Switzerland. Zürcher Geographische Schriften, 21:166 pp.
- BROCK, B. W., WILLIS, I. C., SHARP, M. J. AND ARNOLD, N. S. (2000): Modelling seasonal and spatial variations in the surface energy balance of Haut Glacier d'Arolla. Annals of Glaciology, 31:53–62.
- DICKINSON, W. T. AND WHITELEY, H. (1970): Watershed areas contributing to runoff. In: Symposium on the Results of Research on Representative and Experimental Basins, pages 12–26, Wellington, New Zealand. IAHS, Publ. no. 96.
- ENDRES, J. (2001): Farborthophotokarte "Vernagtferner 1999" aus Amateur-Luftbildern. Master's thesis, Technische Universität München.  
[http://www.lrz-muenchen.de/~a2901ad/webserver/webdata/download/da\\_endres2001.pdf](http://www.lrz-muenchen.de/~a2901ad/webserver/webdata/download/da_endres2001.pdf)
- ESCHER-VETTER, H. (2000): Modelling meltwater production with a distributed energy balance method and runoff using a linear reservoir approach – Results from Vernagtferner, Oetzal alps, for the ablation seasons 1992 to 1995. Zeitschrift für Gletscherkunde und Glazialgeologie, 36:119–150.
- ESCHER-VETTER, H., BRAUN, L. N., SIEBERS, M. AND WEBER, M. (2005): Water balance of the Vernagtferner high alpine basin based on long-term measurements and modelling. Landschaftsökologie und Umweltforschung, TU Braunschweig, 48:19–32.
- FEDERER, C. AND LASH, D. (1978): BROOK: A hydrologic simulation model for eastern forests. Technical Report 19, Water Resource Research Centre, University of New Hampshire.
- HEINDL, W. AND KOCH, H. (1976): Die Berechnung von Sonneneinstrahlungsintensitäten für wärmetechnische Untersuchungen im Bauwesen. Gesundheits-Ingenieur, 97(12).
- HEWLETT, J. D. (1961): Soil moisture as a source of baseflow from steep mountain watersheds. Technical Report 132, US Forest Service Southeast.
- HEWLETT, J.D. AND NUTTER, W.L. (1970): The varying source area of streamflow from upland basins. In: Proceedings of the Symposium on Interdisciplinary Aspects of Watershed Management, pages 65–83, New York. American Society of Civil Engineers.
- KAGER, H. (1989). Orient: A universal photogrammetric adjustment system. In: Optical 3-D Measurement Techniques, pages 447–455. Wichmann Verlag, Karlsruhe.
- KASTEN, F. AND CZEPLANK, G. (1980): Solar and terrestrial radiation dependent on the cloud amount and type of cloud. Solar Energy, 24:177–189.
- KIRNBAUER, R. AND SCHÖNLAUB, H. (2006): Vorhersage für den Inn. Wiener Mitteilungen, 199: 69–84.
- KLEINDIENST, H. (1996): Erweiterung und Erprobung eines anwendungsorientierten hydrologischen Modells zur Gangliensimulation in kleinen Wildbacheinzugsgebieten. Master's thesis, Ludwig-Maximilians-Universität, München.
- LEONHARDT, G., SENFTER, S., SCHÖBERL, F. AND SCHÖNLAUB, H. (2006): Ein hybrider Ansatz zur adäquaten Berücksichtigung des Betriebs von Wehr- und Kraftwerksanlagen im Rahmen des Hochwasservorhersagemodells Inn. In: Wasserbaukolloquium 2006: Strömungssimulation im Wasserbau, volume 32, pages 23–30. Dresdner Wasserbauliche Mitteilungen.
- LISTON, G.E. AND ELDER, K. (2006): A distributed snow-evolution modeling system (SnowModel). Journal of Hydrometeorology, 7(6):1259–1276.
- NASH, J.E. (1958): The form of the instantaneous hydrograph. In: General Assembly of Toronto, pages 114–118. IAHS, Publ. No. 42 (3).
- RANZI, R. AND ROSSO, R. (1991): A physically based approach to modelling distributed snowmelt in a small alpine catchment. In: Snow, Hydrology and Forests in High Alpine Areas, pages 141–150. IAHS, publ. No. 205.
- REICHEL, G. AND BAUMHACKL, G. (2000): A new simulation tool for flood routing in man-controlled river systems focusing on to the needs of operational hydrology. In: TÖNSMANN, F. AND KOCH, M. (editors) (2000): International Symposium on Flood Defence, Germany. Kassel Reports of Hydraulic Engineering, No. 9/2000, Universität-Gesamthochschule Kassel.
- SCIETEC (2005). Flux<sup>DSS/DESIGNER</sup> Referenzhandbuch. SCIETEC Flussmanagement GmbH, Linz, Austria.  
<http://www.sciotec.at/ps/tools/download.php?file=/doc/cudb/psfile/doc/99/Referenzha4339349b904e3.pdf&name=Referenzhandbuch.%20Ver.4.0.pdf>
- STRASSER, U., CORRIPIO, J. BROCK, B., PELLICCIOTTI, F., BURLANDO P. AND FUNK M. (2004): Spatial and temporal variability of meteorological variables at Haut Glacier d'Arolla (Switzerland) during the ablation season 2001: Measurements and simulations. Journal of Geophysical Research, 109(3).
- TROFIMOVA, E.B. (1970): Metod rascheta otrazhayushchej sposobnosti snezhnogo pokrova (Eine Methode zur Berechnung der Reflexionseigenschaften von Schneeoberflächen). Sredneaziatskij Nauchno Isseledovatel'skij Gidrometeorologicheskij Institut, Leningrad, 52 (67): 21–25.
- U.S. ARMY CORPS OF ENGINEERS (1956): Snow hydrology, Summary report of the snow investigations. North Pacific Division, Portland (Oregon).
- VAN GENUCHTEN, M.Th. (1980): A closed-form equation for predicting the hydraulic conductivity of unsaturated soils. Soil Science Society of America Journal, 44:892–898.

## 2 Provision of snow information from satellite data within Polar View and application example for a mesoscale Alpine catchment using PROMET

HEIKE BACH<sup>1</sup>, FLORIAN APPEL<sup>1</sup> AND WOLFRAM MAUSER<sup>2</sup>

<sup>1</sup> VISTA Remote Sensing in Geosciences, Gabelsbergerstr. 51, D-80333 Munich, Germany

<sup>2</sup> Department of Geography, Ludwig-Maximilians University (LMU), Luisenstr. 37, D-80333 Munich, Germany

### Abstract

Information on snow cover and snow properties is an important factor for hydrology and runoff modeling. Frequent updates of snow cover information can help to improve water balance and discharge calculations. Within the frame of Polar View, snow products from multi-sensoral satellite data are operationally provided to control and update water balance models for large parts of Southern Germany. This snow service is described and results are presented. Example applications are given using the PROMET model in the mesoscale Alpine catchment of the Upper Danube. Through assimilation of the remote sensed information in the PROMET model, enhanced snow water equivalent distributions, that can not directly be observed by remote sensing, were calculated. Accurate snow storage simulations are a prerequisite to correctly simulate runoff during the melting phase.

### 1. Introduction

#### 1.1 Scope of Polar View

Polar View is an earth observation (EO) program, mainly focused on both the Arctic and the Antarctic. Polar View is supported by the European Space Agency (ESA) and the European Commission (with participation by the Canadian Space Agency). It presents one of the GMES Service Elements and is supported by ESA until 2008. GMES stands for Global Monitoring for Environment and Security, a European initiative which intends to provide tools operational services to improve our environment (<http://www.gmes.info>). As major goal ESA's GMES services promote the utilization of satellites for public good and in support of public policy in the areas of sustainable economic development, marine safety, and environment. The Polar View Team consists of companies, government agencies and research institutes across Europe. Each organization contributes its diverse, complementary skills to the Polar View program and is committed to establish a dedicated service for addressing polar issues using earth observation

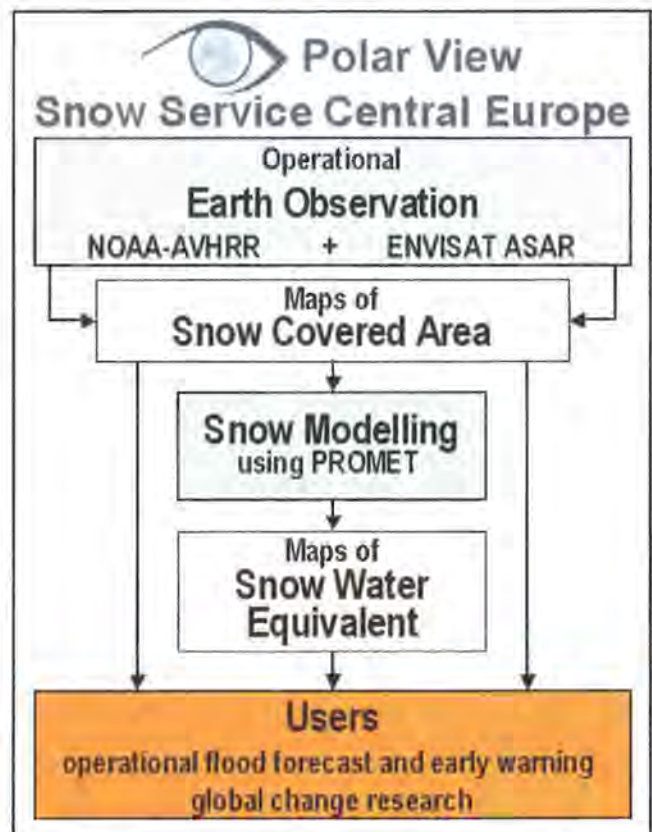


Figure 1: Overview on Polar Views Snow Service Central Europe.

technologies. More about Polar View, the GMES/GSE initiatives and the services can be found at [www.polarview.org](http://www.polarview.org)

#### 1.2 Polar View's Snow Cover Services

Although Polar View has a focus on the Arctic and Antarctic regions with services ranging from the monitoring of sea ice, icebergs, ice edge, and ice drift, also outside the polar regions snow and ice products are provided by the team. The snow services cover Northern and Central Europe with the Alps as one area of interest. Each of these regions has his own characteristics of the snow cover, its seasonal extent and temporal dynamics. The lower mountainous regions in Central Europe show the characteristic, that due to frequent temperature changes the snow pack accumulates and melts off several times during a winter season. Especially rainfall in combination with snow melt is one of the most critical causes for floods there. In higher mountainous areas, the Alps, longer consisting snow coverage is characteristic. This Alpine snow pack is also an important contribution to local and cross-region energy production. Therefore a good knowledge of the stored snow water equivalent (SWE) is essential. To cover this diversity and to properly spatially characterize the snow properties, Earth observation from satellites together with spatial water balance modeling is an ideal tool.

## 2. Methodology

### 2.1 Operational Snow Products from Earth Observation

Within Polar View VISTA is in charge of Central Europe and provides binary snow cover maps for the Alpine Region and Southern Germany with frequent updates and spatial resolutions of 1 km. The provision of information on Snow Water Equivalent from joint observation and modeling with PROMET (see next section) was included into the services. The operational satellite observation service provides daily snow cover as input information to the water balance model. The snow services use two different processing chains for optical and microwave data. Optical AVHRR sensors of the NOAA operational series of satellites are used for snow mapping and snow line delineation. Although these acquisitions are available several times per day, cloud cover hinders regular frequent updates of snow cover maps. As an additional remote sensing data source microwave data, which are not affected by cloud cover, from Advanced Synthetic

Aperture Radar (ASAR) on ENVISAT is used. The wide swath mode of ASAR is selected as input data source that provides a medium spatial (150 m) and also good temporal coverage (up to 2 times per week). Since C-band SAR sensors are only sensitive to snow when the snow has a high content of liquid water, the application of ASAR is limited to the melting periods. However under these conditions the developed procedure allows to delineate the snow cover in a comparable way as from optical data. In addition information on where the snow is melting can be provided (APPEL et al., 2005).

Data processing is performed fully automatically with direct data reception of the optical data at the University of Munich and near real time provision of ASAR data by ESA within a couple of hours after data take via FTP. The output of both automatic processing chains for the different sensor types consist of satellite observation based snow cover maps and snow line delineation with comparable classes and identical spatial resolution. The different chains are shortly described in the following section and illustrated in Figure 2:

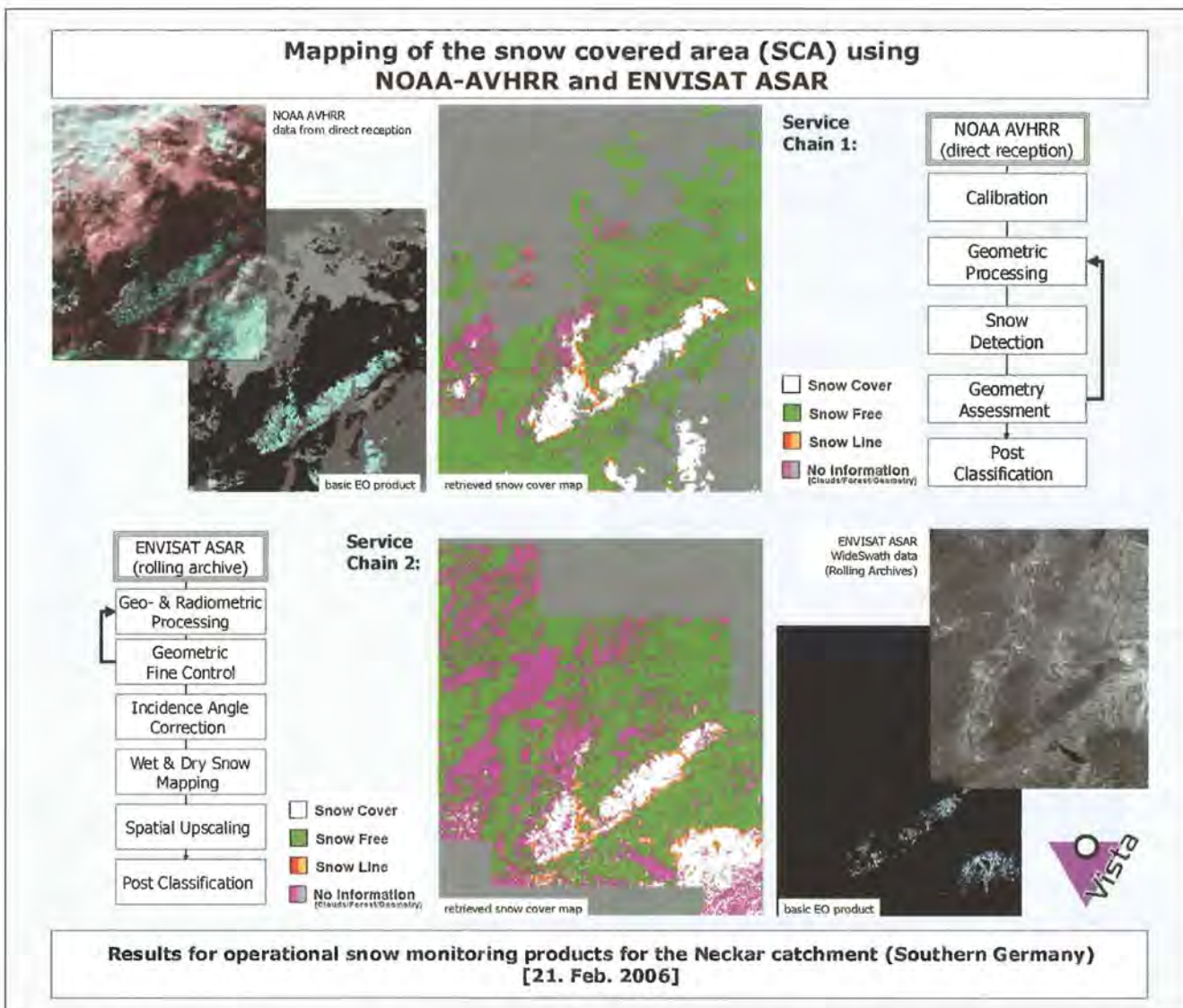


**Figure 2:** Overview of the two different service chains to obtain comparable Snow Covered Area (SCA) maps from the different sensors (NOAA-AVHRR and ENVISAT ASAR).

- The first processing chain provides daily information of snow covered area, the snow line, and snow free areas using medium resolution optical imagery (NOAA-AVHRR) from direct reception. Also areas that could not be classified due to cloud cover or sensor limitations are clearly marked. Snow is detected using ratio and threshold techniques for several spectral bands of the sensor. This allows a clear discrimination of snow from other surfaces and clouds.
- The second processing chain identifies the extent of snow with a high content of liquid water from microwave SAR data using ENVISAT ASAR in wide swath mode. A semi-empirical backscatter model and change detection techniques are applied. The combination of the classified wet snow areas from SAR with GIS information and spatial analyses is the basis to derive a snow cover map and deliver a snow line comparable to the optical product. Products are provided within 6 hours after data acquisition using ESA's Near Real Time (NRT) rolling archive.

The basic products from optical and microwave data analyses are enhanced and standardized in a final step. In order to provide user demanded products the snow line detection and quality assessment is performed. Resulting products of snow cover maps (several classes, including snow line information) are archived and provided via FTP to the users in formats defined by them. A validation with station measurements for the last 3 winter seasons proved the high quality of the operational snow classification. For NOAA 95% and for ASAR 85 % of the 1km<sup>2</sup> raster cells were correctly classified.

The temporal frequency of the provision of hydrological meaningful products is irregular, since it depends on the occurrence of a snow cover, snow melt conditions (in case SAR is used) and on the cloud cover (in case optical data are used). However during the winter season 2005/2006 more than 20 hydrological relevant products could be provided.

The snow service is up to now regularly used by two flood forecast centers in Germany (Flood Forecast Center - LUBW Baden-Württemberg; Flood Information Service - LUWG Rheinland-Pfalz), responsible for the runoff and flood forecast for the Neckar, Upper Rhine, and Mosel. Also the German Weather service (DWD) uses these maps in order to optimize their snow water equivalent model results provided with SNOW-D (BLÜMEL et al. 2004)

## 2.2 Hydrological modeling of the Upper Danube with PROMET

In order to demonstrate how the remote sensing products can be used for improved water balance modeling, an application example for the Upper Danube is presented. This catchment is the research area of the integrative research project GLOWA- DANUBE that is conducted by the University of Munich (MAUSER & LUDWIG 2002). Basic characteristics and a satellite image of



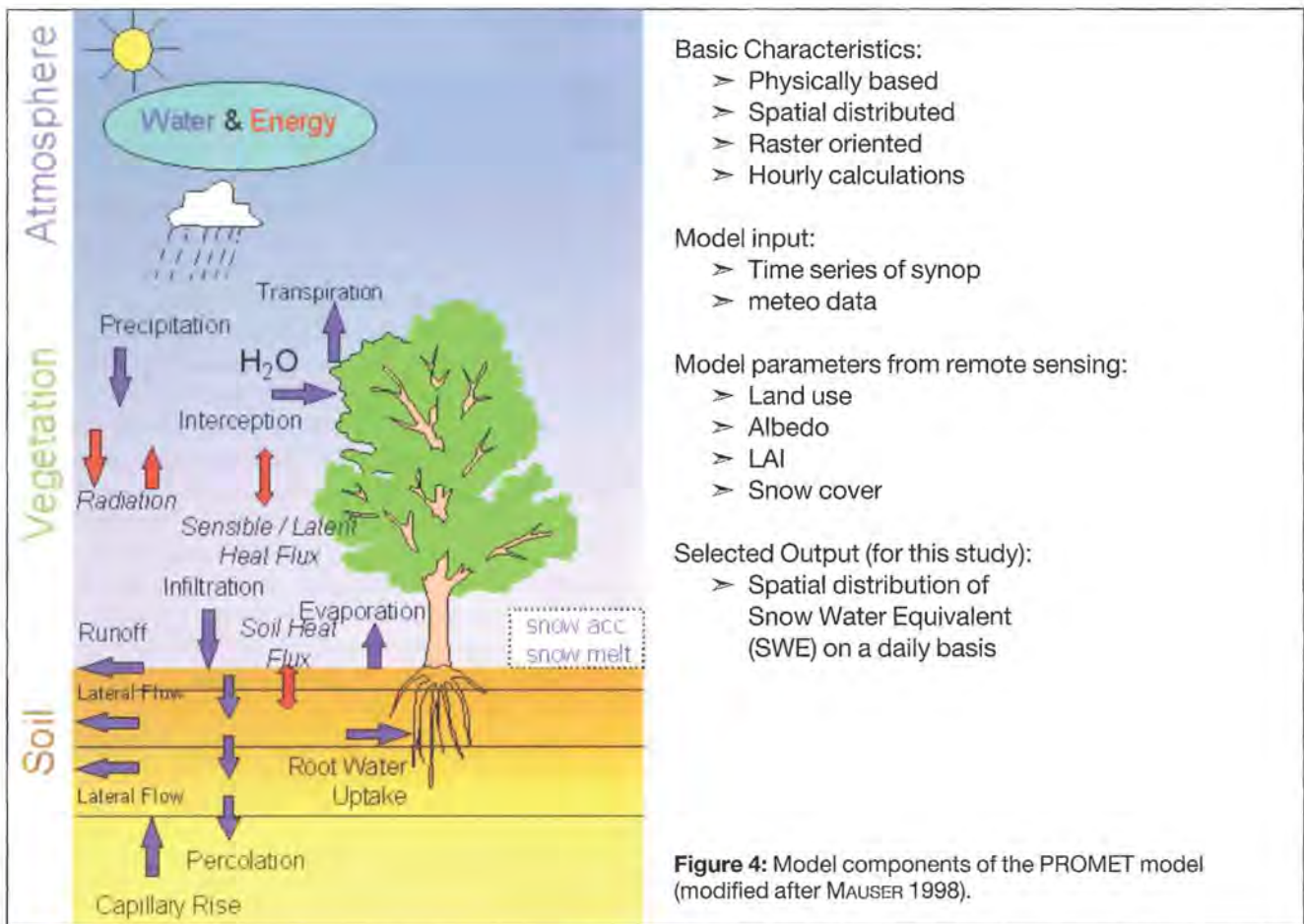
**Figure 3:** Watershed of the Upper Danube up to Passau (catchment size 76 643 km<sup>2</sup>).

this test area are shown in Figure 3. In the Southern part of the catchment the Alps show up in white due to snow cover at the higher elevations.

As hydrological model, the Process Oriented Model for EvapoTranspiration PROMET is applied. PROMET is a physically based Soil-Vegetation-Atmosphere-Transfer Scheme (MAUSER 1998, LUDWIG AND MAUSER 2000). It simulates fluxes of water, energy and matter in the system soil-vegetation-atmosphere. On the basis of the Penman-Monteith equation, the actual evapotranspiration is modeled spatially distributed as a function of water availability, radiation balance and physiological regulation mechanisms of heterogeneous plant stands. In the applied PROMET version a snow model as developed by STRASSER (STRASSER & MAUSER 2000) was used.

The specific advantage of PROMET is that it is optimized for the integration of satellite observation data. The raster based infrastructure is one of the features that allow that information on land use, albedo, leaf area index and snow cover, that can be derived from remote sensed satellite images, can be used for an improved parameterization of the spatial characteristics of the watershed. Examples for the integration of satellite observations in the model and description of the data assimilation schemes can be found in MAUSER et al. 1998 and BACH et al. 2003.

The calculations in PROMET are conducted in hourly time steps. The model is driven by meteorological inputs like precipitation, radiation and wind. Within PROMET the meteorological station data (only Synop - stations are available for the complete catchment) are spatially and temporally interpolated considering terrain influences. In the model a critical threshold air temperature decides where precipitation falls as rainfall or snow. This critical temperature is an important parameter that determines the snow accumulation phase. It can be varied between -3 and +3°C.

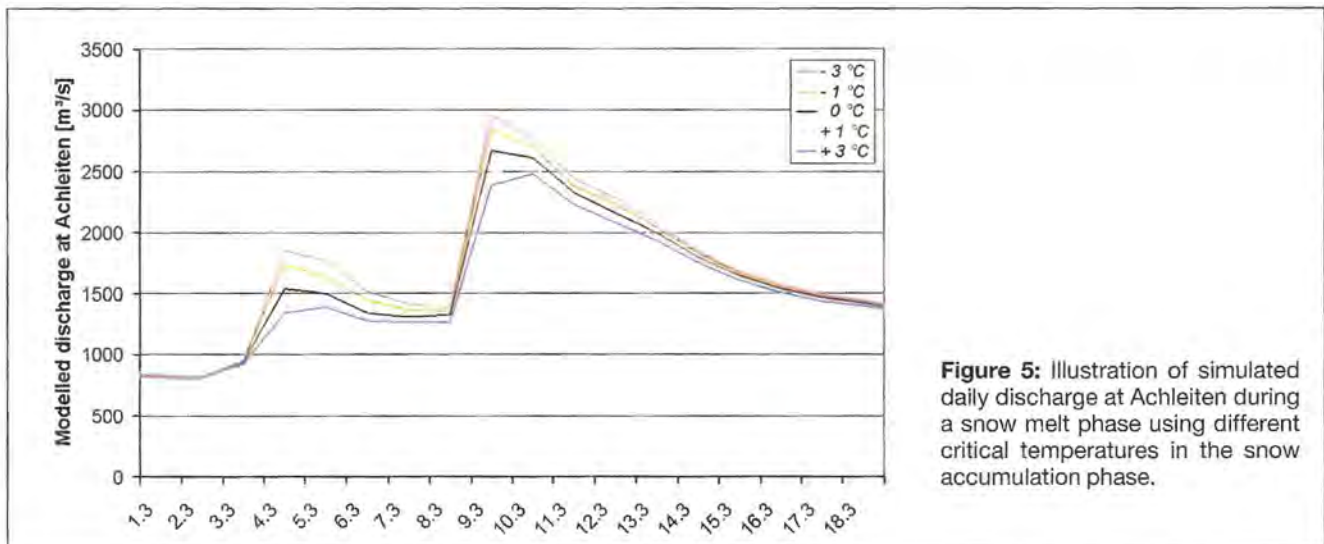


### 2.3 Sensitivity Studies

The critical temperature is not only important for the snow model. Since it is one of the factors that determine to which extent the precipitation is temporally stored in the snow cover, it also significantly affects the runoff formation. As an example, Figure 5 shows simulated discharge at the outlet of the catchment at Achleiten assuming 5 different critical temperature values in the snow model. For this sensitivity study, during the whole winter period the critical temperature was kept constant in

each test case. If the critical temperature is larger e.g. 3°C then the water storage in the snow cover increases and as a consequence during snow melt more runoff is created. The difference of the runoff peak can easily vary by +/- 10% when we use +/-3°C instead of the nominal values 0°C.

The Polar View snow service provides snow cover maps that highlight the snow line as illustrated in Figure 2. During the accumulation phase of the snow cover, the spatial extent of the snow cover and thus the modeled snow line is depending on the applied critical temperature.



This makes it possible to compare the modeled snow cover, assuming variable critical temperature values in a kind of ensemble run, with the observed snow cover. This comparison is done for each subwatershed in order to estimate the best threshold for the decision on the critical temperature and thus the occurrence of snow fall. Accordingly, the critical temperature is parameterized using the observed snow cover from satellite data analyses. As an example Figure 6 illustrates such a retrieved parameterization of the critical temperature for each subwatershed. As can be seen neighboring subwatersheds often have similar values and cluster together.

The impact of this kind of parameterization on the modeled snow water equivalent (SWE) is illustrated at the right side of Figure 6. The increase or decrease of the snow water equivalent as result of the assimilation of the satellite information into the model is related to the snow water equivalent that is simulated assuming a constant critical temperature of 0°C. Thus the green regions on the left side on Figure 6, where 0°C was judged to fit best, show up on the right side of this figure as white regions where no change of SWE could be identified. For the other regions the impact is quite complex with the strongest increase of SWE in the North East part of the watershed.

### 3. Results

Through the described data assimilation technique, the modeled snow cover agrees better with the mapped snow cover information from satellite. The satellite image thus succeeds to bring in more realism in the simulations. The PROMET model on the other hand provides maps of snow water equivalent, which is a land surface property that can not directly be assessed by remote sensing. This is one typical example how remote sensing and hydrological modeling can both benefit from each other, if data assimilation techniques are applied. Examples of calculated snow water equivalent distributions using data assimilation are illustrated in Figure 7 for 2 different dates.

### 4. Discussion

The presented examples show principle ways to integrate remote sensing information in land surface models and especially in snow models. However data assimilation has its limitations. For example, in some cases it is not possible to obtain an agreement between model and satellite results by optimizing the critical temperature within its valid ranges. In these cases other sources of errors in the simulation must be identified. One should always consider that hydrological models should not be forced to the observation without assuming meaningful physics behind the forcing and to take into account the inaccuracies and uncertainties of the remote sensing products. Concerning the critical temperature adjustments this means that the range of +/-3°C can not be extended. As a result of an uncertainty analysis of the remote sensing products, it was identified that the snow classification has a significant lower accuracy for thin snow layers of less than 5 mm SWE. Accordingly, the assimilation process considers this threshold in order not to overinterpret the satellite image.

In the presented cases the applications of remote sensing data was found meaningful for the accumulation phases of the snow cover. For the melting phases comparisons of model results and snow height measurements indicate that the melting process is partly modeled too intense. This shall be overcome in the near future when integrating a new version of the snow sub-module in PROMET using the ESCIMO principles, as described in PRASCH et al. (2007). Additionally it will be investigated how the observations of wet/melting snow regions, possible with SAR, can improve the spatial modeling of the melting process.

### Acknowledgement

This work was supported by ESA within the GMES-GSE project Polar View.



**Figure 6:** Distribution of estimated critical temperatures in the catchment for a snowfall period (12.2.-18.2.2006) derived from comparison with snow maps observed with satellites (left) and resulting increase or decrease of simulated snow water equivalent (right).

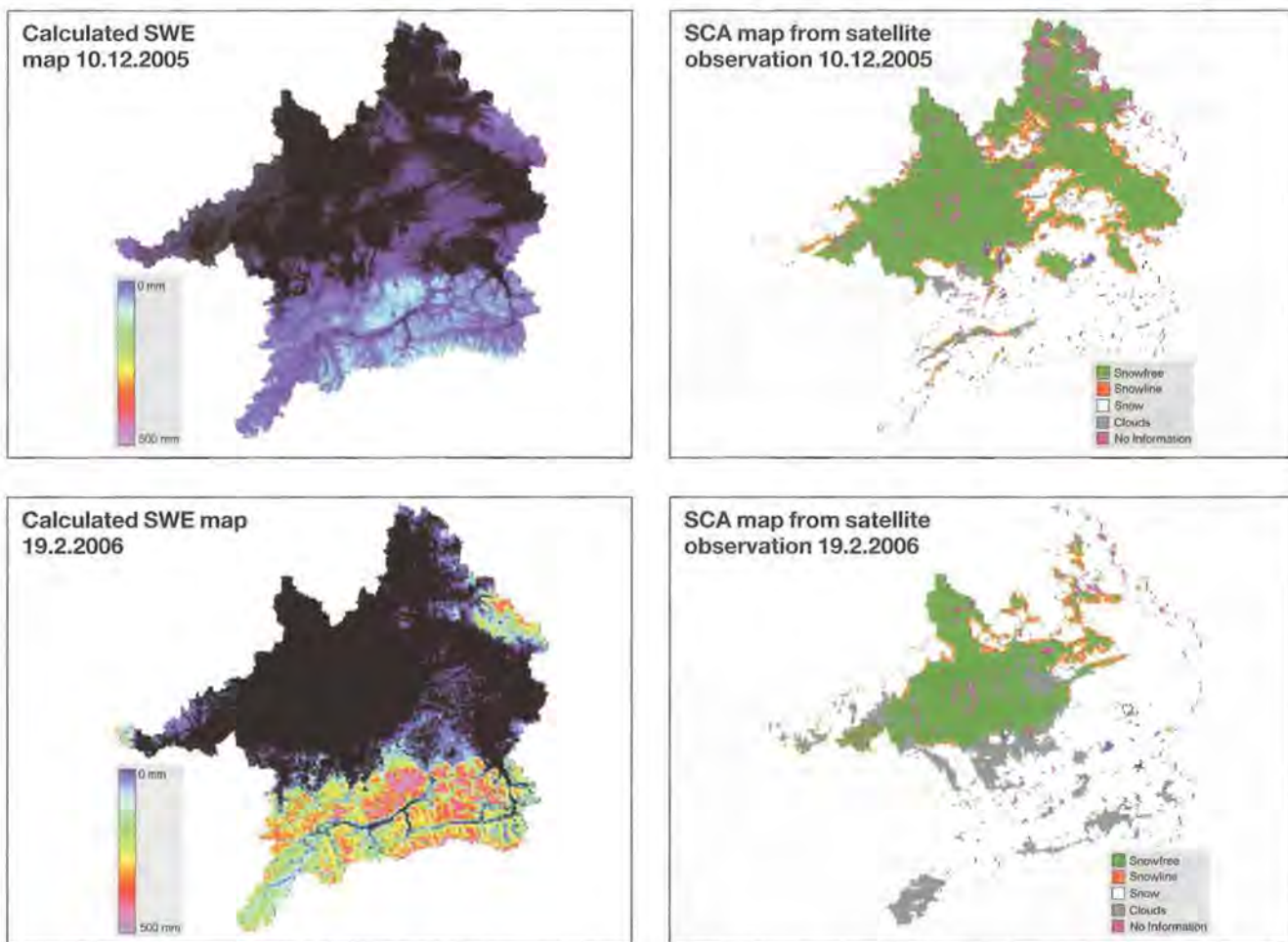


**Figure 7:** Simulated snow water equivalent for the Danube catchment and snow cover maps classified from satellite data used as input to data assimilation.

## References

- APPEL, F., BACH, H., LÖW, A., LUDWIG, R., MAUSER, W., SCHULZ, W. (2005): Operational Monitoring of the Snow Cover Dynamics in Southern Germany, Capabilities of Optical and Microwave Remote Sensing for Improved Flood Forecast, IEEE Int. Geos RS Symposium, 25-29. July 2005, Seoul, Korea. Vol. III, pp. 1955-1958.
- BACH, H., BRAUN, M., LAMPART, G., MAUSER, W. (2003): The use of remote sensing for hydrological parameterization of Alpine catchments, *Hydrology and Earth System Sciences*, 7 (6), pp.862-876
- BLÜMEL, K., SCHNEIDER, G. (2004): Bereitstellung von operativ nutzbaren Vorhersagedaten zur Schmelz- und Niederschlagswasserabgabe aus der Schneedecke für das Beratungsgebiet Rheinland-Pfalz, Saarland, für Teile von Nordrhein-Westfalen und Hessen sowie das französische Moselgebiet, Luxemburg und Baden-Württemberg (SNOW-BW2003), Abschlussbericht, Deutscher Wetterdienst, Geschäftsfeld Hydrometeorologie, Berlin-Buch, 158 p.
- MAUSER, W., SCHÄDLICH, S. (1998): Modeling the Spatial Distribution of Evapotranspiration on Different Scale using Remote Sensing Data, *J. Hydrol. (Special BAHC Issue)* 212-213(1998)250
- MAUSER, W., LUDWIG, R. (2002): GLOWA-DANUBE – A research concept to develop integrative techniques, scenarios and strategies regarding global changes of the water cycle. In: Beniston, M. (ed), *Climatic Change: Implications for the Hydrological Cycle and for Water Management. Advances in Global Change Research*, Vol. 10 (2002), Kluwer Academic Publishers, Dordrecht and Boston, pages 171-188
- MAUSER W., BACH H., STRASSER U., SCHNEIDER K. (1998): The contribution of remote sensing data to distributed hydrologic modeling, *Information for Sustainability*, ISBN82-7542-040-7, Proceedings Int. Symp. Rem. Sens. Envir., pp.295-299
- LUDWIG, R., MAUSER, W. (2000): Modelling Catchment Hydrology within a GIS-based SVAT-model framework. In: *Hydrology and Earth System Sciences HESS*, Vol. 4(2), p. 239-249
- PRASCH, M., STRASSER, U., MAUSER, W. (2007): Validation of a physically based snow model for the simulation of the accumulation and ablation of snow (ESCIMO), this issue
- STRASSER, U., MAUSER, W. (2001): Modelling the Spatial and Temporal Variations of the Water Balance for the Weser Catchment 1965-1994; *J. Hydrol.*, 254 (2001) 199-214.

### 3 High resolution modelling of snow transport in complex terrain using simulated wind fields

MATTHIAS BERNHARDT<sup>1</sup>, GLEN E. LISTON<sup>2</sup>,  
GÜNTHER ZÄNGL<sup>3</sup>, ULRICH STRASSER<sup>1</sup>  
AND WOLFRAM MAUSER<sup>1</sup>

<sup>1</sup> Department of Geography, Ludwig-Maximilians Universität (LMU), Luisenstr. 37, D-80333 Munich, Germany

<sup>2</sup> Cooperative Institute for Research in the Atmosphere, Colorado State University, Fort Collins, Colorado, 80523 USA

<sup>3</sup> Department of Physics, Institute for Meteorology, Ludwig-Maximilians University (LMU), Theresienstr. 37, D-80333 Munich, Germany

#### Abstract:

Snow transport is one of the most dominant processes influencing the snow cover accumulation and ablation in high alpine mountain environments. Hence, the spatial and temporal variability of the snow cover is significantly modified with respective consequences on the total amount of water in the snow pack, on the temporal dynamics of the runoff and on the energy balance of the surface. For the presented study we used the snow transport model SnowTran3D in combination with MM5 (Penn State University - National Center for Atmospheric Research MM5 model) generated wind fields. In a first step the MM5 wind fields were downscaled by using a semi-empirical approach, which accounts for the elevation difference of model and real topography, as well as aspect, inclination and vegetation. The target resolution of ten m corresponds to the highest resolution of the available DEM and the land cover map. For the numerical modelling, data of five automatic meteorological stations were used, comprising the winter season of 2004/05. In addition we had automatic snow depth measurements and periodic manual measurements of

snow courses available for the validation of the results. In this paper we describe the downscaling of the wind fields and discuss the results of the snow transport simulations with respect to the measurements.

#### 1. Introduction

In alpine terrain wind induced snow transport leads to a significant redistribution of the existing snow cover (DOESKEN AND JUDSON 1996; BALK AND ELDER 2000; DOORSCHOT 2002, BOWLING et al., 2004, BERNHARDT et al. 2007). In succession one can observe snow accumulation in lee regions, in sinks, and on the windward side of taller vegetation (POMEROY et al. 1993, LISTON AND STURM 1998, HIEMSTRA et al. 2002). The resulting heterogeneity has effects on the energy balance, the total amount of snow water equivalent (SWE) and the timing and intensity of snowmelt runoff as well as the avalanche risk (LISTON 1995, LISTON AND STURM 1998, LISTON et al. 2000, LEHNING 2006). Furthermore snow transport can lead to an increase of the sublimation rates of the snow cover itself and of airborne snow particles. Losses from 40-50% of the winter snow precipitation can be assumed for high alpine terrain which is due to the high frequency of blowing snow events within these regions (HOOD et al. 1999, ESSERY 1999 et al., LISTON 2004). For the reproduction of all these processes many models were developed over the last years (LISTON AND STURM, 1998; DÉRY, 1999; ESSERY et al., 1999; WINSTRAL AND MARKS, 2002; LEHNING et al., 2006). Nevertheless, the appropriate reproduction of snow transport processes not only depends on the model itself, but also on the ability to provide representative meteorological information for the model used. In this context, very sensitive parameters are wind speed and direction (ESSERY 2001; LEHNING et al. 2000; EIDSVIK et al. 2004, BERNHARDT et al. 2007). WINSTRAL AND MARKS (2002) outlined the difficulties of constraining this parameter in alpine terrain. BERNHARDT et al. (2007) utilized a library of MM5 wind fields for providing physically derived wind fields to the snow transport model (fig.1).

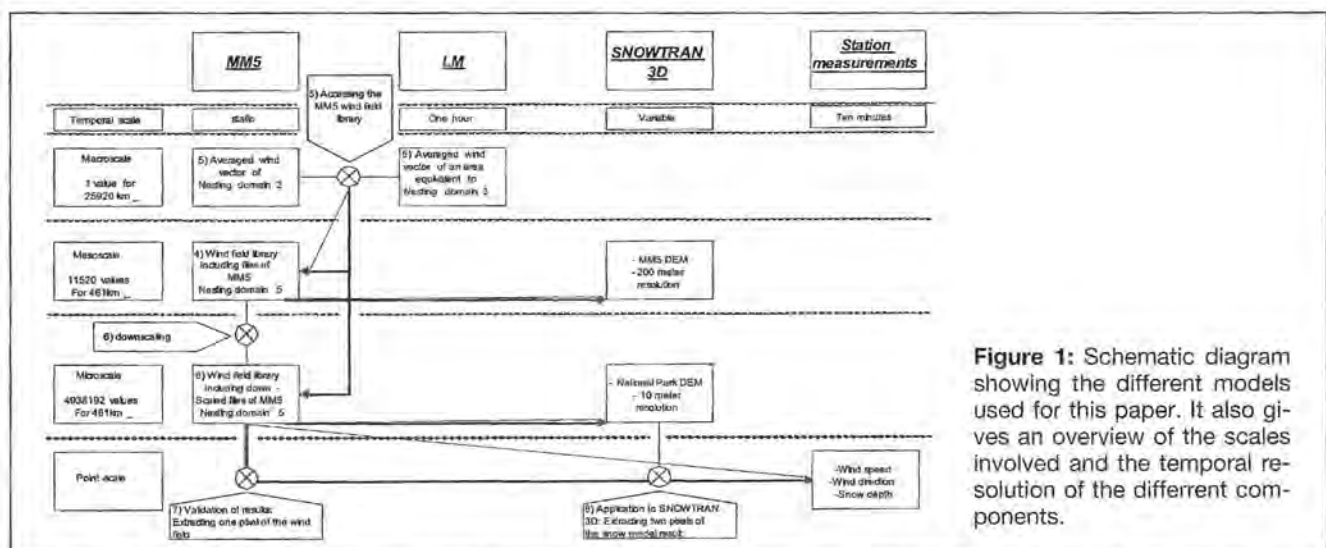


Figure 1: Schematic diagram showing the different models used for this paper. It also gives an overview of the scales involved and the temporal resolution of the different components.

## 2. Study area

The "Berchtesgaden National Park" is located in the southeast of Germany within the Free State of Bavaria (fig. 2). The park is centered near 47°36'N, 12°57'E and covers an area of 208 km<sup>2</sup> with an average altitude of approximately 1010 m a.s.l.. The high alpine area is characterised by rapid changes in elevation (minimum altitude: 501 m a.s.l., maximum altitude 2713 m a.s.l.). The difference between the "Königssee" (lake level 603 m a.s.l.) and "Watzmann" summit (2713 m a.s.l.) is about 2110 m at a horizontal distance of about 3.5 km.

The climate of the National Park area is subject to significant spatial variability, strongly influenced by the elevation. Small scale local differences are caused, by the general position in the mountainous landscape, the position whether windward or lee to the prevailing winds, and solar incidence angles.

Due to its status as a biological reserve, we can assume undisturbed testing conditions and human influences can be neglected. The described study investigates the winter season of 2004/2005; meteorological data for this period were available from five automatic weather stations (table 1). Snow depth measurements were provided by a field campaign accomplished by the National Park rangers (fig. 2).

GIS information of vegetation and topography were provided by the National Park authority. The vegetation dataset is based on an interpretation of coloured infrared aerial photographs (personal communication). The used DEM was derived from 20 m contour lines. Both data sets provide a spatial resolution of 10 m.

For the described study we applied our model on two sites: "Reiteralm" and "Kühroint".

### Field campaign

During the winter season 2004/05 a field campaign was carried out in the area around the meteorological stations of "Kühroint" and "Reiteralm". The precise location of the sample points can be seen in figures 3 and 4. The sample points were chosen randomly. Four sample points are located within the forest at "Kühroint", whereas 10 sample points are located between the mountain pines and within the canopy stands at Reiteralm.

A continuous series of weekly measurements was planned (at Kühroint and Reiteralm), but in some cases the aspired interval could not be maintained because of critical meteorological conditions and high avalanche risk (fig.11). The National Park rangers measured the snow depth via snow poles and pre-installed staff gauges. The results of the realized measurements can be seen in table 2 and 3.

**Table 1:** Meteorological stations which were used, their abbreviations, geographical coordinates, elevation, and meteorological recordings: wind speed (WS), wind direction (WD), temperature (T), humidity (H), snow height (SH), global radiation (GR), and precipitation (P).

Station	Elev (a.s.l.)	Long (deg)	Lat (deg)	Temporal resolution	Parameters provided
Reiter Alm I	1755 m	12,80532	47,80532	10 min.	WS, WD
Reiter Alm II	1670 m	12,80984	47,64949	10 min.	T, H, SH
Reiter Alm III	1615 m	12,81133	47,64720	10 min.	T, H, GR, P, SH
Jenner I	1200 m	13,01926	47,58648	10 min.	T, H, GR, WS, WD, P
Schönau	617 m	12,98332	47,60941	10 min.	T, H, GR, WS, WD, P

**Figure 2:** Test site (National Park Berchtesgaden) (Bayerisches Landesvermessungsamt 1994, modified). Reiteralm 1 is located at the Wartsteinkopf (1755 m a.s.l.). The locations of Reiteralm 2 and 3 are marked with arrows.



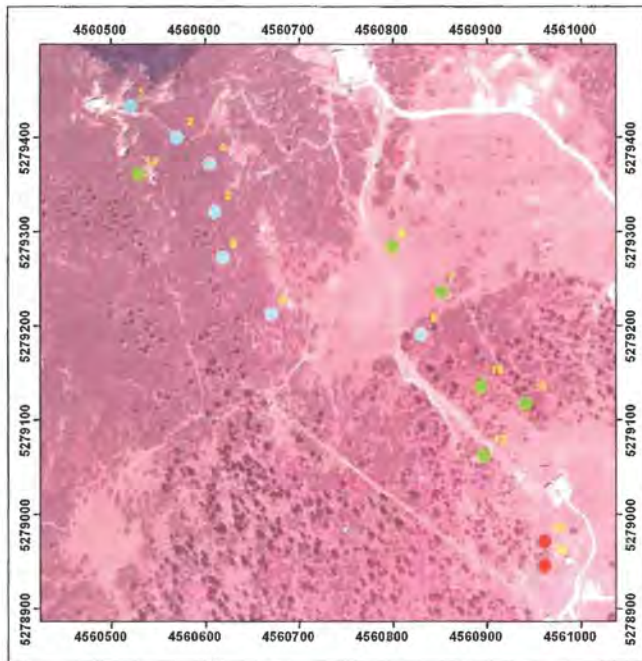


Figure 3: Sample points Reiteralm 2004/2005.

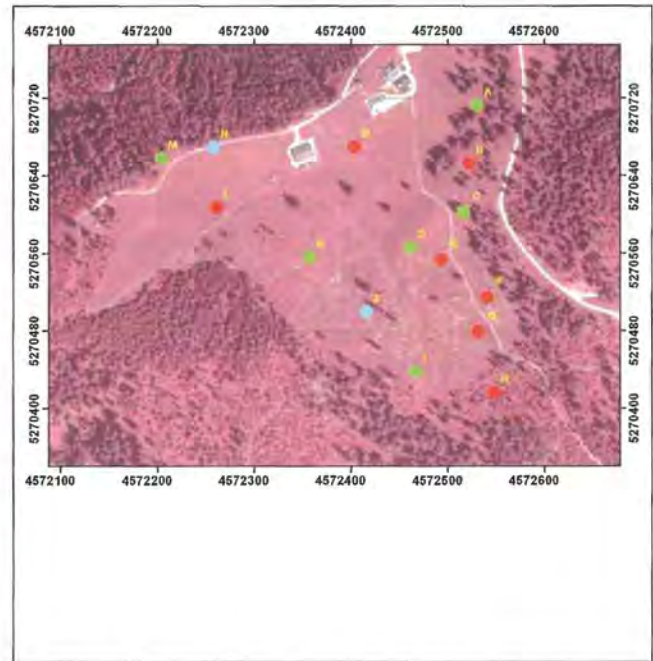


Figure 4: Sample points at K uhroint 2004/2005.

Table 2: Snow depth (cm) at the sample points at Reiteralm (2004/2005).

Point	08.02.2005	15.02.2005	23.02.2005	02.03.2005	10.03.2005	14.03.2005	23.03.2005	30.03.2005	05.04.2005	14.04.2005
1	76	126	116	114	104	101	74	57	48	39
2	138	189	175	174	204	176	124	97	70	58
3	151	196	179	175	183	172	118	100	85	83
4	133	186	173	167	184	170	125	97	89	82
5	146	204	188	185	202	187	139	112	105	101
6	140	178	164	158	196	172	126	122	105	94
7	173	214	198	219	235	212	155	141	119	117
8	94	144	131	125	139	122	80	59	36	35
9	147	168	163	156	197	174	119	95	48	72
10	220	260	231	231	235	200	154	141	118	109
11	169	218	192	180	210	230	122	107	53	56
12	202	257	215	209	255	232	157	130	115	101
13	176	230	209	198	250	234	161	138	118	118
14	224	264	240	240	305	270	209	178	157	157
15	230	259	238	238	320	320	218	197	160	149

Table 3: Snow depth (cm) at the sample points at K uhroint (2004/2005) (-999 is an error value).

Point	08.02.2005	15.02.2005	22.02.2005	02.03.2005	08.03.2005	15.03.2005	22.03.2005	29.03.2005	12.04.2005	19.04.2005
A	128	114	156	133	146	145	102	80	81	51
B	175	161	165	174	188	189	139	115	102	78
C	95	73	86	95	102	108	53	21	40	0
D	111	-999	128	132	240	105	-999	71	0	0
E	173	153	160	168	183	188	125	102	92	62
F	165	147	155	165	173	175	120	101	83	58
G	164	152	160	166	178	178	125	105	94	73
H	183	176	177	180	200	207	155	142	135	113
I	121	110	123	126	142	146	105	99	72	46
J	76	82	90	85	100	95	60	38	0	0
K	122	113	120	124	140	142	96	69	59	40
L	177	63	166	176	189	202	154	136	123	89
M	88	87	95	105	116	122	60	53	23	0
N	86	77	84	87	100	108	83	29	0	0
O	165	149	146	146	169	177	127	104	92	66

### 3. Models

We used the snow transport model Snowtran3D (LISTON AND STURM 1998) and the Penn State University - National Center for Atmospheric Research MM5 model (MM5), version 3.3 (GRELL et al. 1995).

SnowTran3D is based on the mass balance equation which describes the temporal variation of snow depth at any grid cell:

$$\frac{d\zeta}{dt} = \frac{1}{\rho_s} \left[ \rho_w P - \left( \frac{dQ_s}{dx} + \frac{dQ_t}{dx} + \frac{dQ_s}{dy} + \frac{dQ_t}{dy} \right) + Q_v \right] \quad (1)$$

$Q_s$  = changes in horizontal mass-transport rates of saltation ( $\text{kg m}^{-1}\text{s}^{-1}$ ),  $Q_t$  = changes in horizontal mass-transport rates of turbulent suspended snow ( $\text{kg m}^{-1}\text{s}^{-1}$ ),  $Q_v$  = sublimation of transported snow ( $\text{kg m}^{-2}\text{s}^{-1}$ ),  $P$  = Water equivalent precipitation rate ( $\text{m s}^{-1}$ ),  $\zeta$  = change of snow depth,  $t$  = time (s),  $x$  and  $y$  horizontal coordinates (m),  $\rho_s$  = snow density ( $\text{kg m}^{-3}$ ),  $\rho_w$  = water density ( $\text{kg m}^{-3}$ ).

The model predicts the horizontal mass transport rates of saltation, changes in horizontal mass transport rates of turbulent suspended snow, sublimation of transported particles and the water equivalent precipitation rate (LISTON AND STURM 1998, LISTON AND ELDER 2006a) SnowTran3D has proven its applicability for a wide range of environments from Arctic plains (LISTON AND STURM 1998; LISTON AND STURM 2002) to mountainous terrain (GREEN et al. 1999; LISTON et al. 2000; PRASAD et al. 2001; HIEMSTRA et al. 2002; HASHOLT et al. 2003; BRULAND et al. 2004, HIEMSTRA et al. 2006, BERNHARDT et al. 2007).

Additionally we used an MM5 generated wind field library as input for Snowtran3D. Due to performance reasons this library was created in advance and was connected to the snow model over the Deutscher Wetterdienst (DWD) Lokalmodell (LM) (BERNHARDT et al. 2007). For the creation of the wind field library an adapted version of MM5 was utilized (ZÄNGL 2002, ZÄNGL 2003, BERNHARDT et al. 2007). This adapted version allowed us to produce wind fields with a spatial resolution of 200 m. Nevertheless the 200 m DEM had to be smoothed at some loca-

tions (fig. 5) due to stability requirements of MM5 (BERNHARDT et al. 2007). These modifications lead to some inaccuracies, which are corrected with the approaches applied here.

### 4. Reasons for the downscaling

A precise description of the results at the 200 m scale is given in BERNHARDT et al. (2007). In general it can be claimed that the snow transport activities increase under usage of the MM5 wind fields. Furthermore it pointed out that erosion is much more intensive at windward location as ablation processes are dominant at the leeward sites of the ridges. This is in line with the expectations (BARRY 1992) but was not fulfilled when using the interpolated wind fields (BERNHARDT et al. 2007). A more precise prediction of the location of accumulation and erosion zones is impossible at the 200 m scale (LISTON et al. 2006). For determining these locations, model-runs, with a higher spatial resolution become necessary. SnowTran3D and all other components of the snow model package are completely scale independent and permit model-runs up to a resolution of 1 m (LISTON et al. 2006). For the presented study a target resolution of 10 m should be used which corresponds with the GIS data and makes a comparison to field campaign data possible. Therefore the MM5 wind fields had to be downscaled to this resolution. The downscaling procedure is described in the following sections.

#### a) Spatial correction

For the high resolution modelling it was necessary to get the most exact geometry of the MM5 wind fields. Due to the scale of the coarser DEM used within MM5 and the smoothing of topography which was necessary for MM5 (BERNHARDT et al. 2007) this requirement was not fulfilled in the case of very exposed areas like station 1 at Reiteralm (fig. 5). In this special case the crest of "Wartsteinkopf" still appears, but not in the position like as in reality. The consequence is that in the model the meteorological station is not located at the mountains crest, but at the slope (fig. 5).

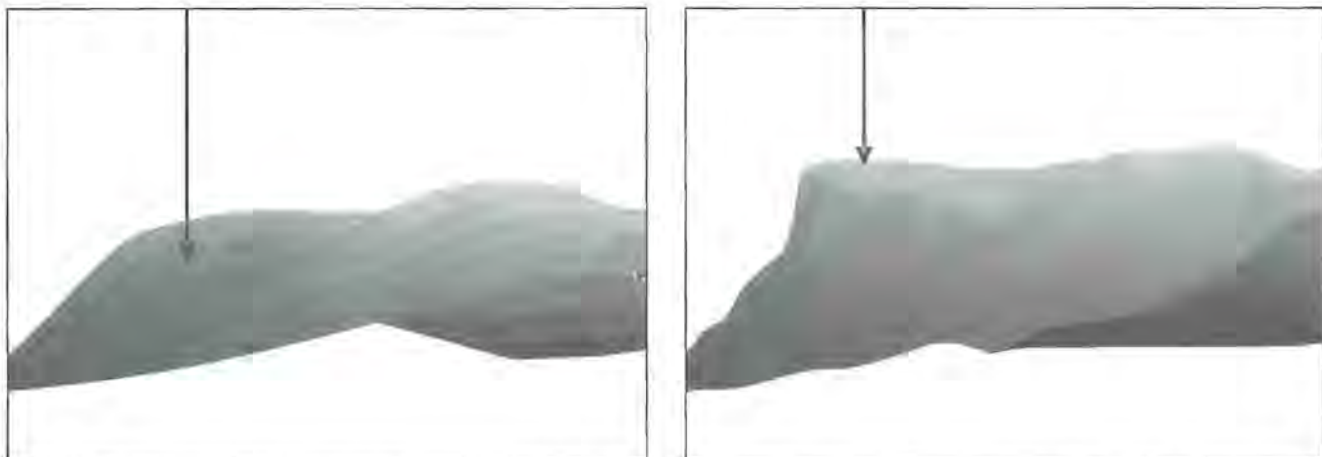


**Figure 5:** The smoothed Reiteralm area within the MM5 DEM (200 m resolution) compared to the National Park DEM (10 m resolution).

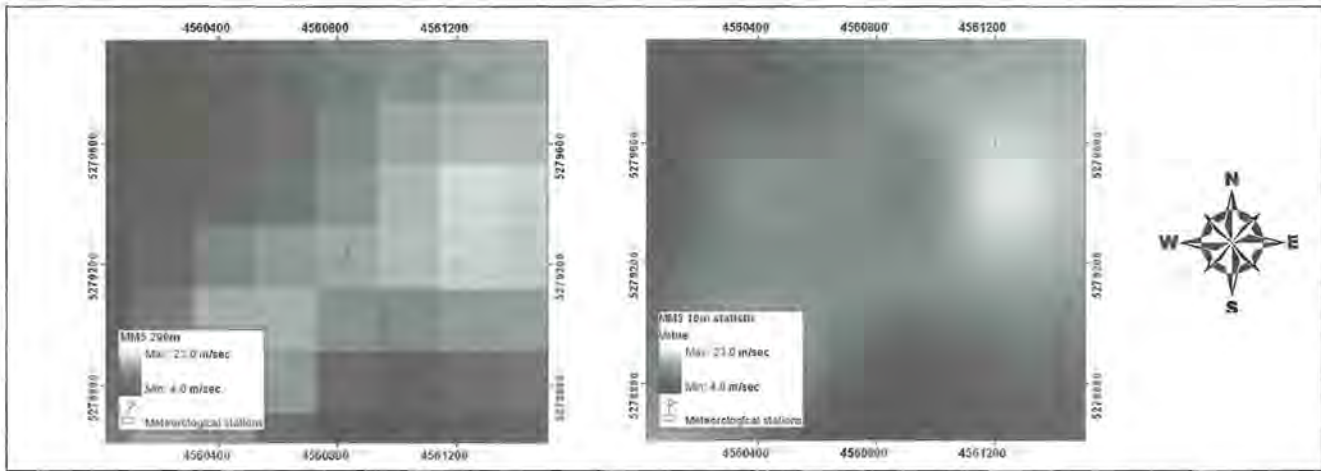


Figure 6: 1) Cutout of the original wind field (200 m) with Reiteralm station. Figure 6/2).

Due to the fact that a lot of such examples could be found a correction of the 200 m DEM and of the wind fields, in direction of the 10 m data becomes necessary. The correction happened via two 2 dimensional second order polynomials:

$$Z' = a1 * Z^2 + a2 * S^2 + a3 * Z + a4 * S + a5 * Z * S + a6 \quad (2)$$

$$S' = b1 * Z^2 + b2 * S^2 + b3 * Z + b4 * S + b5 * Z * S + b6 \quad (3)$$

Equation 2 stands for the new row coordinate and equation 3 for the new column coordinate. We used pass points for the determination of the coefficients a1-a6 and b1-b6. Under usage of more than six pass points the system of equations becomes over-determined and could be solved over the smallest quadratic deviance between the coefficients a1-a6 and b1-b6. So the MM5 DEM could be straightened to the 10 m DEM.

#### b) Statistical revision

The statistical revision was done in order to prevent of artefacts of the former 200 m pixels within the downscaled 10 m data and in succession within the snow model results (fig 6). Hence a Radial Basis Function (RBF) (Eq. 4) was used for smoothing the wind fields and for eliminating the coarse grid structure by conserving the total amount of energy of any wind field.

RBF is a local statistical technique, calculating predictions from measured points within a defined neighborhood which is smaller than the total area. As this approach is correct the modeled values will be conserved. For verification, mean wind speeds were compared before and after applying this statistical approach for any 200 m grid cell. The discrepancies were close to zero (table 3).

Table 4: Column I: Mean value of all 220 wind fields between the average value of the original and the modified MM5 wind speeds. Column II: Maximal observed difference between original and modified MM5. Column III: Minimal observed difference.

Mean deviation	Maximal deviation	Minimal deviation
0.03 [m/s]	0.02 [m/s]	0.00 [m/s]

The completely regularized spline function that was used is:

$$\phi(r) = -\sum_{n=1}^{\infty} \frac{(-1)^n (\sigma * r)^{2n}}{n!n} = \ln(\sigma * r/2)^2 + E_1(\sigma * r/2)^2 + C_E \quad (4)$$

$\phi(r)$  = Radial basis function,  $r$  = the Euclidean distance ( $r = \|s_i - s_j\|$  is the distance between the prediction location  $s_j$  and each data location  $s_i$ ),  $\sigma$  = the smoothing parameter,  $\ln$  = natural logarithm,  $E_1$  = exponential integral function,  $C_E$  = Euler constant.

After these calculations, wind fields were smoothed and the resolution was reduced to 10 m.

#### c) Inclusion of the height difference between MM5 and 10 m DEM

The coarser resolution of the modified MM5 DEM leads to smoothed elevation minima and maxima. This has a direct effect on the generated wind fields, which also show over- or underestimated wind speeds. For taking this into account the difference of the two DEM was calculated in a ten meter resolution. In a next step the gradient in wind speed with elevation was calculated for each modelled wind field. By doing so, it was distinguished between two elevation intervals which were significant dissimilar within the datasets.

Thus there is one gradient for the interval from 500 to 1800 m a.s.l., and another for 1800 to 2700 m a.s.l.. This separation was necessary because the gradient above 1800 m a.s.l. was much steeper than the gradient for the underlying interval. Caused by this analysis, it was possible to get a value for the increase of wind speed per meter in elevation for the two intervals. These gradients were then combined with the difference in elevation of the two DEMs. As a result, a surplus on wind speed was generated at locations with positive divergences, and there negative wind speed correction values were generated at locations where MM5 DEM values are higher than the ones of the 10 m DEM. So the resulting file contains a positive or negative correction value for any 10 m pixel. These values were added to the dedicated statistical reworked MM5 wind field.



Figure 7: Cutout of the original wind field (200 m) containing Watzmann massive. b) Same clipping after the downscaling process.

#### d) Integration of subgrid topography

Most of the small scale sinks and hills of the 10 m DEM were not respected during the MM5 modelling procedure which means that they have not had any influence on the generated wind fields. That makes a subsequent inclusion of this subscale information necessary. Therefore we used an algorithm of LISTON (1998):

$$S(a) = 1 + x * \text{slope} + y * \text{curvature} \quad (5)$$

S(a) = modification factor of the original wind speed,  
x and y = empirical factors.

The algorithm was utilised for the distribution of meteorological station wind speed data, but it can also be applied to the MM5 wind fields if one is regarding any grid value as a station measurement.

An algorithm of RYAN (1977) was used for modifying the wind direction, again with respect to the 10 m topography:

$$Md = -255 + sl * \sin*(2(e - d)) \quad (6)$$

Modification of the wind direction (RYAN 1977): Md=Modified direction, sl=slope in wind direction, e = exposition in wind direction, d = wind-direction.

The effect of vegetation on wind speed was considered with:

$$w_m = \exp((-L) * \left(1 - \left(\frac{0.6 * \text{veg}_{ht}}{\text{veg}_{ht}}\right)\right)) \quad (7)$$

Modification of the wind speed by vegetation:  $w_m$  = Modified speed,  $L = 0.9 * \text{LAI}$ ,  $e = \text{veg}_{ht}$  = vegetation height.

#### Validation of the MM5 data and application to the snow transport model Snowtran3D

The accordance of measured and modelled data is quite well at the daily scale ( $r^2=0.63$ , mean of the years 2002-

2005), but  $r^2$  is lower at the hourly scale (0.5, mean of the years 2002-2005). The lower convergence of measured and modelled data on hourly basis is conditional to the higher frequency, in the wind speeds of the station measurements due to local phenomena. These are not inherent within the MM5 wind fields. Furthermore, the determination of the current wind field depends on the synoptic situation which changes less frequent than the local conditions but determine the general course of data. So results are in line with the expectations. In addition, data become more confident if the wind speed is increasing which makes the wind fields applicable, because high wind speed is the steering factor for snow transport events.

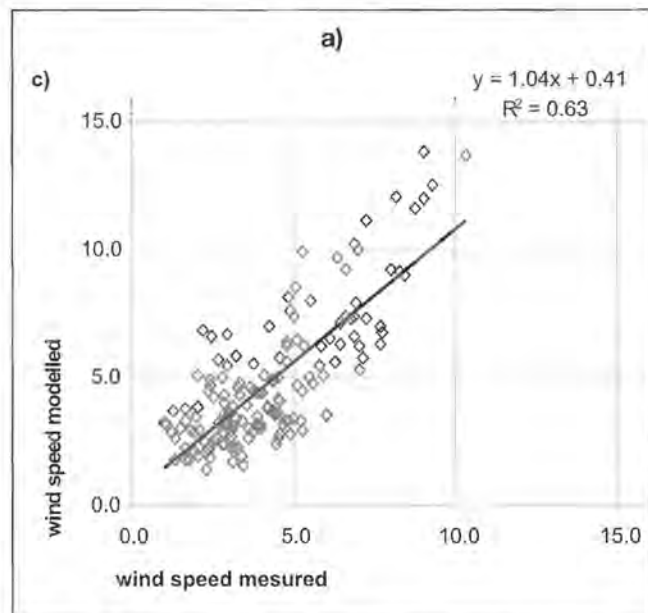


Figure 8 a: Correlation between MM5 results and station wind speed (Reiteralm 1, daily resolution).

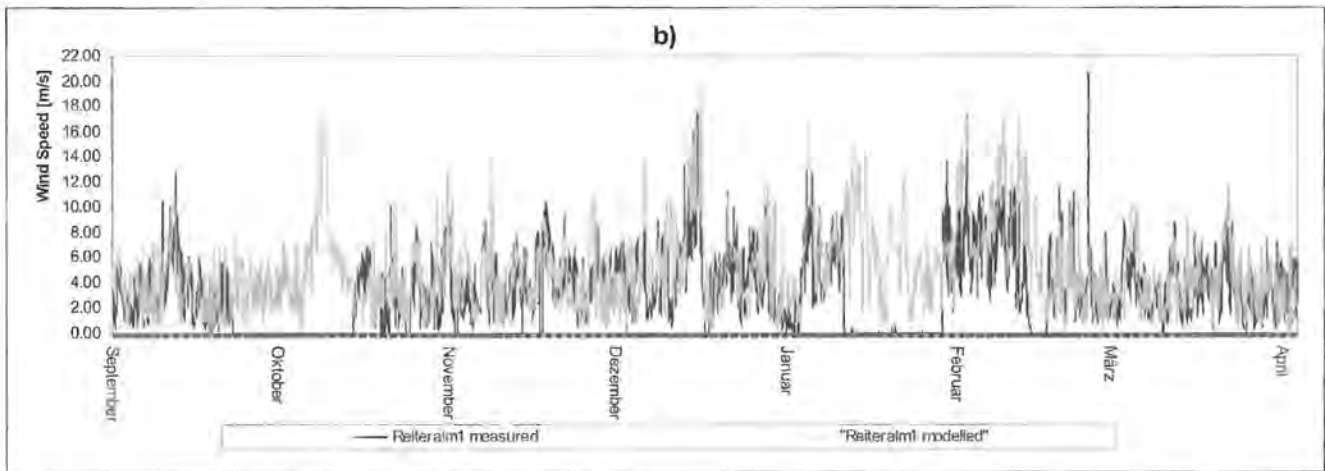


Figure 8 b: Time series of MM5 results and station measurements (Reiteralm 1, hourly resolution).

### Methodology

We simulated the snow evolution from August 1, 2004, to June 1, 2005. Snowtran3D runs were performed with a temporal resolution of one hour and a spatial resolution of 10 meters. The model requires humidity, air pressure, radiation and temperature information from the meteorological stations (table 1). Interpolated and MM5 generated wind speeds and directions (BERNHARDT et al. 2007) were used. At "Reiteralm" an area of about 2 km<sup>2</sup> or 20 000 pixels was modelled. The two available automatic stations at Reiteralm which were especially installed for observing snow transport processes, measured the snow depth in a ten minute resolution. At "Reiteralm" it should be proved that the Snowtran3D/MM5 wind field couple is able to reproduce the transport events. At "Kühroint" (1 km<sup>2</sup> / 10 000 pixels) we examine that the couple is able to reproduce no transport conditions. Caused by very low wind speeds, at winter season 2004/05, there almost was no energy available for snow transport at "Kühroint". Hence, modelled transport rates should be low under usage of the MM5 wind fields, too.

For the first model run, at "Reiteralm", the parameterisation of the vegetation classes was adopted from LISTON AND STURM (1998). After that, the vegetation type "mountain pine" was introduced and modified with respect to field measurements and to model results. In addition, a vegetation type "sporadic trees" was created for areas with sparse canopy stands.

### Results and Discussion

#### Results Reiteralm

First results at "Reiteralm" have shown a satisfying convergence of modelled and measured values. However, the snow depth was generally overestimated at the upper part of "Reiteralm" (marked as blue dots in fig. 3) as the snow depth was underestimated at the lower parts (red dots in fig. 3). The variance between the sample points could be reproduced by some extent, but is too small within the model results (fig. 9). Long lasting experiences of the Avalanche Warning Service of Bavaria have shown that respectable amounts of snow were blown

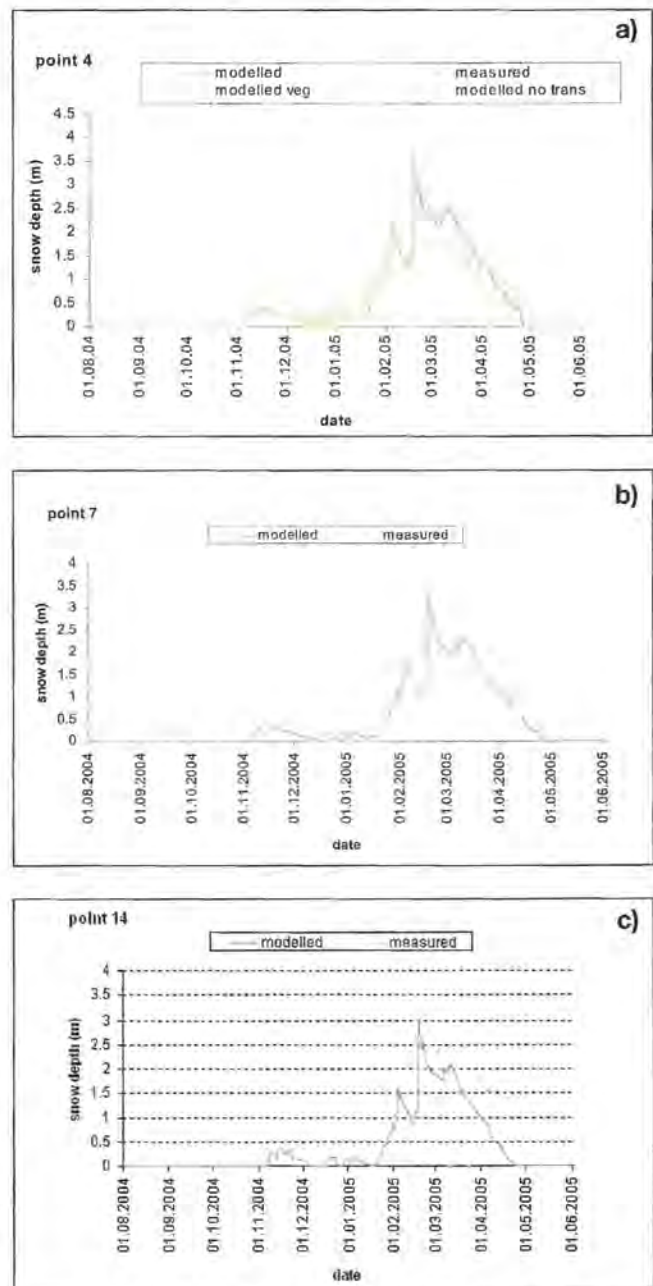


Figure 9: a) is representative for the upper part of Reiteralm. b) For the central region and c) for die lower part.

from the upper (characterised by sample points 1-8) to the lower part of the site (sample points 14 and 15). This experience is confirmed by the snow depth measurements of the automatic meteorological stations "Reiteralm" 2 and 3 but was only reproduced to some degree by the snow transport model. Hence the transport processes were underestimated at the first model run and under usage of the existing vegetation snow holding capacities.

Under usage of the new vegetation types and MM5 wind fields the model results could be improved at the upper part of the "Reiteralm", but we found minor changes at the lower part. A transport of snow from the higher area to the forest which subdivides "Reiteralm" into two parts could be observed. Nevertheless the forest appears as a physical barrier. The introduction of the vegetation class "sporadic trees" shows no improvement which is conditioned by the general model setup. For allowing snow transport over the forest, two different wind velocity layers would be required (only one is available).

A difference between modelled and interpolated wind fields can only be found at the upper stations. The other stations are close to the forest or within the forest which makes the differences negligible.

### Results Kühroint

Fig. 10 shows three sample points at "Kühroint". Point N is located at the edge of the forest at the northern part of "Kühroint"; point F is located at the clear cut area, as point K can be found on the meadows at the western part of the area. The three points represent: maximum overestimation (N), best fit (K) and maximum underestimation (F) of snow depth. In general, the overall variance of the modelled data is too small with respect to the snow depth differences between the sample points. The variation between the modelled pixels was especially low at the centre parts of "Kühroint". This might be due to the used DEM which describes the centre of "Kühroint" as an almost flat area, but it is undulated in reality. This lack between real and model topography certainly is one reason for the gap between measurements and model results. Nevertheless there are some other possible reasons, like a misinterpretation of the snow density or a wrong calculation of the solar radiation.

It matters that there are almost no differences in amount and timing of snow transport processes between the MM5 wind fields and interpolated wind fields, for the observed winter season. This proves the applicability of the MM5 wind fields, because the wind speed and direction measured by the meteorological station "Kühroint" should be representative for the whole clearance. As the MM5 wind fields producing equivalent results, they can also be regarded as representative for "Kühroint".

### Discussion

At both test sites snow begins to accumulate in early November, the maximum snow cover is reached in late February and the snow period ends in May.

The results at "Reiteralm" and "Kühroint" fit well to the measurements. Results at "Reiteralm" could be partly improved by the inclusion and adjustment of additional

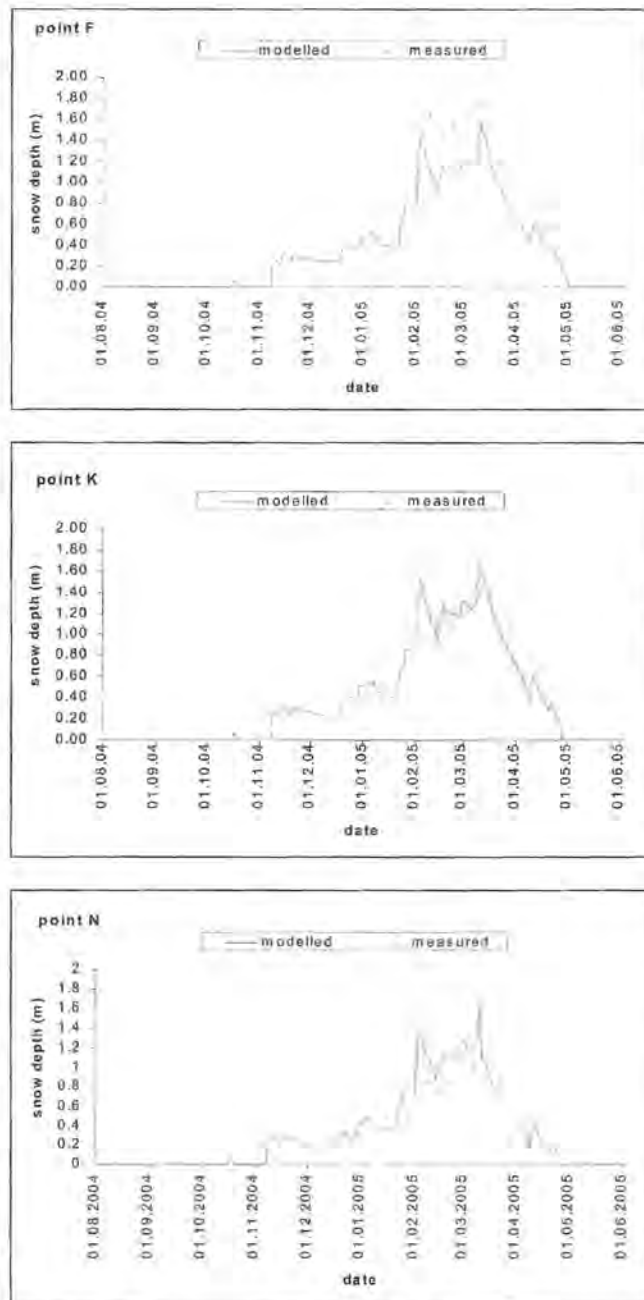


Figure 10: Three representative points at "Kühroint".

vegetation classes and by the usage of the MM5 wind fields. At Kühroint the results do not differ between the used methods (MM5 or interpolated wind fields). This is due to the wind conditions at "Kühroint" in the winter season 2004/05. The mean wind speed was below 1 m/s and only 69 hours with wind speeds of more than 3 m/s were registered, thus we could assume low snow transport rates. Hence it is a satisfying result that Snowtran3D is not generating higher transport rates under usage of the MM5 wind fields because this would indicate a systematic misinterpretation of the local situation at Kühroint.

The minor differences between the two methods at both sites are in line with the expectations according to BERNHARDT et al. (2007). They have found that the MM5 and the interpolated wind fields are significantly

different for heights from 1800 m a.s.l. upwards. Nevertheless the coincidence between Snowtran3D results which could be achieved in the direct environment of an anemometer and under usage of interpolated or MM5 wind fields show that MM5 data is applicable. The overall performance of the MM5 approach is mostly similar or better than the performance of Snowtran3D in combination with the interpolation routine. As the accuracy of the presented approach is not dependent on the general location of the observed area, it could be a helpful alternative for alpine environments, independent if they are well, bad or not equipped.

### Acknowledgements

The authors want to thank the National Park authority for providing the GIS information and the meteorological data, as well as the Bavarian Avalanche Warning Service, for meteorological data. A special thank goes to the National Park rangers, who accomplished the snow

depth measurements; the latter encouragement of the rangers can not be acknowledged high enough (fig. 11).

### References:

- BALK, B. AND ELDER K. (2000): Combining binary decision tree and geostatistical methods to estimate snow distribution in a mountain watershed. *Water Resources Research*, 36, 13-26.
- BARRY, R.G. (1992): *Mountain Weather and Climate*. Routledge, Taylor & Francis Books Ltd.
- BERNHARDT, M., STRASSER, U., ZÄNGL, G. AND MAUSER, W. (2005): Using MM5-derived wind fields for the modelling of snow transport processes. In: *Abstracts of the 3rd Symposium for Research in Protected Areas*.
- BERNHARDT, M., ZÄNGL, G., LISTON, G.E., STRASSER, U. AND MAUSER, W. (2007): Using wind fields from a high resolution atmospheric model for simulating snow dynamics in mountainous terrain. *Hydrological Processes* (accepted).



**Figure 11:** Field work (Wolfgang Palzer, Josef Egger, Matthias Bernhardt, Helmut Franz, Picture: Ulrich Strasser).

- BOWLING, L.C., POMEROY, J.W. AND LETTENMAIER, D.P. (2004): Parameterization of Blowing-Snow Sublimation in a Macroscale Hydrology Model. *Journal of Hydrometeorology*, 5, p 745-762.
- BRULAND, O., LISTON, G.E., VONK, J., SAND, K. AND KILLINGTVEIT, A. (2004): Modelling the snow distribution at two high arctic sites at Svalbard, Norway, and at an Alpine site in central Norway. *Nordic Hydrology*, 35, 191-208.
- DÉRY, S.J. AND YAU, M.K. (1999): A Bulk Blowing Snow Model. *Boundary Layer Meteorology*, 93 Issue 2, p 237-251.
- DOESKEN, N.J. AND Judson, A. (1996): *The Snow Booklet: A guide to the science, climatology, and measurement of snow in the United States*. Colorado State University, Fort Collins, CO.
- DOORSCHOT, J. (2002): Mass transport of drifting snow in high alpine environments. <http://e-collection.ethbib.ethz.ch/show?type=diss&nr=14515>
- EIDSVIK, K.J., HOLSTAD, A., LIE, I. AND UTNES, T. (2004): A Prediction System for Local Wind Variations in Mountainous Terrain. *Boundary-Layer Meteorology*, 112 Issue 3, p557-586.
- ESSERY, R.L.H., LI, L. AND POMEROY, J.W. (1999): A Distributed Model of Blowing Snow over Complex Terrain. *Hydrol. Process.*, 13, 2423-2438.
- ESSERY, R.L.H. (2001): Spatial statistics of windflow and blowing-snow fluxes over complex terrain. *Boundary-Layer Meteorology*, 100, 131-147.
- GREENE, E.M., LISTON, G.E. AND PIELKE, R.A. (1999): Simulation of above treeline snowdrift formation using a numerical snow-transport model. *Cold Regions Science and Technology*, 30, 135-144.
- GRELL, G.A., DUDHIA, J. AND STAUFFER, D.R. (1995): A description of the fifth generation Penn State/NCAR mesoscale model (MM5). Technical report, National Centre for Atmospheric Research, Boulder, Colorado, USA.
- HASHOLT, B., LISTON, G.E. AND KNUDSEN, N.T. (2003): Snow-distribution modelling in the Ammassalik region, south east Greenland. *Nordic Hydrology*, 34, 1-16.
- HIEMSTRA, C.A.A., LISTON, G.E. AND REINERS, W.A. (2002): Snow redistribution by wind and interactions with vegetation at upper treeline in the Medicine Bow Mountains, Wyoming, USA. *Arctic Antarctic and Alpine Research*, 34, 262-273.
- HIEMSTRA, C.A., LISTON, G.E. AND REINERS, W.A. (2006): Observing, modelling, and validating snow redistribution by wind in a Wyoming upper treeline landscape. *Ecological Modelling*, in press.
- HOOD, E., WILLIAMS, M. AND DCLINE, D. (1999): Sublimation from a seasonal snowpack at a continental, mid-latitude alpine site. *Hydrol. Process.*, 13, 1781-1797.
- LEHNING, M., DOORSCHOT, J., RADERSCHALL, N., BARTELT, P. (2000): Combining snow drift and SNOWPACK models to estimate snow loading in avalanche slopes. *Snow Engineering*, 113-122.
- LEHNING, M., VÖLKSCH, I., GUSTAFSSON, D., NGUYEN, T.A., STÄHLI, M. AND ZAPPA, M. (2006): ALPINE3D: A detailed model of mountain surface processes and its application to snow hydrology. *Hydrological Processes*, in press.
- LISTON, G.E. (1995): Local Advection of Momentum, Heat, and Moisture during the Melt of Patchy Snow Covers. *Journal of Applied Meteorology*, 34, 1705-1715.
- LISTON, G.E. AND STURM, M. (1998): A snow-transport model for complex terrain. *Journal of Glaciology*, 44, 498-516.
- LISTON, G.E., WINTHER J.G., BRULAND, O., ELVEHOY, H., SAND, K. AND KARLOF, L. (2000): Snow and blue-ice distribution patterns on the coastal Antarctic Ice Sheet. *Antarctic Science*, 12, 69-79.
- LISTON, G.E. AND STURM, M. (2002): Winter Precipitation Patterns in Arctic Alaska Determined from a Blowing-Snow Model and Snow-Depth Observations. *Journal of Hydrometeorology*, 3, 646-659.
- LISTON, G.E. (2004): Representing Subgrid Snow Cover Heterogeneities in Regional and Global Models. *Journal of Climate*, 17, 1381-1397.
- LISTON, G.E. AND ELDER, K. (2006): A distributed snow-evolution modeling system (SnowModel). *Journal of Hydrometeorology*, 7, 1259-1276
- PRASAD, R., TARBOTON, D.G., LISTON, G.E., LUCE, C.H. AND SEYFRIED, M.S. (2001): Testing a blowing snow model against distributed snow measurements at Upper Sheep Creek, Idaho, United States of America. *Water Resources Research*, 37, 1341-1356.
- POMEROY, J.W., GRAY, D.M. AND LANDINE, P.G. (1993): The Prairie Blowing Snow Model - characteristics, validation, operation. *Journal of Hydrology*, 144, 165-192.
- RYAN, B.C. (1977): A mathematical model for diagnosis and prediction of surface winds in mountainous terrain. *Journal of Applied Meteorology*, 16, 571-584.
- WINSTRAL, A. AND MARKS, D. (2002): Simulating wind fields and snow redistribution using terrain-based parameters to model snow accumulation and melt over a semi-arid mountain catchment. *Hydrological Processes*, 16, 3585-3603.
- ZANGL, G. (2002): An Improved Method for Computing Horizontal Diffusion in a Sigma-Coordinate Model and Its Application to Simulations over Mountainous Topography. *Monthly Weather Review*, 130, 1423-1432.
- ZANGL, G. (2003): Orographic Gravity Waves Close to the Nonhydrostatic Limit of Vertical Propagation. *Journal of the Atmospheric Sciences*, 60, 2045-2063.

## 4 Snow variability and change in Romania

ROXANA BOJARIU<sup>1</sup> AND MIHAELA DINU<sup>2</sup>

<sup>1</sup> National Meteorological Administration, Sos. Bucuresti-Ploiesti 97, 013686 Bucharest, Romania

<sup>2</sup> Romanian American University, Bucharest, Romania

### 1. Introduction

Snow cover is considered to be a useful indicator of climate change because of its sensitivity to temperature (KARL et al. 1993, GROISMAN et al. 1994). The presence of snow cover affects the planetary albedo and has been shown to exhibit a close negative relationship with hemispheric air temperature over the period of relative homogenous satellite data (ROBINSON et al., 1993). This relationship is consistent with a positive snow-albedo feedback mechanism. The importance of snow cover as an indicator of change was highlighted in a number of papers. MYENI et al. (1997) documented an increase in the active growing season of plants across much of the Northern Hemisphere high latitudes from 1981 to 1991. This change was attributed to the earlier disappearance of spring snow cover which appears to be part of a recent trend toward enhanced warming of spring temperatures and earlier disappearance of spring snow and ice cover over much of North America and Eurasia (BROWN AND GOODISON 1996, DYE 2000).

As for the linkage with large scale circulation pattern, a number of recent studies show that positive-anomalous snow cover in late autumn and winter over Eurasia, and especially over Siberia, is associated with a negative North Atlantic Oscillation (NAO) phase (COHEN AND ENT-KHABI 1999, GONG et al. 2003). Two out-of-phase relationships between the NAO and Eurasian snow-cover extent are documented: a quasi-simultaneous connection (from January to March) and a lagged one (from April to October) (BOJARIU AND GIMENO 2003, SAITO AND COHEN 2003, SAUNDERS et al. 2003). The simultaneous correlation between positive (negative) NAO and negative (positive) snow cover extent anomalies is mostly due to the warm (cold) thermal advection over the continental area in mid and late winter but a positive feedback is also revealed in modeling studies with prescribed snow cover anomalies (WATANABE AND NITTA 1998).

On regional scales, the snow cover strongly impacts climate fluctuations due to feedbacks generated through its influence on surface energy and moisture fluxes, clouds, and precipitation (YASUNARI et al. 1991). The main goal of this paper is to investigate the snow fluctuations over the Romanian regions, where the complex topographical constraints may play an important role on the local response to both large scale natural variability and global warming.

### Data and analysis

The primary dataset used here consists of monthly means of snow depth sum from 94 Romanian meteorologi-

cal stations (from which 26 stations are situated at altitudes higher than 500 m) spanning the time interval from November 1961 to December 2000. Monthly geopotential heights at 500 hPa level over the Northern Hemisphere are extracted from the NCEP/NCAR reanalysis (KALNAY et al. 1996). The NCEP/NCAR reanalysis uses a global data assimilation system which is kept unchanged and their data base has been enhanced with ship, rawinsonde, aircraft and satellite data. In addition we also use monthly temperature and precipitation from 94 Romanian stations for the cold season (November to March) in the analyzed interval (1961-2000).

Best-fit linear trends and non-parametric Mann-Kendall rank statistics ( $\tau$ ) (MANN 1945, KENDALL 1970, SNEYERS 1990) are used to analyse the regional variability of snow depth sum, temperature, and precipitation. The Canonical Correlation Analysis (CCA) is applied to the Northern Hemisphere geopotential heights at 500 hPa level and snow depth sum over Romania to identify large scale mechanisms responsible for the snow fluctuations. The CCA selects a pair of spatial patterns of two variables such that their time evolution is optimally correlated (PREISENDORFER 1988, BRETHERTON 1992, VON STORCH 1995). Before canonical correlation analysis, the original data are usually projected onto their Empirical Orthogonal Functions (EOFs), retaining only a limited number of them in order to minimize the noise. The CCA patterns are normalized such as the coefficients have standard deviation units, so the patterns represent typical anomalies in their specific units. The CCA time evolutions of snow depth sum are compared with a NAO index taken from the Climate Prediction Center (CPC, USA) ([ftp://ftp.cpc.ncep.noaa.gov/wd52dg/data/indices/tele\\_index.nh](ftp://ftp.cpc.ncep.noaa.gov/wd52dg/data/indices/tele_index.nh)).

### 2. Results

Downward trends in the sum of snow depth were identified for the entire cold season (November to March) in northern western and central Romanian regions, while other areas from southern part of the country and Southern Carpathians show positive trends. However, the ( $\tau$ ) values of the Mann-Kendall test show significant downward trends at confidence levels higher than 90% only in north-eastern and western Romanian regions. Also, significant upward trends are present in limited areas in the southern and center parts of Romania. The mixed signals revealed by snow depth variability over Romanian regions pose the question of an intra-seasonal structure in the climate data, masked by the November to March averaging. Many papers have documented such type of structures. For instance, FREI et al. (1999) identified a shift in the snow seasons which begin earlier and end sooner over North America. Further evidence for this shift was documented in an analysis of Canadian annual snow cover statistics that revealed widespread significant trends toward earlier dates of maximum snow depth and earlier disappearance of snow over the period 1955-97. BROWN (2000) noted that monthly temperature trends for both Western Eurasia and North

America show that the strongest warming during the snow season has occurred in February and March, consistent with snow cover feedback information generated by GROISMAN et al. (1994) for the mid-latitude regions.

To investigate this intraseasonal feature, the cold season was split in two parts: early winter (November to December) and mid-late winter (January to March). Over Romanian territory, linear trend assessment and Mann-Kendall statistics show significant differences in the variability of snow depth sum in the first and second part of the cold season (figure 1). The downward trends in snow depth sums are extensively present in the mid and late winter, while upward trends characterize the early winter. These trends can mainly be attributed to temperature trends. The upward trends in snow depths are consistent with a downward trend signal in early winter temperatures over Romania (figure 2b). As for decreasing snow depths in the mid-late winter, they are associated with upward thermal trends and downward precipitation trends over a large part of the country (figure 2a). It is interesting to note that the spatial patterns of changes in precipitation are similar for both early and mid-late winter, although the January to March trends are more pronounced and statistically significant over larger areas. The trends and non-parametric Mann-Kendall rank statistics ( $\tau$ ) derived from the 94 stations were interpolated onto a 0.5 degree longitude-latitude grid by applying a Cressman procedure (CRESSMAN 1959). Note that the observing stations cover only the Romanian territory and features outside the Romanian borders are due to the spatial interpolation procedure.

The mid-late winter signal in snow depths over Romania seems to be a regional manifestation of a larger scale phenomenon. To investigate this further, the CCA is applied to the pair consisting of Northern Hemisphere geopotential height at 500 hPa and snow depth sum over Romania. Prior to the analysis, the geopotential and snow data have been standardized. The spatial patterns of first CCA mode are presented in figure 3. The first 5 EOFs of geopotential height and snow depth sum have been retained for the CCA. The correlation coefficient associated with the first CCA mode is 0.71 and the fraction of total variance represented is 11% for the geopotential height and 35% for snow depth sum. Again, the local spatial coefficients derived from the 94 stations were interpolated onto a 0.5 degree longitude-latitude grid by applying a Cressman procedure and features outside the Romanian borders are due to the spatial interpolation procedure. The enhancement of mid-tropospheric zonal circulation over Central and Northern Europe determines snow depth reduction over almost all Romanian regions. The time evolution of first CCA mode and a JFM NAO index are illustrated in figure 4. The correlation coefficient between CCA time series and NAO index is 0.66. Both time series show trends significant at confidence levels greater than 95%.

The snow depth reduction due to changes in large scale circulation is modulated by the presence of Carpathian Mountains which represent an element of roughness for

the atmospheric flow, acting as a complex barrier in the lower troposphere. The Carpathian chain stretches between 45°N and 50°N, sheltering inside the Hungarian Plain and the Somes-Transylvanian Plateau. The chain's total length is 600 km and covers a total area of 170.000 km<sup>2</sup>. The south-eastern part of Carpathians situated on the Romanian territory has a double-bent shape and are generally higher than the North Western and Middle Carpathians. Romanian Carpathians cover an area of 66 700 km<sup>2</sup> which represents 27.8% of Romanian territory. The uplift across the Carpathian slopes substantially modulates the precipitation and snow patterns over the region (ION-BORDEI 1988). The contrasting sign of snow depth trends in mid-late winter near the bent of Carpathians may be due to the foehn winds effect melting the snow rapidly on the leeward side of the mountains under westerly and north westerly atmospheric circulation conditions (see figure 1 a). Also, the temperature patterns due to the thermal advection are modified by the topographic forcing imposed on the lower tropospheric flow by the Carpathian Mountains (ION BORDEI 1988, BOJARIU AND PALIU 2001). The manifestation of this forcing is revealed by the presence of a stronger center of variability to the east of the Carpathian Massif, which is more intense due to the greater roughness of the eastern Carpathians (see figure 2a).

As for the snow depths at higher altitudes, only 5 stations from the analyzed 26 mountain locations show statistically significant trends. The downward trends in snow depths are statistically significant at confidence levels greater than 90% in the case of two stations situated in the Apuseni Mountains (Baisoara -1385 m and Vladeasa - 1410 m) and one in the north-eastern mountains (Rarau -1572 m). These trends are consistent with upward (downward) trends in temperature (precipitation) and seem to be due to nonlinear response imposed by the topography and other local factors to NAO-type atmospheric circulation. The Apuseni Mountains (Western Carpathians) has been considered a region suitable for winter sports.

However, trend analysis for almost all Romanian areas with ski resorts in the Southern and Eastern Carpathians reveals no changing conditions over the last four decades. Exceptions are Paltinisi (1442 m) and Lacauti (1776 m), even where snow depths have upward trends which are statistically significant at confidence levels greater than 90%. The snow depth variability at Paltinisi and Lacauti show different behaviour in comparison with the rest of the stations due to their specific locations inside the Carpathian arch.

There, the zonal atmospheric flow (positive NAO phase) leads either to more precipitation and snow depths due to the uplift of moist air focused at the inner façade of Carpathians (Lacauti) or to other local unidentified effects (Paltinisi). However, observed snow variability at many mountain stations seems to be decoupled to the NAO-type atmospheric circulations, probably due to the altitude and/or local slope orientation relative to the large scale flow.

### 3. Conclusions

Our results show that over Romania, like over many mid-latitude land areas of Northern Hemisphere, the strongest warming during the snow season and associated downward trend in snow depth are observed in mid-late winter (January to March). Many studies documented that most of the warming related to this changes has occurred over the last half of this century and seems to be associated with large scale circulation patterns such as NAO (e.g. HURRELL 1996). Indeed, our CCA reveal that the diminishing snow depth over Romanian territory is related to the tendency toward the positive phase of NAO. In mid-late winter, snow amounts exhibit significant downward trends in the western, north-eastern and some south-western Romanian regions. So, the tendency of prevailing zonal circulation in mid-late winter (JFM) over the Central Europe can partially explain the snow reduction, especially for the regions situated at low altitude, in extra-Carpathian areas. As for the Romanian mountain regions, the local and regional factors seem to

play a more important role in snow pack variability, in contrast with other mountain regions (e.g. Swiss Alps) (BENISTON 1997) where large-scale forcing plays a dominant role in controlling the timing and amount of snow. The present analysis draw the attention to possible climate-change related impacts on snow in several Romanian regions and hence to the climate-change influences on related socio-economic activities. Numerical experiments with regional climate models have to be used to investigate in more detail the physical mechanisms involved in regional response to present and future global warming.

### Acknowledgements

This work is partially supported by the EU Framework 6 program under contract 003903-GOCE (DYNAMITE). We would like to thank two anonymous reviewers for their helpful comments.

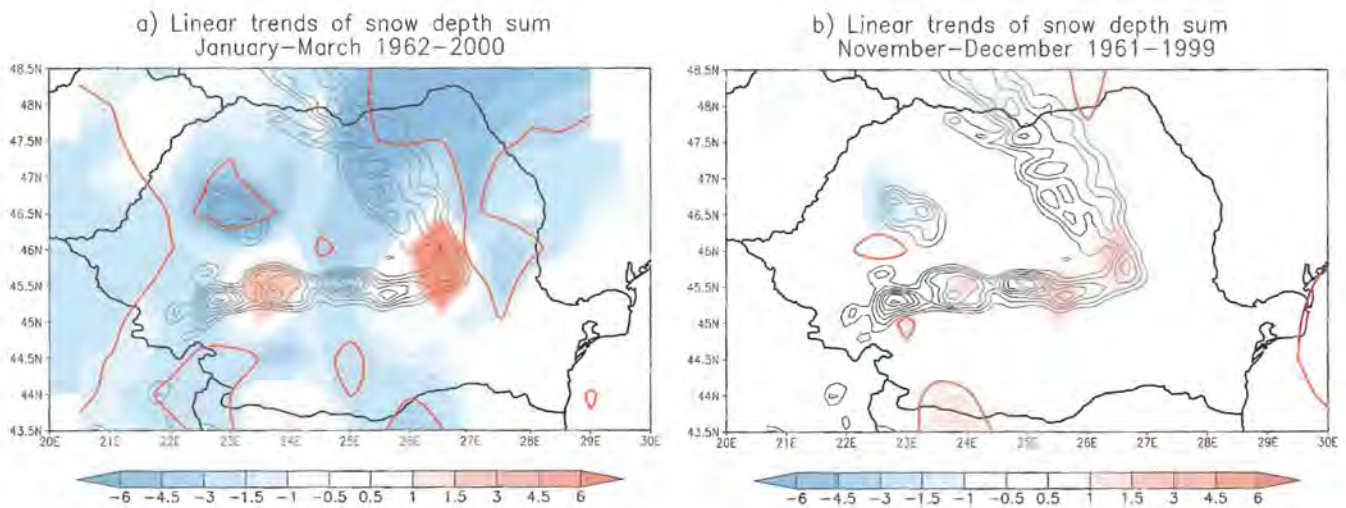


**Figure 1:** Linear trends of snow depth sum (color shaded, in m) for January to March (a) and November to December (b). Red contour lines show border regions with trends statistically significant at confidence levels greater than 90 %.

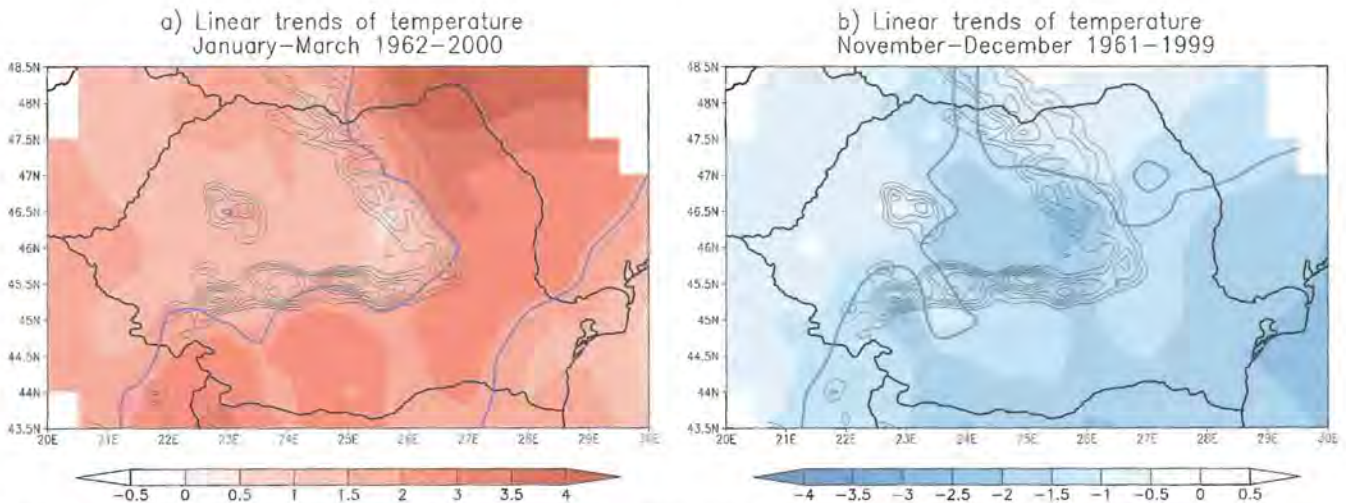


**Figure 2:** Linear trends of temperature sum (color shaded, in °C) for January to March (a) and November to December (b). Blue contour lines show border regions with trends statistically significant at confidence levels greater than 90 %.

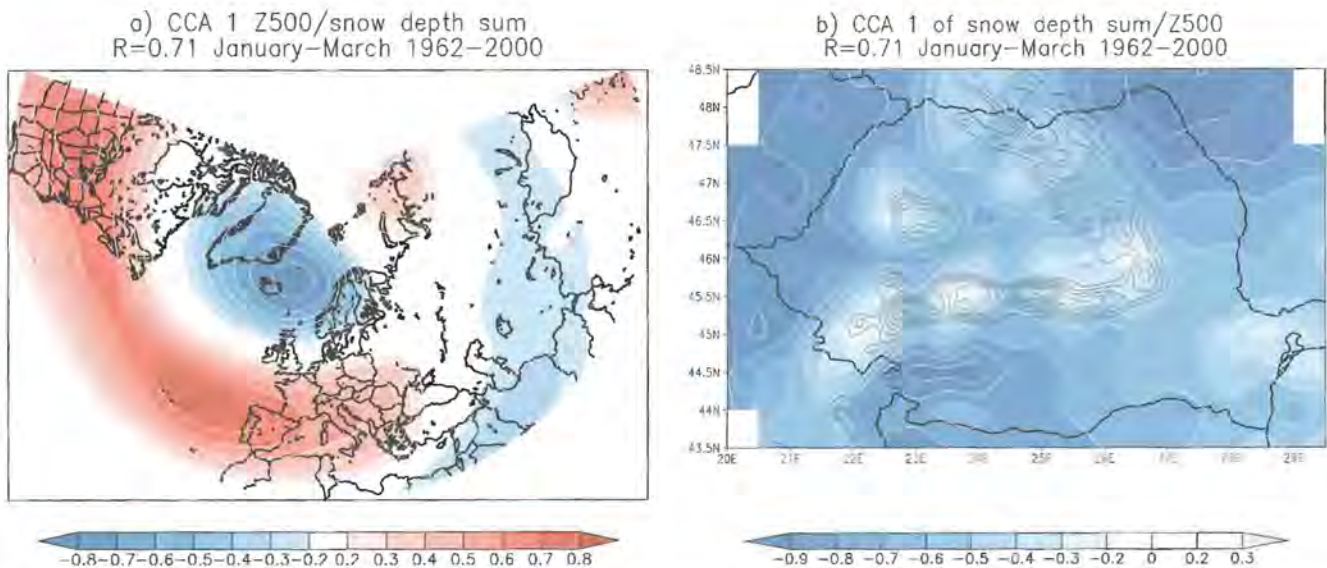


**Figure 3:** Spatial patterns of 1st CCA mode for geopotential height at 500 hPa (a) and snow depth sum (b). The input data were standardized, so the spatial coefficients are in standard deviation units.

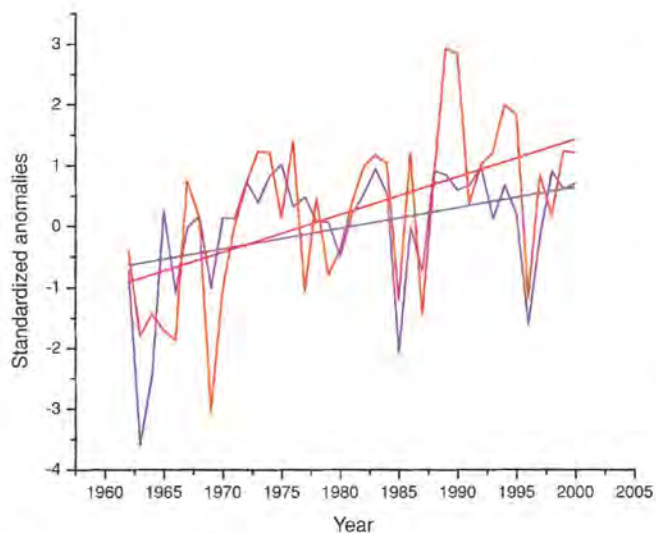


**Figure 4:** Time evolution of 1st CCA mode illustrated in figure 3 and its associated linear trend (blue lines) and NAO index and its associated trend (red lines) for the time interval January-March 1962-2000.

## References

- BENISTON, M. (1997): Variations of snow depth and duration in the Swiss Alps over the last 50 years: links to changes in large-scale climatic forcings. *Climatic Change*, 36(3-4), 281-300.
- BRETHERTON, C.S., AND WALLACE, J.M. (1992): An intercomparison methods for finding coupled patterns in climate data. *J. Climate*, 5, 541-560.
- BOJARIU, R., GIMENO, L. (2003): The influence of snow cover fluctuations on multiannual NAO persistence. *Geophysical Research Letters*, 30(4), 1156, doi:10.1029/2002GL015651.
- BOJARIU, R. AND PALIU, D. (2001): North Atlantic Oscillation projection on Romanian climate fluctuations in the cold season. *Detecting and Modelling Regional Climate Change and Associated Impacts*, M. Brunet and D. Lopez Eds., Springer-Verlag Berlin-Heidelberg, 345-356.
- BROWN, R.D. (2000): Northern Hemisphere snow cover variability and change 1915-97. *J. Clim.*, 13, 2339-2355
- BROWN, R.D. AND GOODISON, B.E. (1996): Interannual variability in reconstructed Canadian snow cover, 1915-1992. *J. Clim.*, 9, 1299-1318.
- COHEN, J. AND ENTEKHABI, D. (1999): Eurasian snow cover variability and Northern Hemisphere climate predictability. *Geophys. Res. Lett.*, 26, 345-348.
- CRESSMAN, G.P. 1959. An operational objective analysis system. *Mon. Wea. Rev.*, 87:367-374.
- DYE, D.G. (2000): Variability and trends in the annual snow-cover cycle in Northern Hemisphere land areas, 1972-2000. *Hydrological Processes*, 16(15), 3065-3077.
- FREI, A., ROBINSON, D.A. AND HUGHES, M.G. (1999): North American snow extent: 1900-1994. *International Journal of Climatology*, Volume 19, Issue 14, Pages 1517-1534.
- GONG, G., ENTEKHABI, D., COHEN, J. (2003): Modeled Northern Hemisphere Climate Response to Realistic Siberian Snow Anomalies. *J. Climate*, 16, 3917-3931.
- GROISMAN, P.YA, KARL, T.R. AND KNIGHT, R.W. (1994): Observed impact of snow cover on the heat balance and the rise of continental spring temperatures. *Science*, 263, 198-200.
- HURRELL, J.W. (1996): Influence of variations in extratropical wintertime teleconnections on Northern Hemisphere temperatures. *Geophysical Research Letters*, 23, 665-668.
- ION-BORDEI, N. (1988): *Meteclimatic phenomena induced by the Carpathian configuration in the Romanian Plain*. Ed. Academiei, Bucharest, 174 pp (in Romanian with abstract in English).

- KENDALL, M. (1970): Rank correlation methods. Griffin, London, 4 edn., 258 pp.
- KALNAY, E., KANAMITSU, M., KISTLER, R., COLLINS, W., DEAVEN, D., GANDIN, L., IREDELL, M., SAHA, S., WHITE, G., WOOLLEN, J., ZHU, Y., CHELLIAH, M., EBSUZAKI, W., HIGGINS, W., JANOWIAK, J., MO, K.C., ROPELEWSKI, C., WANG, J., LEETMA, A., REYNOLDS, R., JENNE, R. AND JOSEPH, D. (1996): The NCEP/NCAR 40-year reanalysis project, *Bull. Amer. Meteor. Soc.*, 77, 437-470.
- KARL, T.R., GROISMAN, P.YA., KNIGHT, R.W. AND HEIM JR, R.R. (1993): Recent variations of snow cover and snowfall in North America and their relation to precipitation and temperature variations. *J. Clim.*, 6, 1327-1344.
- MANN, H. (1945): Nonparametric test against trends. *Econometrica*, 13, 245-259.
- MYENI, R.B., KEELING, C.D., TUCKER, C.J., ASRAR, G. AND NEUMAN, R.R. (1997): Increased plant growth in northern high latitudes from 1981 - 1991. *Nature*, 386(6626): 698-701.
- PREISENDORFER, R.W. (1988): *Principal component analysis in Meteorology and Oceanography*. Elsevier. 425 pp.
- ROBINSON, D.A., DEWEY, K.E. AND HEIM, R.R. (1993): Global snow cover monitoring: An update. *Bull. Am. Meteorol. Soc.*, 74, 1689-1696.
- SAITO, K. AND COHEN, J. (2003): The potential role of snow cover in forcing interannual variability of the major Northern Hemisphere mode. *Geophys. Res. Lett.*, 30(6), 1302, doi:10.1029/2002GL016341.
- SAUNDERS, M.A., QUIAN, B. AND LLOYD-HUGHES, B. (2003): Summer snow extent heralding of the winter North Atlantic Oscillation. *Geophys. Res. Lett.*, 30(7), 1378, doi:10.1029/2002GL016832.
- SNEYERS, R. (1990): *On the Statistical Analysis of Series of Observations*, W.M.O. Technical Note 143, 6-15.
- VON STORCH, H. (1995): Spatial patterns: EOFs and CCA. In: VON STORCH, H. AND NAVARRA A. (eds): *Analysis of climate variability: applications of statistical techniques*, Springer, 227-258.
- WATANABE, M. AND NITTA, T. (1998): Relative impact of snow and sea surface temperature anomalies on an extreme phase in the winter atmospheric circulation. *Journal of Climate*, 11, 2837-2857.
- YASUNARI, T., KITOH, A. AND TOKIOKA, T. (1991): Local and Remote Responses to Excessive Snow Mass over Eurasia Appearing in the Northern Spring and Summer Climate. *J. Meteor. Soc. Japan*, 69, 473-487.

## 5 Evaluation of snowmelt from modis images

ANGELO COLOMBI<sup>1</sup>, ANNA RAMPINI<sup>1</sup>,  
FRANCESCO ROTA NODARI<sup>2</sup>

<sup>1</sup> IREA-CNR Institute for Elektromagnetic Sensing of the Environment-National Research Council, Via Bassini 15, 20133, Milano, Italy

<sup>2</sup> Remote Sensing Data Engineering (RSDE), Via Washington 78, 20146 Milano, Italy

### Abstract

This work is aimed at simulating the snowmelt in an Alpine watershed and at modelling the discharge in a certain section of the river. To evaluate snowmelt at regional scale, ground data collected by weather stations are not enough and should be integrated with remotely sensed data. Remote sensing, in fact, allows the monitoring of the whole Earth surface by providing spatialized information. Snowmelt Runoff Model (SRM), developed by MARTINEC et al. (1994), was selected for the analysis. This model estimates the snow melting phenomenon by a simple degree-day approach, in which air temperature is considered the only variable affecting the process. Then, in order to spatialize the analysis, SRM requires, as input, the estimation of the snow covered catchment area during the snowmelt season. For this specific goal, satellite images with medium/coarse resolution were considered the most useful, since they provide daily information about the same area. To evaluate the snow coverage, MODIS (*MODerate-resolution Imaging Spectroradiometer*) sensor onboard the EOS TERRA platform was selected. The obtained results of SRM calibration showed high values for all the accuracy coefficients (correlation coefficient  $r$ , Nash-Sutcliffe coefficient  $R^2$ , deviation of volume DV), achieved by obtaining calibrated values of model parameters that agree with literature values and historical analyses. Moreover, the use of MODIS images (250 meter spatial resolution), together with the un-mixing classification methodology, produced an improvement in the snow cover maps, with respect to other available sensors such as NOAA-AVHRR (1 km spatial resolution) and to other typical MODIS hard classifications at 500 meters of spatial resolution.

### 1. Introduction

The simulation of the river discharge is a basic step for a correct use of the available water, e.g. for the hydropower production and the irrigation, and act as help to announce and prevent flood risks. The snowmelt is the main process affecting the river discharge for those mountain watersheds characterized by high altitudes. In fact, during the snowmelt season, the discharge observed in a river is a direct consequence not only of the rainfall within the basin, but above all of the snowmelt. The purpose of this study is the assimilation of remotely sensed data within a snowmelt hydrological model. This

kind of observation provides spatially distributed information about all Earth surface and therefore their integration with punctual ground data collected by weather stations turns out to be very useful. In this study MODIS images were analysed. This sensor, onboard EOS TERRA NASA's platform, provides daily information in 36 different spectral bands, at a spatial resolution variable from 250 meters to 1 km, according to the different spectral channels. Moreover, the choice of such a satellite with medium/coarse resolution is a direct consequence of the daily step required for the hydrological modelling. SRM (Snowmelt Runoff Model, MARTINEC et al. 1994) was selected in order to simulate river discharge. It simulates in a semi-distributed - by sub-dividing the watershed into elevation zones - and conceptual way - temperature index approach - the physical phenomena. The choice of this model, after an accurate evaluation of the available ones (WMO 1986, CUNDERLIK 2003), was led by its capacity of assimilating satellite derived information. This model simulates the river discharge at the watershed scale as a function of daily precipitation and air temperature, derived from ground stations, and the snow covered area retrieved from EO data. Besides, the selection of such a semi-distributed model is the half-measure between lumped models, usually characterized by a scarce accuracy, and the distributed ones that require several data with great spatial resolution, often not available. The selected study area is the upper-Adda sub-basin, located in the Italian Alps. The basin size (506 km<sup>2</sup>, Cepina outlet) and the elevation range (1120-3851 meters) led the choice of the watershed. Since MODIS images are characterized by a moderate spatial resolution, the study area should not be too small, otherwise the snow cover area can't be estimated accurately. Moreover, the high elevations suggest the presence of a huge snow coverage and consequently a great river discharge dependence on the snowmelt.

## 2 Materials and methods

### 2.1 SRM description

SRM was applied to the 2003 snowmelt season, by considering the 1<sup>st</sup> of April as the starting date, as suggested from literature. The simulation of the river discharge was obtained by the following equation (MARTINEC et al. 1994): [1]

$$Q_{n+1} = [c_{in} * DDF_n * (T_n + \Delta T_n) * S_n + c_{rn} * P_n] * (A_n * 10000/86400) * (1 - k_{n+1}) + Q_n * k_{n+1}$$

where

<p>Q = daily mean discharge (m<sup>3</sup>/s)</p> <p>c = runoff coefficient of snow (c<sub>s</sub>) and rain (c<sub>r</sub>)</p> <p>T = number of degree-day (°C * d)</p> <p>ΔT = correction of T in order to extrapolate its value at the hypsometric mean elevation of zone from the station values</p> <p>DDF = degree-day factor (cm*°C<sup>-1</sup>*d<sup>-1</sup>)</p>	<p>S = ratio between snow covered area and whole area</p> <p>A = area (km<sup>2</sup>)</p> <p>P = precipitation (rainfall only, cm)</p> <p>k = recession coefficient</p> <p>n = temporal step (daily)</p> <p>i = elevation zone</p>
--	---

For this work the watershed was sub-divided in the following three elevation zones.

**Table 1:** Watershed subdivision into elevation zones

Zone	Altitude Range (m)	Mean Elevation (m)	Area (km <sup>2</sup> )	Area (% of the basin)
1	1120 - 1900	1594	88	17.4
2	1900 - 2600	2283	228	45.1
3	2600 - 3851	2896	190	37.5

## 2.2 Snow cover classification

The snow cover classification within the basin was performed by analysing MOD09\_L2 daily products. This kind of data, characterized by a spatial resolution of 250 meters, provides information in terms of surface reflectance only about two spectral bands: the first one in the Visible (VIS) region (0.62-0.67  $\mu\text{m}$ ) and the second one in the Near Infra-Red (NIR) region (0.841-0.876  $\mu\text{m}$ ). By analysing the spectral trend of different land covers it can be inferred that snow differs from all the other coverage because of its highest reflectance in both VIS and NIR regions. These two bands allow therefore the mapping of snow cover with the highest available spatial resolution.

The main constraint in using only these two bands is the spectral similarity between snow and clouds, that can be clearly discerned only by analysing Short-Wave Infra-Red (SWIR) and Medium Infra-Red (MIR) channels. In this context a preliminary step of the analysis consisted in the choice of clear sky images. This procedure

was carried out by analysing different MODIS products, containing also SWIR and MIR bands. In particular, MOD02 and MOD09 products are available at a spatial resolution of 500 meters too; with this resolution other 5 spectral channels are investigated, two of them in the SWIR and MIR region.

A typical index used to map snow coverage and above all to discern snow from the clouds is the Normalized Difference Snow Index (NDSI, HALL et al. 1995), based on the different reflectance between snow and clouds in the SWIR region - high reflectance for the clouds and low in the case of snow - and defined by the following equation:

$$\text{NDSI} = (\text{MOD4} - \text{MOD6}) / (\text{MOD4} + \text{MOD6}) \quad [2]$$

where MOD4 is the surface reflectance in the MODIS band 4, in the VIS region (0.54-0.56  $\mu\text{m}$ ), and MOD6 is the surface reflectance in the MODIS band 6, in the SWIR region (1.63-1.65  $\mu\text{m}$ ).

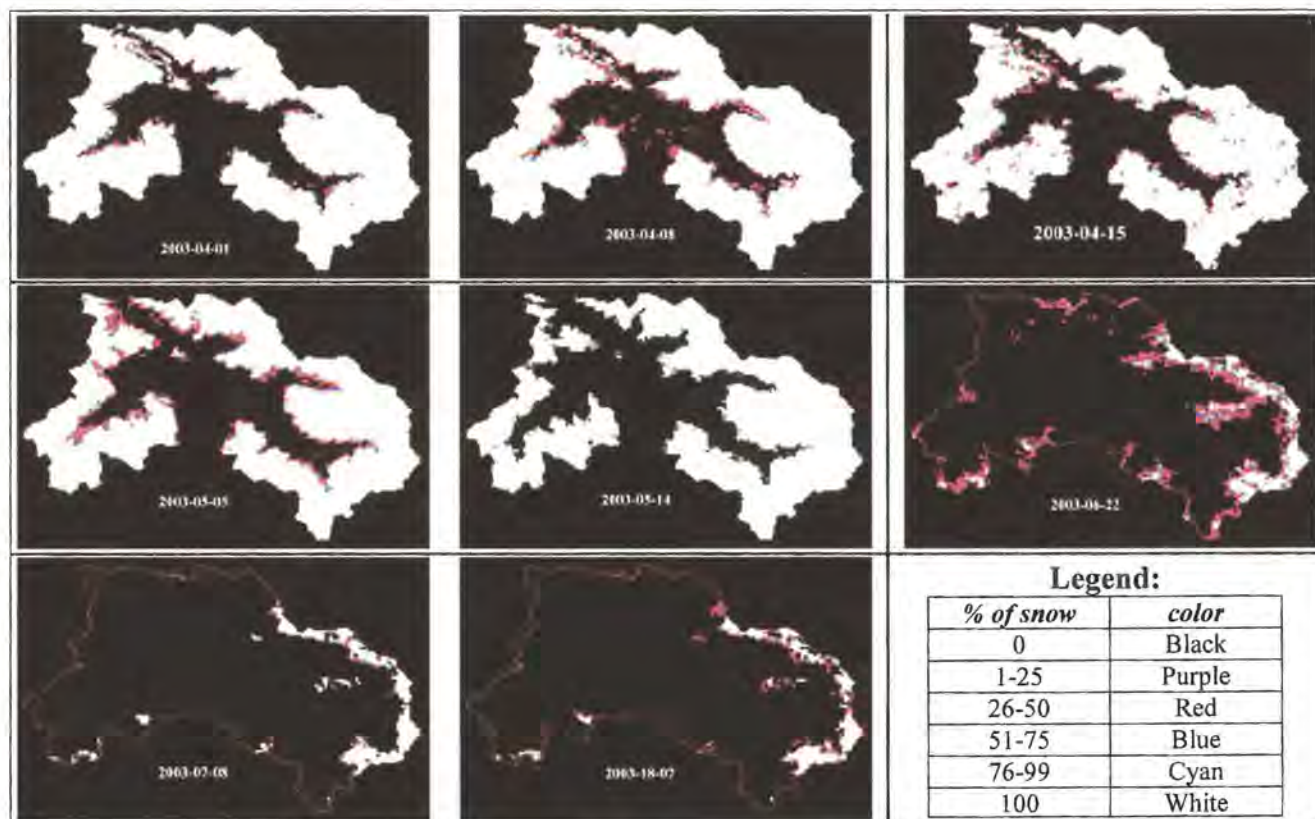


**Figure 1:** Snow coverage within the upper-Adda watershed during the 2003 snowmelt season. Coloured pixels represent pixels partially covered by snow, resulting from the un-mixing classification method.

Once selected clear sky images, the classification of MOD09 at 250 m was performed by using an un-mixing technique: the fuzzy set classification. This method (WANG 1990) doesn't classify pixels with only a membership class of land cover, but a degree of membership – variable between 0 and 1 - is provided for each class (*soft classification*). The main improvement of such a classification method is the possibility of retrieving accurate information about those 'mixed' pixels, not characterized by only one land cover, really frequent near the snowline, because of the moderate spatial resolution of the MODIS pixels. Through this technique, the classification accuracy improves greatly, since every pixel contains values in terms of percentage of snow coverage. Figure 1 shows the decreasing snow covered area within the watershed, during the 2003 snowmelt season, coming from the clear sky classified images.

After having estimated the snow coverage percentage for these dates, a temporal interpolation is necessary in order to obtain the daily input as required by the SRM. This interpolation, performed separately for each elevation zone, was obtained by using different polynomial depletion curves, as shown in figure 2. In the first zone the snow is almost absent since the beginning of the snowmelt season; on the contrary, in the second zone we get a typical depletion trend in which snow coverage decreases from the maximum extent to zero with a second order polynomial curve. Finally, the third zone shows the general dynamic of high altitudes, in which the snow covers all the area and remains constant for several days, followed by a quick decrease, that doesn't complete because of the glaciers presence. These three different dynamics show the difficulty in the definition of snowmelt season and its dependence on the altitude. In this context we decided to analyse the snow cover extent from the 1<sup>st</sup> of April, according to literature.

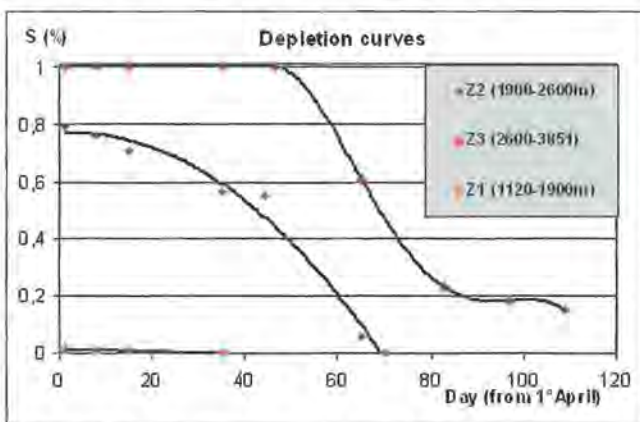


Figure 2: Depletion curves obtained for the three elevation zones.

### 2.3 Evaluation of snowmelt: degree-day approach

Since SRM simulates the snowmelt using a degree-day approach, it is necessary to obtain the air temperature from ground measurements to evaluate the volume of the water from snowmelt for each elevation zone. In fact,

the model simulates the melted snow using the following equation:

$$M = DDF * T \quad [3]$$

where M (cm) is the depth of melted snow, in terms of Snow Water Equivalent (SWE), T is the daily mean air temperature (degree-day) and DDF is the degree-day factor: it represents the snowmelt depth of each degree-day unit. While the evaluation of the air temperature is quite simple, using the temperature lapse rate to estimate the variable at the mean hypsometric altitude of each zone, the degree-day factor must be evaluated by calibration. However, this parameter is not constant during the snowmelt season and it varies as a function of the snow properties, in particular it increases with the snow density (MARTINEC 1960). In this context, a different value of DDF should be evaluated for each month (or twice a month) and zone. In order to estimate its range of variability in the selected study area, ground data from snow gauges and the associated air temperature were used. The analysis regarded historical series from 1992 to 2002.

In particular, from ground measurements, M was calculated using the following equation:

$$M_n = SWE_n - SWE_{n-1} \quad [4]$$

where n indicates the day and SWE was obtained from snow depth and density measurements.

Therefore, DDF was calculated by inverting formula [3], where T values were directly available from ground data measurements. Finally, a range of possible DDF values was retrieved by averaging daily values and by subdividing the analysis taking into account the altitude and the month.

Results showed that from April to June the DDF (cm for each degree-day) generally varies from a minimum of 0,36 to a maximum of 0,57; however for the snow gauges located at the highest altitudes, in June and July the DDF touches and also exceeds 0,6.

### 3 Calibration of the model

Since the selected study area is greatly overworked for hydropower production, the river discharge observed at the watershed outlet can not be compared with the simulated one because it doesn't describe the natural discharge. Therefore, to calibrate the model other information from the hydropower society was necessary. In this context the natural discharge was calculated by taking into account all the water contributes incoming and outcoming the two dams within the watershed (Cancano and San Giacomo) and all data from the electric power stations. Figure 3 shows the observed river discharge and that evaluated by considering all the other contributions: the great difference shows how the elevated anthropic disturbance for hydropower production results in a very low constant discharge.

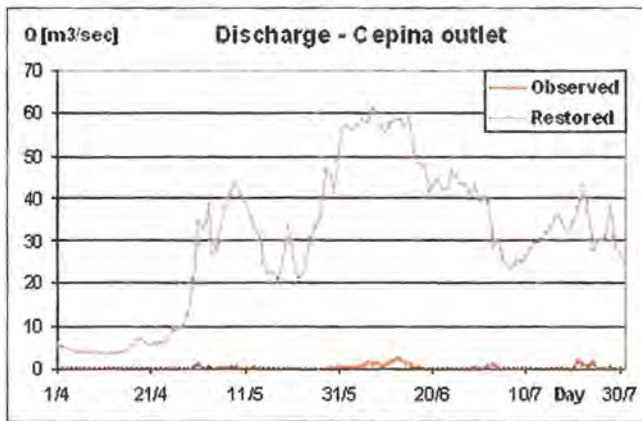


**Figure 3:** Differences between observed and restored discharge at the basin outlet (Cepina).

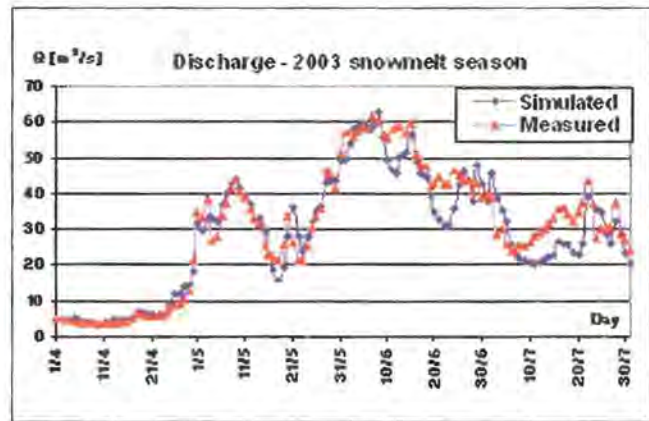


**Figure 4:** Simulated (blue) and measured (red) discharges for the 2003 snowmelt season in the upper-Adda watershed.

Then, we calibrated the model in order to evaluate the right values of the parameters (DDF, runoff coefficient of snow -  $c_s$  - and rain -  $c_r$ ); whereas, the recession coefficient was indirectly estimated on the basis of other watershed values (MARTINEC AND Rango 1986).

The two hydrographs drawn in figure 4 show a good model performance, since the simulated discharge appears very close to the measured one. In particular, to evaluate the model accuracy, three coefficients were calculated, according to the SRM user manual (MARTINEC et al. 1994). The first one was the correlation coefficient ( $r$ ) that indicates if measured and simulated river discharge are correlated; the second is the Nash-Sutcliffe coefficient ( $R^2$ ) that tests the accuracy of the simulated discharge with respect to the measured one; while the last one (DV) tests the accuracy in terms of water vo-

**Table 2:** Model accuracy for the case study

$r$	$R^2$	DV (%)
0.959	0.911	-4.94

lume. Table 2 shows the obtained results of these three indexes.

Finally, Table 3 shows the obtained values of the calibrated DDF values, different for each zone and variable twice a month. These obtained DDF values agree with the estimated range.

With calculated DDF values, it was possible to evaluate the water volume from the snowmelt, for each elevation zone and for each month, and to draw their seasonal graphs (see figure 5 - cumulated and daily).

**Table 3:** Calibrated values of DDF. The variability of this parameter during the snowmelt season was considered by varying it twice a month, according to literature.

	April 1 - 15	April 16 - 30	May 1 - 15	May 16 - 31	June 1 - 15	June 16 - 30	July 1 - 15	July 16 - 30
Z 1	0.5	0.5	-	-				
Z 2	0.5	0.5	0.42	0.45	0.55	-	-	-
Z 3	0.5	0.5	0.35	0.4	0.65	0.7	0.7	0.65

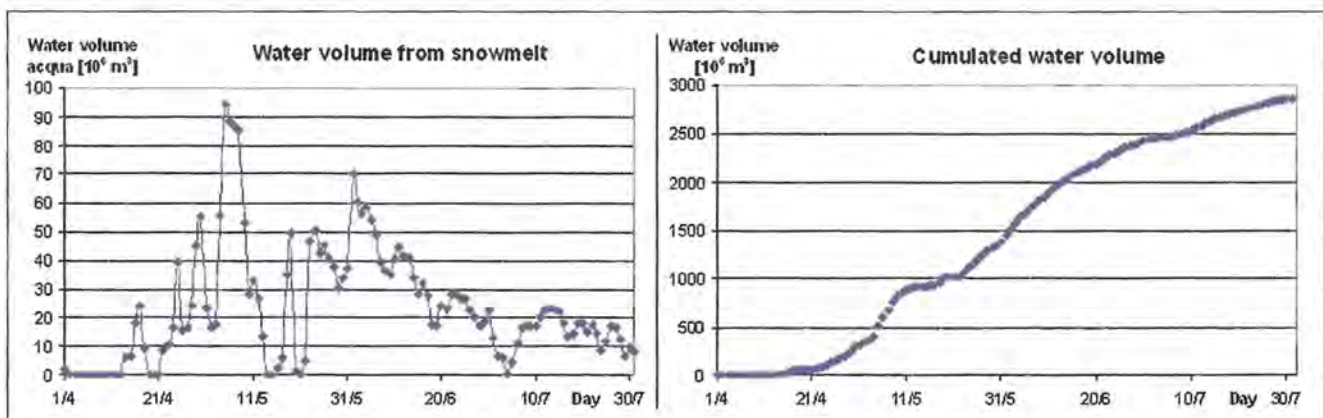


**Figure 5:** Water volume from snowmelt, daily and cumulated.

#### 4. Conclusions

The SRM calibration was very good, since high values for all the accuracy coefficients ( $r$ ,  $R^2$ , DV) were achieved by obtaining calibrated values of model parameters that agree with literature values and historical analyses. This study also demonstrated the importance of snowmelt within the upper-Adda watershed, since local peaks of the discharge values are a direct consequence of the water volume from snowmelt (see figures 4 and 5).

Moreover, the application of the model to such a watershed greatly disturbed by the anthropic modifications doesn't affect the results and didn't represent a constraint, thanks to the restoration of discharge. This is due to the parametric and conceptual approach of SRM too; otherwise, energy balance equations wouldn't have been capable of simulating this disturbance.

Finally, the use of MODIS images, together with the un-mixing classification methodology, represents an improvement in the snow cover map spatial resolution, with respect to other available sensors such as NOAA-AVHRR (1 km spatial resolution) and to other typical MODIS hard classifications at 500 meters of spatial resolution. For further developments, SRM could be improved by introducing other EO data, e.g. the air temperature, since MODIS, for instance, provides 1-km information about the Land Surface Temperature.

#### Acknowledgements

This study was performed in the framework of AWARE (A tool for monitoring and forecasting Available Water Resource in mountain environment) project, a STREP Project in the VI F.P., GMES Initiative.

The authors wish to thank ARPA Lombardia for all the ground data provided from its weather stations, NASA for all the MODIS products and AEM S.p.A. for the restoring of the natural river discharge.

#### References

- CUNDERLIK, J.M. (2003): Hydrologic model selection for the CFCAS project: Assessment of water Resource Risk and Vulnerability to Changing Climatic Conditions. Project Report 1.
- HALL, D.K., RIGGS, G.A., SALOMONSON, V.V. (1995): Development of Methods for Mapping Snow Cover Using Moderate Resolution Imaging Spectroradiometer Data, *Remote Sensing of Environment*, 54:127-140.
- MARTINEC, J. (1960): The degree-day factor for snowmelt runoff forecasting, IUGG General Assembly of Helsinki, IAHS Commission of Surface Waters, IAHS Publ. No. 51, 468-477.
- MARTINEC, J., RANGO, A., ROBERTS, R. (1994): The Snowmelt Runoff Model (SRM) User's Manual (ed. by BAUMGARTNER, M.F.). Geographica Bernensia, P29, Departments of Geography, Univ. of Berne, Berne, Switzerland.
- MARTINEC, J. AND RANGO, A. (1986): Parameter values for snowmelt runoff modelling, *Journal of Hydrology* 84, 197-219.
- Wang F. (1990): Fuzzy Supervised Classification of Remote Sensing Images. *IEEE Transaction on Geoscience and Remote Sensing*, 28: 194-200.
- WMO - WORLD METEOROLOGICAL ORGANIZATION (1986): Inter-comparison of models of snowmelt runoff. Operational Hydrology Report No.23, WMO.

## 6 Heavy Snowfalls and avalanche activity over eastern pyrenees: A study of two extreme cases

PERE ESTEBAN, GLORIA MARTÍ<sup>2</sup>, CARLES GARCIA<sup>2</sup>,  
MONTSE ARAN<sup>2</sup>, JORDI GAVALDÀ<sup>3</sup> & IVAN MONER<sup>3</sup>

<sup>1</sup> CENMA/IEA-Snow and mountain research center, Principality of Andorra

<sup>2</sup> Institut Geològic de Catalunya, Barcelona, Spain

<sup>3</sup> CONSELH GENERAL D' ARAN, Vielha, Spain

### 1. Introduction

Extreme avalanche events occurred in the Alps (VILLECROSE et al. 1999) draw the attention to the importance of the meteorological-related snow patterns from the standpoint of risk, hazard and vulnerability. The present study analyses two important nivometeorological and avalanche patterns that occurred during the winter seasons 2002-2003 and 2005-2006. A detailed description of the episodes is made using atmospheric circulation maps, water-vapour images, radiosonde profiles, among others, in order to distinguish potential meteorological elements that could be the cause of intense avalanche activity in those events.

We consider this type of studies to be useful in two ways: firstly, in the operational mountain weather and avalanche forecasting by making easier the short-term detection of potential elements that could lead to an extreme event. This kind of short-term approach is nowadays largely explored in some mountain regions. How-

ever, it is used to a lesser extent over the Pyrenees (e.g. ESTEBAN et al. 2002) due to the short meteorological series available, although vulnerability in this mountain region has steadily increased together with tourism and associated urbanisation boom. Secondly, the main nivometeorological and/or avalanche patterns can be related to large-scale patterns of atmospheric circulation using downscaling techniques. These relationships could be further used for a long-term assessment of snow-related risk and vulnerability. The cases analysed in this study could be exploit to validate the results of such long-term approaches. In this context, one should recall the existing historical event analyses (e.g. BARRIENDOS et al. 2006) and statistical downscaling studies (e.g. ESTEBAN et al. 2005) for our analyzed area – the Pyrenees.

The Pyrenees are characterized by their southward location in Europe (43°N) and their east-west orientation. Consequently, the influence of water masses such as the Atlantic Ocean and the Mediterranean Sea strongly imprints the annual and interannual climate variability and the two cases analyzed in this study add extra evidence in this context.

### Nivometeorology and avalanche activity over the Pyrennes - an overview

#### Case Study 1: Episode 26-31/01/2003

##### Nivometeorological pattern

This episode began in the time interval 26th-27th of January when the Azores High generated a northerly flow over the Pyrenees pumping Atlantic warm air mass

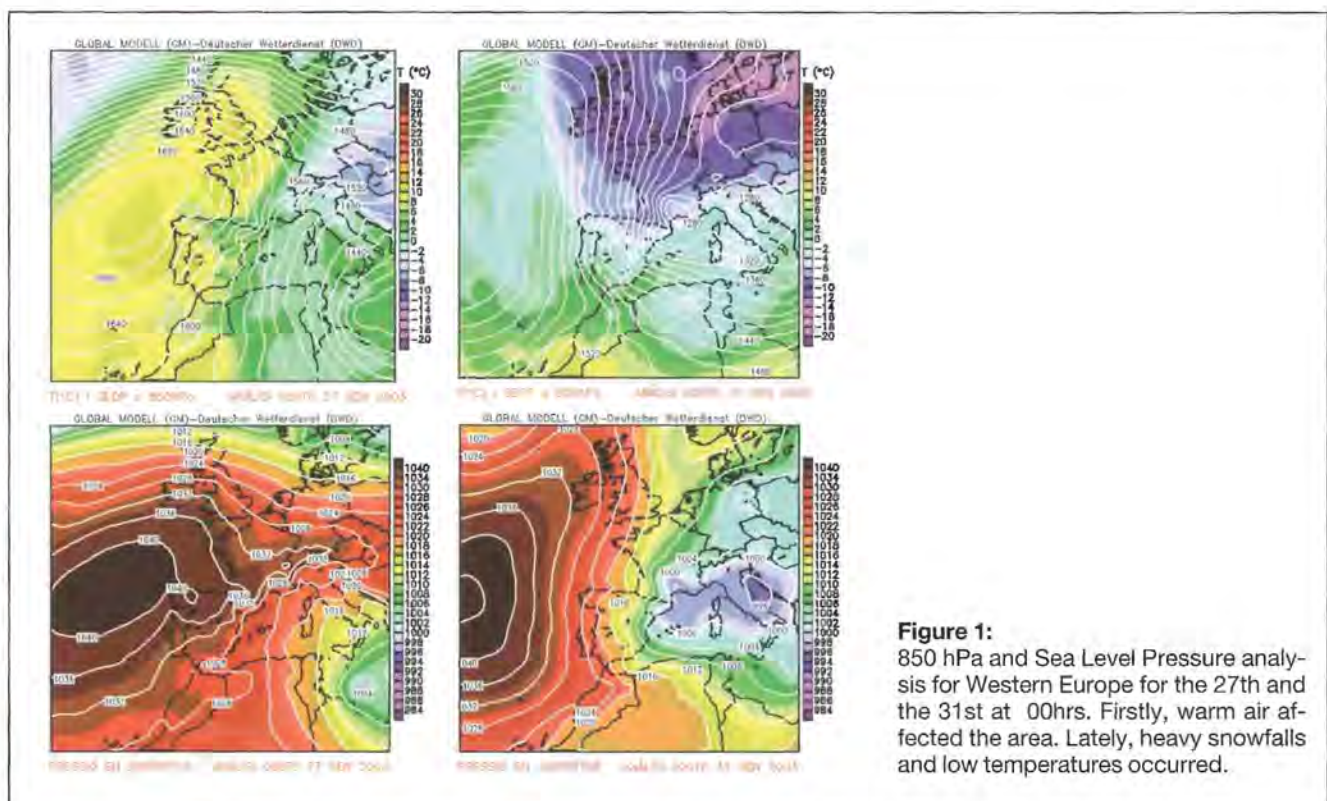


**Figure 1:** 850 hPa and Sea Level Pressure analysis for Western Europe for the 27th and the 31st at 00hrs. Firstly, warm air affected the area. Lately, heavy snowfalls and low temperatures occurred.

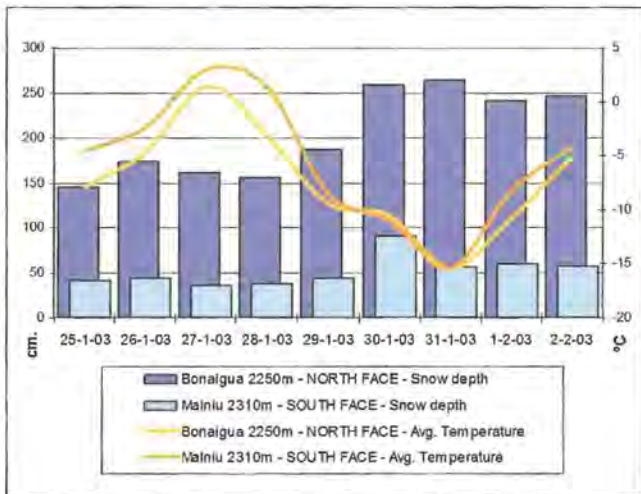


**Figure 2:** Daily average of the snow depth and temperature for the period studied. The high temperatures period is centred on the 27th, and the heavy snowfalls on the 30th of January.

(figure 1). Fresh snow cover having depths between 30 and 70 cm developed over the north face of western side of the area (Val d'Aran), with snow level rising from 1000 to 2200 m and strong northerly winds at high elevations. Temperature began to go down on the 28th of January and did not stop until the end of the episode (see figure 2).

On the 29th of January, a cold front from the northeast intensified the snowfalls (30-60 cm.), but the snow and temperature falls were heavier in the morning of the 31st of January (figure 1). As a result, an average of 1m of fresh snow was accumulated, although it was difficult to accurately measure the data due to the snow drifting at weather stations. During this period, water vapour images show how a cyclonic system crossed rapidly France from northwest to southeast. Between the evening of the 30th and the morning of the 31st (figure 3), this weather system was situated over the eastern part of the Pyrenees with a relative low at surface level and a well located jet-stream. According to this, we consider the

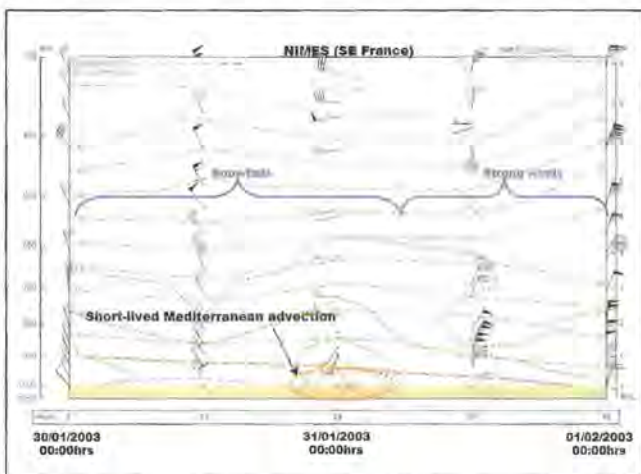


**Figure 4:** Radiosonde profiles for Nîmes from 00UTC of the 29th of January to 0 UTC of the 1st of February. The change of the wind direction at low levels, related to the vortex at higher levels, favours a weak Mediterranean air advection over this area of the French coast.



**Figure 3:** Water vapour image at 23:30 UTC of the 30th. We can observe a vortex located just northerly the Catalan Pyrenees and the jet-stream south-westerly the massif.

possibility of a short-lived advection near surface when this low was close to the Mediterranean Sea, which might increase the humidity supply. In this context it's noteworthy that the radiosonde profile at Nîmes (figure 4) showed a change of the wind direction at low levels and an increase of the mixing ratio.

This heavy snowfall also over passed the massif, and affects low altitudes of the southern side. At 2200m, minimum temperatures were about  $-15^{\circ}\text{C}$ , and maximum values  $-9^{\circ}\text{C}$ . On the 31st the snowfalls stopped, simultaneously with the occurrence of extremely low temperatures and very strong winds (up to around 90 km/h). The total amount of snow accumulations corresponds to a return period of 30 years drawing the attention to the severity of the event.

#### Avalanche activity

Just after the snowfalls an intense avalanche activity occurred in the Val d'Aran where the total amount of snow accumulated was more than 2 m at 2200 m altitude, in part due to the drifting by northerly and northwesterly winds in lee slopes. During this avalanche episode, 39 major avalanches occurred. Both air blast and dense part of these avalanches reached populated areas damaging buildings and collapsing infrastructures and avalanche defense structures. One of the most relevant avalanches fell on the 31st January reaching the urbanised area named La Pleta (1500 m altitude), which became the track zone of the event. The snow profile of the day after showed at the top three well differentiated parts of the recent snow (figure 5): 1) at the top, drifted snow in lee slopes deposited by strong winds during and after the snowfalls, 2) in the middle, new snow accumulated by the episode itself and 3) at the bottom, crusts and weak interfaces generated by the previous warm front and the fall of temperatures. Even though weak interface on the crust is not visible in the profile, snow and weather conditions from 27-30th are favourable to the growth of a weak interface over the crust

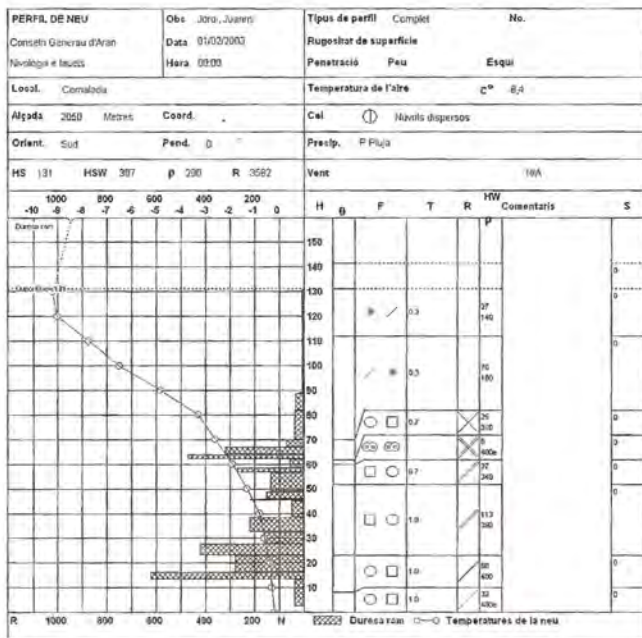


**Figure 5:** Snow profile showing the crust at 60 cm and the upper new snow both deposited during the snowfalls and during the drifting process.

(BIRKELAND 1996). Before the heavy precipitation of 30th, on 29th few new snow falls at low temperatures (about -8° - -10°C) and it deposits on the crust which temperature ranges between -1°C and zero degrees. The strong thermal gradient in the contact between the crust and the new fallen snow could favour the formation of a weak interface. Afterwards, the new fallen snow by itself could act as a weak layer so. Snow and meteorological data analysed come from the high altitude automatic

station of the Meteorological Survey of Catalunya for the avalanche prediction. The majority of the avalanches were in southward or sheltered slopes where the higher part of the snowpack moved over the snow crusts in the starting zone involving from that point more snow in the track zone and becoming major avalanches. For this reason, not only the great amount of precipitation seems to have an important role in avalanche activity but also the wind during and after the episode and the existence of sliding interfaces.

**Case Study 2: Episode 28-31/01/2006**  
*Nivometeorological pattern:*

This snowfalls event began on 27th of January, firstly affecting the low lands of the Iberian Mediterranean area (MATEO et al. 2006). These precipitations were related to a deep and cold low-pressure system situated in the north-northwest of the Iberian Peninsula (figure 6). Over the Pyrenees, there were small dry snow accumulations. During the 28th of January, the warm Mediterranean advection caused a clearly increase in temperatures (figure 7). Different types of precipitation were observed, such as, freezing rain and sleet, associated with the warm front (figure 8) (MATEO et al. 2006). The Pyrenees were mainly affected between the 29th and 30th of January. On the 29th of January, the upper low broke away from the main flow producing a cut-off (figure 6). These synoptic situations are not very frequent during winter in the Iberian Peninsula (NIETO et al. 2005). This low moved from the northwest of Iberian Peninsula to south and impinges wet and warm air over Catalonia (figure 6). Warm air displaced, from east to

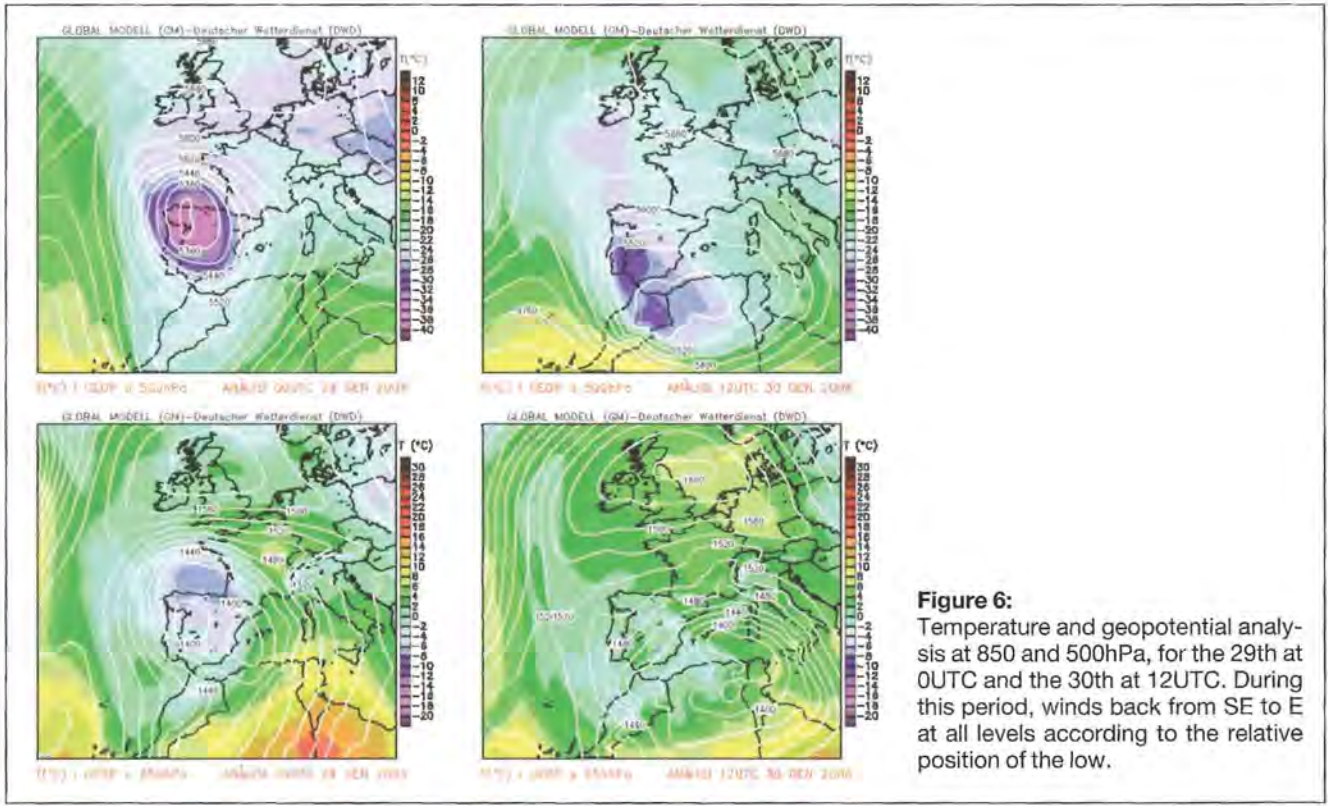


**Figure 6:** Temperature and geopotential analysis at 850 and 500hPa, for the 29th at 0UTC and the 30th at 12UTC. During this period, winds back from SE to E at all levels according to the relative position of the low.





**Figure 10:** Hoar surface formed before the events of January 2006 (Picture: Karen and Jason Skinner).

pes were the non-cohesive hoar surface layer (figure 10) was specially developed.

## 2. Conclusions

Two important events of heavy snowfalls and avalanche activity over the Catalan Pyrenees has been analysed using circulation data, high elevation meteorological and radiosounding observations, and the corresponding snow profiles and avalanche data collected.

In the first episode, in 2003, the location of the jet-stream near the Pyrenees, joined with a short-lived low increasing instability looks as the main reason for the important amount of snow and the increase on the intensity of precipitation during the morning of January 31st. Major avalanches were produced on the northern side of the Catalan Pyrenees, isolating the Val d'Aran, the most populated area of the range. Three factors seem to be the most relevant for the major avalanche release:

- 1- Possible existence of a weak interface due to a fall of temperatures, located between the crust related to the warm front crossing the 27th and the heavy snow-fall.
- 2- Great amount of new snow due to the instability related to the jet-stream joined with the short-lived low.
- 3- Overload with drifted snow, a usual pattern over the analyzed area after snowfalls.

The second example studied is related to a low-pressure system also pumping humid air from the Mediterranean. Important amounts of precipitation related to strong and well-oriented winds at low-levels and, especially, the steadily increases of the snow level are the most relevant elements for this situation. In this case, major avalanches were produced over almost all analyzed area but they were more relevant on the southern and eastern side. In this case, the avalanches were mainly caused by:

- 1- Specially, the existence of buried weak layers, related to a cold air advection in December and nocturne irradiation processes through high pressures episodes.
- 2- The great input of dry fresh snow thanks to a cold low at mid troposphere located westerly of the Pyrenees,
- 3- The help of a overloading of new wet snow caused by the warm Mediterranean air mass entering to the mountain and inland areas.

These two examples reveal the importance of a good and accurate high mountain weather forecast to detect and prevent avalanche risk situation, implying not only the detection of heavy snowfalls but also the variation of the snow level and wind during and after the episode. Moreover, in future works, more detailed studies on synoptic situation responsible of weak layer formation during snow season should be carried out. On the other hand, the episodes analysed fit well with the circulation patterns related to heavy snowfalls over the area obtained with automatic methods (ESTEBAN et al. 2005). These results encourage the authors to look for strong relationships between the atmospheric circulation and the natural triggers of avalanches, being also useful for studies of climate change over the Pyrenees based on GCM.

## Acknowledgements

Patrick Bornuat (MétéoFrance), Institut Geològic de Catalunya and Jordi MATEO (Catalan Meteorological Service), Tomas Mas Pascual (photos).

## References

- BARRIENDOS, M., RODÉS, P., GARCÍA, C., MARTÍ, G., GAVALDÀ, J. (2006): La reconstrucció de riscos naturals en el contexto climàtic de la miniglaciació. El caso del alud catastròfic de abril de 1855 en el Valle de Torán. *Boletín Glaciológico Aragonés* 6, 61-85.
- BIRKELAND, K.W., JOHNSON, R.F. AND SCHMIDT, D.S. (1996): Near-surface faceted crystals: Conditions necessary for growth and contribution to avalanche formation, southwest Montana, U.S.A. *Proceedings of the International Snow Science Workshop, Banff, Alberta*, 75-79.
- CONSELH GENERAL D'ARAN (2003): L'allau del 31 de Gener de 2003 a la carretera C-28bis d'accés a Beret i la Pietra de Baqueira. Internal report. Vielha, Catalonia, Spain.
- ESTEBAN, P., JONES, P.D., MARTÍN-VIDE, J., MASES, M. (2005): Atmospheric circulation patterns related to heavy snowfall days in Andorra, Pyrenees. *International Journal of Climatology* 25: 319-329.
- ESTEBAN, P., MARTÍN-VIDE, J., MASES, M. (2002): Climatology for avalanche forecasting: the Les Fonts avalanche of Arinsal, Andorra, February 8th of 1996. *Horitzó: Revista del Centre en Ciències de la Terra* 2: 10-19 (in Catalan).
- MATEO, J., ANDRÉS, A., BALLART, D., FIGUEROLA, F., MIRÓ, A., ARAN, M. (2006): Different precipitation-type in a snow event in Catalonia. A mesoscale analysis. 6th Annual Meeting of the European Meteorological Society, Ljubljana, Slovenia.
- NIETO, R., GIMENO, L., DELA TORRE, L., RIBERA, P., GALLEGÓ, D., GARCÍA-HERRERA, R., AGUSTÍN, J., NUÑEZ, M., REDAÑO, A., LORENTE, J. (2005): Climatological Features of Cutoff Low Systems in the Northern Hemisphere. *Journal of Climate* 18: 3085-3103.
- VILLECROSE, J., COLEOU, C., GIRAUD, G. (1999) : Février 1999 dans les Alpes du Nord. Note de travail du Centre d'Études de la Neige 14. Météo France, Saint Martin d'Hères.

## 7 Weather and snowpack conditions of major avalanches in the Catalan Pyrenees

CARLES GARCÍA<sup>1</sup>, GLÒRIA MARTÍ<sup>1</sup>, ALBERT GARCÍA<sup>2</sup>, ELENA MUNTAN<sup>3</sup>, PERE OLLER<sup>4</sup>, PERE ESTEBAN<sup>5</sup>

<sup>1</sup> Institut Geològic de Catalunya, Barcelona, Spain

<sup>2</sup> Grup de Climatologia. Universitat de Barcelona, Barcelona, Spain

<sup>3</sup> Grup de Dendrologia. Universitat de Barcelona, Barcelona, Spain

<sup>4</sup> Institut Geològic de Catalunya, Barcelona, Spain

<sup>5</sup> CENMA/IEA-Snow and mountain research center, Principality of Andorra

### Abstract

The goal of this presentation is to identify the nivometeorological conditions releasing major avalanches in the Catalan Pyrenees (NE Spain). One of the main points of this study is dating and reconstructing major avalanches occurred before the avalanche warning system was started in 1989. In this way, dendrochronology information on major avalanches activity is added to the usual sources of information in avalanche research such as historical documents, population inquiry and intensive, local avalanche observations. After identifying and dating major avalanches, weather and snowpack conditions releasing these events have been reconstructed and analysed. The results show a great variety of different nivometeorological patterns compared to areas with a similar extension over the Alps. The singular geographical factors of the Catalan Pyrenees as proximity to the Mediterranean Sea and the Atlantic Ocean, zonal disposition of the axial range, and relatively low latitude of the massif, determine the complexity of the Catalan Pyrenees' climate. On the other hand, comparisons with previously established circulation patterns for heavy snowfalls at the synoptic scale over the study area highlight the robustness of the results. Since not all major avalanches are linked to heavy snowfalls, these major avalanche events have been also related with low-frequency patterns as NAOi (North Atlantic Oscillation index), showing consistent results. Looking at the obtained results, we can conclude that both the identification of several weather and snow conditions patterns releasing major avalanches and the relationship with low frequency atmospheric circulation patterns will clearly contribute to improve short and mid term forecasting of major avalanche events over the Catalan Pyrenees.

### 1. Introduction

The growth of tourism in the recent decades, in the Catalan Pyrenees, has resulted in an increase in building, opening of mountain roads during winter, and related infrastructures. The policy of territorial planning aims to

develop new ski resorts in the Catalan Pyrenees and to build thousands of new lodgings. As a consequence, exposure to natural hazards has increased and so has the risk; its trend is to rise. The number of skiers and mountaineers who have died due to an avalanche has grown in the last years (MARTÍNEZ AND OLLER, 2004). As there are not studies dealing with avalanche situations in the Catalan Pyrenees, this article tries to open a line of research on this subject. The aim of the article is to characterize the atmospheric circulation patterns responsible of major avalanches in the Catalan Pyrenees. This work will attempt to detect the diverse atmospheric conditions producing different avalanche situations in different parts of the Catalan Pyrenees. First of all, even though it could seem few ambitious it's essential to identify major avalanche days. This search will be done by means of different sources at a different temporal resolution. The study of the avalanche situations from a synoptic point of view understood as past and present weather conditions, not only based on behaviour of current meteorological parameters triggering avalanches, let's know further the causes of the avalanches and to predict them.

A lot of research in this field has been achieved in the United States and Canada. Avalanches activity has been related to climate in a regional scale by LACHAPPELLE (1966), SCHAEFER (1986) and ARMSTRONG AND ARMSTRONG (1987), for instance. Studies for specific sites analysing the relationship between regional atmospheric circulation patterns and avalanche data has been undertaken by FITZHARRIS (1981) and MOCK (1996) as two examples. Most recently, BIRKELAND (2001) has emphasized that differences in avalanche activity with distinctive atmospheric conditions can be observed even in sites located in a similar intermountain avalanche climate. His conclusions remark that the local topography explains the different effects of synoptic patterns on avalanches.

In the Alps, studies taking into account circulation patterns to explain major avalanches in a regional scale have been developed by HÄCHLER (1987) in the Swiss Alps. He differentiated circulation patterns responsible of severe avalanches in the Northern and Southern Alps focusing on both geographical factors as distance from the nearest sea and mountains disposition and dynamic factors as the direction of the upper-level airflow. In the French Alps, VILLECROSE (2001) showed the difficulty of comparing major avalanche situations when studying the main catastrophic crisis in the French Alps. This study tries to define and to compare extreme situations by means of quantitative avalanche activity, damages, number of fatalities and depth of fresh snow. It concludes that those parameters are not enough and they must be put in relation with the snow and weather context.

There are few works focused on the Pyrenees. The extreme avalanche situation of 1996, the most catastrophic of the second half of the twentieth century in the Catalan Pyrenees, has been described attending to synoptic weather patterns in a report issued by the Cartographic Institute of Catalonia (GARCÍA et al. 2000). This study has highlighted the importance of taking into account the previous snowpack structure in order to ex-

plain the effectiveness of the synoptic patterns giving major avalanches. An attempt to explain one extreme avalanche event of the 1996 crisis by means of a synoptic approximation has been shown by ESTEBAN (2002). Studies focusing in making regions in the Catalan Pyrenees on the basis of variations in the avalanche activity are very scarce, which is one aspect of the present research. Some internal reports from the Geological Institute of Catalonia have shown the relative magnitude of each major avalanche winter looking at the intensity and geographical extent of the major avalanches recorded for each winter.

The present paper uses a new method based on dendrochronology techniques (MUNTAN 2004) to identify avalanche winters as a first step to hunt for avalanche events in different kind of historical documentation. After, we will try to assign each major avalanche episode to an atmospheric circulation pattern and define which areas are affected for each weather pattern. Finally we will attempt to analyse the relationship between the low-frequency pattern NAOi (North Atlantic Oscillation index) and the regional occurrence of major avalanches.

## 2. The Study Area

The Pyrenees constitute a mountainous system of about 450 km from the Atlantic Ocean (west) to the Mediterranean Sea (east). They rise from the isthmus that links the Iberian Peninsula with the rest of the Euro Asiatic continent. The study area, the Catalan Pyrenees, is located in the eastern half part of the range. It spreads 146 km long per 52 km wide at the western part and 19 km wide at the eastern part. The region is divided geographically in the Western (61%) and the Eastern Pyrenees (39%). The Western Pyrenees are higher than the Eastern. Highest elevations reach 3,000 m, but in general they range bet-

ween 2,500 and 3,000 m. The highest peak in this region is the "Pica d'Estats" with 3,143 m. The timber line is located between 2,100 and 2,300 m. The highest mountain villages are located from 1,500 m to lower altitudes. The highest winter opened roads reach 2,300 m and 9 alpine ski resorts spread on altitudes over 1500 m height. Two main kinds of relief can be differentiated: the glacial cirque areas, plateaus over 2,000 m, with abrupt peaks but with vertical drops not higher than 700 m, and the valley areas, with smoother relief, but with vertical drops in some cases higher than 1,500 m.

The Catalan Pyrenees has been divided in 7 regions attending to weather and snow conditions (figure 1). Avalanche coerture is shown too (OLLER et al. 2006). These regions are the empirical result of 15 years of avalanche prediction tasks and it is not a climatic classification since long data series don't exist. The singular geographical factors affecting the climate of the Catalan Pyrenees bears three different climatic conditions in a relatively small area. The zonal disposition of the axial range lets the retention of humid air masses, both polar and arctic maritime air masses from north advections and tropical maritime air masses from south and southwest flows. The meridian valleys configuration favours the penetration and the placement of the unstable air masses pointed out; the forced lifts by the relief sometimes result on heavy and persistent snowfalls. The proximity to Mediterranean Sea and less to the Atlantic Ocean avoids extreme temperatures as it occurs in inland ranges but surprisingly extensive pluviometric shadows exist as well. Finally, the relatively low latitude of the massif becomes the Pyrenees in a boundary range between the humid ocean climate and subtropical dry climate. Three climatic conditions could be defined. The northwest part of the Catalan Pyrenees shows a humid ocean climate as the main river basin drains to the Atlantic Ocean through France. Precipitations are abundant

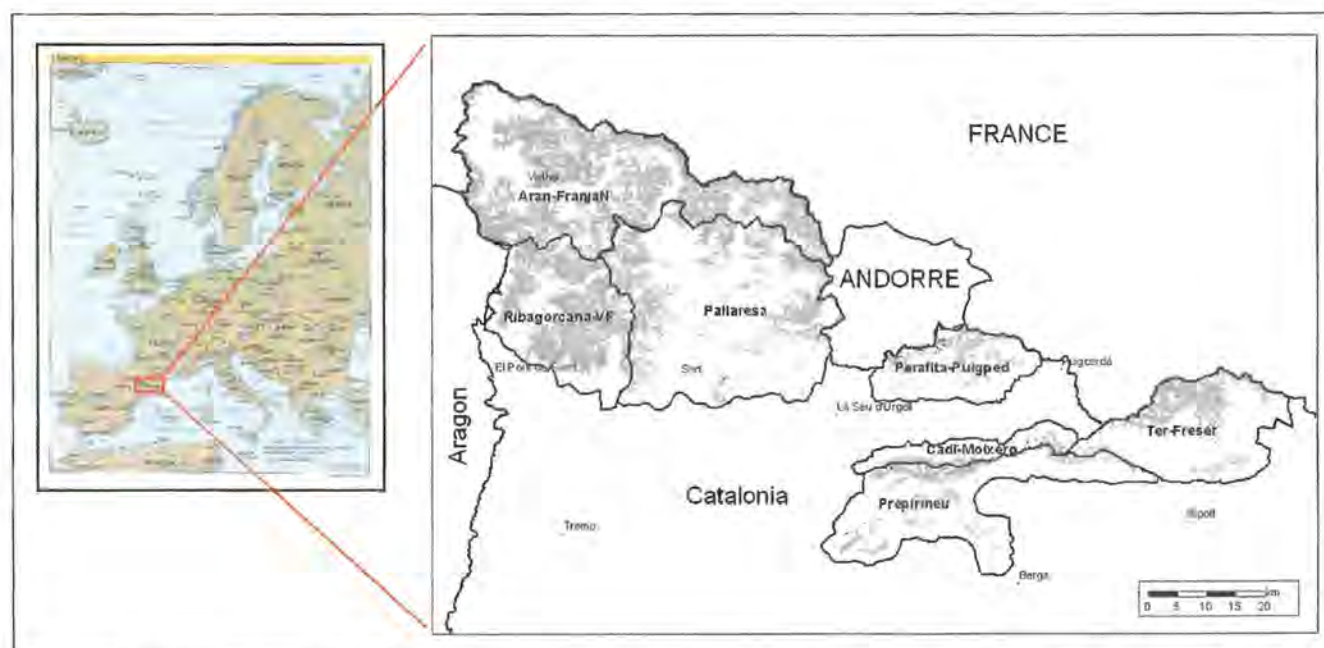


**Figure 1:** The Catalan Pyrenees are located on the eastern part of the Pyrenees. The range has been divided in seven nivoclimatic regions for a better description of the avalanche forecasting. Avalanche coerture is also shown (OLLER, 2006).

and show a regular interannual distribution. The total amount of fresh snow at 2200 m height is about 500–600 cm per year. The oceanic influence crosses the range to the south face but diminishing quickly. So, climate gains continental features towards the south and east. Winter precipitation reduces being the winter the driest season and snow precipitation increases in spring and autumn seasons. Interannual variability of precipitation increases. The total amount of fresh snow at 2200 m height exceeds slightly 250 cm per year. Predominant winds come from north and northwest, often with gusts over 100 km/h. Oceanic influence disappears completely in the most eastern part of the Catalan Pyrenees and Mediterranean Sea influence plays a significant role. It means heavy snowfalls, but not frequent, due to lows centred on the Mediterranean sea blowing very humid, maritime flow from the east. Interannual variability of snowfalls is high. The total amount of fresh snow at 2200 m height is about 350–450 cm per year. Predominant winds come from north (mistral, or locally tramuntana) and maximum gusts sometimes exceed 200 km/h at 2200 m height due to the formation of a persistent low in the lee-side of the Alps over the Lion Gulf.

The nivoclimatic regions in which the Catalan Pyrenees have been divided are, from west to east, "Aran-Northern border of Pallaresa" (Oceanic conditions); "Ribagorçana-Vall Fosca", "Pallaresa", "Perafita-Puigpedrós", "V. N. Cadí Moixeró" (Continental conditions); "Prepirineu" and "Ter-Freser" (Mediterranean influence).

### 3. Data and Methods

An essential part of this work is to look for major avalanche events, it means, dating and localizing them. We have considered major avalanches in a wide sense, as defined by SCHAEFER (1986), avalanches larger than usual, arriving to the bottom of the valley, destroying mature forest, damaging structures. In order to date major avalanches episodes a new method based on dendrochronology has been developed and applied. Avalanche data utilized in this study has been dated in three temporal resolution classes, that is to say, daily, monthly and annual resolution. Avalanches have been dated in a daily resolution from 1996 till now. In 1996 the Nivometeorological Observers Network (NIVOBS) begun a winter surveillance making transects every day to report snow conditions and avalanche events. All the episodes have been dated and mapped due to systematic observations in all the regions, even by means of helicopter flights. The NIVOBS was started in 1986 but avalanche observations were not undertaken systematically till 1996, so monthly or weekly resolution on avalanche dating prevails from 1986 to 1996. Before 1986, avalanche dating is scarce and without continuity and data comes from enquiries to inhabitants; annual and monthly resolution prevails and the errors in dating are possible. In order to enhance the knowledge of avalanche events from the past a new method to look for major avalanches has been essayed by means of dendrochronological techniques.

Dendrochronology is the study of tree rings. It can be used to date geomorphological processes accurately with annual resolution (POTTER 1969). A study carried out by MUNTAN (2004) in Núria valley, in the eastern part of the Catalan Pyrenees, has dated different avalanche events in an avalanche track and run out zone by means of the study of tree rings and observed damages in different transects. She synthesizes the method in three steps. First of all a reference chronology must be built with trees from the surrounding forest; trees that haven't been affected by avalanches. This is the guarantee for a correct dating. Samples are taken with an increment borer. Afterwards cores are measured to produce the reference chronology. In a second step, trees affected by avalanches are sampled to search for tree-ring signals. Trees can be tilted several times and they react producing a special kind of wood; they can develop scars from an injury, and they can be overthrown and die. Finally, events can be dated by counting the tree-ring signals from a representative amount of trees from the avalanche path. Some of the events can be exceptional avalanches (1930, 1971 and 1996 in Núria). Of course, its resolution is annual, but it let us concentrate the search in a concrete year, investigating in historical documentation from the councils and ecclesiastic registers in case of fatalities (avalanches dated in 1855 and 1991). With this information, we can search in the meteorological registers to find out the synoptic situations responsible for the avalanche episodes.

This research comes from a joint project among the Geological Institute of Catalonia, the University of Barcelona and the Meteorological Survey of Catalonia called ALUDEX to date major avalanches in the Catalan Pyrenees ([www.igc.cat](http://www.igc.cat)).

Daily weather data has been analysed for all the major avalanche events from 1855 until now. Data comes from manual and automatic meteorological networks of the National Institute of Meteorology of Spain and Meteorological Survey of Catalonia. Daily synoptic scale atmospheric situations for major avalanches have been selected from the NCEP-NCAR reanalysis data (KALNAY et al. 1996) by using maps of sea-level pressure (SLP), 850 hPa and 500 hPa. Atmospheric circulation patterns have been defined using manual classification. In cases of major avalanche situations due to heavy snowfall days, the synoptic situation has been compared with the synoptic patterns related to heavy snowfall days in the Pyrenees obtained by using principal components analysis and clustering techniques (ESTEBAN et al. 2005). Finally, major avalanches episodes are put in relation to the North Atlantic Oscillation index (NAOI) as this low frequency circulation pattern determines strongly the variability of the temperature and precipitation behaviour in Europe (OSBORN et al. 1999). Monthly NAO values from December to March comes from the Climatic Research Unit of the University of East Anglia, UK ([www.cru.uea.ac.uk/cru/data/nao.htm](http://www.cru.uea.ac.uk/cru/data/nao.htm)), currently revised and modified with Gibraltar SLP data till the year 2000. Data till March 2006 has been updated in the present work.

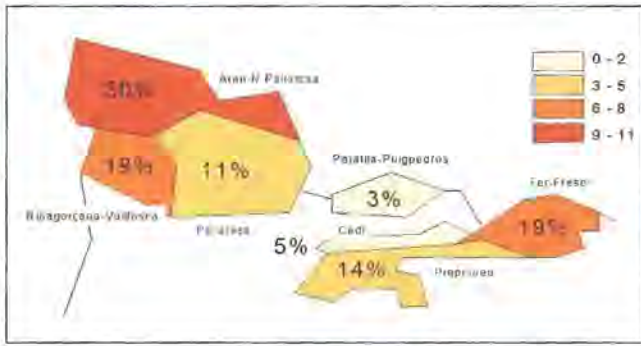


**Figure 2:** Frequency (%) of affectation of major avalanches for each region. The legend corresponds to the number of episodes.

#### 4. Results

From 1939 to 2006, each of the seven nivoclimatic regions has been affected in 37 occasions by one major avalanche at least. The frequency of affectation shows a clear spatial variability (figure 2). Since no quantity of major avalanches for each region has been taken into account, the results don't depend on the number of observers or quantity of inhabitants. The most affected region is Aran (30%, 11 events), the northwestern, and the minor the central regions (3%, 1 event). The regions closer to the seas are more favoured by major avalanches than regions located in intermountain sites. The spatial distribution of regions affected by major avalanches suggests a positive correlation with the distribution of winter precipitation.

The spatial distribution of atmospheric patterns producing major avalanches events is very heterogeneous over the seven regions, that is to say, their effects are local. We call magnitude of each atmospheric pattern to the averaged quantity of affected regions due to that pattern; the maximum is 1.8 regions for south-western advections and the minimum 1.0 for eastern advections. Magnitudes are low specially taking into account that we are considering an extension of only 150 km. It means a complex mosaic of different snow and weather conditions where orography and topography determines how upper flows and air masses act. Table 1 shows the number of major avalanche episodes for each synoptic pattern that affects each region.

The most intense major avalanche episode occurred at the end of January 1996 due to a southwestern synoptic situation (figure 3, A). Many big avalanches of new fallen, humid, dense snow fell down a few hours after the precipitation. Four regions were affected by major avalanches, some of them extreme one since timber analysis of died trees by the avalanches indicated ages about 80 years. A deep low pressure was located over the northwest coast of the Iberian Peninsula. From surface to upper levels south and southwestern winds flew carrying warm and humid air from the Atlantic and even the Mediterranean on lower levels over the Pyrenees. High instability prevails as a deep cold core exists at 500 hPa. A maximum snowfall of 220 mm of snow water equivalent (SWE) in 24 hours was registered and many other exceeding 150 mm of SWE in several regions due to processes of convective cells growth. It means Gumbel recurrence periods exceeding 100 years (GARCÍA et al. 2000). As ESTEBAN et al. (2005) have shown, heavy precipitation even torrential affects the southern side of the Pyrenees in such a synoptic circulation pattern. Nevertheless, snow is registered only in the highest elevations, normally over 2200 m height, reflecting the warm air mass near the surface in contrast with low temperatures at higher levels. Southwestern pattern is responsible of the 16% of the major avalanche episodes recorded, but its average spatial magnitude is the highest, 1.8 regions. Southern pattern seldom appears but it could be associated to a phase of southwestern pattern (8% of the synoptic patterns releasing big avalanches and 1.5 spatial magnitude score).

Another significant synoptic pattern causing major avalanches is a northern synoptic situation. Its spatial distribution in terms of avalanche releasing is very reduced but intense in number and size as it mostly affects one region (the Aran-Northern border of Pallars). Its average magnitude is 1.3 regions and it is responsible for 16% of the major avalanche episodes recorded. At the end of January 2003 a north advection involved the Pyrenees (figure 3, B). The Azores high pressures were extended in a north-south axis over the Atlantic Ocean, while a deep low pressure was located on the Baltic Sea. This configuration pumped an arctic air mass over the Pyrenees directly from the North Pole. Snowfalls about 100-150 cm in 24 hours were recorded on the Aran-

**Table 1:** Synoptic patterns responsible of major avalanches for each region and spatial magnitude for each one (northwestern, NW; north, N; south, S; southwest, SW; low centered, L; eastern, E; high pressure, H).

Pattern	Spatial magnitude	Episodes %	Aran	Ribagorç.	Pallaresa	Perafita	Cadi	Ter-Freser	Prepirineu
NW	1.4	32	6	2	1	0	0	1	1
N	1.3	16	3	1	1	1	0	0	0
S	1.5	8	0	2	1	0	0	0	0
SW	1.8	16	0	1	1	0	0	2	2
L	1.7	12	0	1	0	0	1	2	1
E	1.0	4	0	0	0	0	0	1	0
H	1.7	12	2	0	0	0	1	1	1
			<b>11</b>	<b>7</b>	<b>4</b>	<b>1</b>	<b>2</b>	<b>7</b>	<b>5</b>

Northern border of Pallars, a region of oceanic conditions. Powder avalanches with more than 2 km of path produced damages in roads and buildings and the region was cut off from the neighbouring regions. North pattern generates very low temperatures (-15° to -20°C at 2200 m height), intense snowfalls, strong winds and very active drift snow processes. The Precipitation gradient decreases strongly to the south. Major powder avalanches prevail during the few hours after the precipitation, specially located in southern slopes due to the enormous overaccumulations of snow deposited on lee side aspects.

We want to focus on concrete features and synoptic conditions of the Pyrenees, sometimes associated to mesoescalar phenomena with strong consequences in the avalanche dynamic. It happens in eastern synoptic pattern. At the beginning of December 1991 big avalanches, some extremes, felt down in the Ter-Freser region, the nearest to the Mediterranean Sea. High pressure existed on surface (about 1024 hPa) over the Pyrenees, but a cold core was centred slightly south

of the Pyrenees. Cyclonic circulation ruled on upper levels (figure 3 C). A slight warm, humid Mediterranean flow on surface penetrated from the east affecting the closest mountain range to the Mediterranean Sea. Amounts of precipitation about 400 mm (SWE) were recorded during four days, with a snow level around 1800-2000 m height. It's a synoptic pattern observed usually in September-October giving torrential precipitations in mountain ranges close to the Mediterranean but seldom in winter (JANSÀ 1990).

Normally eastern synoptic patterns are associated to deep lows centred at south of the Pyrenees pumping Mediterranean warm air from surface to 500 hPa levels. This weather pattern generates heavy snow precipitations in the most eastern part of the Pyrenees and major avalanches use to affect Ter-Freser and Prepirineu. Eastern pattern and lows centred suppose the 16% of synoptic patterns producing major avalanches and show 1.5 spatial magnitude score. The rest of the circulation patterns (northwestern pattern and high pressure associated to warm and dry ad-

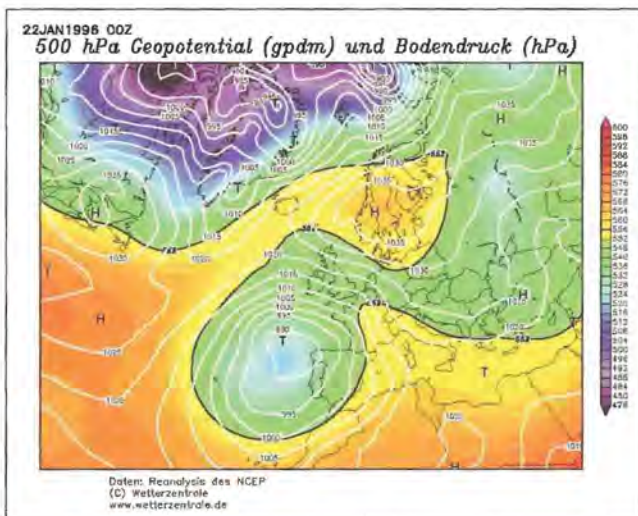


Figure 3a: Southwestern synoptic pattern, SLP and 500 hPa surfaces (1996/01/22).

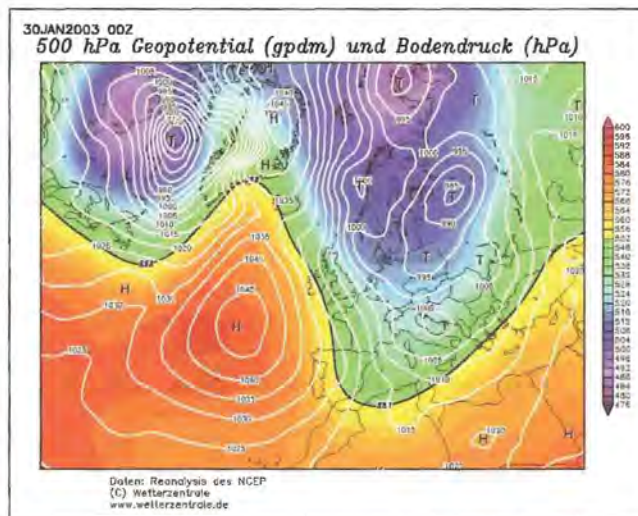


Figure 3b: Northern synoptic pattern, SLP and 500 hPa surfaces (2003/01/30).

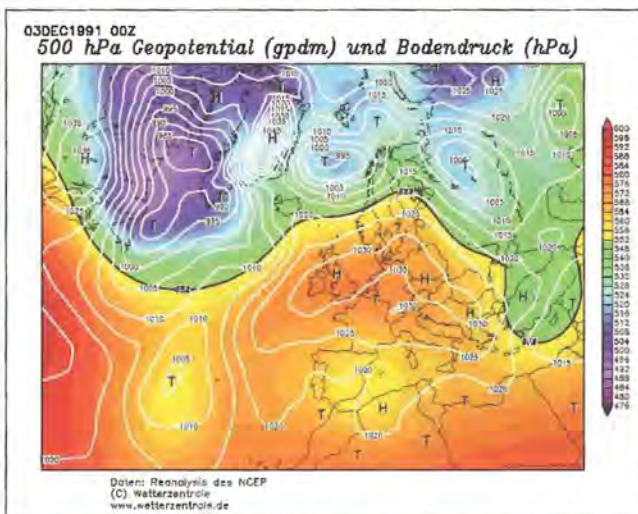


Figure 3c: Eastern synoptic pattern, SLP and 500 hPa surfaces (1991/12/03).

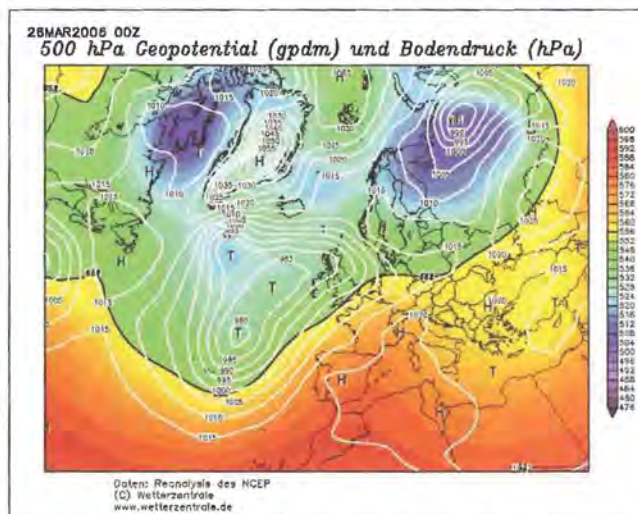


Figure 3d: High pressure synoptic pattern, SLP and 500 hPa surfaces (2006/03/26).

vection on lower levels) produce major avalanches depending on the previous conditions of the snowpack. Northwestern pattern provokes heavy precipitations in the Aran-Northern border of Pallars. Snowfalls lead major avalanches of powder snow and slab avalanches in that region. Nevertheless, strong winds drift snow in neighbouring regions in case snowpack consists on uncohesive, cold and loose crystals. In this situation big slab avalanches occurs over south and east slopes of several regions.

It's the most frequent synoptic pattern giving big avalanches (32%) and affecting 1.4 regions. Finally, high pressure on surface installed on the western Mediterranean Sea and southwestern flow at 500 hPa over the Pyrenees sometimes generate major melting avalanches on several regions (figure 3 D). The necessary conditions are cold and uncohesive snowpack at the end of the winter (March, April), warm and dry advection at 850 and 700 hPa associated to the high pressures centred over the Western Mediterranean. The collapse of loose snow is suddenly produced due to melting processes affecting all the depth of the snowpack, normally over north slopes where uncohesive layers persist all through the winter. Sometimes ground melting avalanches fall down. It supposes 12% of synoptic patterns and affects 1.7 regions.

As pointed out, precipitation and previous conditions of snowpack are essential for avalanche releasing (McC-LUNG and others, 1993). Avalanche episodes and snowfall days with 50 cm per day have been put in relation from 1985-86 winters till 2005-06 in the Catalan Pyrenees. The correlation is high (Pearson's  $r=0.71$ ), but the number of major avalanches episodes is markedly lower than heavy snowfall events (figure 4). By means of the synoptic classification of heavy snowfalls days in Andorra proposed by ESTEBAN et al. (2005), the present study has attempted to look for the synoptic patterns leading heavy snowfalls with no major avalanche activity. Andorra is a country located in a valley flowing to the Mediterranean Sea in the middle of the Catalan Pyrenees. Climatic and orographic conditions don't differ

from the surrounding Catalan Pyrenees (LEFEVRE 1998). ESTEBAN'S classification is based on the principal component analysis and clustering techniques and seven circulation patterns leading to heavy snowfalls have been established. Synoptic patterns associated to zonal circulation or west advection and westerly anticyclonic advection have not provoked major avalanche activity. It could be due to frontal precipitation in these situations usually begin with wet snow at high altitudes and ending with few dry snow due to a descend of temperature. It favours stability processes of snowpack as settlement, bonding and freezing and so no major avalanches occur.

Taking into account that the evolution of the main meteorological parameters as temperature, precipitation and winds are conditioned by the North Atlantic Oscillation index (NAOI) in mountain ranges as the Alps, as BENISTON et al. (1996) demonstrated, in the present study major avalanches episodes have been put in relation with the evolution of the NAO. The relationship between winter precipitation and NAOI has been investigated in the Pyrenees (MARTÍN-VIDE et al. 1999, ESTEBAN et al. 2001) and results show a negative correlation. A monthly index has been obtained from the pressure differences between Reykjavik and Gibraltar. The index of NAO approximately ranges between 3 and -3. Positive values indicate zonal, westerly atmospheric circulation; low pressures are located over the North Atlantic and high pressures over the Azores Islands. In the opposite case, low pressures circulate more southern than usual due to a weakening of the Azores high pressures and vortexes across the Iberian Peninsula.

The magnitude of the spatial affectation of the major avalanche episodes shows a high negative correlation with the values of the North Atlantic Oscillation for each winter (Pearson's  $r = -0,61$ ) from 1985-86 to 2005-06. It means that winters with avalanches episodes of high spatial magnitude correspond to negative values of the NAO index. These events are due to anticyclonic blocking over northern Europe patterns (blue cases in the figure 5), as could be expected for negative values of

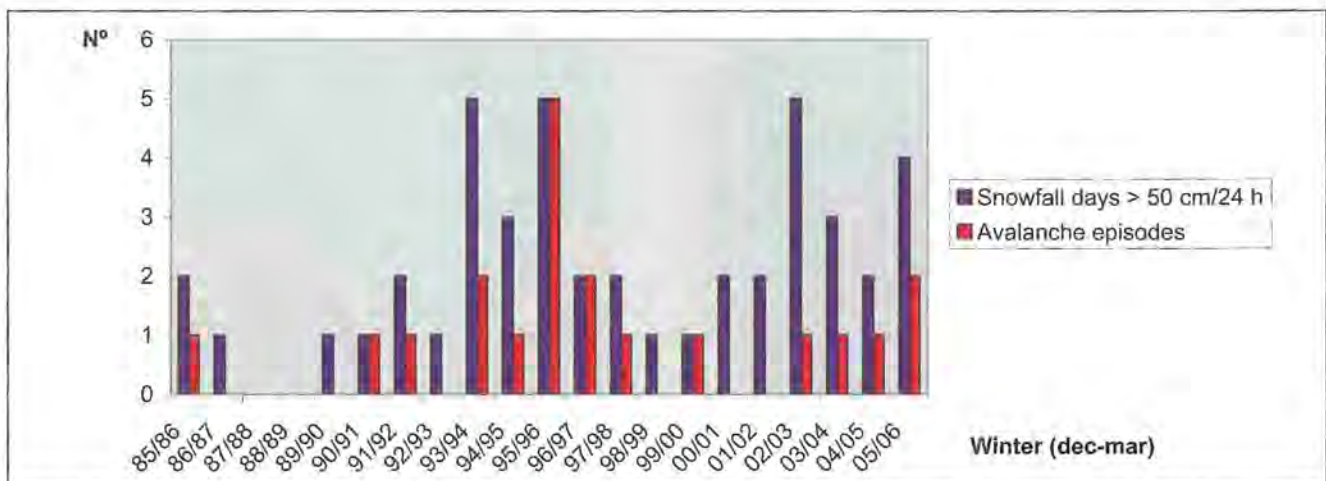
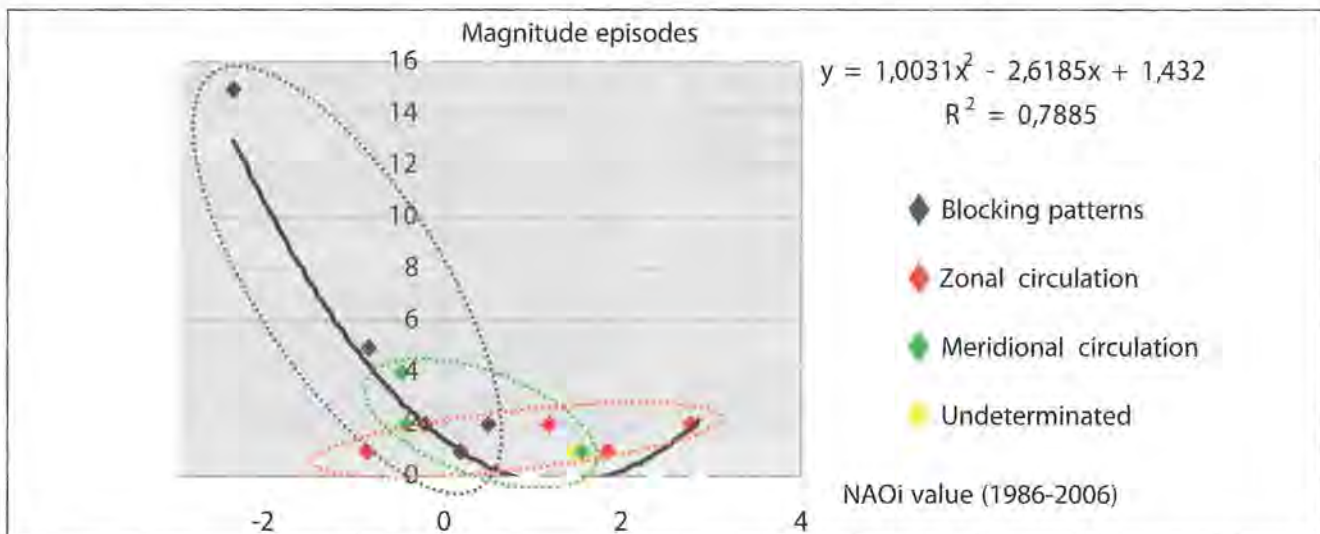


Figure 4: Days with heavy snowfalls and major avalanche episodes for each winter.



**Figure 5:** Relationship between spatial avalanche magnitude and NAOi for winters from 1985-86 to 2005-06.

NAO. On the other tail of the distribution, the winters with smallest values of spatial magnitude correspond usually to positive values of NAO, when avalanche events were produced by zonal circulation patterns, which are shown in red in the figure 5. Meridional circulation patterns associated to major avalanches seem to occur when NAO values are close to 0 and are shown in green in the figure 5. The function describing the relationship between winter NAOi and spatial magnitude of major avalanche episodes shows a coefficient  $R^2 = 0.79$ , which explains the great part of the variance of the distribution.

Positive values of the NAO up to 1 include northwestern patterns, roughly zonal circulation; values between 1 and -1 are composed of meridional circulation patterns as north and south advections; finally negative values less than -1 are linked to atmospheric circulation associated to anticyclonic blocking situations over northern Europe and lows centred over the Iberian Peninsula, southwestern advection, eastern advection and high pressures centred over the Western Mediterranean Sea are included in the negative NAOi category.

## 5. Conclusions

The relationship between atmospheric circulation patterns and major avalanche activity in the Catalan Pyrenees is complex since the avalanche activity is produced by many synoptic patterns, compared to other mountain ranges as the French Alps (VILLECROSE et al. 2001). Each synoptic pattern responsible of major avalanches determines a specific spatial distribution pattern of the avalanches, often very contrasted from one to another. That's is explained by the geographic characteristics of the Catalan Pyrenees, especially the orientation of the valleys, the alignment of the orography, the distance from the nearest seas which modify the general conditions of incoming flows and air mas-

ses. Searching on precipitation and wind behaviour generated by highs and lows generated at mesoscalar scale associated to orographic dipole over the Pyrenees due to perpendicular flows could contribute to improve the knowledge on snow and avalanche conditions.

Considering the NAO index in the occurrence of major avalanche episodes let take into account the previous evolution and stability of the snowpack before the event. High negative correlation between major avalanches and NAOi shows that high pressures blocking over north and central Europe is the most frequent circulation pattern responsible of major avalanche episodes and even of the highest spatial magnitude. Nevertheless, the small dimension of the sample doesn't allow assuming strong conclusions, but it seems to exist an interesting relation between magnitude and the NAO index which could improve the avalanche prediction at a medium term.

On the other hand it is necessary to recuperate major avalanche events from the past to reinforce the results of this article. So, dendrochronology could be a useful tool to search avalanches in the past. In addition, it would be interesting to approach historians to look for in documentary sources.

As future work, once gathered more avalanche events, it would be useful to apply the BIRKELAND (2001) method based on PCA analysis to advance in the spatial distribution of atmospheric patterns associated to major avalanches.

Results from the relationship between avalanche magnitude and atmospheric circulation patterns could be applied to advance in the classification of winter climate regions in the Catalan Pyrenees.

## Acknowledgements

We want to thank the financial support of the Project ALUDEX (MICYT-FEDER: REN2002-02768).

## References

- ARMSTRONG, R.L., ARMSTRONG, B.R. (1987): Snow and avalanche climates of the western United States: a comparison of maritime, intermountain and continental conditions. International Association of Hydrological Sciences Publication, 162. 281-294.
- Beniston, M., Rebetez, M. (1996): Regional behaviour of minimum temperatures in Switzerland for the period 1979-1993. *Theor. Appl. Climatol.* 53, Springer-Verlag, pp. 231-243.
- BIRKELAND, K.W., MOCK, C.J. SHINKER, J.J. (2001): Avalanche extremes and atmospheric circulation patterns. *Annals of Glaciology* 32, pp.135-140.
- ESTEBAN, P., SOLER, X., PROHOM, M., PLANCHON, O. (2001): The precipitation distribution by using NAOi. The effect of the relieve at local scale: the eastern Pyrenees. In: "El Agua y el Clima - L'Aigua i el Clima" JOSÉ A. GUIJARRO PASTOR, MIQUEL GRIMALT GELABERT, MERCEDES LAITA RUIZ DE ASÚA Y SERGIO ALONSO OROZA (Eds.) Publicaciones de la Asociación Española de Climatología (AEC), 2002, Serie A, nº 3. Planográfica Balear, Marratxí (Mallorca), xii+594 pp (in Spanish).
- ESTEBAN, P., MASES, M., MARTÍN-VIDE, J. (2002): Climatology for avalanche forecasting: Les Fonts avalanche of Arinsal, Andorra, February 8th of 1996. *Horitzó: Revista del Centre de Recerca en Ciències de la Terra* 2, 10-19 (in Catalan).
- ESTEBAN, P., JONES, P.D., MARTÍN-VIDE, J., MASES, M. (2005): Atmospheric circulation patterns related to heavy snowfall days in Andorra, Pyrenees. *International Journal of Climatology* 25: 319-329.
- FITZHARRIS, B.B. (1981): Frequency and Climatology of Major Avalanches at Roger Pass, 1909-1977. National Research Council, Canadian Association Committee on Geotechnical Research, Ottawa. 99 pp.
- GARCÍA, C., GAVALDÀ, J., MARTÍ, G., MARTÍNEZ, P., OLLER, P. (2000): Avalanche Bulletin. Winter 1995-1996. Institut Cartogràfic de Catalunya, Barcelona, 125 pp (in Catalan).
- HÄCHLER, P. (1987): Analysis of the weather situations leading to severe and extraordinary avalanche situations. International Association of Hydrological Sciences Publication, 162. 295-303.
- JANSÁ, A. (1990): Notes on meteorological mesoscalar analysis at lower levels. Instituto Nacional de Meteorología, 70 pp. (in Spanish).
- KALNAY, E., KANAMITSU, M., KISTLER, R., COLLINS, W., DEAVEN, D., GANDIN, L., IREDELL, M., SAHA, S., WHITE, G., WOOLLEN, J., ZHU, Y., CHELLIAH, M., EBISUZAKI, W., HIGGINS, W., JANOWIAK, J., MÓ, C.K., ROPELEWSKI, C., WANG, J., LEETMA, A., REYNOLDS, R., JEENE, R., JOSEPH, D. (1996): The NCEP/NCAR 40 years reanalysis project. *Bulletin of the American Meteorology Society* 77: 437-471.
- LACHAPPELLE, E.R. (1966): Avalanche forecasting. A modern synthesis. International Association of Hydrological Sciences Publication, 69. 350-356.
- LEFEVRE, C. (1998): Some characteristic situation. The Pyrenees. In: *La Meteorología de Montaña*, THILLET, J.J. (ed.). Ediciones MARTÍNEZ-ROCA. Barcelona:189-196 (in Spanish).
- McCLUNG, D., SCHAEFER, P. (1993): *The Avalanche Handbook*. The Mountaineers: Seattle
- MARTÍN-VIDE, J. BARRIENDOS, M., PEÑA, J.C., LLASAT, M.C., RODRÍGUEZ, R. (1999): Potenciality of the NAOi in the prediction of heavy precipitation in Spain. In: *Análisis*, GR 67, pp. 19-29 (in Spanish).
- MARTÍNEZ, P., OLLER, P. (2004): The avalanche accidents in Catalonia. I Jornades Tècniques de Neu i Allaus. Institut Cartogràfic de Catalunya, Barcelona, 4 pp (in Catalan).
- MOCK, C.J. (1996): Avalanche Climatology of Alyeska, Alaska, U.S.A. *Arct. Alp. Res.*, 28(4), 502-508.
- MUNTÁN, E., ANDREU, L., OLLER, P. GUTIÉRREZ, E., MARTINEZ, P. (2004): Dendrochronological study of the avalanche path Canal del Roc Roig. First results of the ALUDEX project in the Pyrenees. *Annals of Glaciology*, V. 38. 173-179.
- OLLER, P.; MUNTÁN, E.; MARTURIÀ, J.; GARCIA, C.; GARCIA, A.; MARTÍNEZ, P. (2006): The avalanche data in the Catalan Pyrenees. 20 years of avalanche mapping. Proceedings of the International Snow Science Workshop. Telluride, Colorado (USA). P. 305-313.
- OSBORN, T.J., BRIFFA, K.R., TETT, S.F.B., JONES, P.D., TRIGO, R.M. (1999): Evaluation of the North Atlantic Oscillation as simulated by a coupled climate model. *Climate Dynamics*, 15: 685-702.
- POTTER, JR.N. (1969): Tree-ring dating of snow avalanche tracks and the geomorphic activity of avalanches, northern Absaroka Mountains, Wyoming. *Geol. Soc. Amer. Special Paper*, 123. 141-165.
- SCHAEFER, P. (1986): Weather patterns for major avalanches. *The avalanche Review*, vol. 4, nº 3, 2 pp.
- VILLECROSE, J. (2001): Les avalanches de janvier et février 1999 dans les Alpes du Nord Françaises. *La Météorologie* 8° série, 32, pp. 11-22.

<http://www.icc.es>  
<http://www.wetterzentrale.de>  
[www.cru.uea.ac.uk/cru/data/nao.htm](http://www.cru.uea.ac.uk/cru/data/nao.htm)

## 8 Mathematical modelling of metamorphic structural evolution in the snow cover and soil

ELENA GUSEVA-LOZINSKI,  
Immenhoferstr. 38, D-70180 Stuttgart, Germany

### 1 Introduction

The proposed thermomechanical mathematical model uses meteorological data to simulate the snow-cover and soil characteristics for the purpose of clarifying the structural and physical-mechanical properties alteration in the stratified snow cover under changing weather conditions. This mathematical model is based on previous mathematical models for snow cover and soil (GOLUBEV AND GUSEVA 1987, 1989, 1990; GUSEVA-LOZINSKI 1997, 1998, 1999, 2000, 2001, 2006) and is the thermo-mechanical structural mathematical model for snow cover and soil layer. The structure and texture of snow are very sensitive to the temporal variations of the heat and mass transfer in snow cover and soil. Snow structure, texture and thermomechanical properties are a key to avalanche forecasting. Metamorphic processes include isothermal and temperature gradient parts. The result of these processes is the transformation of the surface shape crystals due to metamorphic processes within snow cover. This mathematical formalisation makes it possible to unite the main equation of snow cover with soil layer and allows it to differ between various forms of snow crystals like depth hoar, faceted crystals, skeletal, dendrite and over riming crystals, rounded - fine and coarse crystals and to calculate the changes of the forms of the snow crystals due to metamorphism - fresh deposited and old snow. The model allows it to retrace the thermomechanical and structural transformations inside of the snow cover and the evolution of the boundary's layer at the snow-soil boundary.

Snow cover formed in various meteorological conditions consists of some snow layers. The snow layers have different parameters like temperature, density, water vapour pressure, structure and mechanical properties. The mathematical nonlinear model (GOLUBEV AND GUSEVA 1987-1990; GUSEVA-LOZINSKI 1997-2001) includes the heat balance equation, the diffusion equation for water vapour migration, the densification, and the structural and strength relations in the snow cover and the layer of soil. This approach includes the mathematical description of the water vapour migration mechanisms in soil and water vapour migration between frozen soil layers - snow cover. The common equation for the water vapour migration in the snow cover and together with the water vapour migration in soil was used. Macro and micro diffusion coefficients for snow depend on temperature and snow porosity. The diffusion coefficients in soil depend on temperature, porosity and tortuosity. The definition of the tortuosity coefficient is based on the Magnus-

Thompson and the Laplace law. The sublimation of the frozen soil with relative big water vapour flux into the snow cover accelerates the depth hoar appearance at the soil-snow boundary and in the layer boundaries within the snow cover due to the mechanisms of water vapour transition that is temperature degree and different structure of layers. Using this approach I can calculate the water vapour migration from the frozen soil layer to snow cover with colder temperature. Mass transfer between the frozen or unsaturated unfrozen soil and snow cover accelerates the metamorphic processes and the depth hoar appearance at the soil-snow boundary and in the snow layer boundaries with various structural features within of snow cover.

### 2. Model description of the water vapour migration in snow cover and soil

The crystallization process of the snow grains, ice around of soil grains and metamorphism of the fresh snow (snowflakes-grain) involve changes to a state of lesser free energy.

The conditions controlling the crystallization are the over saturation of water vapour or super cooling of the initial medium contents of water vapour. The mathematical model (GOLUBEV AND GUSEVA 1987, 1989, 1990; GUSEVA-LOZINSKI 1997, 1998, 1999, 2000, 2001, 2001, 2006) includes the heat balance equation for temperature definition and the diffusion equation for water vapour pressure in all area of snow and soil. The equations of these model were combined with a shape parameter, for snow grains which depend on the temporal evolution of the properties of freshly deposited snow to grain (GUSEVA-LOZINSKI 1999) and equations for soil due to its type, structure, density and tortuosity (GUSEVA-LOZINSKI 2001,2001,2006).

The origin of the vertical axis  $x=0$  is defined in soil at a depth  $x=H^*$  from the surface,  $x=H$  is a boundary soil-

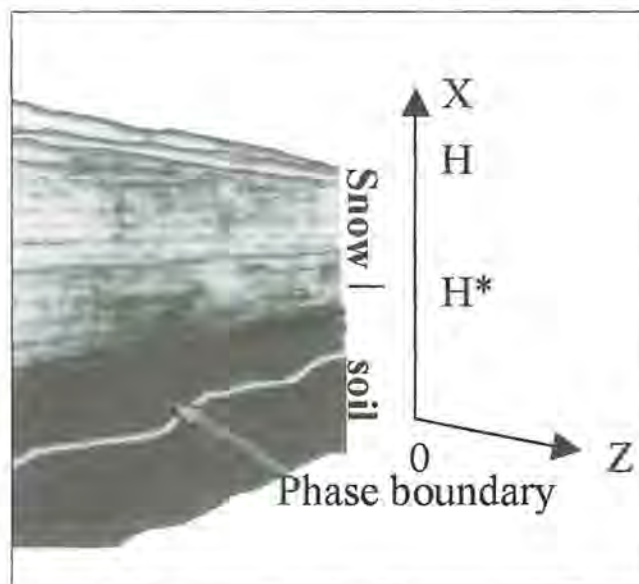


Figure 1: Scheme coordinate system of the snow cover - soil area.

snow and the horizontal axis  $z$  is parallel to the main slope direction. The snow cover consists of layers with various structural and mechanical properties due to precipitation depositions according to various weather conditions. The soil layer consists of various types of soil and can be in unfrozen or frozen state.

The heat balance equation is as follows:

$$C_i(\rho_i) \frac{\partial T}{\partial t} - C_a V_a \frac{\partial T}{\partial x} = \nabla \cdot (K_i(\rho_i) \nabla T) + f(x) + L_i j \quad (1)$$

where  $0 \leq x \leq H$  is thickness of the soil and snow cover,  $i$  is an index  $i = s$  for snow parameters and for soil parameters  $i = r$ ,  $K_i$  is the snow/soil heat conductivity coefficient,  $C_i$  is capacity,  $f(x)$  is the absorbed sun radiation distribution,  $L$  is the specific sublimation heat due to water vapour-ice sublimation-evaporation processes in frozen zone,  $\rho_i$  is a snow/soil density, and  $v_a$  is wind velocity, which is defined as airflow Darcy velocity. The local pore geometry controls the air flow through snow medium Darcy velocity, which is small that means about  $10^{-10} \frac{m}{s}$  without wind pumping and is limited by the first 0.2 m from the top of snow cover surface (BARTELT et al. 2004). At the snow surface and at the soil depth  $z=0$  the boundary condition for the heat flux is applied. At the vertical boundaries heat flux equals zero, due to symmetry. The origin of the vertical axis is set at the soil level, the Stephen's condition of heat balance is defined on the phase boundary in the soil (melted-frozen state) (GUSEVA-LOZINSKI 2001, 2006). The initial condition for the temperature is  $T(z, x) = f_i(t) / t = 0$ .

The rate of sublimation is defined by the diffusion equation for the processes, which depend on the temperature gradient and the structural parameters of medium in snow and soil:

$$j = \frac{\partial e_i}{\partial t} - \frac{\partial}{\partial z} \left( D_s^{ef} \frac{\partial e_i}{\partial r} \frac{\partial r}{\partial z} + D_s^{ef} \frac{\partial e_i}{\partial T} \frac{\partial T}{\partial z} \right) + \frac{\partial}{\partial x} \left( D_r^{ef} \frac{\partial e_i}{\partial r} \frac{\partial r}{\partial x} + D_r^{ef} \frac{\partial e_i}{\partial T} \frac{\partial T}{\partial x} \right) + s_f v_a \frac{\partial e_i}{\partial x} \quad (2)$$

where  $e_i$  is the average water vapour pressure in porous media, that is snow or soil,  $j$  is the sum of the condensation and evaporation part of the mass transfer in porous media above the common sublimation/evaporation surface  $s_f$  of the grains with radius  $r_i$  and bonds per grain averaging through one unit of volume,  $D_s^{ef}$  and  $D_r^{ef}$  - are diffusion coefficients in snow, which depend on temperature  $T$  due to diffusion through porous air space and on snow porosity due to diffusion caused by sublimation/evaporation ice on the opposite surfaces of ice grain. These coefficients correspond to the micro- and macro-diffusion (YOSIDA, 1963(13)) processes. The coefficients  $D_r^{ef}$  and  $D_s^{ef}$  are diffusion coefficients in soil layer, which depend on temperature and  $D = D_0 \frac{p}{g}$  (FROLOV 1976, GUSEVA-LOZINSKI 2001, 2006), the coefficient  $D_0$  is diffusion coefficient of water vapour in porous air,  $p$  is the porosity and  $g$  is the tortuosity coefficient,  $t$  is time. The porous air is fast saturated and has a temperature close to the temperature of ice grains (GRAY AND MALE 1981). The mathematical model in (BARTELT et al. 2004) is based on the temperature difference of porous air and snow grain, which is about 3°-5°C. The water vapour density depends on the temperature and it moves to the colder

zones because of the temperature gradient. It depends also on curvatures and surface composition of the ice grains. The water vapour density above ice-matrix elements with curvature  $r_s$  and with the coefficient of surface shape  $F^*$  at temperature  $T$  is defined by the Magnus condition for snow crystal (GOLUBEV AND GUSEVA 1987):

$$e_s(T, r) = e_s(T) (1 + \frac{F^*}{r}) \quad (3)$$

where  $F^*$  is a time dependent surface parameter. The state of fresh snow depends on the combination of wind conditions and on the initial types of deposited crystals. This parameter was defined for depth hoar layers and for fresh deposited snow layers. The surface shape parameter  $F^*$  varies between  $0 \leq F^* \leq 2 \times 10^{-5}$  for snow grains. The oversaturation above the central facets part of the crystal can lead to skeletal forms of crystal, which has a step composition in view of screw dislocation formation. The rapid crystal growth leads to a stepped surface of crystal due to the appearance of the screw dislocations (Fig.2). These steps move and can lead to even in bigger steps. The growth layers of this crystal skirts the screw dislocation and successively climbs up over each other. The stepped surface is formed according to that kind of dislocation in contrast to the crystal without screw dislocation.

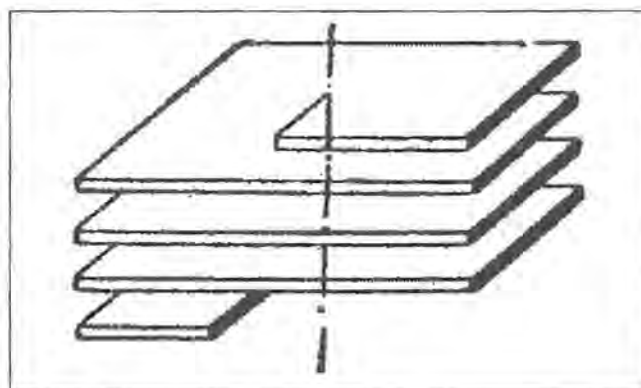


Figure 2: Scheme of screw dislocation.

The shape parameter takes into account the metamorphic changes from dendrites or the over riming snowflakes to rounded grain and stepped form of depth hoar surface. This parameter allow to consider in the model the additional water vapour pressure around faceted crystals like surface and depth hoar, dendricity and over riming of the fresh snow and rounded grains (GUSEVA-LOZINSKI 1999).

A similar equation was used for the water vapour pressure around soil particles in frozen soil, but soil medium varies from snow medium and it causes the difference in the definition of diffusion coefficients in soil layer. Soil medium can be imagined as mineral grain-soil particles -matrix with ice, gas, porous soil water and quasi-fluid adsorption film rounds soil particles, snow and ice crystals with various concentrations (FROLOV 1976).

In unsalted soil when the ion concentration is less than  $C_{cr}$ , ions interact with mineral matrix interior of the film and minimal values for sand and ice was defined

$v_{cr} = 10^{-3} - 10^{-1} \frac{m^2}{s}$  (SCORCELETTI 1979). Unfrozen water contents in frozen soil increase in accordance with ion types:  $Na_2CO_3 - Na_2SO_4 - NaNO_3 - NaCl$  (ERSHOV 1979). The equilibrium water vapour pressure around soil particles depends on the ion concentration in film: increase of ion concentration in film decreases the water vapour pressure around soil particle and ion concentration in film increase to the periphery direction. Salt contents and the film thickness depend on soil humidity and soil types and can be found in study (FROLOV 1976).

Using Raoul law, Vant-Goff law for a weak solutions and Henry law, it is possible to receive osmotic reduction of water vapour pressure around soil particle with film:

$$\Delta e_p = \frac{e_p}{\rho_w} p_m = \frac{e_p}{\rho_w} R T n_i = e_p(T) \frac{F''}{r_s}$$

where  $e_p$  is water vapour pressure,  $p_w$  is film water density,  $n_i$  is concentration of solute substance pro volume in mole. For example, water pressure above saturated solution of  $NaCl$  with  $T=0^\circ C$  is reduced to 76.3% and for  $MgCl_2$  reduced to 35% (RÖDEL 1994). Using Magnus-Thomson equation and Laplace law defined capillarity reduction. The total water vapour pressure above soil particle  $e_s(T, r)$  under account of the osmotic and capillarity pressure reduction was written in following form:

$$e_s(T, r) = e_p(T) \left( 1 + \frac{F'}{r_s} - \frac{F''}{r_s} + 2 \frac{\sigma \cos \theta}{r_s} \right) \quad (6)$$

where  $\sigma$  and  $\theta$  are parameters for Equation (1) depending on type and saturation of soil, the coefficient  $F''$  for frozen soils depends on its type.

The boundary conditions for Equation (1) are as follows.

1. At the snow surface heat flux was defined by way of evaporation from snow surface and turbulent heat exchange due to temperature difference between air and snow surface temperatures:

$$\left[ \alpha_a (T_a - T_s) + L E_s \right]_{x=H} = -k_s \left. \frac{\partial T}{\partial x} \right|_{x=H} \quad (7)$$

and the evaporation  $E_s$  from snow surface and from trees was defined as follows:

$$E_{s\sigma} = N_{\sigma} S_{\sigma} \left( \alpha_f B_f + b_f L_f \right) \left[ E_s + E_s^* \right] \left[ \alpha_f B_f + b_f L_f + 1 \right], \quad (8)$$

where  $E_s^* = j$  is rate of sublimation/condensation water vapour diffusion intensity from snow cover surface and it was defined using the distribution inside the snow cover (below tree or other vegetation),  $\alpha_a$  - is the coefficient of turbulent heat transfer in air above snow surface,  $T_a$  is air temperature above snow pack surface,  $L_f$  is an area parameter: a leaf/needle area index,  $B_f$  is a silhouette woody biomass area index,  $S_{\sigma}$  is a canopy area,  $B_f$  is parameter for deciduous trees ( $\alpha_f = 1, b_f = 0$ ) and  $L_f$  for conifer trees ( $\alpha_f = 0, b_f = 1$ )  $E_s$  is sublimation intensity and defined under supposition about horizontal homogeneity of neutral air boundary layer from the equation, which was written as follows (RÖDEL 1994):

$$E_s = -Sc \rho \kappa^2 \frac{(s(z_2) - s(z_1))(v(z_2) - v(z_1))}{\ln \left( \frac{z_2^2}{z_1^2} \right)} \quad (9)$$

where  $Sc \approx 0.45$  is Schmidt number for water vapour in air,  $\kappa = 0.4$  is Karman constant,  $z_1$  and  $z_2$  are two heights,

$s(z) = \frac{e_s}{e_s + \rho_a}$  is a specific air humidity,  $e_a$  is water density in air above snow surface  $z_1 \approx z_0$  (we suppose that  $e_s$  is constant in the surface layer with thickness  $z_0$ ) and  $s(z) = \frac{e_a}{e_a + \rho_a}$  is a specific air humidity in air at the height  $z_2$ ,  $\rho$  is a dry air density,  $v$  is an average horizontal air velocity and  $\frac{dv}{dz} \neq 0$ , and water vapour density  $e_s$  is defined by Magnus relation for curvilinear surfaces.

Equations (7-9) were used for the estimation of the forest surface sublimation because of wind weather conditions (GUSEVA-LOZINSKI 2001, 2006). The values of wind velocity  $v_x$  which was used for the calculation was limited by 15m/sec, because the trees crowns did not retain snow in windy conditions with bigger wind velocity.

2. Stephan's condition of heat balance was defined in soil at (unfrozen-frozen boundary).

3. At the depth of the soil layer we assumed the absence of heat and mass fluxes. At the vertical boundaries the area fluxes are zero due to symmetry. Water vapour pressure in soil or near the surface soil-snow can be defined as:  $e(T, r) = e(T) W_r$ , where  $W_r$  is the relative soil moisture according to soil type.

Additional surfaces of evaporation  $N_a$  like forest, shrubs, grass, or artificial surfaces of evaporation increase total evaporation and can be estimated with the formula  $E_t = E_s^* + (N_a + 1) E_s$ , where  $E_s^* = j$  is sublimation/condensation water vapour diffusion intensity from the snow cover surface. Sublimation part in windy conditions was estimated, using the Prandtl theory for thermal neutral layer (GUSEVA-LOZINSKI 2006). The water vapour diffusion intensity from the snow cover surface  $E_s^* = j$  was defined using its distribution inside of the snow cover and the air humidity over the snow surface which was defined with the aid of meteorological data.

The thickness of snow cover is defined through the variation of snow density and the quantity of fresh deposited snow. The equation of snow cover densification was used in this form (YOSIDA 1963, VOJTKOVSKY 1977) similar to the mathematical model in (GUSEVA-LOZINSKI 1997). The evolution of the structural parameters, the location changes of weak zones, and the snow pack strength on the mountain slope in a two-dimensional case as a function of heat-, mass-transfer parameters and the mechanical properties of snow were formulated and studied with numerical examples in (GUSEVA-LOZINSKI 2000).

### 3. The Definition of the tortuosity coefficient

Some studies discussed the role of free convection in soil. The value of Raleigh-Darcy index for water in porous soil with relative big size particle was estimated (GRIGORJAN et al. 1987). For porous medium index Raleigh-Darcy was used in following form:  $Ra = \frac{1}{\chi v} \alpha \cdot g \cdot \Delta T \cdot l \cdot k$ , where  $g$  is the acceleration of gravity,  $\Delta T$  is the temperature interval,  $l$  is a representative length of area,  $k$  is a coefficient of permeability of the porous medium,  $\alpha$  is the coefficient of the linear expansion,  $\chi$  is the thermal diffusion coefficient, and  $v$  is the

coefficient of the kinematical viscosity of fluid. Free convection in porous media begins if  $Ra > Ra^* \approx 1500-1700$ . For water in sand with thickness about 100m and  $\Delta T \approx 30^\circ C$   $Ra$  index means about  $Ra \approx O(1) \ll Ra^*$ . The tortuosity coefficient defines the lengthening of the vapour transport way. The values of the tortuosity coefficient depend on the type of soil. The water vapour migration in medium with relative big pores with  $r > 10^{-5} cm$  (micro- and macro-capillary medium) can be described by the law of Fick. The smaller pores are filled by water and do not participate in vapour transport.

The tortuosity coefficient  $g$  in soil was defined using the solution of the shortest trace approach (GRIGORJAN et al. 1987, GUSEVA 1981). The moisture flux chooses the optimal track and most of water flows this way (KOBUS et al. 1993). Hereby the Darcy law was used. For the definition of the mass transfer through fractured rock or through snow/firn it is necessary to know the permeability field. The mathematical approach consists of following parts:

1. Measurements of the concentration peaks and of time of travel of the solution peaks between two bores in 2-D high heterogeneous area. Experimental tracer tests were carried out in a fracture zone and were obtained using pulse tracer injection. These curves have multiple peaks. The behaviour of these multi-peaked curves was observed for a limited range of injection flow rates. Measurements show that the fluid flows in a non-uniform way in by a fracture and chooses its favoured paths. The arrival time and injection magnitude of a pulse in the pulse test were measured.
2. Using geostatistics numerical method for all possible 2-D permeability fields  $K_f^p$  were calculated, where  $p$  is quantity of different permeability distributions between two vertical bore measurements.
3. The optimisation method (OPT) of the 2-D permeability fields definition allows to choose the permeability field in agreement with measurements. Inside the 2-D permeability fields  $K_f^p$  was sorting and ranging the traces by means of mathematical optimisation method and using of the following criteria:

- a. transport time minimum  $t_j$  of the first arrival solute pulsation;
  - b. maximum result peak solution in the arrival bore;
- Using Darcy's law ( $v_f = -K_f^{gradh}$ ) and condition of hydraulic potential  $h$  with relative small changes of  $gradh$ : ( $|gradh| \leq H^*$ ) and criteria a or b, all possible flow traces for every  $K_f^p$  field were ranked.  $V_f$  is flow velocity,  $K_f$  is permeability coefficient and  $H^*$  is maximal value of  $gradh$ . An optimal trace (criteria a or b) was chosen for the every  $K_f^p$  field. All permeability fields were ranked.
4. Using an optimal trace and the field permeability the tortuosity coefficient was defined.
  5. The classical numerical simulation of the flow and mass-transport problem with chosen permeability field was made with the programs Modflow and Modpath based on the finite-differential approach. The model solves the system of coupled partial differential equations which describe a multidimensional water/solute flow through strongly heterogeneous porous media with Darcy law, solute transport equation and salt diffusion equation. The model and the programs Modflow and Modpath can be for the sake of shortness renamed as below in this article as the MM method.

The optimal pathway calculated by the OPT method for the area D with a length of  $x_N = 50 m$  and a thickness of  $z_M = 2.5 m$  is shown in Fig.3.a. The values of arrival time for every trace were calculated by the MM method and are shown in Fig.3.b. The tortuosity coefficient is illustrated in Fig.3 and was defined as follows:  $\tau = \frac{L_N}{x_N}$ , where  $L_N$  is a short-trace length for D.

This mathematical and numerical method (OPT) was extended and was thus applied for solving the shortest-path problem in various inhomogeneous mediums, such as: fractured rock, soil with water and various impurities, and the snow/ice network with water vapour.

The mathematical model for the snow/firn solves the system of coupled partial differential equations which describe a multidimensional air/water vapour flow through

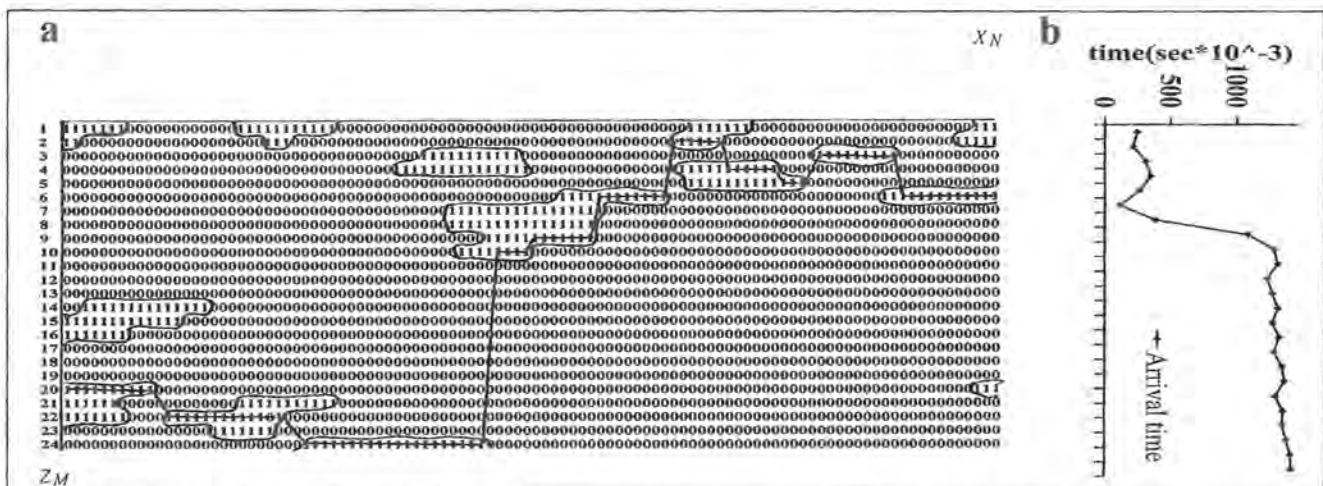


Figure 3: Optimal pathway in area D. with length 50m and thickness 2.50 m. a) Calculated pathway by OPT; b) Arrival time of flux by MM.

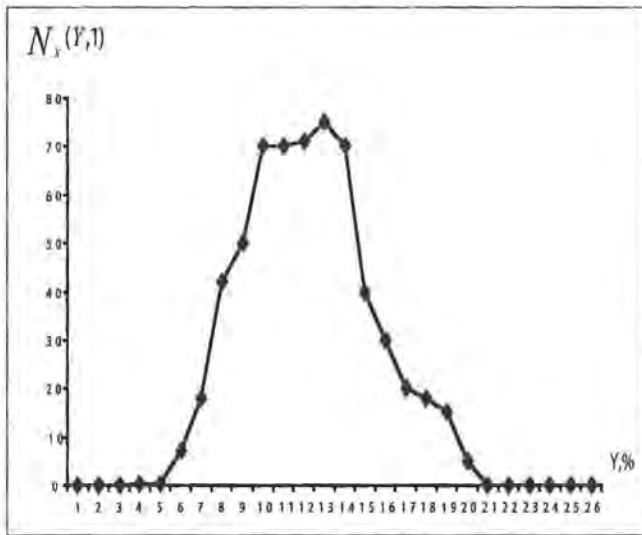


Figure 4: Function  $N_x(Y, I)$  for  $Y: 1\% \leq y \leq 26\%$  and  $I = \pm 1\%$  of the 300 different variants - permeability fields.  $K^P, 1 \leq \eta \leq 300$

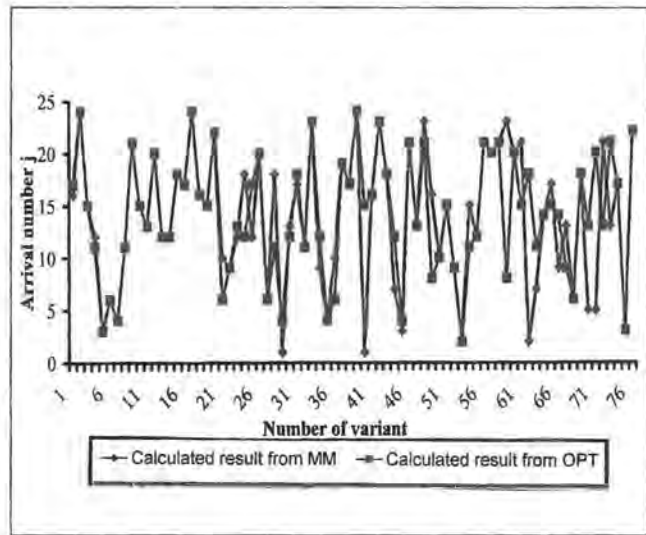


Figure 5: Comparison of calculated arrival numbers of lines in B2 computed by numerical methods MM and OPT.

strongly heterogeneous porous media with advective and diffusive heat transfer, including the effects of vapour transport and sublimation, structure of snow network including adsorption of the chemical species inside snow/firn.

The mathematical model allows the calculation of the distribution of water content in a glacier; the calculation of the snow/firn porosity; the impurity control in the porous soil with contaminated water; the minimal 'time-transport' searching of the contamination spreading inside inhomogeneous medium; the optimal spreading trace definition, and the tortuosity coefficient. This mathematical model was used for the definition of the optimal porous distribution and for calculating all parameters with this coefficients using finite-difference method.

The described method was applied for  $P=300$  permeability fields  $K^P, 1 \leq p \leq 300$  with  $N=100$  - columns and  $M=24$  - lines. The values of permeability coefficients were:  $K_1 = 3.8 \cdot 10^{-3} m/sec$ ,  $K_2 = 5.3 \cdot 10^{-5} m/sec$ . The sizes of the area D are:  $Z_M = 2.5m$ ,  $X_N = 50m$ . All 300 variants were analysed ac-

ording to ratio  $1\% \leq Y \leq$  of the sub-areas with high permeability to common area.  $I$  is an interval, where  $I = \pm 1\%$  applies. The distribution is shown in Fig.4. The short-time pathways were calculated by the geostatistical method OPT and finite-difference method MM. The results were compared.

The comparison was made on the part  $p^*$  of the fields with the similar ratio  $N_x$  of the high permeable sub-areas. The maximal quantity of the fields targets the value of  $N_x(Y, I) \approx 12\%$  and of  $p^*=76$ .

The errors decrease in calculations by OPT of the fields with the lower permeability ratio and with higher  $N_x(Y, I)$ . The comparison of the results shows the agreement of the arrival point  $B_2(Y, I)$  in 56 from 76 fields. The arrival points to  $B_2$  computed by numerical methods MM and OPT are shown in Fig.5. Some discordance in these curves came about through numerical instability of MM in these variants. The numbers of the variants calculated by OPT were reordered in sequence with regards to the transport time increase using (3) (Fig.6). A corresponding sequence computed by MM also increased but with deviations.

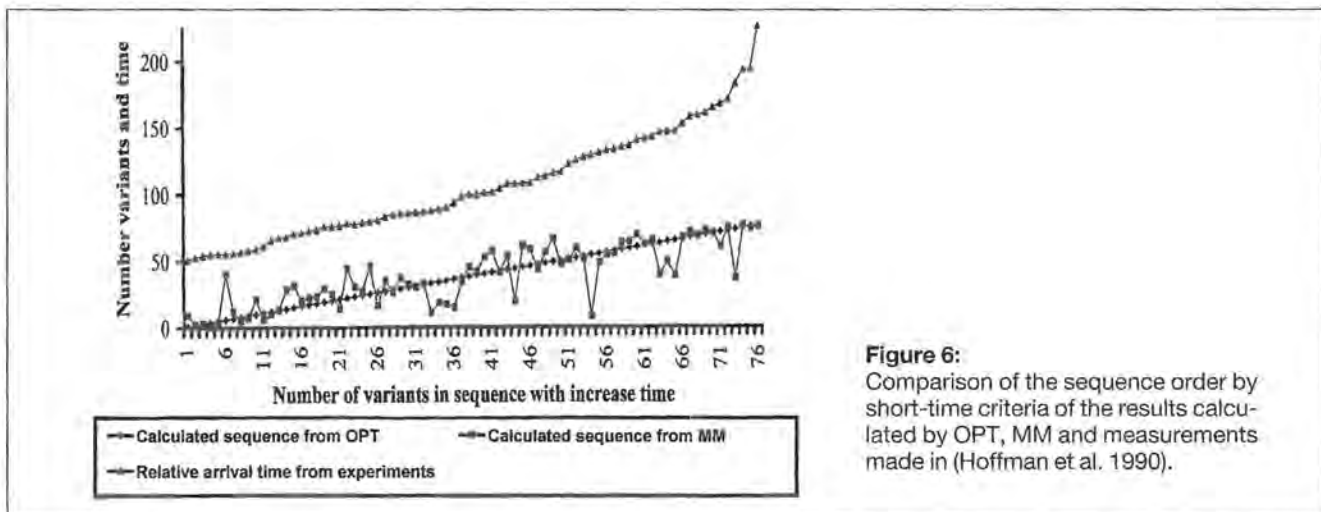
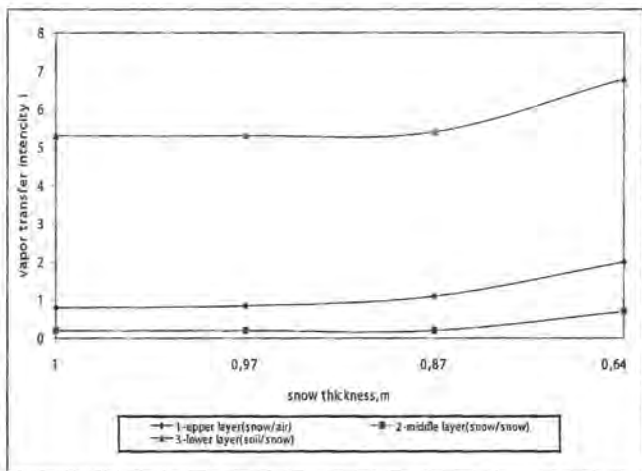
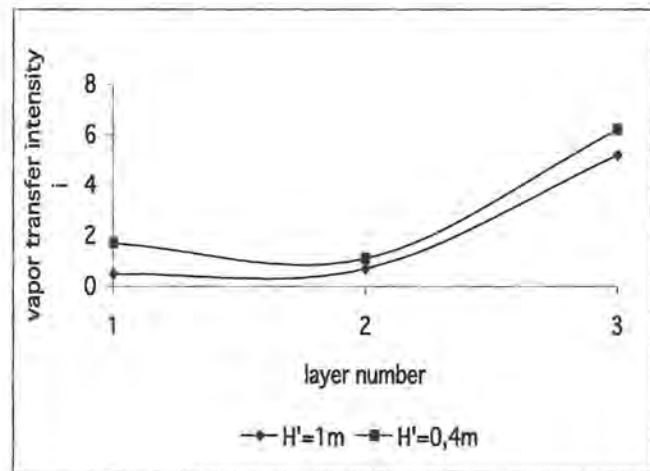


Figure 6: Comparison of the sequence order by short-time criteria of the results calculated by OPT, MM and measurements made in (Hoffman et al. 1990).



**Figure 7a:** A Vapour transfer intensity  $j = \frac{kg}{m^2 \cdot s} \cdot 10^{-4}$  interior of the snow cover for different thickness of snow cover. 1-3 are numbers of horizons inside snow.



**Figure 7b:** A vapour intensity distribution  $j = \frac{kg}{m^2 \cdot s} \cdot 10^{-4}$  with the snow depth for snow cover thickness: 1 m and 0.4 m.

The program was used to find the tracer transport in medium with highly heterogeneous hydraulic, and transport properties. The calculation results of finite-difference model and calculation results of optimisation model agree each other and with observations.

#### 4. Numerical examples

The structural mathematical model and data for calculations (GOLUBEV AND GUSEVA 1987, 1989, 1990; GUSEVA-LOZINSKI 1997 – 2006) was used for calculations of the processes interior snow cover and soil. The mathematical model and Prandtl approach (RÖDEL 1994; GUSEVA-LOZINSKI 2001, 2006) were used for the estimation of the surface sublimation because of wind weather conditions. A structural mathematical model of the mass and heat transfer of the snow cover includes empirical formulae for estimating the evaporation at the upper surface using the Prandtl approach. The mass transfer intensity interior of the snow cover with different thickness computed by mathematical model is shown in the Fig.7.a-b. The values of the vapour fluxes increase at boundaries inside of snow cover and snow-soil boundary.

The measurements of snow evaporation intensity from the snow cover surface  $i = \frac{kg}{m^2 \cdot s}$  (GOLUBEV AND SOKRATOV 1991, SOKRATOV AND SATO, MALE AND GRANGER 1979, SOKRATOV AND MAENO 2000, KAMATA et al. 1999) are calculated using the Prandtl approach for different conditions. Various values of the vapour intensity  $i = \frac{kg}{m^2 \cdot s} \cdot 10^{-4}$  from snow cover surface in just windless conditions were compared. The comparison of the calculated values using present model with the evaporation intensity in isothermal conditions (GOLUBEV AND SOKRATOV 1991), with the evaporation intensity measured in laboratory conditions (SOKRATOV AND SATO 2000), with observations values (MALE AND GRANGER 1979) show a close proximity of these values. The snow surface evaporation flux is

bigger by a factor of 10 than mass transfer fluxes inside snow pack with temperature gradients less than 140°C, and is about  $j = 0.86 - 6.45 \cdot 10^{-4} \frac{kg}{m^2 \cdot s}$  (SOKRATOV AND MAENO 2000). The measurement of the sublimation flux  $j$  evaporated from subsurface snow layer is  $j = 10^{-4} \frac{kg}{m^2 \cdot s}$  (KAMATA et al. 1999). The calculated result of the present mathematical model of flux evaporated from snow cover subsurface is about  $j = 0.4 \cdot 10^{-4} \frac{kg}{m^2 \cdot s}$  and flux evaporated from snow cover subsurface during winter period is about  $j = 0.35 \cdot 10^{-4} \frac{kg}{m^2 \cdot s}$  (MALE AND GRANGER 1979). Comparing laboratory experiment data, observations data, and calculation one can conclude that the sublimation intensity values calculated with the Prandtl approach correspond to real values.

#### 5. Conclusion

The mathematical model for mass and heat transfer was extended for soil area. Some numerical experiments were done using the complete model inside snow/soil cover and real data. Monitoring of the snow properties using the present mathematical model can be an important part of the avalanche warning service which requires the snow-cover mathematical modelling based on the detailed structural approach.

#### References

- BARTELT, P., BUSER, O. (2004): A nonequilibrium treatment of heat and mass transfer in alpine snowcovers Cold Regions Science and Technology vol. 39, 219-242
- ERSHOV, E.D. (1979): Wlagoperenos i kriogennye teksturi v dispersnykh porodah.[Moisture transport and cryogenic textures in dispersal grounds] M., Isd-vo Mosk. Un-ta. 214
- FROLOV, A.D. (1976): Elektricheskiye i uprugiyе svoystva merzlych poros i ldov [Electric and elastic properties of frozen earth materials] Puschchino, Fossiyskoy Akademii Nauk. Izdatelstvo Puschchinskogo Nauchnogo Soveta 513

- HOFFMAN, B., KOBUS, H., PTAK, T., SCHAD, H., TEUTSCH, G. (1991): Institut für Wasserbau/Kernforschungszentrum Karlsruhe: Abschlussbericht (1.Projektphase) -Testfeld WASSER/BODEN Teilprojekt II: Schadstofftransport in Untergrund, Erkundungs- und Überwachungsmethoden 1 Projektphase.
- GOLUBEV, V.N. AND GUSEVA, YE.V. (1987): Osobennosti teplo- i massoperenosa stratificirovannoy sneznoy tolsche [Features of the heat- and mass-transfer in stratified snowpack.] In: VOITKOVSKIY, K.F. AND DYURGEROV, M.B. (eds.): Snezhniyy pokrov v gorah i laviny. [Snowpack in mountain and avalanches.] Moscow, Nauka, Sibirskoye Otdeleniye, Institut Merzlotovedeniya, 62-73
- GOLUBEV, V.N. AND SOKRATOV, S.A. (1991): Snow evaporation in isothermal conditions [Isparenie snega v isotermiceskih uslovijah], Mater. Glyatsiol. Issled.71, 27-32
- GRAY, D.M. AND MALE, D.H. (1981): Handbook of snow. Pergamon press 751
- GRIGORJAN, S.S., KRASS, M.S., GUSEVA, E.V., GEVORKJAN, S.G. (1987): Kolicestvennaja teorija geokryologiceskogo prognoza [Quantative theory of geocryological prognosis] M., Isd-vo Mosk. Un-ta 265
- GUSEVA, E.V. (1981): Algorithm of the water-pumping optimisation from underground water reservoirs. Water research Akad.Nauk SSSR, Moscow, N3, 167-175
- GUSEVA, E.V. AND GOLUBEV, V.N. (1989): Thermomechanical mathematical model of the formation of the structure and properties of the snowpack Geojournal vol. 19(2), 193-200
- GUSEVA, YE V. AND GOLUBEV, V.N. (1990): Matematicheskaya model formirovaniya stroyenijja i svoystv sneznogo pokrova [Mathematical model of the properties and structure of the snowpack] Mater. Glyatsiol. Issled. vol.68, 18-26
- GUSEVA-LOZINSKI, E. (1997): Mathematical modelling of temporal changes in snow-firn properties in the cold period Ann. Glaciol., vol. 24, 309-313
- GUSEVA, E.V. (1998): Evolution of snow-firn properties: a thermomechanical approach. In: INAN, E. AND MARKOV, K.Z. (eds.): Proceedings of the 9 International Symposiums on Continuum models and discrete systems, World scientific, 29-38
- GUSEVA-LOZINSKI, E.V. (1999): Transformation of the snow crystal to a particle of ice. In: HUTTER, K. and others: Advances in cold-region thermal engineering and sciences, Springer, 387-394
- GUSEVA-LOZINSKI, E.V. (2000): Modelling thermomechanical properties of the snowpack. Ann. Glaciol., vol. 31, 309-313
- Guseva-Lozinski, E.V. (2001): Water vapour transport between soil and snow. Advances in cold-region thermal engineering and sciences. Proceedings of 7th International Symposium on Thermal Engineering and sciences for cold Regions, 125-132
- GUSEVA-LOZINSKI, E.V. (2001): Determination of pore connectivity as a function of pore size using mathematical approach. Advances in cold-region thermal engineering and sciences. Proceedings of 7th International Symposium on Thermal Engineering and sciences for cold Regions, 133-138
- GUSEVA-LOZINSKI, E.V. (2006): Structural mathematical model for snow and soil. Proceedings of III International Conference "Avalanches and related subjects", Kirovsk, Russia, September 4-8, 2006, in Print
- GUSEVA-LOZINSKI, E.V. (2006): Modelling snow-cover parameters in mountain forest-covered area and its using for avalanche proection constructions. Proceedings of III International Conference "Avalanches and related subjects", Kirovsk, Russia, September 4-8, 2006, in Print
- KAMAMATA, Y., SOKRATOV, S.A. AND SATO, A. (1999): Temperature and temperature gradient dependencies of snow recrystallisation in depth hoar snow. In: HUTTER, K. and others: Advances in cold-region thermal engineering and sciences, Springer, 395-402
- KOBUS, H., TEUTSCH, G. AND GUSEVA, E. (1993): Optimierungsverfahren zur Identifizierung bevorzugter Fließwege in heterogenen porösen Medien. Wissenschaftlicher Bericht Nr.93/16 (HG 182), Universität Stuttgart, Institut für Wasserbau, Lehrstuhl für Hydraulik und Grundwasser, 124
- MALE, D.H. AND GRANGER, R.J. (1979): In: COLBECK, S.C. AND RAY, M.: Modelling Snow Cover runoff U.S. Army Cold reg. Res. Eng. Lab., Hanover, New Hampshire, 101-124
- RÖDEL, W. (1994): Physik unserer Umwelt. Die Atmosphäre. Springer, 467
- SKORCELETTI, V.V. (1979): Teoreticeskaja elektrohimiija. Theoretical electro chemistry L.: Chemistry, 608
- SOKRATOV, S.A. AND SATO, A. (2000): Wind propagation to snow observed in laboratory Ann. Glaciol., 31, 427-433
- SOKRATOV, S.A. AND MAENO, N. (2000): The effective water vapour diffusion coefficient of snow under a temperature gradient Water Resource Res., vol. 36(5), 1269-1276
- SOKRATOV, S.A., SATO, A. AND KAMATA, Y. (2001): Water vapour in the pore space of snow. Ann. Glaciol., vol. 32, 51-58
- YOSIDA, Z. (1963): Physical properties of snow. In: KINGERY, W.D. (ed.): Ice and snow: properties, processes and applications. Cambridge, MA, M.I.T. Press, 485-527

## 9 Estimation of snow water equivalence using the polarimetric scanning radiometer from the Cold Land Processes Experiments (CLPX03)

LINGMEI JIANG<sup>1,2</sup>, JIANCHEN SHI<sup>3</sup>, SAIBUN TJUANJUA<sup>4</sup>,  
KUNSHAN CHEN<sup>5</sup>, LIXIN ZHANG<sup>1,2</sup>

<sup>1</sup> State Key Laboratory of Remote Sensing Science, Jointly Sponsored by Beijing Normal University and the Institute of Remote Sensing Applications of Chinese Academy of Sciences, School of Geography and Remote Sensing Science, Beijing Normal University, Beijing, 100875 China;

<sup>2</sup> Beijing Key Laboratory for Remote Sensing of Environment and Digital Cities, 100875 China

<sup>3</sup> Institute for Computational Earth System Science, University of California, Santa Barbara, CA 93106-3060 USA

<sup>4</sup> Wave Scattering Research Center, The University of Texas at Arlington, TX 76019-0016 USA

<sup>5</sup> Center for Space and Remote Sensing Research, National Central University, 32054 Chung-Li, Taiwan

### Abstract

In this study, we used a multi-scattering microwave emission model (DMRT-AIEM-MD) including the Dense Media Radiative Transfer Model (DMRT) and Advanced Integral Equation Model (AIEM) to simulate the dry snow layer emission with Matrix Doubling approach. This theoretical snow emission model was evaluated with data from two field measurements conducted in CLPX 2003 and in Switzerland in 1995 (JIANG et al. 2004, JIANG et al. 2006). Model comparisons showed that predictions from the DMRT-AIEM-MD emission model agreed well with the field measurements. A computationally efficient parameterized snow emission model was developed using the database generated by the DMRT-AIEM-MD emission model with a wide range of snow and ground properties under AMSR-E sensor configurations. Based on the parameterized model and the relationship of ground emissivity at different frequencies, we developed a physically-based snow water equivalence (SWE) inversion technique. Finally, we evaluated this physical estimation of SWE using both simulated data and PSR data from CLPX03. The results showed that the new developed inversion technique performs better than AMSR-E.

### 1. Introduction

Terrestrial snow cover is an important climate variable because of its influence on the surface radiative balance, and a significant hydrological variable since it acts as the frozen storage term in the water balance. Characterizing the patterns in regional snow cover and atmospheric triggers to their accumulation and ablation is the-

re more significant given the important role that snow cover plays in global energy and water cycles. Satellite passive microwave imagery has been used as a source of snow cover information because of all weather imaging capabilities, rapid scene revisit time, and the ability to derive quantitative estimates of snow water equivalent (SWE). Understanding, characterizing and predicting snow-related processes across spatial scale in coupled atmospheric and hydrological models requires improved capability for accurately monitoring spatial and temporal distributions of seasonal snow properties on land, especially snow water equivalence (SWE). Passive microwave remote sensing can provide useful information at large scale on snow cover characteristics for hydrological, climatic and meteorological applications.

The NASA Cold Land Processes Experiment (CLPX) was a multi-sensor and multi-scale experiment that focuses on extending a local-scale understanding of water fluxes, storage and transformations to regional and global scales. These campaigns involved one of the most intensive snow sampling efforts undertaken and used as the primary airborne sensor Polarimetric Scanning Radiometer (PSR), which is the first high-resolution (150-500 m) airborne multi-band microwave imagery of snow pack. The data collection of frozen and dry conditions used in this study was from Intensive Observation Period 3 (IOP3), including in situ data, PSR flight data, and Gamma SWE observations.

In this study, we firstly generated a dry snow emission simulated database using our multi-scattering emission model (DMRT-AIEM-MD) with a wide range of snow and underground properties for algorithm development purpose. Using this database and our parameterized model, we developed a physical inversion technique to estimate snow water equivalence. Finally, we demonstrated this technique both using simulated data and field experimental data from CLPX03.

## 2 Model Description

### 2.1 Theoretical model

Our multiple scattering model for microwave emission from dry snow uses the matrix doubling approach to include multiple scattering and combines the Dense Media Radiative Transfer Model (DMRT) (TSANG 1992) for snow volume scattering and emission, the Advanced Integral Equation Model (AIEM) for soil emission (CHEN et al. 2003a), and the interactions of microwave signals between snow and soil to calculate dry snow emission. This study utilizes dense medium radiative transfer (DMRT) model with quasicrystalline approximation (TSANG AND KONG 2001). The DMRT model predictions are in good agreement with numerical solutions of Maxwell's equations based on three-dimensional simulations (NMM3D), with laboratory controlled measurements (CHEN et al., 2003b), and with field measurements for a variety of snow depths, grain sizes and densities (TSANG et al. 2000, JIANG et al. 2004). Furthermore, theoretical modeling of surface emission and scattering has

also significantly improved. The Integral Equation Model (IEM) has demonstrated applicability to a much wider range of surface roughness conditions compared to conventional models. Recently, CHEN et al. (2003b) extended the original IEM and developed the Advanced Integral Equation Model (AIEM), by removing some weak assumptions in the original IEM model development. Comparisons of AIEM with NMM3D-simulated data (CHEN et al. 2003a) and field experimental data over the frequency range from 6 to 37 GHz (SHI et al. 2005) showed significantly better agreement than the original IEM model over a wide range of surface dielectric, roughness, and sensor frequencies. These efforts have established a fundamentally improved understanding of the effects of snow physical parameters and underlying surface dielectric and roughness properties on the microwave measurements of snow-covered terrain, making it possible to characterize microwave emission more accurately.

Vector radiative transfer theory (VRT), which is based on energy transport of partially polarized electromagnetic waves inside a medium, has been used for studying snow effects on microwave signatures. A snow-layer emission model based on VRT accounts for incoherent multiple scattering effects within the layer and the incoherent interactions between the volume and the layer surfaces (FUNK, 1994). The VRT equations for a snow layer can be solved numerically using the eigen-analysis technique or the matrix doubling (MD) method (ULABY et al. 1986). In terms of computation, matrix doubling is a more efficient method for layers that are optically thick, as is usual with snow.

## 2.2 The parameterized model

Through our analyses and comparison with the components of the 0th-order radiative transfer model, we developed our parameterized dry snow emission model that includes multiple scattering (JIANG et al. 2006)

$$E_{mp}^t = (E_p^v \cdot Cf_p^v + L_p \cdot (1 - E_p^v) \cdot Cf_p^{svs} E_p^s) \cdot \Psi_p \quad (1)$$

$$= (\text{Intercept} + \text{slope} \cdot E_p^s) \cdot \Psi_p$$

Here,  $E_{mp}^t$  is the total emissivity simulated by our multiple scattering model. The first term  $E_p^v \cdot Cf_p^v$  is the intercept determined in the linear regression analyses.  $E_p^v$  is direct snow volume emissivity in the 0th-order form.  $Cf_p^v$  is the multiple scattering correction factor that corrects for the difference in the direct volume emission signal between the 0th-order and the multiple scattering models:

$$Cf_p^v = a + b \cdot \omega + \tau' \cdot (c + d \cdot \omega + e \cdot \omega^2) \quad (2)$$

where  $\tau' = \tau / \cos(\theta_r)$  is the optical path length and where the coefficients  $a, b, c, d$  and  $e$  are determined by the linear regression analysis, see JIANG et al. (2006).

The second term in (1), excluding the underground emissivity  $E_p^s$ ,  $L_p \cdot (1 - E_p^v) \cdot Cf_p^{svs}$  represents the slopes determined by the linear regression analyses. The multiple scattering correction factor  $Cf_p^{svs}$  can be expressed as

$$Cf_p^{svs} = \exp[\tau' \cdot (A + B \cdot \omega) + \tau'^2 \cdot (C \cdot \omega + D \cdot \omega^2)] \quad (3)$$

Similarly, the coefficients  $A, B, C,$  and  $D$  are regression constants, see (JIANG et al. 2006). Furthermore, our previous work (JIANG et al. 2006) showed the RMSE of this parameterized model could reach  $10^{-3}$ .

## 2.3 Developing a physically-based inversion algorithm

If we assume the snow temperature and ground temperature are known, then we could get the snow emissivity from the observed brightness temperature. We rearranged eq. (1), then get the underground emission at given frequency as

$$E_p^s(f) = \frac{E_p^t(f) - \text{Intercept}(f)}{\text{slope}(f)} \quad (4)$$

where  $E_p^t(f), E_p^s(f)$ , are the total snow emissivity and subsurface emissivity. Intercept and slope only depend on snow emission and attenuation properties.

We characterized the relationship of the underground surface emission signals at the different frequencies and polarizations under AMSR-E sensor considerations to reduce the number of unknowns to describe the underground surface emission signals in the inversion model. We found that the surface emission at one frequency is almost linear dependent on the polarization difference at another frequency. Through our analysis of underground emissivity at different frequencies with AIEM model, we could derive the following linear relationship for different frequencies (Figure 1).

$$\begin{cases} E_p^s(X) = a(X, Ku) + b(X, Ku) \cdot E_p^s(Ku) \\ E_p^s(Ku) = a(Ku, Ka) + b(Ku, Ka) \cdot E_p^s(Ka) \end{cases} \quad (5)$$

Where  $a, b$  are regression coefficients depending on the snow density and frequencies. Using the equations of (5), we could remove the underground emission signals from the total emissivity.

The top of figure 1 shows the relationship of Ku-band with X-band, and the bottom shows the relationship of Ku-band with Ka-band. The left in figure 1 is for V polarization case, while the right is for H polarization. Based on the parameterized model, we could cancel out the underground surface emission component from the radiometer signals using the ratio of brightness temperature polarization difference at two frequencies. Therefore, at a given polarization and two frequencies, we could get

$$\frac{E_p^s(f1) - \text{Intercept}(f1)}{\text{slope}(f1)} \approx a + b \cdot \frac{E_p^s(f2) - \text{Intercept}(f2)}{\text{slope}(f2)} \quad (6)$$

Where  $f1, f2$  are different frequencies used for snow retrieval. This equation is only related to snow properties and total observed emissivity. After rearranging eq. (6), we get the following relationship:

$$E_p^s(f1) \approx A + B \cdot E_p^s(f2) \quad (7)$$

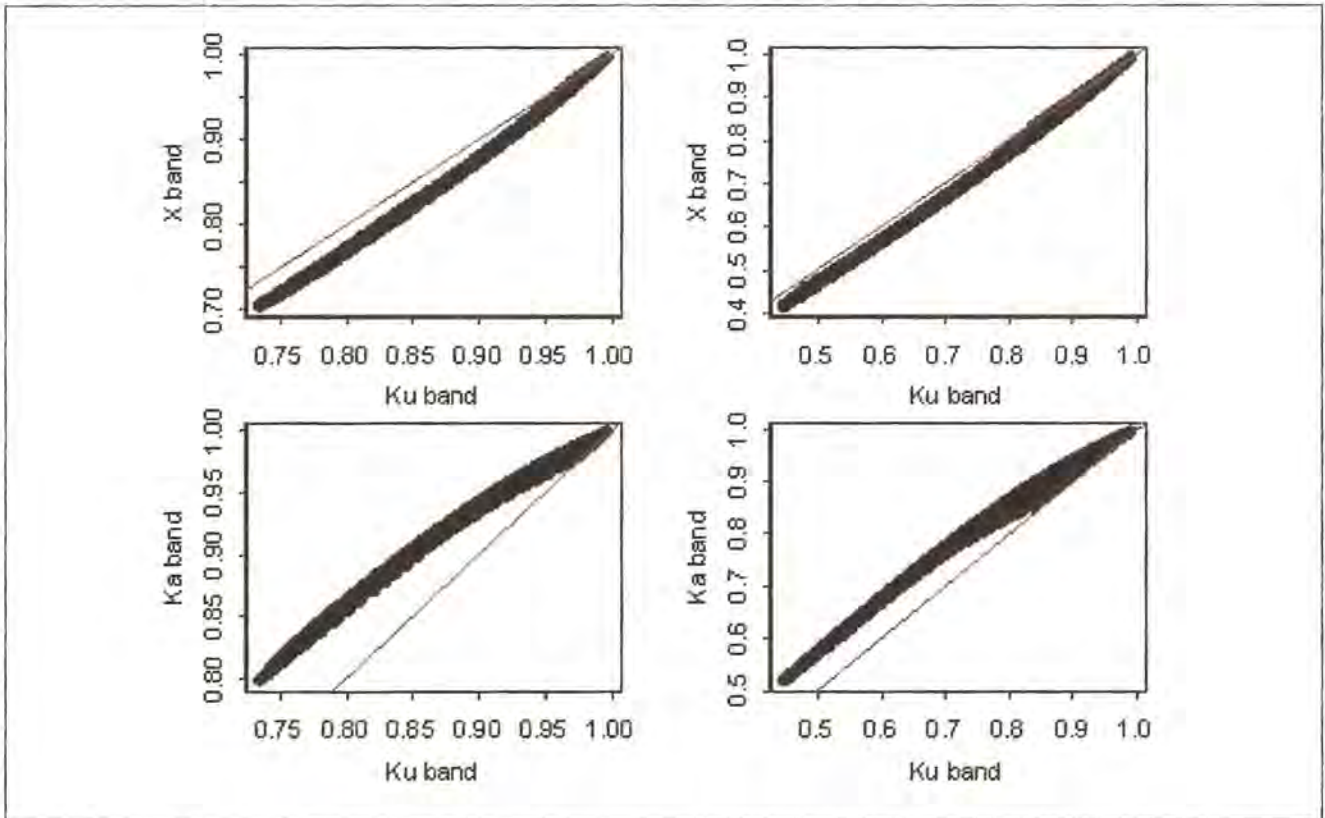


**Figure 1:** The relationships of underground surface emissions with snow cover at different frequencies simulated by AIEM model at 55° incidence angle.

Here  $A$  and  $B$  depended only on the snow properties. Since we assume the snow particles are spherical and randomly distributed in the snow pack,  $A$  and  $B$  are independent with the polarization. Therefore, with measurements at two polarizations and two frequencies, we could derive

$$B = \frac{E_v'(f_1) - E_h'(f_1)}{E_v'(f_2) - E_h'(f_2)} \quad (8)$$

$$A = E_p'(f_1) - B \cdot E_p'(f_2) \quad (9)$$

Where  $B$  is the ratio of brightness temperature polarization difference at two frequencies. In addition, with the simulated database, we obtained good relationships for  $A$  and  $B$  with SWE, respectively (Figure 2).

Based on the relationship of SWE with  $A$  and  $B$ , we developed a physical inversion technique to estimate SWE:

$$swe \approx \exp(a + b \cdot A + c \cdot A^2 + d \cdot \log(-\log(B))) \quad (10)$$

Also here  $a$ ,  $b$ ,  $c$ , and  $d$  are regression coefficients. This is a preliminary algorithm for SWE estimation over pure snow covered pixel.

We tested this inversion algorithm with simulated data first. Figure 3 shows the comparison of the retrieved SWE with the simulated data. The RMSE could be 0.034 m. The results showed this algorithm could estimate snow water equivalence in principal.

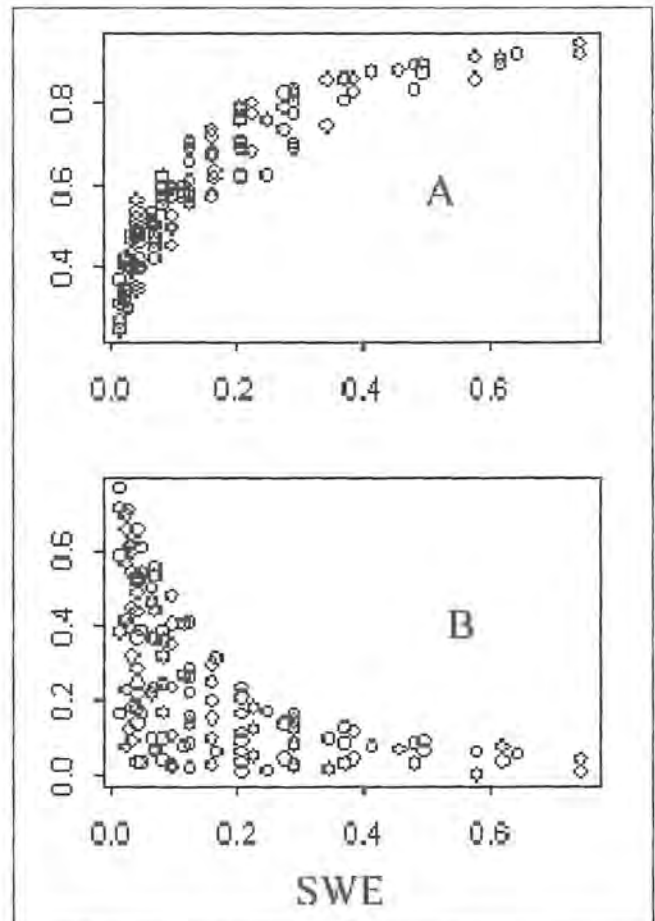


**Figure 2:** The relationship of SWE with  $A$  and  $B$ .

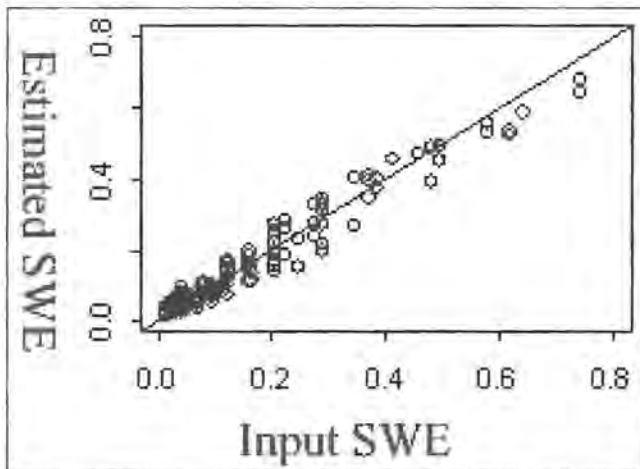


Figure 3: Comparison of retrieved SWE with the simulated data.

### 3 Testing the algorithm with data from CLPX03

#### 3.1 Snow pit data set used in this study

Snow pit data used in this study were collected during the Cold Land Processes Experiment at 2003 (CLPX03) investigations in northern Colorado and southern Wyoming, USA (CLINE et al. 2002). Snow pit data are presented in snow depth, snow density, grain size, wetness, canopy, the snow temperature, ground temperature et al. The snow pit measurements from North Park were applied in this study.

North Park is a broad, high-elevation parkland approximately 40 km in diameter. It has a mean elevation of 2499-m. Most of this Mesoscale Study Area (MSA) has very low relief. It has a total elevation range of 312 m, due largely to the presence of low foothills in the southeastern part in the MSA. This MSA also has very little forest cover. Most of the vegetation is sage-grassland, with willow along riparian areas. Snow packs in this area tend to be shallow and windblown, and are typical of prairie and arctic- and alpine- tundra snow covers 53% of the global seasonal snow cover (STURM et al. 1995).

#### 3.2 PSR airborne data

Data were collected using the NOAA Environmental Technology Laboratory (ETL) Polarimetric Scanning Radiometer (PSR) during a series of flights flown over the three CLPX mesoscale study areas (MSAs) in February 2002 (onboard a NASA DC-8 aircraft) and in February and March 2003 (STANKOV AND GASIEWSKI 2004). This airborne multiband conical-scanning imaging radiometer system provides multiband polarimetric brightness temperature images using AMSR-E bands, at a spatial resolution representative of the topography and vegetation cover.

The PSR/A system operated in conical scanning mode at an incidence angle of 55 degrees from nadir, the same as that of the AMSR-E instrument. Table 1 provides a summary of PSR/A scanhead channels,

There are 42 flights lines collected from Feb. 19 -25, 2003 during IOP3 at North park. In this test, we firstly selected the ground snow water equivalence data from the snow pits with dry snow and no canopy. Then, according to the lat/long information of ground points, we found the nearest PSR pixel close to ground measurements using the minimum least square searching method.

Table 1: PSR/A scanhead imaging bands, polarizations, and beam-widths.

Band (GHz)	Polarizations	Beamwidth <sup>1</sup>	$\Delta T_{rms} (K)^2$
10.6 - 10.8	v,h	8°	0.49
18.6 - 18.8	v,h	8°	0.49
21.4-21.7 (H <sub>2</sub> O)	v,h	8°	0.49
36 - 38	v,h	2.3°	0.14
86 - 92	v,h	2.3°	0.14
9.6 - 11.5 $\mu$ m IR	v+h	7°	0.43

<sup>1</sup> Half-power beam width  
<sup>2</sup> 18 msec equivalent integration time, v & h

#### 3.3 Testing algorithm

Snow cover is identified by the scattering of high frequency microwaves from ice particles and by the fact that scattering reduces high frequency brightness temperature (TB) measurements relative to the lower frequency measurements. Based on this theory, we could

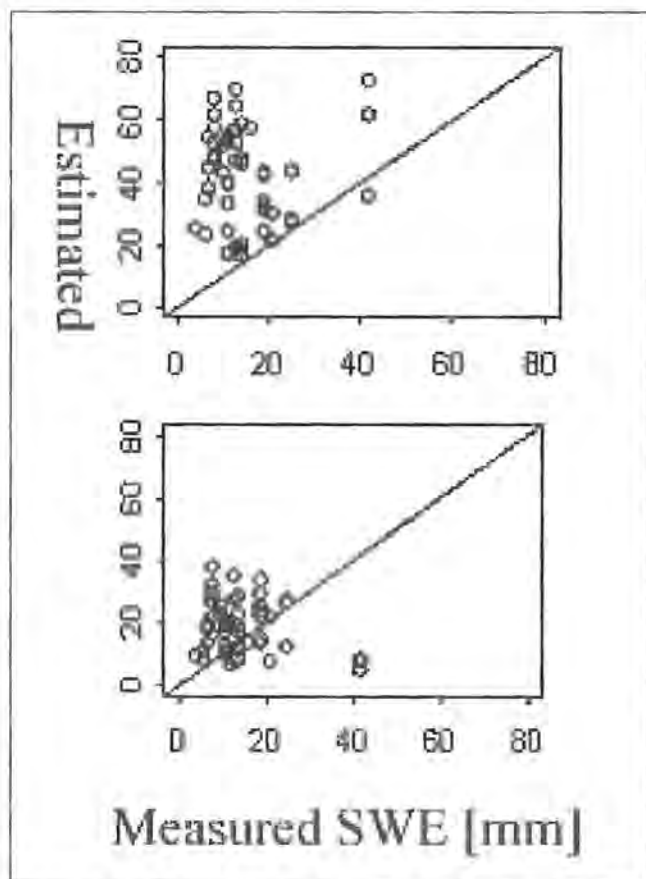


Figure 4: The comparison of different inversion technique to estimate SWE over North Park (left: AMSR-E algorithm; right: new technique).

estimate the snow water equivalent (SWE). AMSR-E baseline algorithm was used the formula  $SWE = 1.59 (TB_{18.7} - TB_{37})$  (mm) (CHANG et al. 1987) to calculate SWE over North Park on IOP3, 20-25 February 2003.

Figure 4 shows the comparison of different inversion technique to estimate snow water equivalence using the measurements over North Park in CLPX03. The left (Fig. 4) tests the linear regression inversion model used from AMSR-E, while the right of figure 4 showed the comparison result with the new technique developed in this study. From the comparison, we could see that both these two techniques overestimated the ground measurements. While the new technique performed better than AMSR-E did over North Park.

#### 4. Conclusion

In this study, we developed a physical inversion technique to estimate snow water equivalence. This algorithm showed better results than AMSR-E algorithm did, although both of these two techniques overestimated the ground measurements of SWE. These are preliminary results for developing physically-based inversion technique. We further need to consider inhomogeneity effects of passive mixed pixel, and consider complex topography effects on snow water equivalence retrieval algorithm.

#### Acknowledgements

This work has been supported by the National Natural Science Foundation of China (90302008), and supported by Program for Changjiang Scholars and Innovative Research Team in Beijing Normal University.

#### References

- CHANG, A.T.C., FOSTER, J.L. and HALL, D.K. (1987): Nimbus-7 derived global snow cover parameters. *Ann. Glaciol.*, vol. 9, pp. 39-44.
- CHEN, K.S., WU, T.-D., TSANG, L., LI, Q., SHI, J. and FUNG, A.K. (2003a): Emission of rough surfaces calculated by the integral equation method with comparison to three-dimensional moment method simulations, *IEEE Transactions on Geoscience and Remote Sensing*, 41(1): 90-101, doi: 10.1109/TGRS.2002.807587.
- CHEN, C.T., TSANG, L., GUO, J., CHANG, A.T.C. and DING, K.H. (2003b): Frequency dependence of scattering and extinction of dense media based on three-dimensional simulations of Maxwell's equations with applications to snow, *IEEE Trans. Geoscience and Remote Sensing*, 41 (8), 1844-1852.
- CLINE, D., ARMSTRONG, R., DAVIS, R., ELDER, K. and LISTON, G. (2002, Updated July 2004): CLPX-Ground: ISA Snow Pit Measurements. Edited by M. Parsons and M.J. Brodzik. Boulder, CO: National Snow and Ice Data Center. Digital Media.
- FUNK, A.K. (1994): *Microwave Scattering and Emission Models and their Applications*, Artech House, Boston, 573 pp.
- JIANG, L., SHI, J., TJUATJA, S. and CHEN, K.S. (2004): A comparison of dry snow emission model with field observations, *Proceedings IGARSS 2004*, 6: 3709-3712, doi: 10.1109/IGARSS.2004.1369926.
- JIANG, L., SHI, J., TJUATJA, S., DOZIER, J. and CHEN, K.S. (2006): A parameterized multi-scattering model for microwave emission from dry snow cover, *Remote sensing of environment*, 2006 (in press).
- SHI, J., JIANG, L., ZHANG, L., CHEN, K.-S., WIGNERON, J.-P. and CHANZY, A. (2005): A parameterized multifrequency-polarization surface emission model, *IEEE Transactions on Geoscience and Remote Sensing*, 43(12): 2831-2841, doi: 10.1109/TGRS.2005.857902.
- STANKOV, B. and GASIEWSKI, A. (2004): CLPX-Airborne: Multi-band Polarimetric Scanning Radiometer (PSR) Imagery. Boulder, CO : National Snow and Ice Data Center, Digital Media.
- STURM, M., HOLMGREN, J. and LISTON, G.E. (1995): A seasonal snow cover classification system for local to global applications. *Journal of Climate*, 8, 1261-1283.
- TSANG, L. (1992): Dense media radiative transfer theory for dense discrete random media with particles of multiple sizes and permittivities. *Prog. Electromag. Res.* 6, 5, 181-225.
- TSANG, L., KONG, J.A. and DING, K.H. (2000): *Scattering of Electromagnetic Waves, Vol. 1: Theory and Applications*. Wiley Interscience, 426 pages.
- TSANG, L. and KONG, J.A. (2001): *Scattering of Electromagnetic Waves, Advanced Topics*, Wiley-Interscience, New York, 432 pp.
- ULABY, F.T., MOORE, R.K. and FUNG, A.K. (1986): *Microwave Remote Sensing: Active and Passive, from Theory to Applications*, Artech House, Boston, 1120 pp.

## 10 Comparison of several sets of modelled and analysed precipitation fields over the French Alps. Impact of different spatial resolutions

LAURENT MERINDOL, YVES DURAND,  
GILBERT GUYOMARC'H

Météo-France / CNRM / CEN, 1441 rue de la piscine,  
38400 St Martin d'Hères, France

### Abstract

Since the nineties, Météo-France has been developing software named SAFRAN in order to produce relevant parameters for a snow cover evolution model named CROCUS. SAFRAN could be described as an objective interpolator and analysis tool for meteorological information for all our massifs. These massifs are considered to be homogeneous in terms of daily precipitation. Each massif represents an average area of about four hundred square kilometres and has a vertical extension between two and three thousand meters. The elevation range is divided into steps of three hundred meters in the French Alps and the Pyrenees. Another vertical step can be chosen. The current vertical step has been defined to avoid under-determination in the analysis scheme.

The analysis version of SAFRAN merges meteorological model output and observations (ground surface, radiosounding, etc.) while the forecast version of SAFRAN runs more like a downscaling operator and uses statistical methods in order to calculate unbiased daily precipitation and also to reduce the main standard deviation errors.

In this paper, we present some comparisons from the French Alps which have been divided into twenty-three massifs. This work focuses on daily precipitation, and mainly two meteorological output sets are used:

- The first one provided by ARPEGE.
- The second one by ALADIN.

Concerning ALADIN, two spatial definitions are extracted from archives, a coarse one similar to an ARPEGE extraction with a latitude-longitude grid mesh of around seven kilometres and a fine one twice as precise in both directions.

The daily data set of ARPEGE and ALADIN ("coarse extraction") is composed of nearly two thousand days and starts on the 27 of December 2000.

The daily data set with ALADIN ("fine extraction") starts on the 18 of March 2004 giving approximately eight hundred days for comparisons in terms of spatial definition input.

Firstly, using some basic statistical criteria, both temporal and spatial forecast errors are discussed. The errors in this section are defined as differences between forecast and analysis. Then, the spatial structures of errors are considered.

In the second part, we use the future numerical model AROME, a new non-hydrostatic model, for the case study. This model is planned to be the operational model at Météo-France for the year 2008.

### Introduction:

#### Part 1: Statistical part

#### 1. Presentation of the models and tools used

##### i. SAFRAN

The model SAFRAN has been used and updated since 1991 at the centre of snow studies CEN / Météo-France. This model is based on both optimal interpolation and variational methods. SAFRAN principally uses two information sets, one from a meteorological numerical model, like a prior estimate, named here "guess field", one from various ground and altitude observations. The results obtained are a new set of analysed parameters over the analysed area with meteorological consistency and with the "best" of all the available information sources taken into account. This procedure also makes it possible to scan all observations and to have an automatic procedure to reject a part of those considered as erroneous.

The basis for the output of the SAFRAN model is defined in terms of massif elevation and aspect. Concerning the French Alps, there are 23 massifs; the elevation is discretized into 300m steps. The vertical range varies between two and three thousand meters depending on the massif. The aspect is discretized as "flat", "North", "East", "South", and "West". Following CLÉMENT (1979), for the daily precipitation, the massifs are considered as climatologically homogeneous, so the daily precipitation is the same for each aspect. The other SAFRAN output data not studied in this paper are temperature, wind speed and direction, humidity, cloudiness, and radiation (three kinds). We use an hourly time frame for output. In this study, daily precipitation is used because most of the precipitation observations for the French Alp massifs are based on two observations per day, one in the morning at 8 a.m. local time, and one in the afternoon at 1 p.m. local time. See figure 1.

We want to identify the main advantages or disadvantages of each model according to input, and not to test our hourly temporal interpolation scheme.

After this general presentation of the SAFRAN analysis model, see DURAND (1993) for more details, each input model used for the SAFRAN "guess" is described briefly here.

##### ii. ARPEGE

Since the end of the eighties, this model has been used for operational needs at Météo-France. It was a joint development project with the ECMWF's team. ARPEGE uses a highly stretched grid. The grid for ARPEGE is more precise over the pole of interest (~30 km) than over the antipode (~300 km). Both models are global. The main physical equations are solved by a spectral repre-

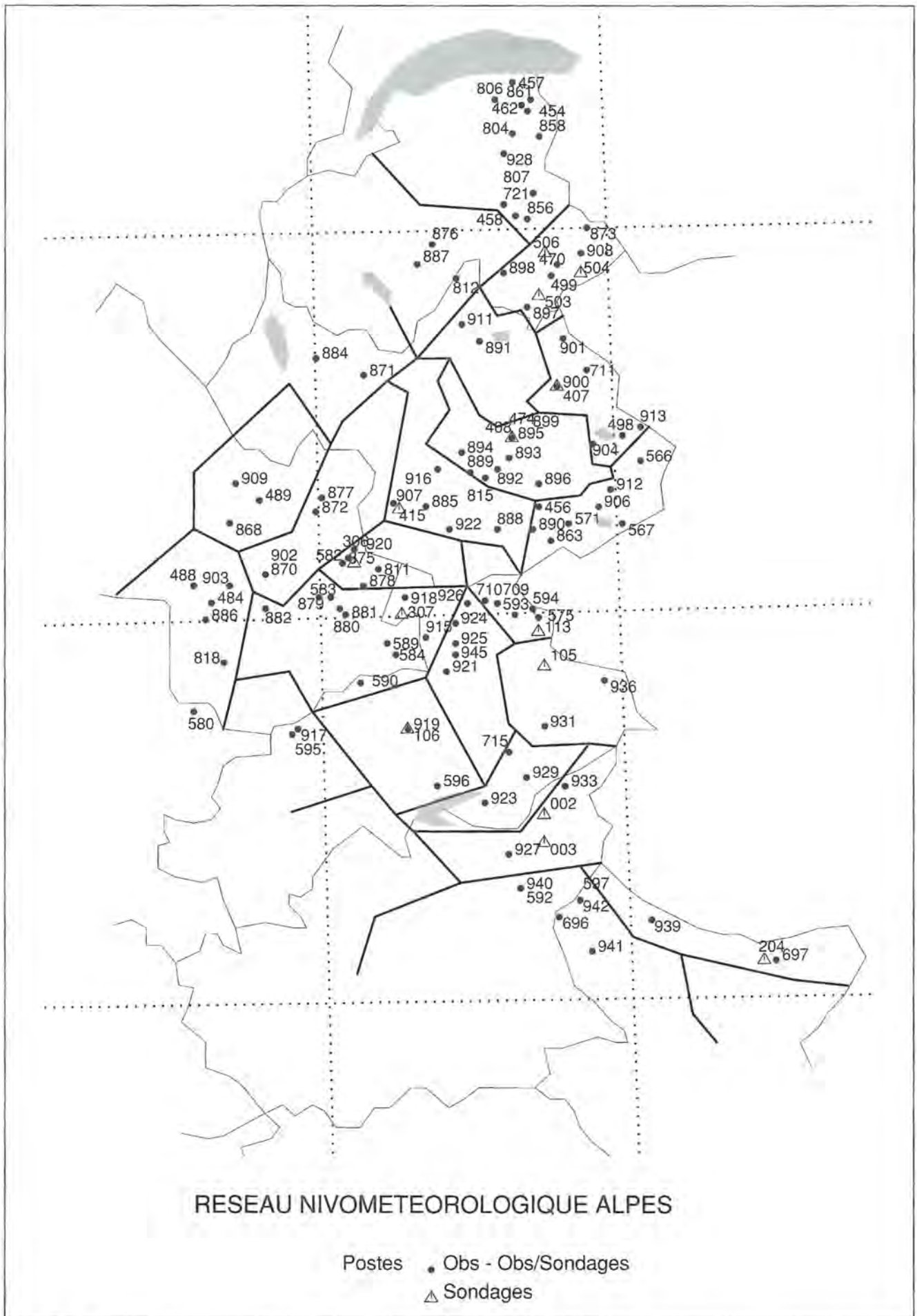


Figure 1, with observation points and border massifs.

sentation. At the current time, the number of vertical levels is 41. Near the ground, the levels are denser than in the upper part of the atmosphere. The orography under the ARPEGE model represents the main features influencing the synoptic atmospheric circulation with quite good accuracy, like the Alp barrier or the Rhone valley. On the contrary, the "sillon alpin" between Grenoble and Chambéry, is not represented and so local effects like Foehn can not be simulated. See the figure 2 to visualize the orography used by ARPEGE in our zone.

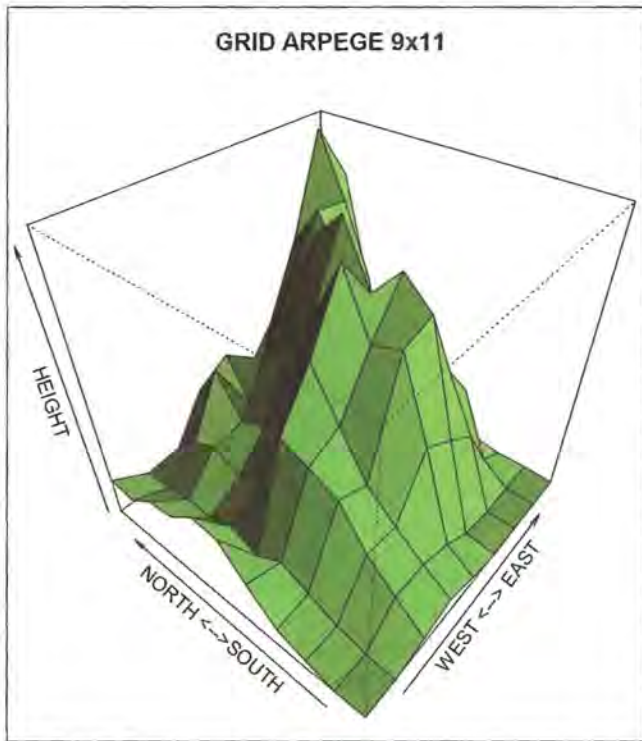


Figure 2, orography ARPEGE 9 x 11

### iii. ALADIN

ALADIN is a limited area model. The boundary conditions are given by ARPEGE every six hours. In the operational version, the hydrostatic assumption is used. In our study, we used two kinds of extractions from the ALADIN model. The first one is the same as with ARPEGE and the second one is twice as fine for latitude and longitude. See the following chapter concerning the data sets for more details.

## 2. Data sets and statistical tools used

### i. grid 9 x 11

Over the French Alps, we choose a regular longitude-latitude grid with 99 verticals, covering the whole French Alps and the surrounding area. The main characteristics of this extraction are a  $0.375^\circ$  step in longitude and a  $0.5^\circ$  step in latitude. For each vertical, from ground to 500hPa, the following parameters: atmospheric pressure, geopotential, temperature, zonal wind, meridian wind, humidity are taken at each model level and standard level. Precipitation exists only at ground level. This grid is used with both the ARPEGE and ALADIN models. What we call "coarse ALADIN", is when this

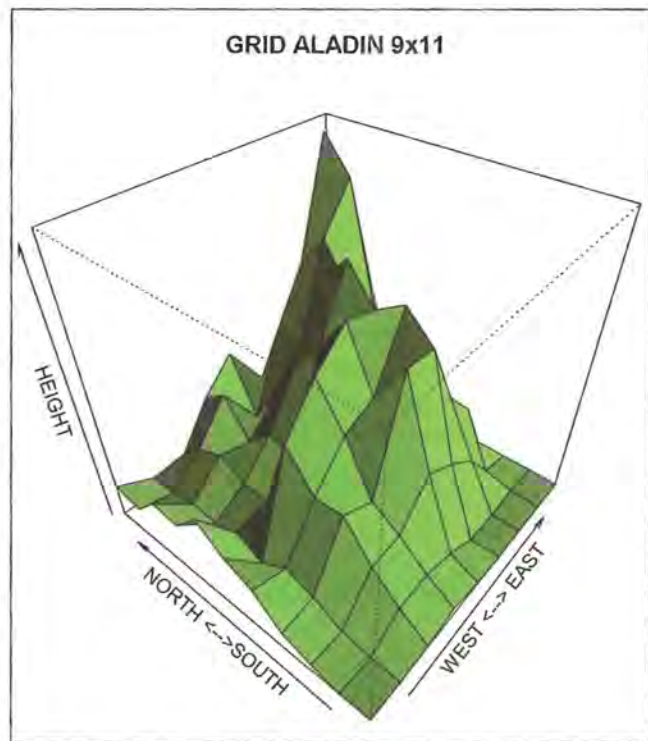


Figure 3, orography ALADIN 9 x 11

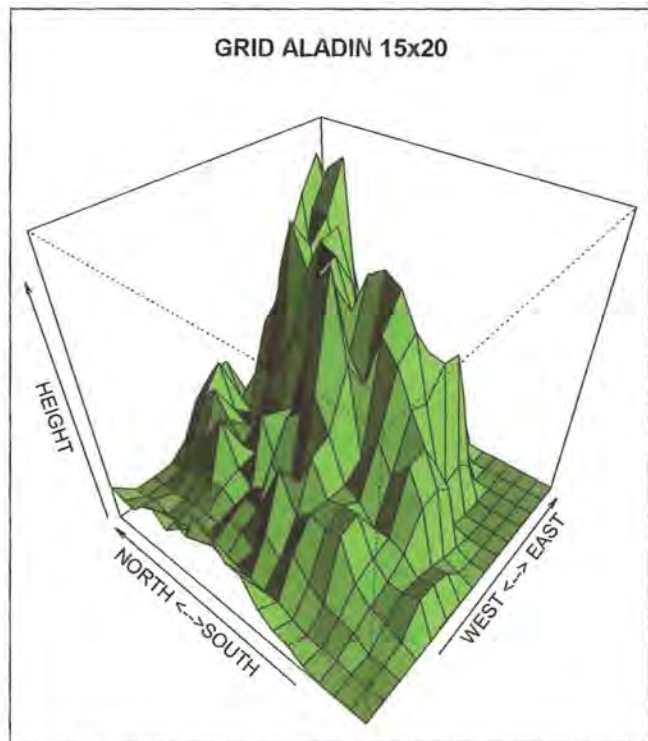


Figure 4, orography ALADIN 15 x 20

9x11 grid is used. See figure 3 to visualize the ALADIN orography representation with this grid.

### ii. grid 15x20

In the same way, we extract a regular longitude-latitude grid with 300 verticals, covering nearly the same zone as the previous one. The latitude step is now  $0.2^\circ$  and the longitude step  $0.3^\circ$ . The same parameters are extrac-

ted. This grid is used only with the ALADIN model. Hereafter, these fields are called "fine ALADIN" when this 15x20 grid is used. See figure 4, to visualize the ALADIN orography with the finer extract.

### iii. temporal view

For each day, the data sets consist of the analysis and one of the forecasts available. The analysis part is the output from SAFRAN with the amount of precipitation in mm for each massif. The forecast part is the output from the ARPEGE or ALADIN models. The value given for each massif is a mean value after an interpolation between the verticals inside and surrounding each massif. The value used in each vertical is obtained for cumulative precipitation from a 30-hour forecast minus the forecast after the first 6 hours. We used the forecast starting at 0h00. So we obtain, a daily forecast between 6h00 and 6h00 the next day in mm per day for each massif. Figure 5 illustrates the temporal view of the different available data sets.

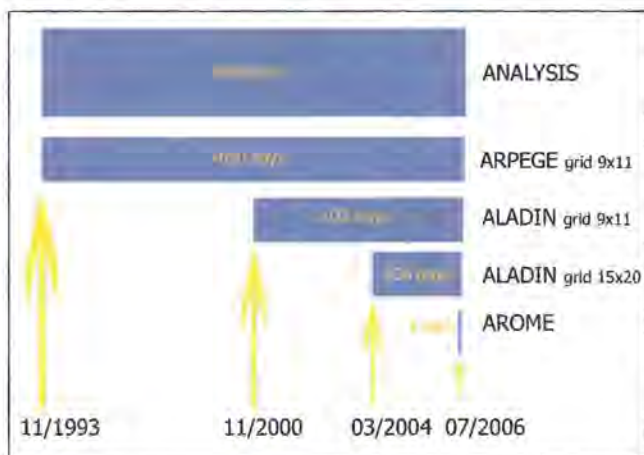


Figure 5, temporal view of data sets.

### iv. statistical criteria

We use some statistical indexes like bias as a position parameter, root mean square (RMS) as a dispersion parameter and correlation ( $R^2$ ) as an association parameter. However, in this part, we shall also focus on another index based on a contingency table less frequently used than the previous ones, defined by ROUSSEAU (1980) and noted  $I_R$ . In a 2x2 contingency table as in table 1:

Table 1

	Precipitation observed	No precipitation observed
Precipitation simulated	a	b
No precipitation simulated	c	d

We can define, if N is the total number of observations:

- the observed frequency by  $F_{obs} = (a+b)/N$
- the forecast frequency by  $F_{for} = (a+c)/N$ .

The ROUSSEAU index is then defined by:

$$I_R = 1 - ((b+c)/N) / (F_{obs} + F_{for}) (1 - F_{obs} - F_{for})$$

$I_R$  varies between -1 and 1. If the forecast follows the observed climatology, then  $I_R=0$  and we have  $I_R=1$  for a perfect forecast. This statistical index is stricter than a

traditional index on a contingency table such as the "success index". Another advantage is the neutrality of this index in terms of false alarms and non-detection. If we obtain, a value of  $I_R$  greater than 0.5, the detection of the phenomenon is very good. This index could be generalized to a contingency table with more categories.

### 3. General results on data sets

First, we show in figure 6, an operational real-time evaluation; on the Y axis, there is the correlation  $R^2$  between the model used and the SAFRAN analysis. This correlation is calculated for all the massifs with an averaged moving window of three months. Since the beginning of October 2002, "coarse ALADIN" has replaced ARPEGE previously used as "guess" since the beginning with the same 9x11 grid extract. We can observe an annual cycle, namely, every summer the correlation decreases. One reason is the difficulty to correctly represent convective precipitation in a mountainous region. With ALADIN (yellow bars), we have a better correlation in winters but a slightly worse one in summer. Very often ALADIN over-reacts on rainy summer days. In the following part, we concentrate our comparisons on a common period (in pink in figure 5), to allow global comparisons to be made. And, because our centre is mainly devoted to avalanche forecasting, we have focused on "winter" periods defined as all the months from October to March. The sample is thus composed of 363 days.

### 4. Comparison ARPEGE / ALADIN 9 x 11 / ALADIN 15 x 20

In the following table, the results obtained from the common "winter" sample of 363 days covering the twenty-three massifs in the French Alps are shown. The first block column gives the bias for the three types of input data respectively ARPEGE, coarse ALADIN and fine ALADIN. The second block gives the RMS and the third, the results for the Rousseau Index.

It can be observed that for the bias criterion, the ARPEGE input gives the best results. Globally, for this model, the bias is slightly negative for the Pre-Alps and positive otherwise. With the ALADIN input, the bias is greater and more chaotic especially with the 15x20 grid. But in the SAFRAN process of analysis, this climatological behaviour of the input guess could be partly filtered afterwards by a seasonal statistical adaptation. We find relatively speaking the same features for the RMS criteria. Concerning the ALADIN 9x11 grid, we have a block in the western part of the Alps with a too high RMS (Vercors, Oisans, Dévoluy). On the other hand, we can observe, that the shape of the precipitation field, in terms of rain/no rain, is better with the finer spatial definition given by ALADIN 15x20 as seen by the Rousseau Index block. This fact is more evident near the central part of the French Alps, near the Swiss and Italian borders.

### 5. First Conclusions

The better reactivity with a limited area model such as the ALADIN grid 15x 20 is obtained at a high cost in terms of bias or RMS, but with a better shape of precipitation fields. So, careful statistical adaptations must be

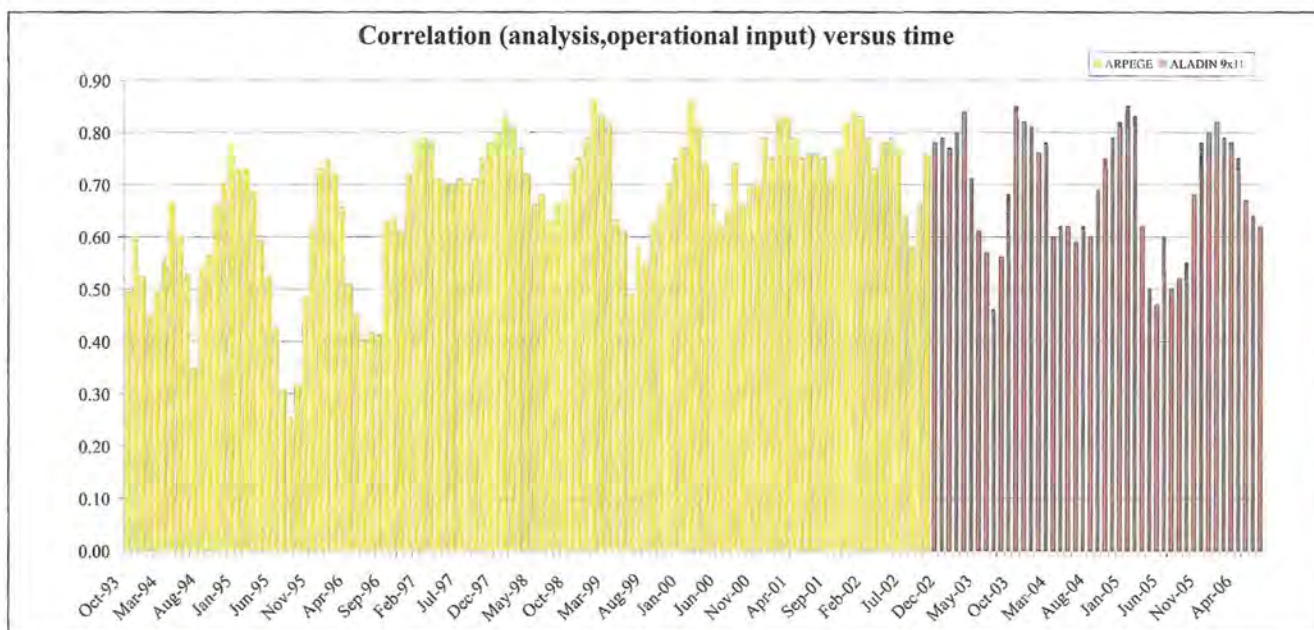


Figure 6, correlation versus time (see explanations in text).

Table 2

	BIAS			RMS			ROUSSEAU		
	ARPEGE	ALADIN 9 x 11	ALADIN 15 x 20	ARPEGE	ALADIN 9 x 11	ALADIN 15 x 20	ARPEGE	ALADIN 9 x 11	ALADIN 15 x 20
Chablais	-0,70	<b>-0,61</b>	1,08	<b>4,64</b>	5,03	4,76	<b>0,78</b>	0,74	0,77
Aravis	-0,82	<b>0,05</b>	0,36	5,01	<b>4,41</b>	4,68	0,78	0,79	<b>0,81</b>
Mont Blanc	<b>0,05</b>	-0,56	2,07	<b>5,09</b>	5,59	5,14	<b>0,70</b>	0,69	0,61
Beaufortin	<b>0,53</b>	0,62	3,12	4,61	<b>4,05</b>	7,22	0,74	<b>0,78</b>	0,74
Haute Tarentaise	<b>0,26</b>	-0,34	0,62	4,34	4,63	<b>4,11</b>	0,68	0,74	<b>0,80</b>
Vanoise	0,36	<b>0,28</b>	0,80	<b>3,53</b>	3,81	3,70	0,70	0,75	<b>0,77</b>
Maurienne	<b>0,65</b>	0,71	2,24	<b>3,65</b>	3,92	5,46	<b>0,65</b>	0,63	0,63
Haute Maurienne	0,38	<b>-0,18</b>	-0,30	3,73	<b>3,25</b>	3,42	0,60	<b>0,65</b>	0,62
Bauges	<b>0,04</b>	1,14	1,61	<b>4,47</b>	5,19	5,31	0,73	<b>0,76</b>	<b>0,76</b>
Chartreuse	<b>-0,26</b>	-0,55	0,66	5,30	<b>5,28</b>	9,02	0,67	0,65	<b>0,68</b>
Vercors	-0,77	1,90	<b>0,63</b>	<b>5,39</b>	6,74	4,95	<b>0,64</b>	0,59	0,63
Belledonne	<b>0,88</b>	0,90	2,21	4,80	<b>4,72</b>	6,40	0,73	0,74	<b>0,75</b>
Grandes Rousses	<b>0,41</b>	1,51	0,70	<b>4,55</b>	5,42	4,94	0,63	0,61	<b>0,64</b>
Oisans	<b>1,09</b>	3,69	2,43	<b>4,66</b>	9,61	7,16	<b>0,71</b>	0,67	0,66
Pelvoux	-0,36	0,49	<b>-0,12</b>	4,35	3,96	<b>3,79</b>	0,61	0,60	<b>0,68</b>
Thabor	<b>0,01</b>	0,14	-0,18	4,01	4,12	<b>3,63</b>	0,54	0,57	<b>0,64</b>
Champsaur	<b>-0,07</b>	1,49	2,99	<b>3,66</b>	5,06	9,10	<b>0,69</b>	<b>0,69</b>	0,68
Dévoluy	<b>0,01</b>	1,98	0,98	<b>5,46</b>	6,93	5,75	0,65	<b>0,66</b>	0,65
Queyras	0,46	<b>0,31</b>	-0,33	3,72	3,47	<b>3,11</b>	0,67	0,65	<b>0,71</b>
Parpaillon	0,36	0,97	<b>-0,03</b>	2,90	3,56	<b>2,67</b>	0,61	0,69	<b>0,73</b>
Ubaye	0,39	0,75	<b>0,28</b>	3,53	3,24	<b>2,92</b>	0,61	<b>0,68</b>	0,64
Alpes Azuréennes	<b>-0,12</b>	0,73	0,68	<b>4,06</b>	4,51	4,08	0,70	0,68	<b>0,72</b>
Mercantour	0,45	<b>0,07</b>	0,19	6,31	5,90	<b>5,73</b>	0,60	<b>0,67</b>	0,57

carried out to avoid this drawback and at the same time to take into account the better precision obtained in terms of localisation of the precipitation zones.

## Part 2: Study case

Presently, a new model with non-hydrostatic equations is under development. Its name is AROME. Because of computer limitations, the tests with this limited area mo-

del are presently being made on different zones covering a surface of nearly a quarter of France: south-east, north-east, etc. Twenty-two massifs of the French Alps are located inside the south-east zone, and only twelve in the north-east zone. The two zones do overlap. So, we have chosen to work with the south-east zone. In order to calculate daily precipitation, a 30-hour forecast is needed with a starting point based on 00h UTC. We obtain, at each point, the value of the daily precipitation by:  $RR24 = \sum RR30 - \sum RR06$ , where  $\sum RR06$  (resp.  $\sum RR30$ )

represents the cumulative precipitation from 00 to 06 H UTC (resp. from 00 to 30 H UTC). The digital elevation model under AROME is fine enough to see the Pre-Alps. See figure 7.

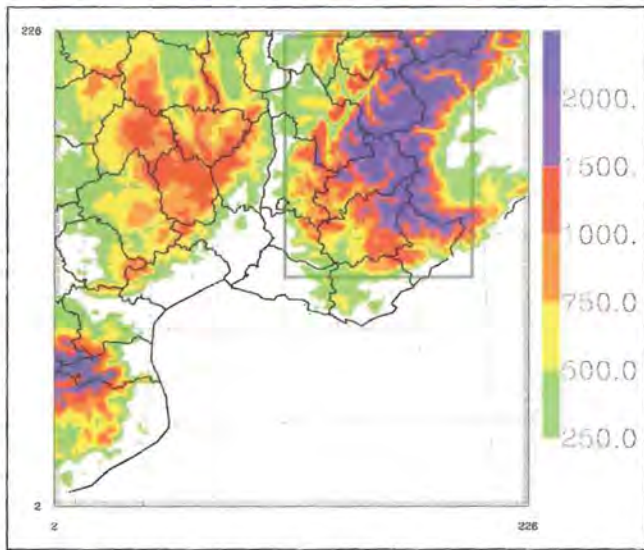


Figure 7, orography AROME

The step is 1 km in both directions in a Lambert II projection. So, we use a 240 x 240 grid of input for our "guess field".

### 1. Presentation of the four days chosen

AROME is a limited area model using ALADIN as a coupled model which gives the initial and lateral conditions every six hours. With this study case, we aim to have a first evaluation of this new model in particular for days with relatively strong precipitation in the Alps. To avoid

discrepancies due to the coupled model, we chose winter days which have a good correlation ( $R^2 > .8$ ) between the ALADIN forecast and the SAFRAN analysis and a daily precipitation greater than 20 mm per day on average in all massifs, at the same time.

The following days were chosen for the 2005-2006 season:

Date	RR24h Analysis	$R^2$ (Analysis, Aladin 15 x 20)
From 30 December 6h to 31 December 6h	25 mm	0,809
From 15 February 6h to 16 February 6h	29 mm	0,822
From 8 March 6h to 9 March 6h	19 mm	0,895
From 30 March 6h to 31 March 6h	24 mm	0,876

For the south-east zone, only the Chablais massif could not be calculated with AROME.

### 2. Synoptical view

We will rapidly describe the four days chosen.

#### Case from 30 December 6h to 31 December 6h

At the end of the year 2005, a storm crossed the French Alps associated with westerly winds. Most of the precipitation was fallen inside the warm sector with an enhancement by orographic effect. See the figure 8 representing the "ANASYG" at 18 h UTC for this situation. For further explanation of this graphic representation of synoptic features, see (SANTURETTE 2002).

#### Case from 15 February 6h to 16 February 6h

Very active westerly storm, with strong winds. The associated warm front is undulating over the Alps. See the figure 9 representing the "ANASYG" at 18h UTC.

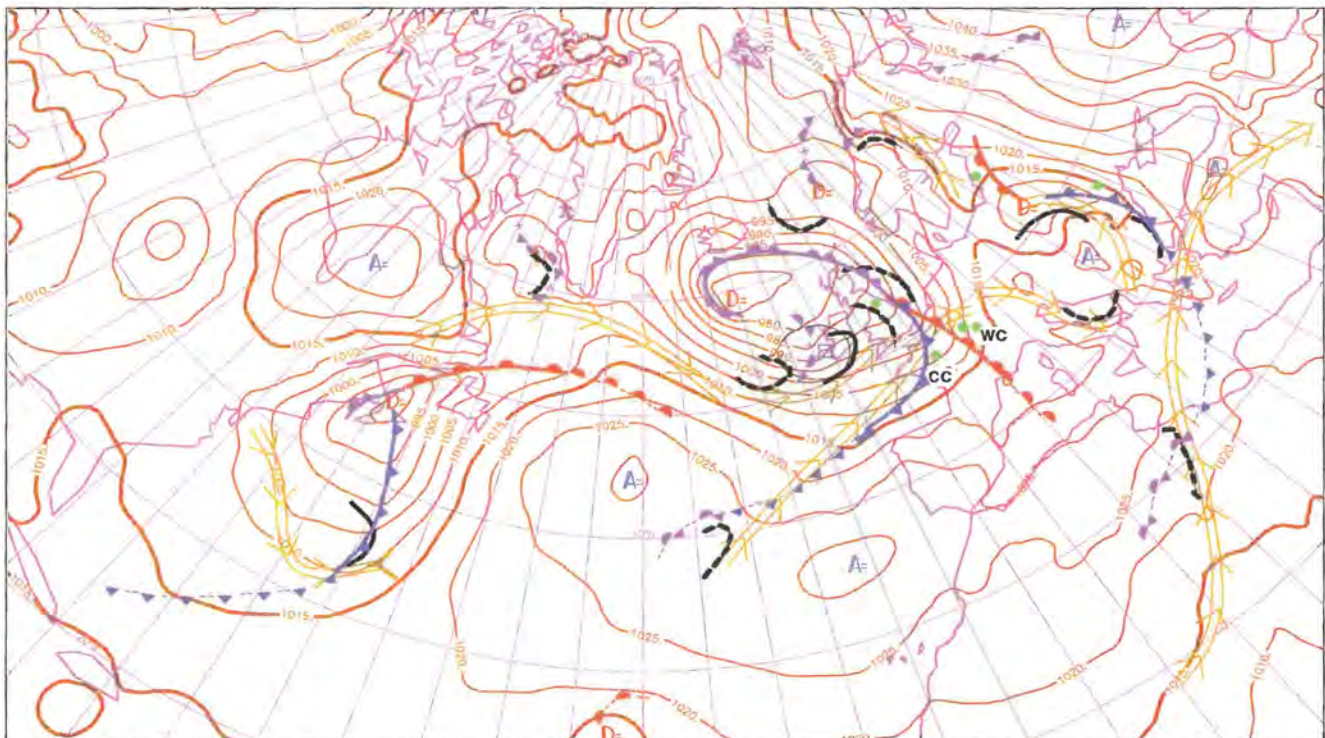


Figure 8, ANASYG the 30 December 2005 at 18h UTC.

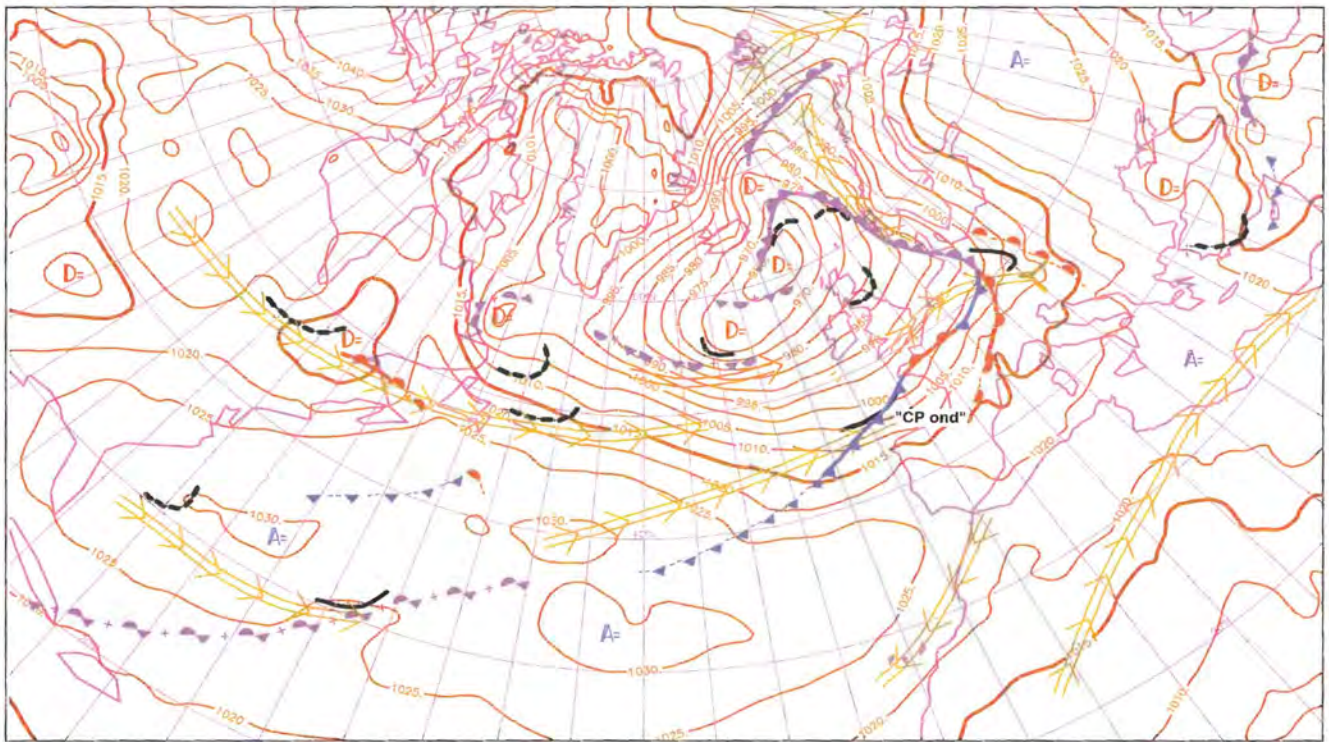


Figure 9, ANASYG the 15 February of 2006 at 18h UTC.

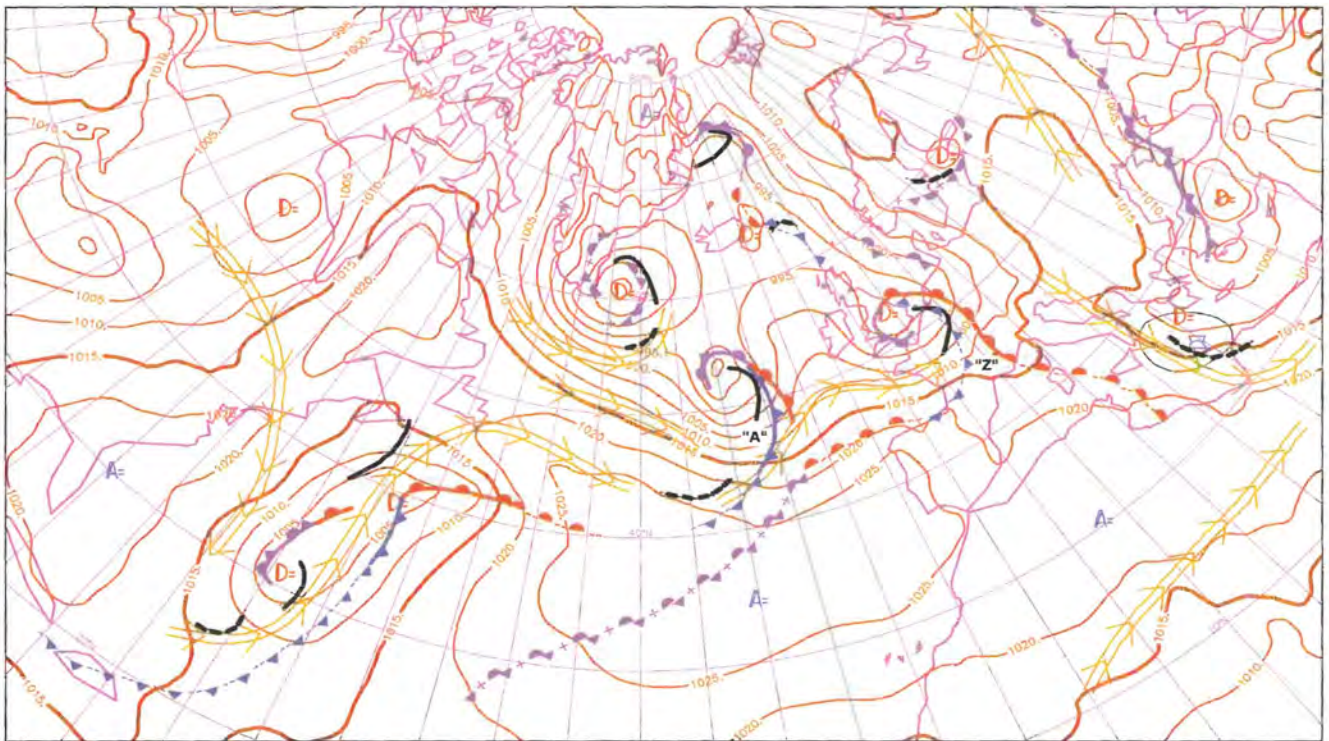


Figure 10, ANASYG the 8th March of 2006 at 18h UTC.

#### Case from 8 March 6h to 9 March 6h

Westerly perturbation with convective activity near the cold front. The warm front with orographic precipitation reaches our zone at approximately 13h UTC and the cold front around 19h UTC. See the figure 10 representing the "ANASYG" at 18h UTC.

#### Case from 30 of March 6h to 31 of March 6h.

WSW occlusion perturbation with a jet stream. The north-

ern part of the French Alps is rainier than the southern part. See the figure 11 representing the "ANASYG" at 18h UTC.

#### 3 Analysis results versus forecasts with ARPEGE input to AROME input

The absolute bias with the AROME model is in a narrower range than for the other models. The daily values fit the analyses really well except for the case 8-9 of March.

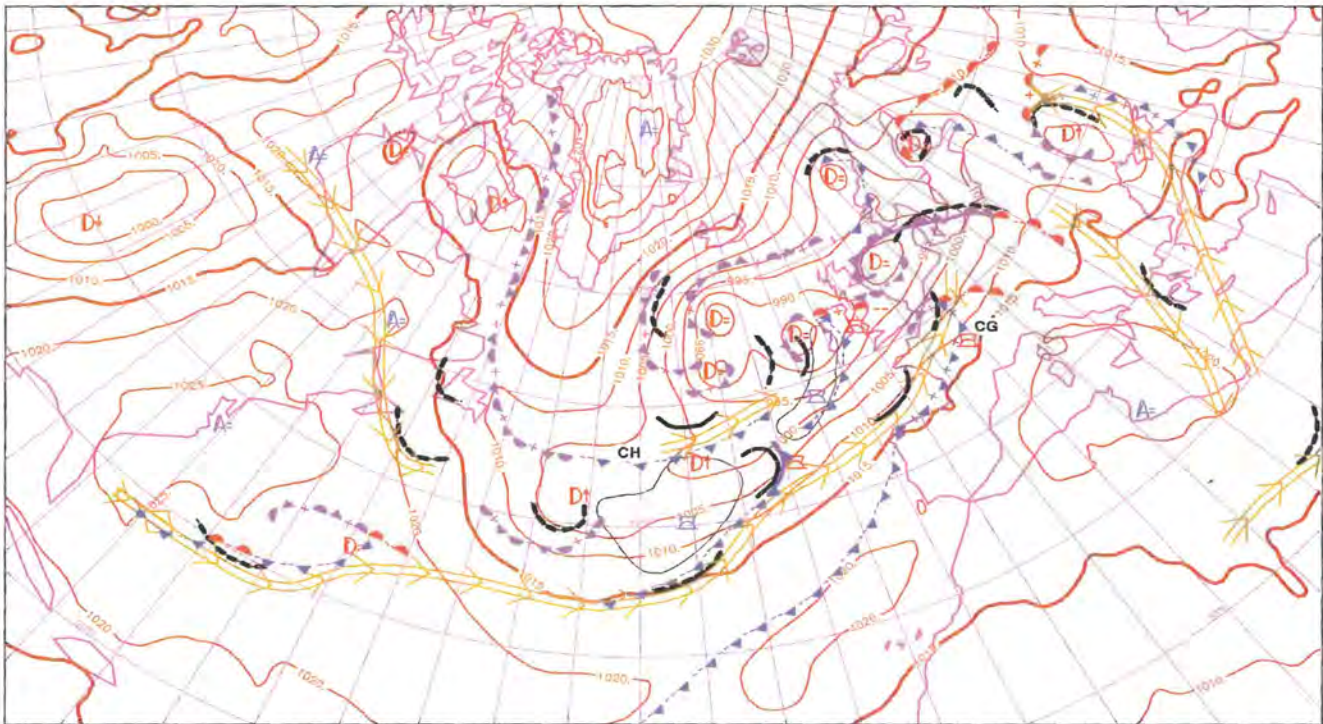


Figure 11, ANASYG the 30 March 2006 at 18h UTC.

The mix of orographic and convective precipitation could be an explanation for the over-estimation of all the models for this situation.

Table 3, daily precipitations for the days chosen, in each block, we have a first analysis value, followed by the AROME, ALADIN 9 x 11, ALADIN 15 x 20 and ARPEGE forecasts.

	31/12/2005					16/02/2006					09/03/2006					31/03/2006				
Aravis	35	30	39	40	27	47	48	46	48	32	53	65	64	71	42	52	38	41	42	30
Mont Blanc	44	41	20	42	26	52	44	22	45	30	61	64	40	68	45	61	58	23	52	33
Beaufortin	35	38	35	53	30	57	46	40	60	40	45	100	52	85	47	44	41	38	65	29
Haute Tarentaise	32	33	12	23	14	35	36	13	25	21	35	76	25	39	27	31	44	13	27	19
Vanoise	37	33	19	27	20	41	36	20	26	27	28	68	39	49	35	33	34	17	26	18
Maurienne	42	38	21	37	24	38	44	21	36	30	22	61	40	61	37	25	25	19	40	20
Haute Maurienne	27	17	6	5	3	20	19	7	5	9	15	35	16	11	11	13	14	7	7	7
Bauges	30	29	41	39	29	45	68	46	44	37	33	69	60	64	37	38	32	35	37	27
Chartreuse	44	36	26	45	30	50	51	27	45	35	17	34	35	59	34	32	20	23	31	21
Vercors	34	31	58	39	27	39	42	66	39	20	15	45	62	43	32	22	16	38	26	13
Belledonne	44	47	34	50	35	47	51	29	44	40	18	55	49	71	44	35	29	30	42	28
Grandes Rousses	36	36	32	32	23	43	42	29	28	31	25	40	51	49	33	35	36	34	28	18
Oisans	31	38	49	37	23	28	42	48	44	34	15	52	71	49	31	20	28	52	39	18
Pelvoux	11	10	2	0	6	15	13	8	10	13	5	13	13	10	11	16	10	9	10	7
Thabor	21	20	5	9	7	17	11	5	9	11	9	32	14	19	14	14	14	6	8	6
Champsaur	25	23	12	16	7	21	23	18	33	18	9	34	19	16	11	13	18	14	25	7
Devoluy	13	27	23	17	12	17	33	34	28	22	7	51	28	20	17	7	12	20	18	9
Queyras	1	5	0	0	2	3	7	2	4	6	2	10	4	6	5	6	5	3	6	3
Parpaillon	7	8	3	5	3	11	20	8	11	12	6	20	6	9	5	15	11	5	9	4
Ubaye	4	8	3	0	3	9	16	9	0	9	3	17	6	5	4	16	7	5	5	2
Alpes Azuréennes	2	7	6	5	4	5	14	14	8	10	1	17	11	9	6	7	6	8	7	3
Mercantour	0	0	0	0	0	0	4	0	0	0	0	1	0	0	0	1	0	0	0	0
	ANALYSE	AROME	ALADIN 9 x 11	ALADIN 15 x 20	ARPEGE	ANALYSE	AROME	ALADIN 9 x 11	ALADIN 15 x 20	ARPEGE	ANALYSE	AROME	ALADIN 9 x 11	ALADIN 15 x 20	ARPEGE	ANALYSE	AROME	ALADIN 9 x 11	ALADIN 15 x 20	ARPEGE
R <sup>2</sup>	0,94	0,66	0,88	0,87	0,89	0,65	0,89	0,91	0,81	0,63	0,82	0,82	0,92	0,62	0,84	0,94				

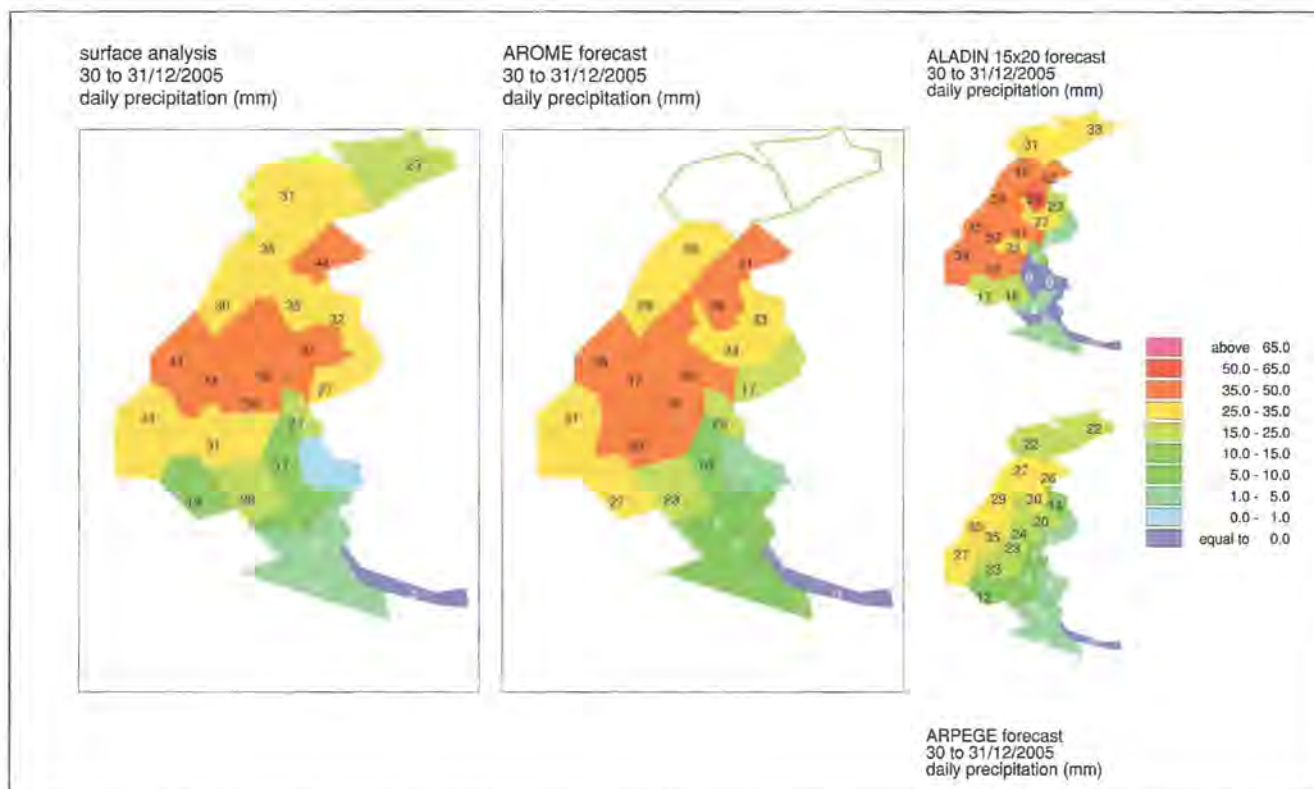


Figure 12: daily precipitation for the 30 to 31 December 2005.

As an illustration of this better fit by AROME in a spatial and bias way, figure 12 shows the analysis and the three forecasts with AROME, ALADIN 15x20 and ARPEGE. The two massifs Diablerets in Switzerland and Chablais in France as well as the northern massifs are not completely included in our AROME extraction zone, so these values for AROME are not comparable to the other panels. The mean value of the precipitation is reproduced well in northern part of the French Alps as well as in southern part with less precipitation. ALADIN has a good fit in the western part, but in the inner southern massif the three massif forecasts show no rain whereas in the analysis panel there is between 5 and 10 mm per day.

#### 4. Some preliminary results

This new approach with better orography representation and also with a better physical resolution which take into account the non-hydrostatic effects seems to be a promising way. However, with just four days in our study case at present, we must be very careful in our conclusions. For the convective part of the precipitation, the mesh is not yet sufficient to explicitly resolve the convection. And the 8-9 March case shows that this convective precipitation could occur during our "winter" period defined in part I chapter 3 from October to March.

#### Conclusion

This study shows that with some post statistical processing, the limited area model ALADIN with an as fine as possible extraction grid currently gives the best result

for the distribution of precipitation in the French Alps. The post processing consists of statistical adaptation in respect to the bias observed over the four seasons. Concerning the evaluation of the new AROME model, further work should be carried out. Currently, some pre-operational tests are being conducted with 30-hour forecasts. A first statistical study could be made at the end of the year 2007. It is ongoing work in collaboration with the AROME team.

#### References:

- CLÉMENT, R. (1979): La neige dans les Alpes Françaises. La Météorologie, 6ième série n°16, p157-165.
- DURAND, Y., BRUN, E., MÉRINDOL, L., GUYOMARC'H, G., LESSAFRE, B. AND MARTIN, E. (1993): A meteorological estimation of relevant parameters for snow models. Annals of Glaciology Vol. 18, p65-71.
- ROUSSEAU, D. (1980): A new skill score for the evaluation of yes/no forecasts. WMO Symposium on probabilistic and statistical methods in Weather Forecasting, September 1980, p167-174.
- SANTURETTE, P. AND JOLY, A. (2002): ANASYG/PRESYG. Météo-France's new graphical summary of the synoptic situation. Meteorology Applied 9, p129-154.

# 11 Validation of a physically based snow model for the simulation of the accumulation and ablation of snow (ESCIMO)

MONIKA PRASCH, ULRICH STRASSER AND  
WOLFRAM MAUSER

Department of Geography, LUDWIG-Maximilians University (LMU), Luisenstr. 37, D-80333 Munich, Germany

## Abstract

The one-layer snow model ESCIMO (Energy Balance Snow Cover Integrated Model) is designed as a physically based model for the hourly simulation of the energy balance, the water equivalent and the melt rate of a snow cover. In this paper, we perform a three-step validation strategy: first we compare model results of snow water equivalent (swe) with locally observed measurements, using hourly meteorological recordings. For this experiment, we apply data from the Weissfluhjoch (Swiss Alps), Col de Porte (French Alps), Sleepers River (USA), Goose Bay (Canada) and Kühroint (German Alps) stations. Secondly, we use a temporally and spatially interpolated meteorological forcing as provided by the SVAT-model PROMET (Process Oriented Model for EvapoTranspiration) to validate the models distributed application. For this second experiment, we compare model results with German Weather Service (DWD) station recordings of swe from selected representative weather stations within the Upper Danube catchment; there, temporal resolution of the meteorological recordings is three-times-a-day. In a last step, we compare simulated snow covered area with NOAA-AVHRR satellite data derived snow products. In this step, the influence of the meteorological data provision of PROMET on snow modelling, especially on the precipitation phase is validated. The paper gives an overview of the validation of the snow model for applications ranging from high temporal resolution at the point scale up to much coarser temporal resolution at the catchment scale.

## 1. Introduction

Snow is not only a fascinating, but a very important variety of precipitation with a significant function as a temporal storage of water with delayed release. Due to climate change, the availability of water for humans, plants and animals will be one of the most essential issues for the future (IPCC 2001, IUCN 2003). Research projects dealing with this topic are, for example, ENSEMBLES, Euro-impacs, KLIWA and many others ([www.ensembles-eu.org](http://www.ensembles-eu.org), [www.eurolimpacs.ucl.ac.uk](http://www.eurolimpacs.ucl.ac.uk), [www.kliwa.de](http://www.kliwa.de)). Within the integrative projects GLOWA-Danube ([www.glowa-danube.de](http://www.glowa-danube.de)) and Brahmatwinn ([www.brahmatwinn.uni-jena.de](http://www.brahmatwinn.uni-jena.de)) a main focus is directed on hydrological modelling and the determination of the im-

pact of future climate change scenarios on the water balance. For simulating the water cycle in the test sites of the Upper Danube and the Upper Brahmaputra catchments, the accumulation and ablation of snow has to be considered due to the alpine character of the headwaters. On the point scale the physically based one-layer snow model ESCIMO (Energy Balance Snow Cover Integrated Model) (STRASSER 1998, STRASSER AND MAUSER 2001, STRASSER et al. 2007) is applied in a stand-alone mode without any temporal or spatial interpolation of the required input data. For distributed applications it is integrated into the raster oriented SVAT-scheme PROMET (Process Oriented Model for EvapoTranspiration) (MAUSER 1989, MAUSER et al. 1998) which provides the required fields applying a sophisticated interpolation techniques (STRASSER AND MAUSER 2001). PROMET is applied on different scales from the single field (1ha) over a microscale region (100 km<sup>2</sup>) to a mesoscale catchment (100 000 km<sup>2</sup>) in a variety of studies (MAUSER AND SCHÄDLICH 1998, STRASSER AND MAUSER 2001, LUDWIG AND MAUSER 2000, LUDWIG et al. 2003). This paper gives an overview of the validation of ESCIMO for both kinds of applications. After the description of the two simulation models, the validation at the point scale as well as at the catchment scale is presented in detail. Finally, simulated snow cover extent is compared to satellite data derived snow cover, and the relevant effects are discussed. The paper ends with a discussion of the quality and quantity of the results and a future perspective.

## 2. The models

### 2.1 The snow model ESCIMO

The one-layer snow model ESCIMO (Energy Balance Snow Cover Integrated Model) is designed as a physically based model for the hourly simulation of the energy balance, the water equivalent and the melt rate of a snow cover. For the simulation of the energy balance the short- and long-wave radiation, the sensible and latent heat fluxes, the energy conducted by solid or liquid precipitation as well as condensation/sublimation and a constant soil heat flux are taken into account. The snow albedo is modelled using a function considering the age and the surface temperature of the snow pack. For each time step the following scheme is followed: First it is distinguished between potential melting conditions (air temperature  $\geq 273.16\text{K}$ ) and no melt (air temperature  $< 273.16\text{K}$ ). In the first case (potential melt), the energy balance is calculated analytically. After the decision whether possible precipitation is solid (air temperature  $\leq 273.16\text{K}$ ) or liquid (air temperature  $> 273.16\text{K}$ ) (if not detected automatically), the water mass budget and the energy budget are calculated, assuming no snowmelt at the current time step. In the next step, the total available energy is compared with the energy status of the snow pack at 273.16K, assumed as the minimum energy status for snowmelt. Then the snowmelt produced by the available excess energy is calculated. Finally the mass and energy budgets are updated, adding rain to melt

and snow to the existing snow water equivalent (swe) in the case of precipitation.

In the case of no melt an iterative procedure is applied to adopt the snow surface temperature for closing the energy balance (with re-calculation of the energy balance in each loop). A detailed description of the model physics and its algorithms is given in (STRASSER et al. 2007) in this volume.

## 2.2 The SVAT-model PROMET

The **PR**ocess **O**riented **M**odel for **E**vapo**T**ranspiration **PROMET** is a physically based Soil-Vegetation-Atmosphere-Transfer Scheme (MAUSER 1989, MAUSER et al. 1998, STRASSER AND MAUSER 2001, LUDWIG AND MAUSER 2000, LUDWIG et al. 2003). **PROMET** is used to model the fluxes of water, energy and matter in the system soil-vegetation-atmosphere on the basis of the Penman-Monteith equation (MONTEITH 1965) for the distributed simulation of actual evapotranspiration as a function of water availability, radiation balance and physiological regulation mechanisms of heterogeneous plant stands. **PROMET** consists of the following five interdependent modules, delivering the required inputs for the distributed application of the Penman-Monteith equation:

- (a) The *radiation module* calculates the radiation balance according to its geographical location, sun angle and cloud cover (MAUSER 1989),
- (b) the *soil hydraulic module* calculates the soil water content as a function of infiltration, exfiltration, percolation and capillary rise (EAGLESON 1978),

- (c) the *plant physiological module* calculates the water transport in plants as a function of the specific stomatal resistance, determined by absorbed photosynthetic active radiation, temperature, humidity and soil moisture (BALDOCCHI et al. 1987),
- (d) the *aerodynamic module* calculates the removal of transpired water vapour into the atmosphere (MONTEITH 1978 and
- (e) the *snow module ESCIMO*, described above (see 2.1).

If snowfall occurs (air temperature  $\leq 273.16\text{K}$  and precipitation  $> 0$ ) (a) or if a snow cover exists from the previous time step (b) the snow module is called within the simulation. Each raster element is either completely snow covered or snow free. In case of snow cover, the vegetation is assumed to be not active (STRASSER AND MAUSER 2001). The snow module returns the actual snow water equivalent and the gain/loss of swe to the previous time step (accumulation or ablation) to the other modules. For example, in case of ablation, the contribution to the surface runoff and respectively the infiltration of the melted water runoff through the soil is modelled in the soil hydraulic module (fig.1).

### Input data

For the simulations presented here, **PROMET** uses a temporal resolution of one hour and a spatial resolution of one kilometer. To run the model, input data fields of topography, landuse/landcover, soil texture and meteorology are required as raster fields. Slope and aspect

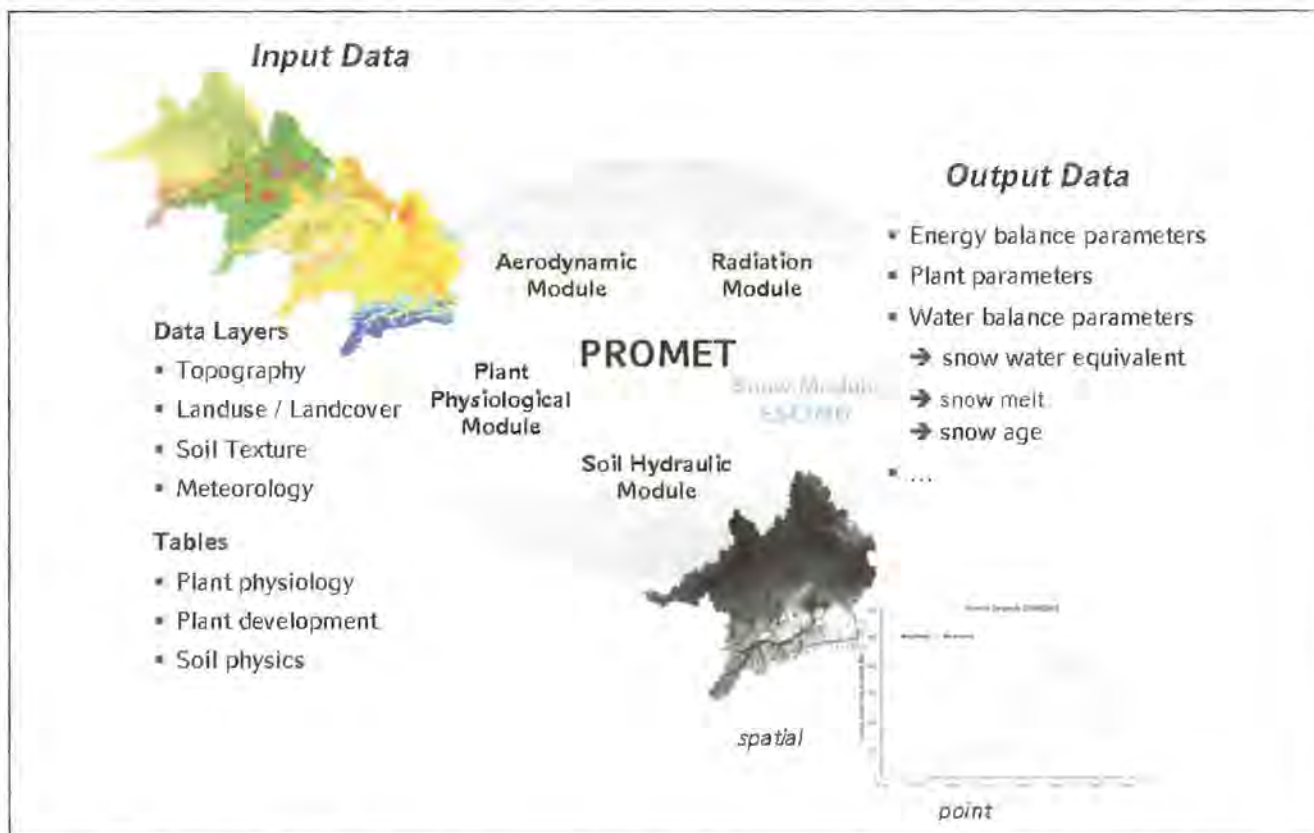


Figure 1: Structure of **PROMET**

is deduced from the digital elevation model. Detailed information of soil physics, e.g. pore size distribution or hydraulic conductivity, and to landuse/landcover, e.g. dynamic parameters like leaf area index or canopy height are derived from literature and/or field campaigns (LUDWIG et al. 2003).

For providing the meteorological input data fields of air temperature, precipitation, wind speed, relative humidity and cloudiness, point measurements at the stations of the German Weather Service (DWD) network are interpolated: The three daily recordings at 7 a.m., 2 p.m. and 9 p.m. ("Mannheimer Stunden") are temporally interpolated using a cubic spline function. Precipitation is classified in short events (one single recording) and long-term events (two or more consecutive recordings). In the first case, a Gaussian distribution of the precipitation is assumed, whereas in the second case, it is equally distributed in time. For the spatially interpolation of the meteorological parameters a linear regression between the measured values and the station altitudes is superposed with the spatially interpolated residuals of the regression. This ensures the reproduction of the station's recordings as well as the consideration of the relief gradient of the parameters (STRASSER AND MAUSER 2001).

### Output data

PROMET results consist of both a large variety of output data for each raster element and of spatially distributed fields for the catchment area, describing e.g. the evolution of plants, the water balance with detailed information for surface, soil, plant and atmospheric processes, the actual snow water equivalent or melt rates.

## 3. Validation

The performance of the snow model *ESCIMO* has been validated at various alpine sites at the point scale within the framework of the *Snow models Intercomparison Project (SnowMIP)* in 2002 (ETCHEVERS et al. 2004). To compare the results of the stand-alone version with the integrated PROMET approach, the weather station *Kühroint*, which is located in the *Upper Danube*

*catchment* (the test site of the *Glöwa Danube Project*), is chosen due to its excellent data availability. This experiment allows to isolate the influence of the different data sources (locally measured vs temporally and spatially interpolated). To validate the modelled spatially distributed snow water equivalent (swe), representative weather stations of the catchment with various geographical characteristics are chosen and the model results are compared with the measurements. In this application the performance of the model is validated using interpolated input data. Finally, the modelled distributed snow cover of the Upper Danube catchment is compared to a satellite derived snow cover. This step emphasises the influence of the interpolated meteorological input data, especially of the precipitation phase on snow modelling. Therefore early winter is chosen as validation time.

### 3.1 The Point Scale

Within *SnowMIP* (<http://www.cnrm.meteo.fr/snowmip/>), 23 snow models of varying complexity were compared at four different test sites without any calibration, as validation data were not provided. Tab. 2 summarises the characteristics and the available data for the sites.

The modelled evolution of the swe for the four test sites is presented in fig. 2a and b. At the cold test sites *Weissfluhjoch* and *Goose Bay* (fig. 2a) with almost no rain or melting periods during winter, all simulated snow cover evolutions are very close to each other as well as to the measured values until the melting process starts in spring. With the beginning of ablation, some models tend to overestimate the melt rate while others underestimate it. *ESCIMO* is among the second group, delaying the date of beginning melt at both sites. Nevertheless the melting evolution is modelled very close to the measured values. The different climate and snow characteristics at the temperate sites *Sleepers River* and *Col de Porte* (fig. 2b) with intermediate melting periods during winter and wetter snow packs cause a higher variance in the model results than at the cold test sites. The performance of *ESCIMO* is very good at *Sleepers*

**Table 1:** Characteristics of the test sites (<http://www.cnrm.meteo.fr/snowmip/>, Etchevers et al. 2004, Etchevers et al. 2002).

Name	Coordinates [Lat/Lon]	Elevation [m a.s.l.]	Seasons	Characteristics
Col de Porte (France)	45.30° N / 5.77° E	1340	Oct 6th 1996 - June, 10th 1997 Oct 8th 1997 - Juni 20th 1998	Alpine site, middle elevation, air temperature not very cold, rainfall and snow melt can occur at any time
Goose Bay (Canada)	53.32° N / 60.42° W	46	Aug 1st 1969 - July 31st 1984	Arctic site, very low air temperature
Sleepers River (USA)	44.5° N / 72.17° W	552	Nov 1st 1996 - May 10th 1997	Eastern US site, temperature low during winter
Weissfluhjoch (Switzerland)	46.83° N / 9.81° E	2540	Aug 1st 1992 - July 31st 1993	Alpine site, high elevation, low air temperature, rain not before May

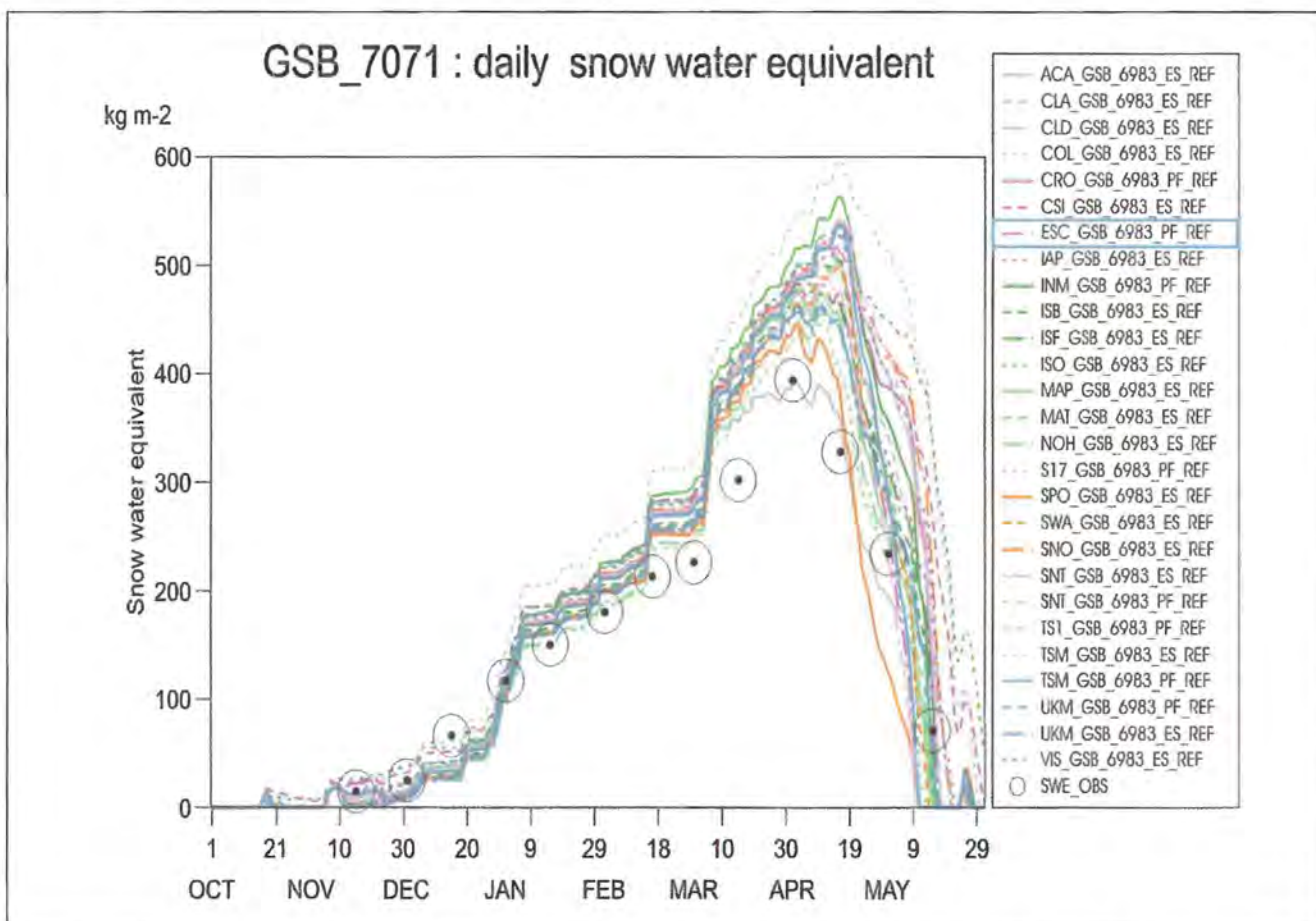
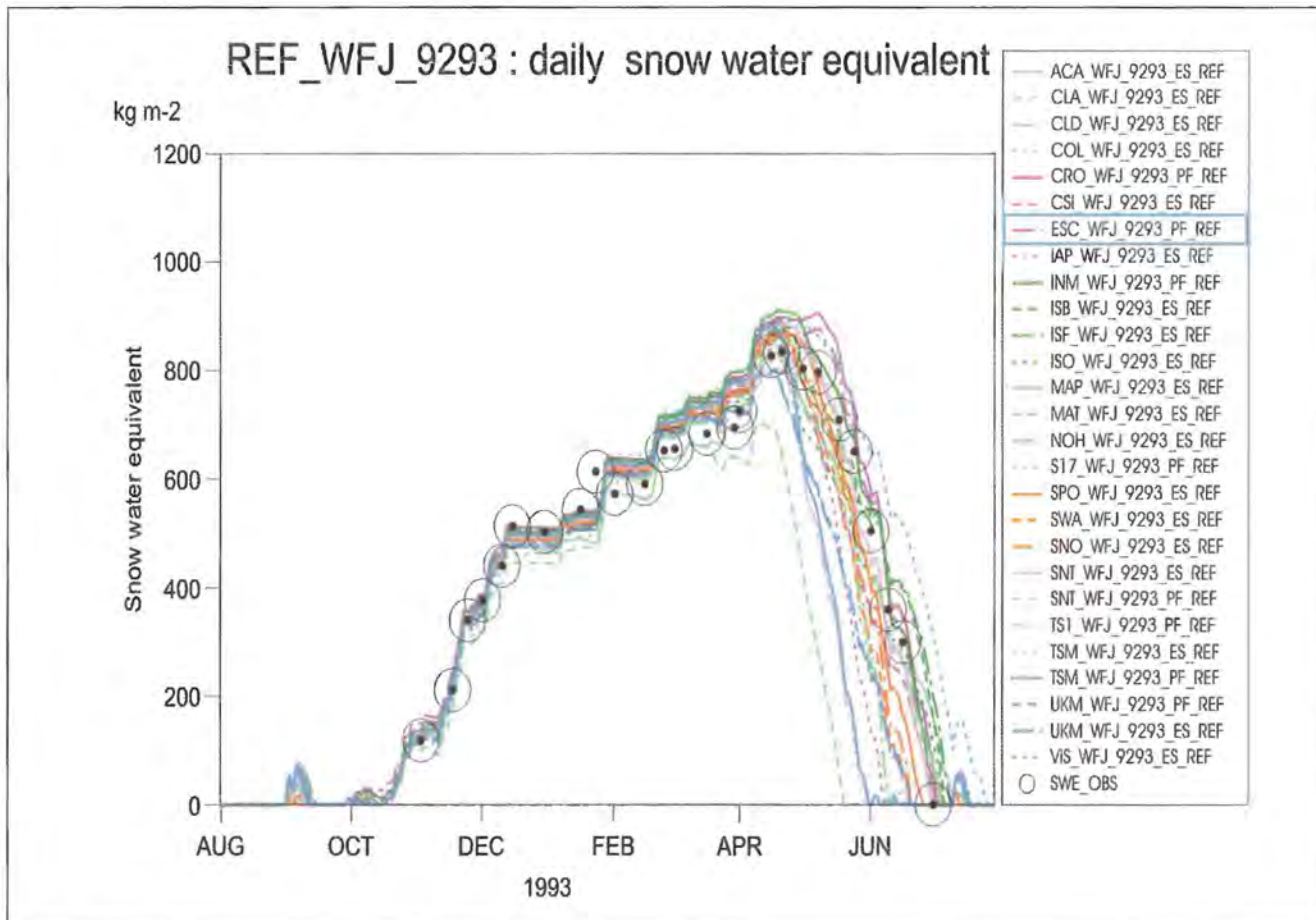


**Figure 2a:** The results for the cold test sites Weissfluhjoch (WFJ) and Goose Bay (GSB) within the models Intercomparison Projekt SnowMIP (<http://www.cnrm.meteo.fr/snowmip>).

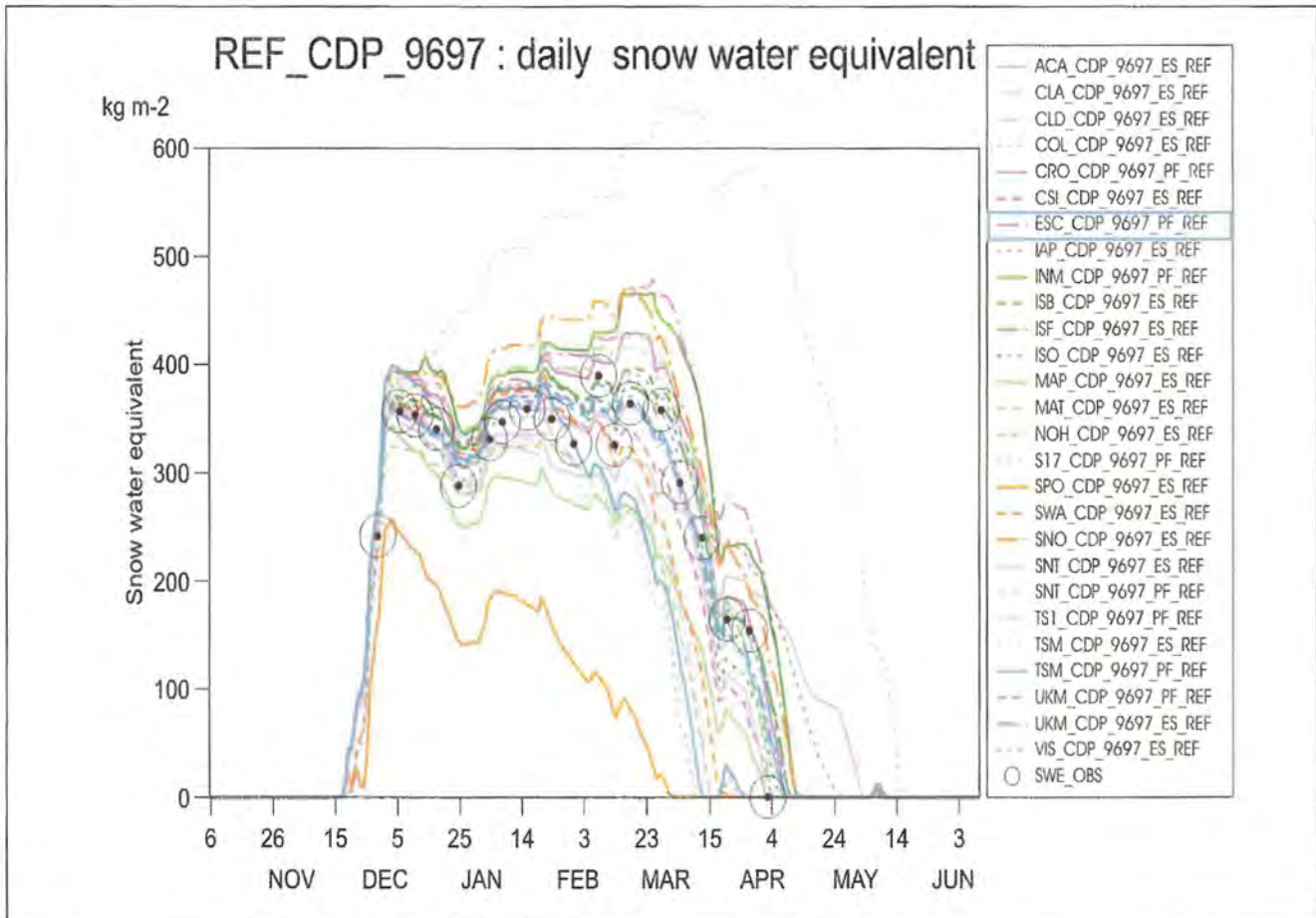
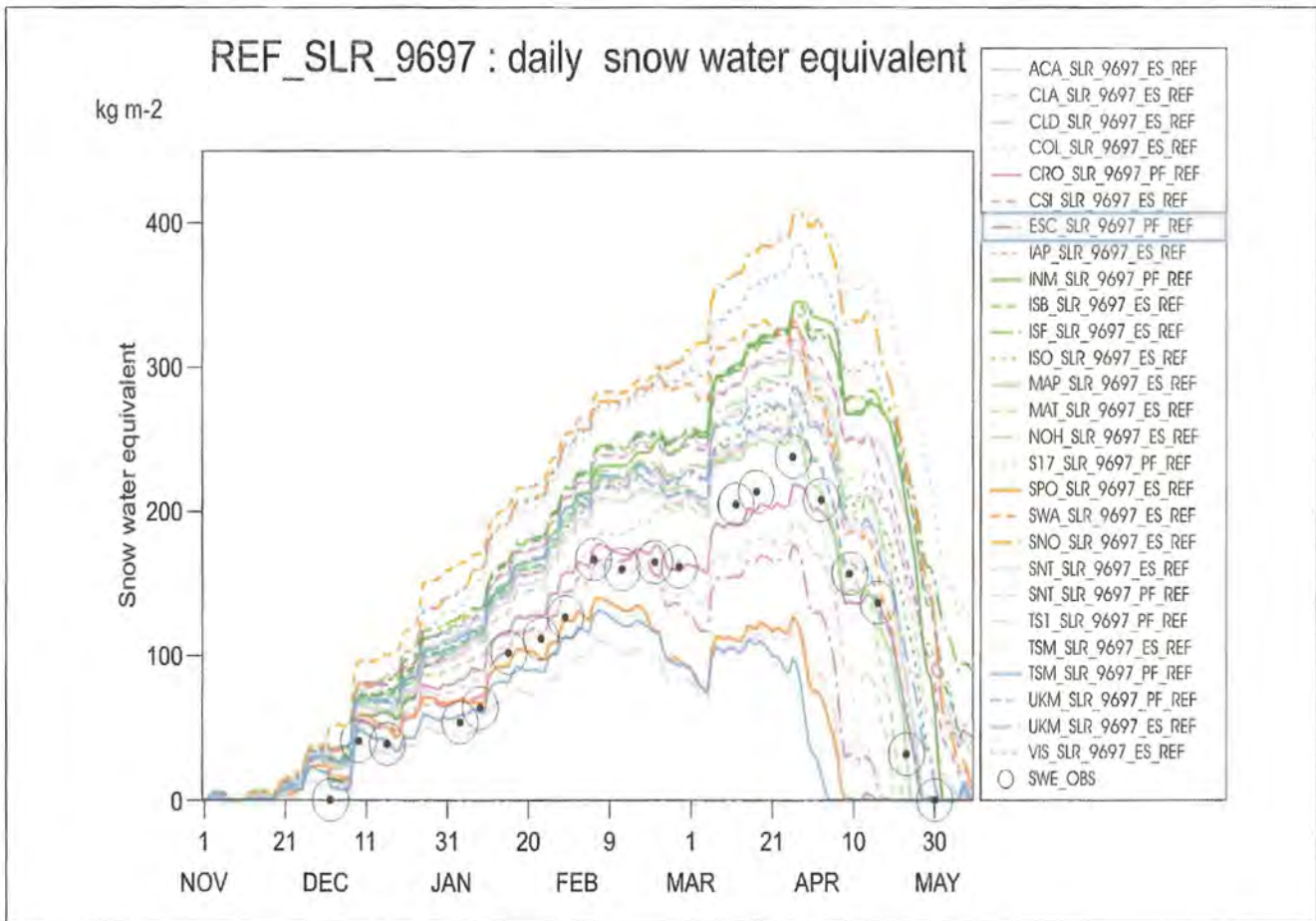


**Figure 2b:** The results for the temperate test sites Sleepers River (SLR) and Col de Porte (CDP) within the models Intercomparison Projekt SnowMIP (<http://www.cnrm.meteo.fr/snowmip>).

River until the first melting starts at the end of February (which is slightly overestimated). But this effect produces an underestimation for the rest of the snow season, resulting in shorter snow cover duration than measured, even though the trend is modelled very well. At *Col de Porte* the opposite occurs in underestimating the melting phase, so that the snow pack remains too long. For the cold test sites the performance of the models is higher than at the temperate test sites due to the characteristics of the winters. The complexity of the models, describing the physical snow processes, is not the determining factor for the performance of the models. More sophisticated snow models (e.g. SNO, SNT, see fig.2a and b) as well as less sophisticated ones (e.g. COL, ISB, see fig.2a and b) both deliver results with high and low deviations (ETCHEVERS et al. 2004, ETCHEVERS et al. 2002).

Another validation of *ESCIMO's* performance at the point is made at the weather station *Kühroint* (1407m) in the *National Park Berchtesgaden* in the Bavarian Alps (fig. 3 and 4), where all the required meteorological input

data (Tab.2) for the stand-alone snow model *ESCIMO* are available. There, a continuous data series of observed swe exist (manual, weekly pit measurements). Fig. 5 shows the modelled (turquoise graph) and measured snow water equivalent (red triangles) for the winter season 2004/2005. The measured evolution as well as the amount of the swe is reproduced very well by the model, which results in a coefficient of determination of 0.93. This coefficient is used to determine how well a regression line fits. It represents the proportion of the variance of observed values that can be explained by the model.

$$R^2 = \frac{\sum_{i=1}^n (\hat{y}_i - \bar{y})^2}{\sum_{i=1}^n (y_i - \bar{y})^2}$$

- with
- n = observations
  - y = observed value
  - $\hat{y}$  = predicted value of regression graph
  - $\bar{y}$  = arithmetic mean

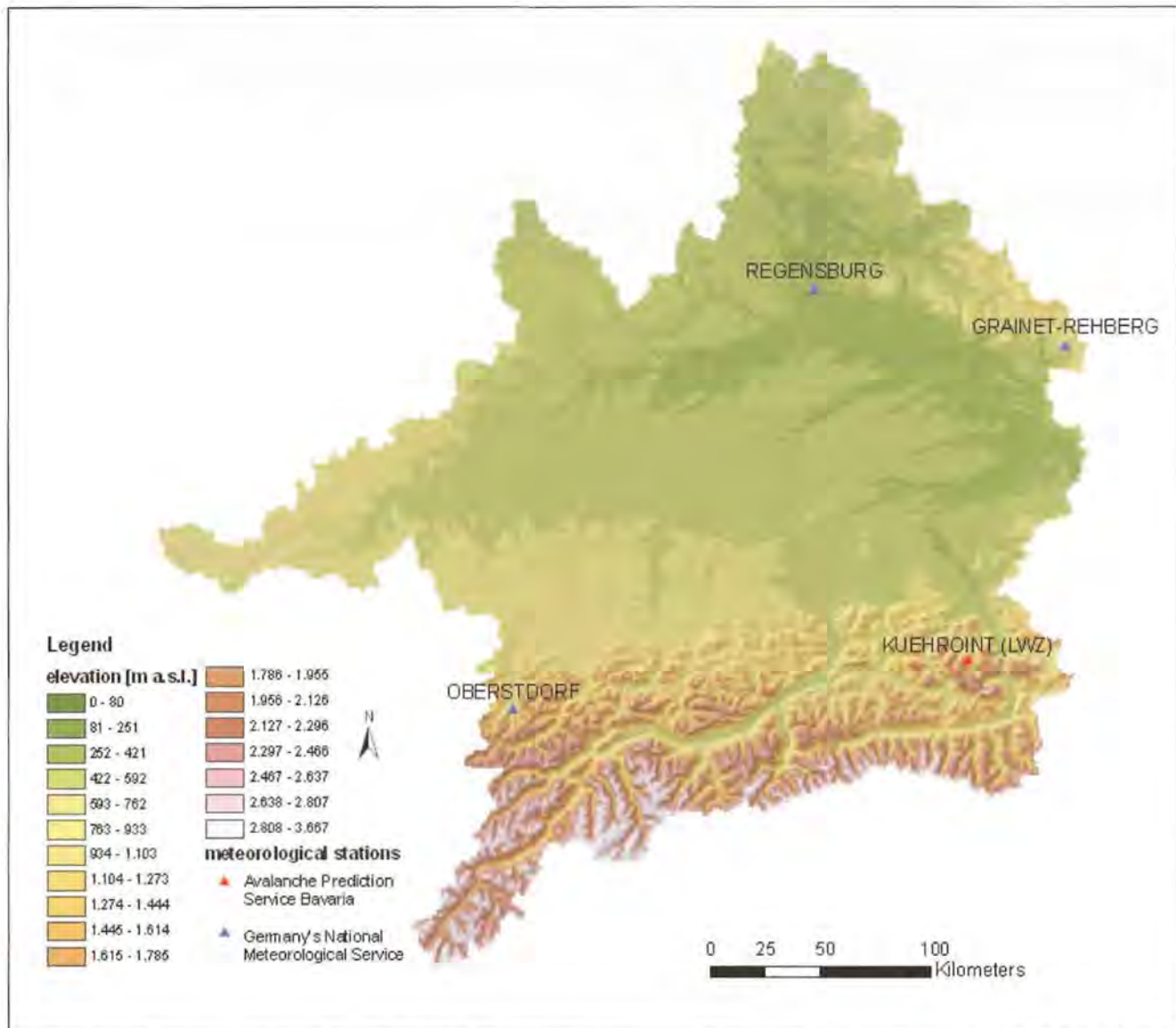


**Figure 3:** The Upper Danube catchment with the meteorological stations of Germany's National Meteorological Service and of the Avalanche Prediction Service of Bavaria.

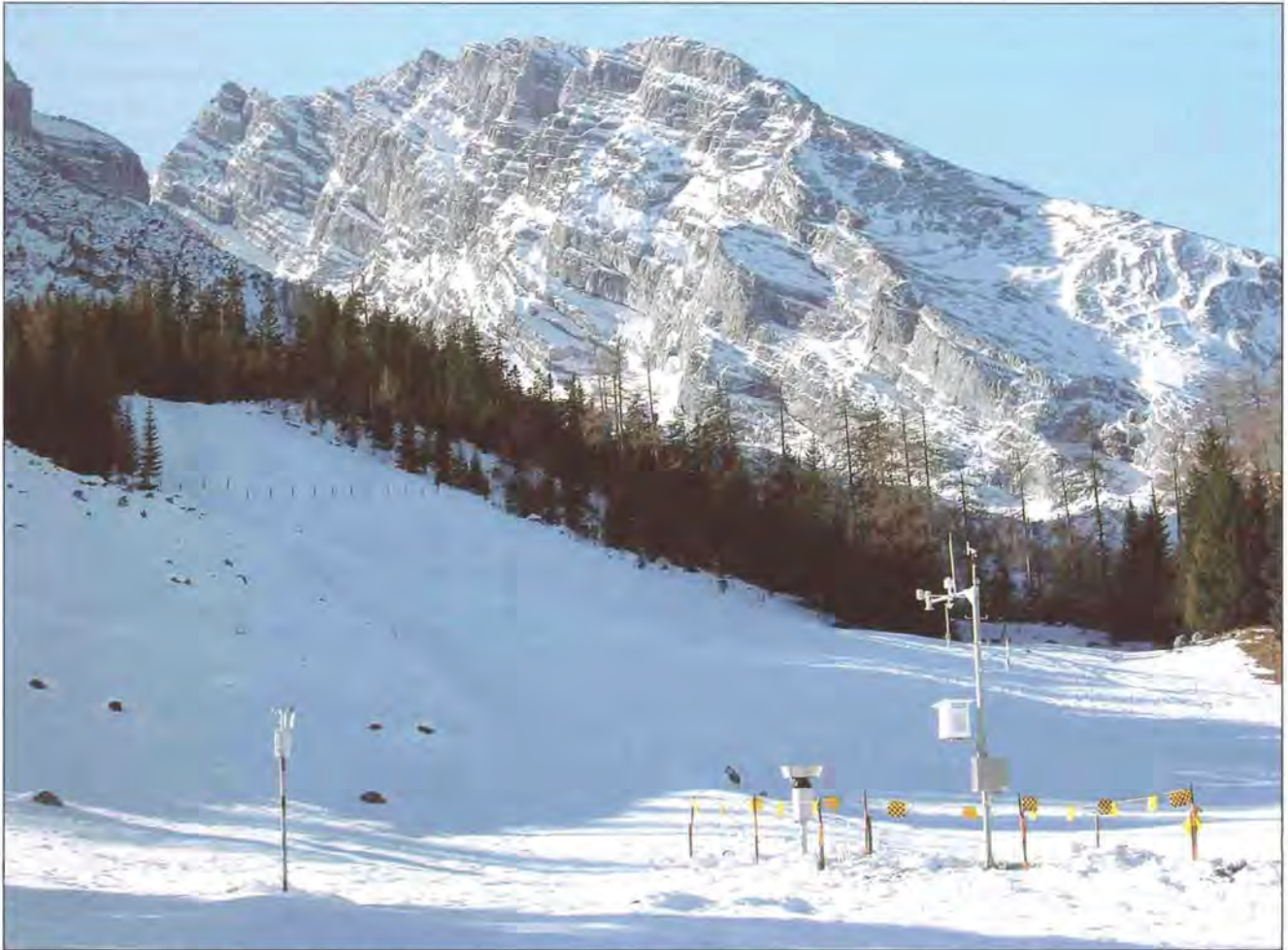


**Figure 4:** The Kühroint station in front of the Watzmann Massiv (Picture: Helmut Franz, December 2006).

**Table 2:** Required meteorological input data for the snow model ESCIMO

Parameter	Unit
Air temperature	K
Wind velocity	m/s
Relative humidity	%
Precipitation	mm
Longwave radiation	W/m <sup>2</sup>
Global radiation	W/m <sup>2</sup>

The blue graph in the diagram (fig. 5) presents the modelled swe as resulting from *PROMET*. As explained in Chapter 2.2, here the meteorological input parameters are derived by spatial and temporal interpolation of six surrounding stations of the German and the Austrian Weather Service, shown on fig. 6. The quality of the model output for the raster element of the Kühroint station decreases, the coefficient of determination is 0.41. Compared to the stand-alone model output (turquoise graph), *PROMET* models the swe at the beginning of the snowfall season similar to *ESCIMO*. From the end of December to the end of the winter season the swe of *PROMET* is continuously lower than of *ESCIMO*. Until the mid of January this even is closer to the measured values, whereas during the following weeks *PROMET* un-

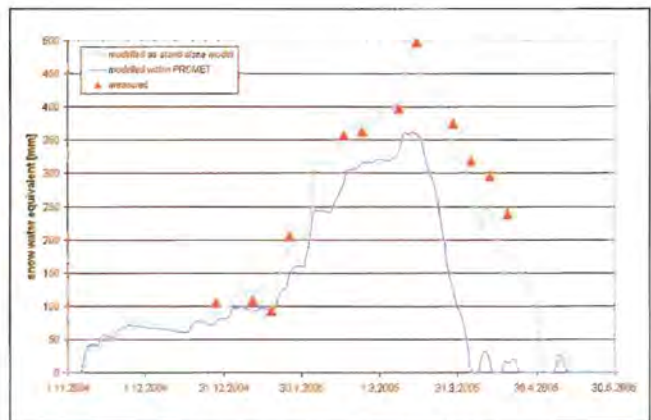


**Figure 5:** Two different applications of *ESCIMO*: modelled and measured snow water equivalent at the weather station Kühroint for the winter season 2004/2005.

derestimates clearly the increase periods of the swe until its' maximum value in March. Therefore the melting period ends up nearly a month earlier than in the *ESCIMO* approach. The differences of the modelled swe between the two models are due to the different input data. Both model approaches simulate the evolution close to the measurements, whereas the quantity of the swe differs noticeably.

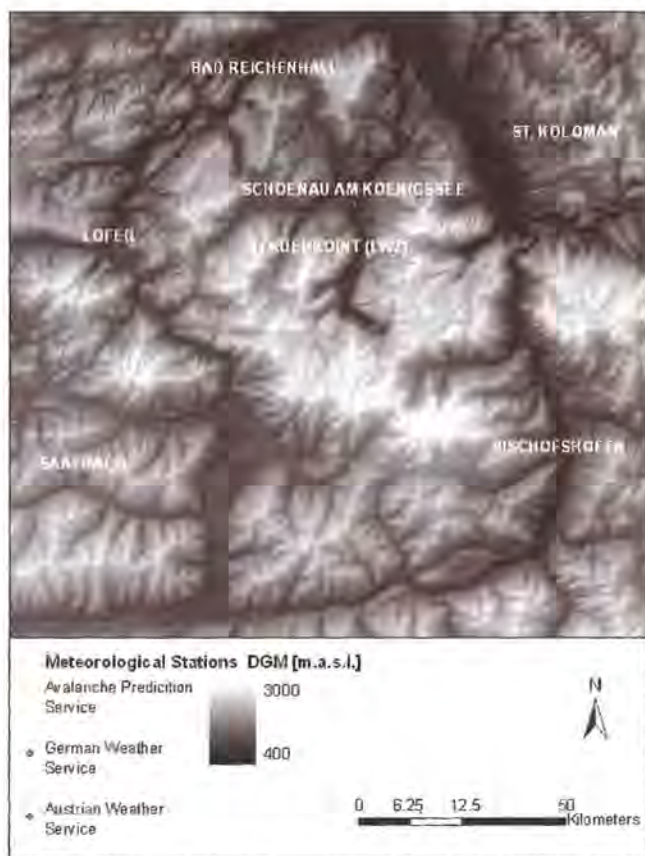


**Figure 6:** Location of the six surrounding weather stations of the German and Austrian Weather Service for the interpolation of the meteorological input data for the raster element of the Kühroint station.

### 3.2 The Catchment Scale

To validate the modelled spatially distributed swe of *PROMET*, weather stations of DWD within the Upper Danube catchment, representing the main characteristics of the catchment, are selected. *Regensburg*, located close to the Danube, stands for low river valleys with alternating melting and accumulation periods in winter, whereas *Oberstdorf* represents an alpine test site with winter temperatures mostly under the freezing point and a continuous snow coverage from December to the end of March. Low mountain ranges like the Swabian Mountains or the Bavarian Forest are represented by the station *Grainet-Rehberg*. Snowfall occurs from November until March, sometimes interrupted by short periods with warmer temperatures and melting conditions. Fig. 3 shows their locations symbolized by blue triangles. The exact geographical position, the elevation as well as the landscape properties of these stations are described in Tab. 3.

The swe was modelled with *PROMET* for the Upper Danube catchment for the period 1970 to 2005. Figs. 7 - 9 show two diagrams with modelled and measured swe for each of the three locations as well as the regressions with the coefficients of determination. At the station *Regensburg*, the snow cover completely melts during characteristically warmer periods in the winter 1984/85. The

**Table 3:** Characteristics of the selected weather stations of the German Weather Service.

Name	Longitude / Latitude [degree minutes]	Elevation [m a.s.l.]	Landscape
Regensburg	12°06' / 49°03'	366	Danube river valley
Grainet-Rehberg	13°37' / 48°48'	655	low mountain range of the Bavarian Forest
Oberstdorf	10°17' / 47°24'	810	Alpine Site

maximum swe reaches 40 mm, which is a small amount compared to the other two stations. The evolution of the swe is more or less simulated in a correct way, except for an underestimation in December 1976 as well as in January 1985. At this time the interpolated temperatures oscillate around the freezing point, so that a small difference in temperature, which effects precipitation to be either assumed as rain or snow, can have a significant effect on the surface energy balance. Furthermore, the resolution of 1 km makes an additional uncertainty which is represented by coefficients of determination of 0.70 and 0.65. In contrast, coefficients of determination of 0.96 and 0.91 prove the qualitatively and quantitatively high performance of the *PROMET* results as modelled at the station *Oberstdorf*. In the winter season 1978/79 the modelled evolution of the swe almost is identical to the measured values until the mid of January. Only the maximum swe and therefore the melting period is a little overestimated. This underestimation of the maximum swe also is modelled in the season 1985/86, whereas at the beginning of the winter season 1985 the swe is overestimated. Nevertheless, the results are of high quality, considering the interpolated input data and the raster element size. At the low mountain site *Grainet-Rehberg*, coefficients of determination of 0.91 and 0.86 are reached. The modelled evolution underestimates the measured swe's in both seasons, whereas the melting periods are modelled close to the measured values. Qualitatively, the modelled swe evolution is correct. As well as for the other two stations, the reason for the underestimation of the swe can be due to the interpolation of the input data on the one hand. On the other hand the sharp threshold value of 273.16K, determining the precipitation phase in the model, can cause differences to nature where the precipitation phase changes within an interval of a few degrees. At the end of December 1976, the temperatures are around freezing point, so that various uncertainties in the temporally interpolated precipitation and its modelled phase (snow or rain) are likely to occur. Furthermore rain is added to melt (see 2.2), the storage of rain in a snow cover is not yet considered.

Comparing the three locations, *PROMET*'s performance is best at *Oberstdorf*. At *Grainet-Rehberg* the simulated swe is acceptable, too, whereas at *Regensburg* the coefficients of determination remain in the lower end of range. Besides the potential source of error in the input data and the spatial raster resolution, the elevation might also have an influence on the modelling. Due to generally little snowfall in lower regions and intermedia-

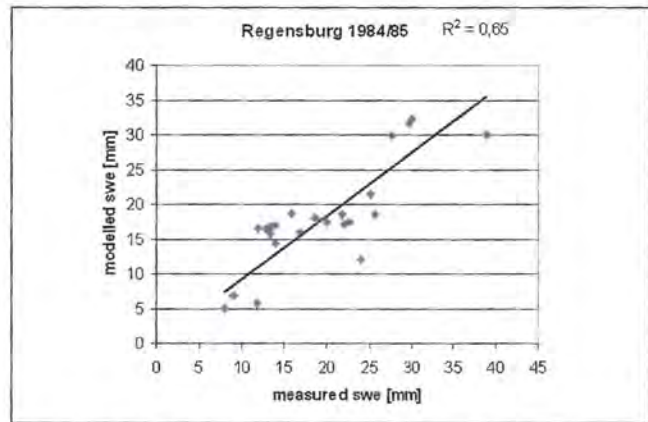
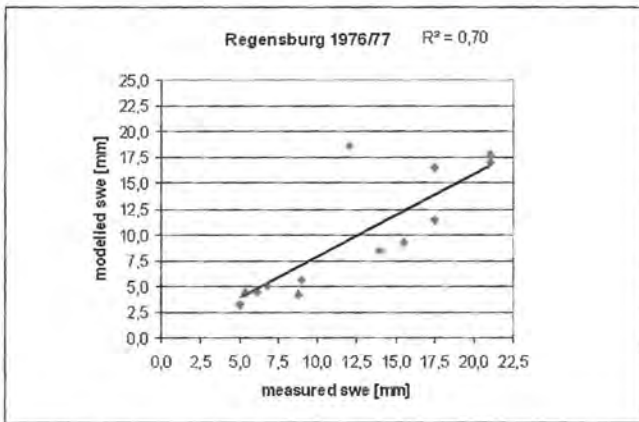
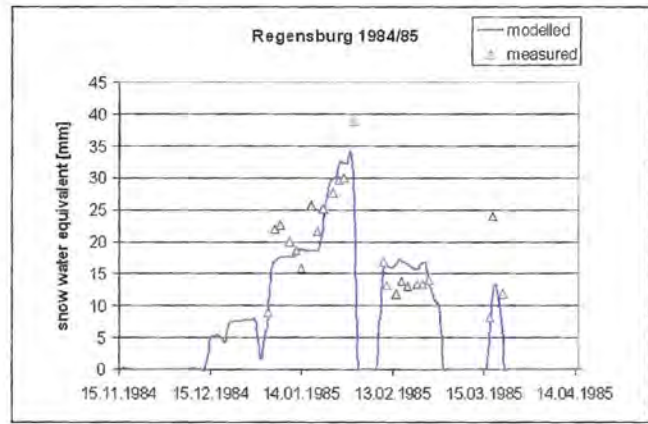
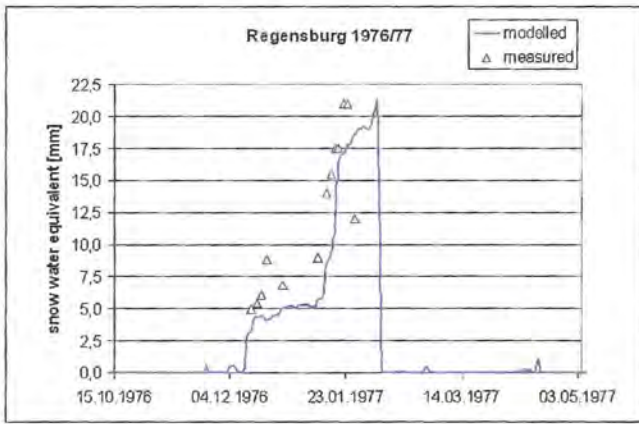


**Figure 7:** The modelled sww by *PROMET* compared to measured values for the station *Regensburg* during the winter seasons 1976/1977 and 1984/1985. The two regressions show the coefficients of determination for the measured to the modelled sww values.

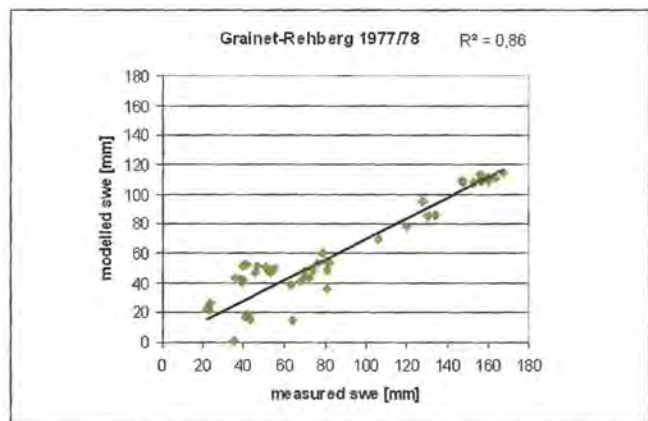
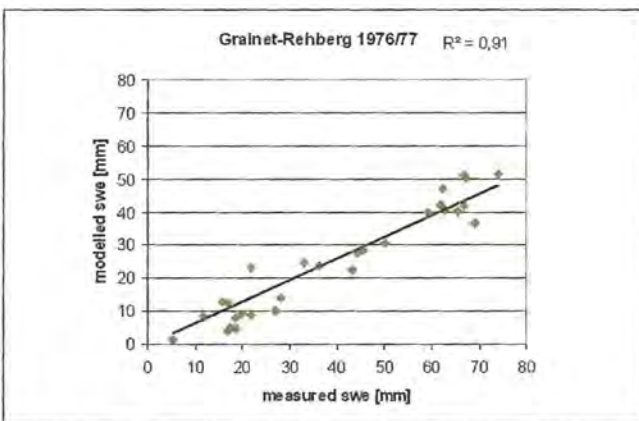
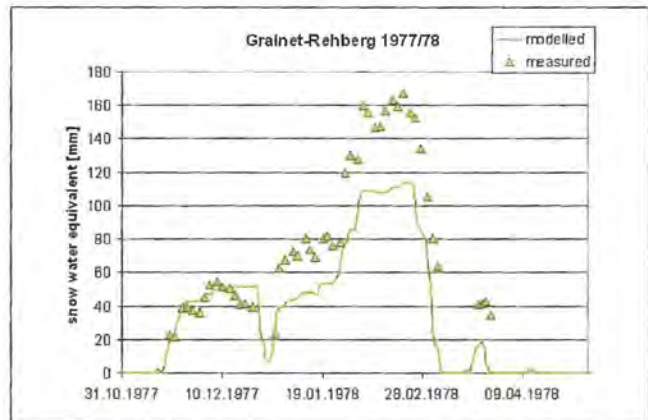
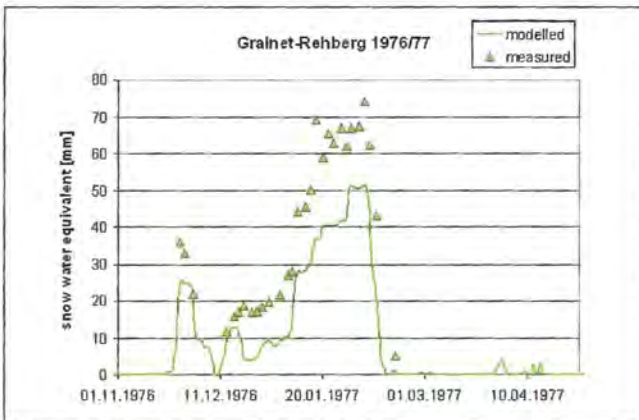


**Figure 8:** The modelled sww by *PROMET* compared to measured values for the station *Grainet-Rehberg* during the winter seasons 1976/1977 and 1977/1978. The two regressions show the coefficients of determination for the measured to the modelled sww values.

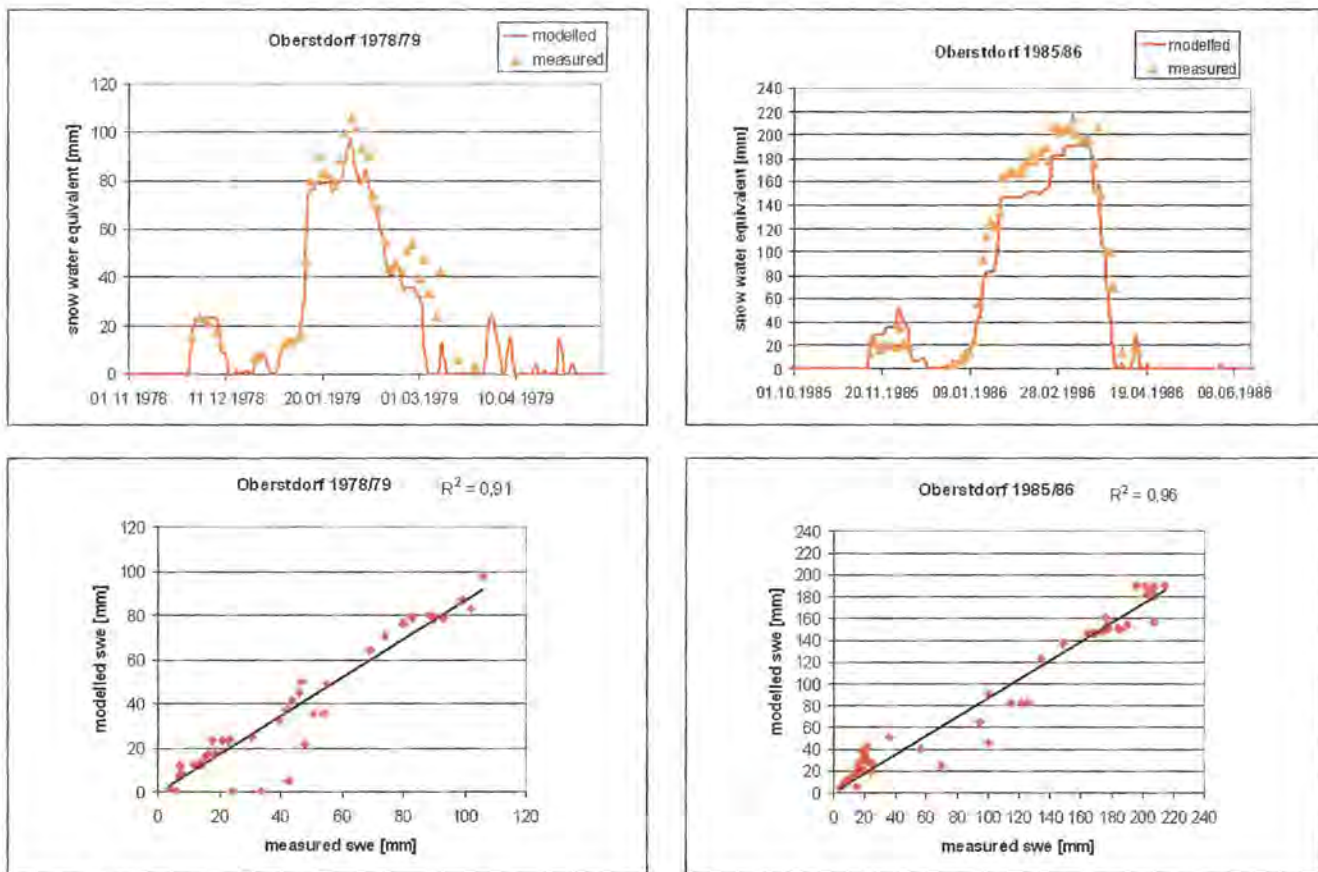


**Figure 9:** The modelled swe by *PROMET* compared to measured values for the station *Oberstdorf* during the winter seasons 1978/1979 and 1985/1986. The two regressions show the coefficients of determination for the measured to the modelled swe values.

te warm periods with melting conditions, the effect of small uncertainties in the data is higher than in mountain regions with seasonal swe's of 80 to 400 mm. Another advantage of the locations *Oberstdorf* and *Grainet-Rehberg* for the validation is the high amount of available measurements, so that the effect of a single error only has a minor effect on the calculation of the coefficient of determination.

Within these two steps, the model physics of *ESCIMO* for the ablation and accumulation of snow are validated in detail at the point scale as well as at the catchment scale with reasonable results. To validate the influence of the interpolation of the meteorological input data (see 2.2) on the snow model, especially on the precipitation phase within *PROMET*, the modelled spatially distributed snow cover for the Upper Danube catchment is compared with satellite derived snow covers. The early winter 2005 is chosen as validation time. At this time of the year the phase of precipitation is the determining factor for getting a snow cover in the model. Not before a snow cover is simulated, the modelling of the accumulation and ablation processes of snow starts. For the validation, images of the medium resolution optical sensor NOAA-AVHRR satellite, classified in snow covered and snow free areas are used. Information about processing these images can be found in BACH et al. (2004), APPEL et al. (2006) as well as at <http://www.polarview.org> and

[www.vista-geo.de](http://www.vista-geo.de). Due to disturbing factors like shadows, a few pixels always remain unclassified. Furthermore, cloud cover and fog constrains an analysis of parts of the images. Tab. 4 shows the dates of the comparison, the modelled snow cover and the difference to the result derived from the satellite data.

**Table 4:** Dates and results of the comparison of modelled to satellite derived snow covers.

Date	percentage of classified image [%]	modelled snow cover [% of the classified image]	difference to the satellite derived snow cover [%]
18.10.2005	88,06	0,10	0,10
27.10.2005	69,45	0,00	-1,79
6.11.2005	8,68	0,00	0,00
13.11.2005	30,53	0,00	0,00
18.11.2005	10,69	0,00	-0,25
27.11.2005	45,06	38,84	-59,13
11.12.2005	83,53	47,31	-10,40
15.12.2005	47,29	65,84	-4,17

As images with classified areas under 30 percent (6th, 13th and 18th of November) do not represent enough information for a comparison, they are not included in the analysis. The dates with a modelled snow cover less than one percent are also not sufficient. As the snow co-

ver at this time is concentrated on high alpine sites, the differences between the two images are marginal. For the remaining three dates of the 27th November, the 11th and 15th of December a snow cover of more than 38 percent is modelled. The resulting snow cover of *PROMET* is shown in *fig. 10a, b, and c* on the left whereas on the right one can see the NOAA/AVHRR classification for the three dates.

On 15th of December the best result is produced by *PROMET* with only little underestimation of four percent compared to the satellite derived snow cover. The model overestimates the snow cover in the Swabian low mountains whereas it is underestimated in the western part of the catchment close to the Alps. Almost the rest of the southern part of the Upper Danube catchment is covered with snow on both images. As 52 percent of the north-eastern part of the catchment is unclassified due to cloud coverage or fog, a sensible part with low elevation can not be analysed. This might be a reason for the difference of up to ten percent on the 11th of December. At this date the Bavarian Forest as well as the Low Bavarian uplands and the Danube River valley are classified. Overall, the spatial pattern of the snow cover is quite similar. The southern part of the catchment, the southern Bavarian Forest as well as the western Swabian Mountains are snow covered on both images. In contrast, in the northern Bavarian Forest and in the Lower Bavarian uplands the snow covered areas are slightly underestimated. This difference might be due to the dependence of the interpolated meteorological input data on elevation in *PROMET*. In regions with low elevation, the determination of the precipitation phase (see 2.2) is more critical than in the higher regions in the southern parts of the catchment, activated through the sharp threshold value in the model. Furthermore the classification algorithm for the NOAA-AVHRR snow product could also be a source of uncertainty. Especially for single raster elements the classification might be difficult due to local effects on the reflected spectrum. As its' validation shows corresponding classifications to the measurements in 95% of all cases, this uncertainty is very low (BACH et al. 2004). For this day the model accuracy is still in a reasonable range whereas on the 27th of November the difference between the two images reaches a maximum of 59 percent. The snow cover along the Danube river valley is simulated as snow free in contrast to the satellite image. The Alpine part of the catchment again is modelled in the right way. Wet snow and/or temperatures around the freezing point with the critical determination of the precipitation phase can cause this high difference.

#### 4. Results and Discussion

The performance of the physically based snow model *ESCIMO* is validated as stand alone model at the point scale at various test sites. In the *Snow models Intercomparison Project* the model is validated among 23 other models at four different alpine locations. At the cold test sites *Weissfluhjoch* and *Goose Bay* as well as at the

temperate test sites *Col de Porte* and *Sleepers River*, *ESCIMO* simulates the *swe* with reasonable accuracy. At the weather station *Kühroint* the snow cover is modelled almost exactly both in amount and evolution with just very small deviations, shown by a coefficient of determination of 0.93. Therefore the results at the point scale with exact input data are of high quality and the model physics simulates the snow accumulation and ablation processes close to the measured values.

With *PROMET*, spatially distributed fields of the meteorological input data are provided, and such a distributed application of an integrated mode of *ESCIMO* is enabled. Compared to the simulations of the stand-alone mode for the station *Kühroint*, the results of *PROMET* do not reach the high quality, but produce good results for the fact that input data is both temporally and spatially interpolated. In a first step, *PROMET*'s results are validated with the measurements of three representative DWD weather stations. The performance at the alpine site *Oberstdorf* is very high with a coefficient of determination of 0.96 and 0.91, respectively. For the low mountain station *Grainet-Rehberg* good results are also achieved, whereas at the station *Regensburg*, representing a location with low elevation, the performance of the model is not as high (coefficient of determination = 0.70 and 0.65) as for the other two stations. Reasons for the differences between the three locations are local climatic conditions with little *swe*'s as well as intermediate changes between melting and accumulation periods due to temperatures around freezing point at *Regensburg*, compared to continuously cold winters with *swe*'s between 80 and 400 mm and a snow cover during the whole winter in *Grainet-Rehberg* and *Oberstdorf*. In the second case, small uncertainties in the temperature have a lower effect on the modelled energy balance than in the first case (the difference between minus 5 and minus 4 degrees Celsius does not imply a phase change, but between minus 0.5 and plus 0.5 degrees Celsius it does). This effect also can be activated through the sharp threshold value of 273.16K in the model, whereas in nature the precipitation phase changes in an interval of a few degrees (BACH et al. 2007). Moreover, the temporally and spatially interpolated input data as provided by *PROMET* strongly depends on elevation, which can be source of errors mainly in lower (and such flat) regions. Finally, the raster area size represents an assumption of homogeneity which results in a certain scale uncertainty (e.g., pixel elevation is not station elevation). These potential sources for deviations are all also part of the comparison between the modelled, spatially distributed snow cover with a satellite derived snow cover in the third step of the validation in early winter. The phase of precipitation due to the spatially interpolated temperatures within *PROMET* is the determining factor for the formation of a snow cover. As the comparison shows, differences between the model results and the images mostly occur in regions with low elevation, e.g. along the Danube River valley or in Low Bavaria, where the initialising temperature for the precipitation phase is critical. This is also shown by the example of the 27th of Novem-

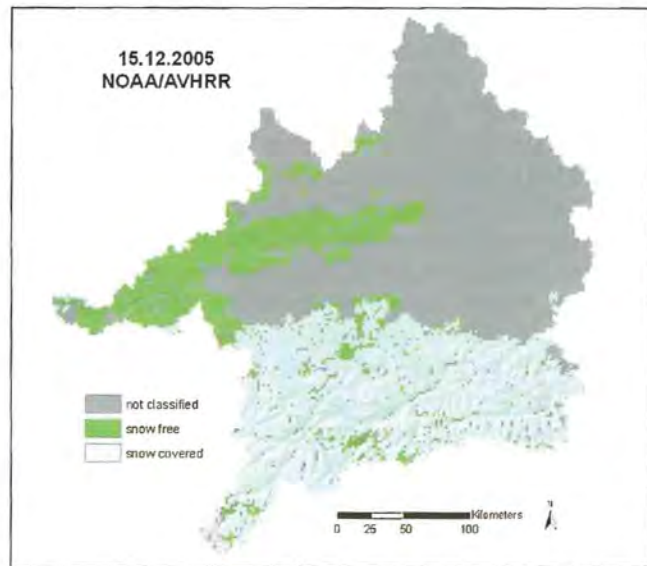
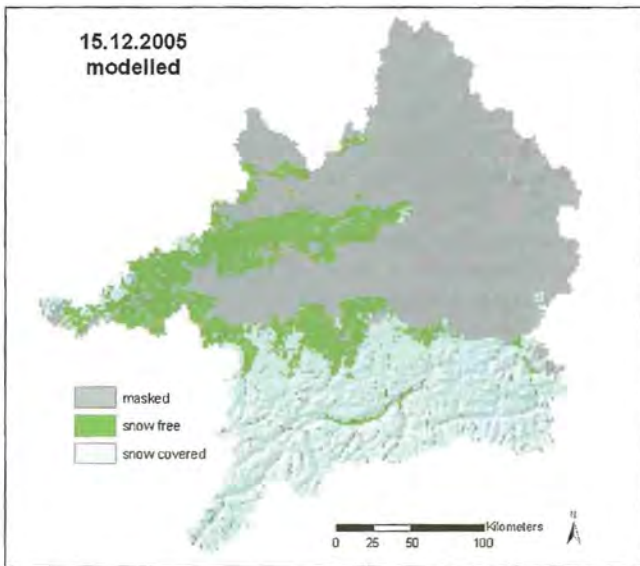


**Figure 10 a:** The modelled snow cover of *PROMET* and the satellite derived snow cover of NOAA-AVHRR for the 15th of December 2005.

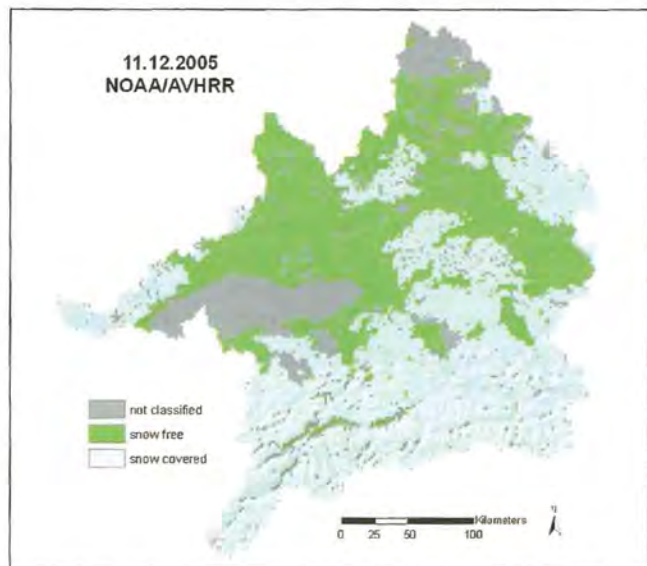
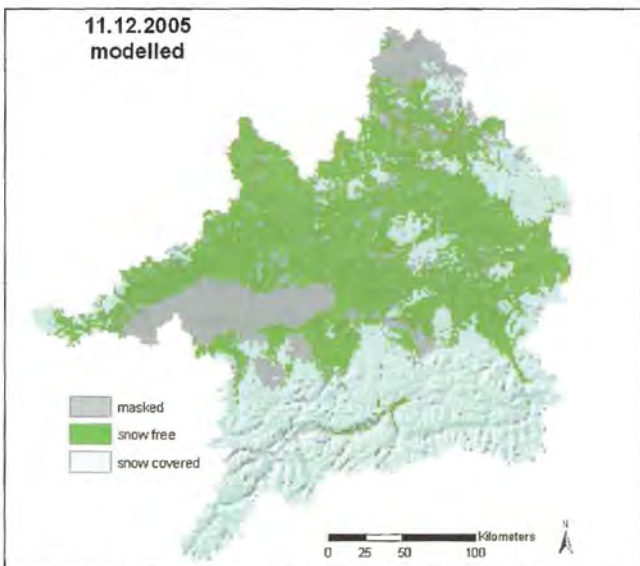


**Figure 10 b:** The modelled snow cover of *PROMET* and the satellite derived snow cover of NOAA-AVHRR for the 11th of December 2005.

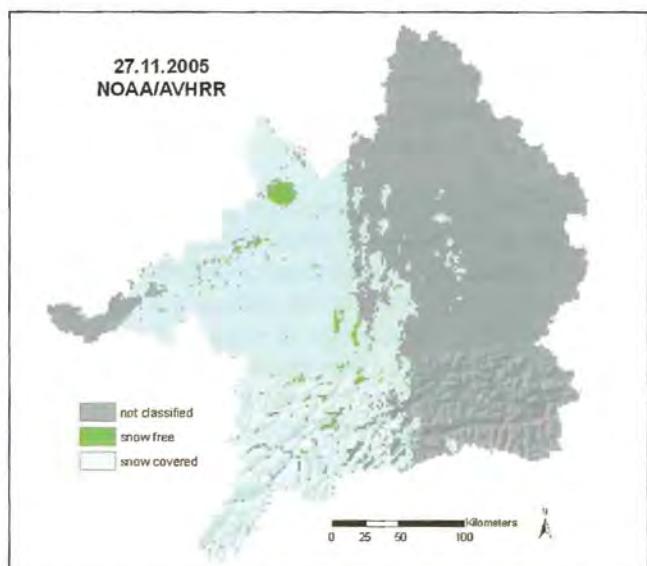
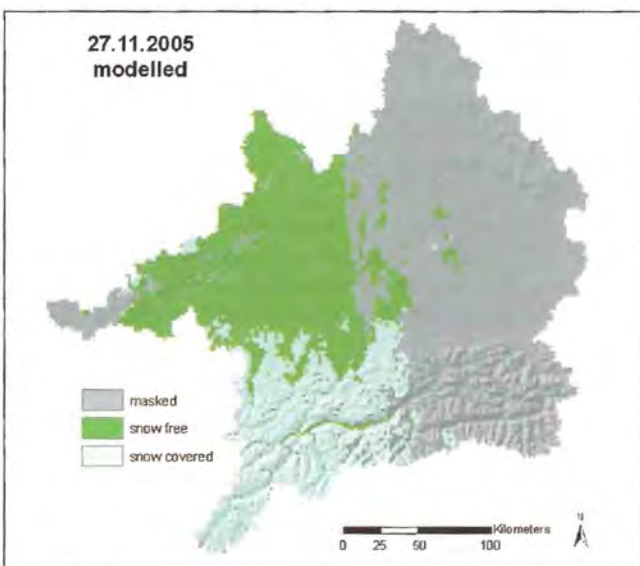


**Figure 10 c:** The modelled snow cover of *PROMET* and the satellite derived snow cover of NOAA-AVHRR for the 27th of November 2005.

ber. In both cases the temperature, oscillating around the freezing point, is a key factor for the model results. Except for the last example, the accuracy of *ESCIMO* within *PROMET* for spatially distributed applications achieves 90 percent, which is in a reasonable range. Overall the model physics of *ESCIMO* produces results of high quality on the point as well as on the catchment scale. Uncertainties are due to the interpolated input data within *PROMET* in sensitive regions with low elevation as well as in seasons with temperatures around the freezing point in early or late winter on the one hand. On the other hand the model threshold value for determining the precipitation phase is too sharp compared to nature. Furthermore, mixed precipitation with rain and snow as well as rain, stored in a snow cover is not yet considered in the model.

## 5. Conclusions and future perspective

*ESCIMO* as stand-alone model as well as included into *PROMET* is a tool which enables to simulate the snow water equivalent with good accuracy in amount and timing. The best performance is achieved for mountain regions and for locations with temporally high resolution input data (e.g. *Kühroint*). But even in other environments with interpolated input data and in low elevation, the results of the snow model are reasonable and sufficient for other applications, e.g. hydrological modelling. Considering the uncertainties due to critical temperature ranges around 273.16 K, *ESCIMO* can be applied for the snow modelling on the point as well as on the catchment scale.

Included into *PROMET* the snow model *ESCIMO* was and is applied in various regions, e.g. in the Weser catchment (STRASSER AND MAUSER 2001). Within the framework of the *Brahmatwinn* research project ([www.brahmatwinn.uni-jena.de](http://www.brahmatwinn.uni-jena.de)), the model will be applied for regional hydrological modelling in the Himalayan catchment of the Upper Brahmaputra. In this EU-funded project we focus on the influence of snow and glacier melt on the spatial variation and temporal dynamics of runoff generation in the Upper Brahmaputra watershed considering scenarios of future climate change up to the IPCC horizon (2001).

Furthermore *ESCIMO* is participating in the *Snow Model Intercomparison Project* for forest snow processes *SnowMIP2* in which the performance of different snow models for the processes in forest canopies is compared. Inside the forest, interception of snow in the trees and various canopy-related interactions influencing the meteorological conditions on the ground have to be considered for an accurate modelling of the ground snow cover (<http://users.aber.ac.uk/rie/snowmip2.html>). For this purpose *ESCIMO* recently was extended with algorithms for the simulation of the forest snow processes interception, sublimation and melt/fall down from the trees of a canopy (STRASSER et al. 2007, LISTON AND ELDER 2006). Results of *SnowMIP2* will be published in 2007.

## Acknowledgements

We would like to thank Helmut Franz and the Rangers of the National Park Berchtesgaden for providing us with the data of the station *Kühroint* as well as Stephanie Mayr for processing these data. The provision with the snow cover maps in the frame of the ESA-GMES activity *PolarView* ([www.polarview.org](http://www.polarview.org)) by Heike Bach and Florian Appel from *VISTA* ([www.vista-geo.de](http://www.vista-geo.de)) is gratefully acknowledged. Special thanks to Dr. Markus Weber for all the discussions about snow modelling. We also would like to thank the German Federal Ministry for Education and Research (BMBF) for funding the *GLOWA* initiative.

## References

- APPLE, F., BACH, H., LOEW, A. AND MAUSER, W. (2006): Snow cover mapping for Central Europe – enhancement of optical and microwave remote sensing methods towards an operational service. European Geoscience Union (EGU), General Assembly, 02.-09, April 2006, Vienna, Austria
- BACH, H., APPEL, F., LÖW, A. AND LUDWIG, R. (2004): Assimilation of Snow Properties Derived from ASAR Wide Swath Data in a Hydrological Model of the Neckar Catchment for Improved Flood Forecast. Proc. ENVISAT Symposium, 6.-10.Sept.2004, Salzburg, = ESA Special publications SP 572.
- BACH, H., APPEL, F. AND MAUSER, W. (2007): Provision of snow information from satellite data within *Polar View* and application example for the a mesoscale Alpine catchment using *PROMET*. In: Research reports, National Park Berchtesgaden (this issue).
- BALDOCCHI, D.D., HICKS, B.B. AND CAMARA, P. (1987): A canopy stomatal resistance model for gaseous depositions to vegetated surfaces. *Atmospheric Environment* 21, 91-101.
- EAGLESON, P.S. (1978): Climate, soil and vegetation. 3. A simplified model of soil movement in the liquid phase. *Water Resour.Res.* 14, 722-730.
- ETCHEVERS, P., MARTIN, E., BROWN, R., FIERZ, C., LEJEUNE, P., BAZILE, E., BOONE, A., DAI, Y.-J., ESSERY, R., FERNANDEZ, A., GUSEV, Y., JORDAN, R., KOREN, V., KOWALCZYK, E., NASONOVA, N.O., PYLES, R.D., SCHLOSSER, A., SHMAKIN, A.B., SMIRNOVA, T.G., STRASSER, U., VERSEGHY, D., YAMAZAKI, T. AND YANG, Z.-L. (2002): *SnowMIP*, an intercomparison of snow models: first results. Proceedings of the International Snow Science Workshop, Penticon, B.C., October 2002.
- ETCHEVERS, P., MARTIN, E., BROWN, R., FIERZ, C., LEJEUNE, P., BAZILE, E., BOONE, A., DAI, Y.-J., ESSERY, R., FERNANDEZ, A., GUSEV, Y., JORDAN, R., KOREN, V., KOWALCZYK, E., NASONOVA, N.O., PYLES, R.D., SCHLOSSER, A., SHMAKIN, A.B., SMIRNOVA, T.G., STRASSER, U., VERSEGHY, D., YAMAZAKI, T. AND YANG, Z.-L. (2004): Validation of the surface energy budget simulated by several snow models (*SnowMIP* project). Papers from the International Symposium on Snow and Avalanches, June 2003, Davos, Switzerland. In: *Ann. Glaciol.*, Vol. 38, pp 150-158.

- IPCC, Intergovernmental Panel on Climate Change (2001): Climate Change 2001: Impacts, Adaption and Vulnerability. Contribution of Working Group II to the Third Assessment Report of the Intergovernmental Panel on Climate Change. – MCCARTHY, J.J., GANZIANI O.F., LEARY, N.A., DOKKEN, D.J. AND WHITE, K.S. (eds.). Cambridge University Press, Cambridge, United Kingdom and New York, NY, USA, 881p.
- IUCN (2003): Change. Adaptation of Water Management to Climate Change. – IUCN, Gland, Switzerland and Cambridge, UK. ix + 53 p.
- LISTON, G.E. AND ELDER, K. (2006): A Distributed Snow-Evolution Modeling System (SnowModel). In: J. Hydrometeor., Vol. 7, No.2, 217-234
- LUDWIG, R. AND MAUSER, W. (2000): Modelling catchment hydrology within a GIS based SVAT-model framework. Hydrology and Earth System Science HESS 4(2), 239-249.
- LUDWIG, R., PROBECK, M. AND MAUSER, W. (2003): Mesoscale water balance modelling in the Upper Danube watershed using sub-scale land cover information derived from NOAA-AVHRR imagery and GIS-techniques. Physics and Chemistry of the Earth 28, 1351-1364.
- MAUSER, W. (1989): Die Verwendung hochauflösender Satellitendaten in einem Geographischen Informationssystem zur Modellierung von Flächenverdunstung und Bodenfeuchte. Habilitationsschrift, Albert-LUDWIGs-Universität, Freiburg i.Br.
- MAUSER, W. AND SCHÄDLICH, S. (1998): Modelling the spatial distribution of evapotranspiration on different scales using remote sensing data. J. Hydrol. 212-213, 250-267.
- MAUSER, W., BACH, H., STRASSER, U. AND SCHNEIDER, K. (1998): The contribution of remote sensing data to distributed hydrologic modeling, Information for Sustainability, I SBN82-7542- 040-7, Proceedings Int. Symp. Rem. Sens. Envir., pp.295-299
- MONTEITH, J.L. (1965): Evaporation and the environment. In: Symp. Soc.Expl. Bio. 19, pp.205-234.
- MONTEITH, J.L. (1978): Grundzüge der Umweltphysik. Dr. Dietrich Steinkopf, Darmstadt.
- STRASSER, U. (1998): Regionalisierung des Wasserkreislaufs mit einem SVAT-Modell am Beispiel des Weser-Einzugsgebiets. Münchner Geographische Abhandlungen, Reihe B, Band 28, 146p, ISBN 3 925 308 88 1.
- STRASSER, U. AND MAUSER, W. (2001): Modelling the Spatial and Temporal Variations of the Water Balance for the Weser Catchment 1965-1994. In: J. hydrol., Vol 254/1-4, 199-214.
- STRASSER, U., FRANZ, H. AND MAUSER, W. (2007): Distributed modelling of snow processes in the Berchtesgaden National Park (Germany). In: Research reports, National Park Berchtesgaden (this issue).
- Internet:  
 Brahmawinn Projekt: URL [www.brahmatwinn.uni-jena.de](http://www.brahmatwinn.uni-jena.de)  
 ENSEMBLES: URL [www.ensembles-eu.org](http://www.ensembles-eu.org)  
 EUROPLIMPAC: URL [www.eurolimpacs.ucl.ac.uk](http://www.eurolimpacs.ucl.ac.uk)  
 GLOWA: URL [www.glowa.org](http://www.glowa.org)  
 GLOWA-Danube: URL [www.glowa-danube.de](http://www.glowa-danube.de)  
 KLIWA: URL [www.kliwa.de](http://www.kliwa.de)  
 POLARVIEW: <http://www.polarview.org>  
 SnowMIP 1: URL <http://www.cnrm.meteo.fr/snowmip/>  
 SnowMIP 2: URL <http://users.aber.ac.uk/rie/snowmip2.html>  
 VISTA: [www.vista-geo.de](http://www.vista-geo.de)

## 12 Snow cover area (SCA) estimation and analysis in the alpine range using moderate resolution satellites

FRANCESCO ROTA NODARI, FRANCESCA SAPIO,  
MICHELA BIAGGI

Remote Sensing Data Engineering (RSDE),  
Via Washington 78, 20146 Milano, Italy

### Abstract

The environmental importance of medium and high latitudes snow cover is well established. Snow melt dynamics generate a complex set of interactions, which dictates a need for long-term monitoring of snow cover in conjunction with other climatological variables.

Suitable data can be derived from satellite observations. Moderate satellite sensors help in the survey of the variations of snow coverages because they provide synoptic information over large territories, have low costs and adequate spectral resolution, even if the low spatial resolution it is still a problem.

Previous works have been focused on the monitoring of American northern regions and the procedures involved have been tuned to large areas. In particular NASA mission on Moderate Resolution Imaging Spectroradiometer (MODIS) have been tailored to monitor spatial phenomena all over large areas.

The work here presented has been performed in the AWARE project funded by EC. This project aims at providing innovative tools for monitoring and predicting water availability and distribution in snowmelt regime Alpine catchments using hydrological models and Earth Observation data integrated.

Among the available EO sensors, MODIS has been chosen as the most suitable for producing the required parameters, according to factors identified in the analysis of requirements, such as temporal coverage and resolution, spectral and spatial resolution.

Snow Cover Area (SCA) has been estimated on the Alpine range. The raw images have been converted in radiance; then water and clouds cover has been masked and a snow index has been calculated. Alpine basins considered have a dimension that not allow the application of NASA MODIS mission elaboration methodology so the procedure has been modified and a new approach, tailored on Alpine basins, have been settled.

### 1. Introduction

In the latest years, a generalized global warming and a continue glacier retreat on the Earth surfaces increase community attention on water availability problems. The environmental importance of medium and high latitudes snow cover is well established. As well as its role in albedo feedback it is an indicator of global climate, though a complex one since a warming climate can have both po-

sitive effect through increased precipitation and a negative effect through increased melting. Snow melt dynamics generate a complex set of interactions, which dictates a need for long-term monitoring of snow cover in conjunction with other climatological variables.

Recent droughts observed in Alpine catchments and the downstream rivers (e.g. the 2003 drought of the Po river in Italy) indicate the need of an efficient technology to predict medium and long-term flows for sustainable water resources management.

Excluding the great ice sheets of Antarctica and Greenland, snow cover is primarily a phenomenon of the northern hemisphere and the mountainous ranges. So, snow coverage analysis all over the mountainous ranges and the cold regions is a key aspect in this climate research challenge that involves all the world populations and countries (CHANG et al. 1987).

Estimate with a global coverage the processes of snow melting will be more and more fundamental for the management of water resource of the globe. There is considerable interest in monitoring their long-term variations and linking these to climate change.

Suitable data can be derived from satellite observations. Moderate satellite sensors help in the survey of the variations of snow coverages because they provide synoptic information over large territories, have low costs and adequate spectral resolution, even if the low spatial resolution it is still a problem.

Previous works (ANDREADIS AND LETTENMAIER 2005) have been focused on the monitoring of American northern regions and the procedures involved have been tuned to large areas. In particular NASA mission on Moderate Resolution Imaging Spectroradiometer (MODIS) have been tailored to monitor spatial phenomena all over large areas.

The activity here presented has been performed in the framework of **AWARE** project (*A tool for monitoring and forecasting Available WATER REsource in mountain environment*), in the Sixth program of the EC. This is a Research Project that aims at providing innovative tools for monitoring and predicting water availability and distribution in snowmelt regime Alpine catchments using *Earth Observation* (EO) data. Different hydrological models will be applied to basins situated all over the Alps to estimate the amount of water availability from snow variations in the melting season (April – July). The duration of the project is of 3 years starting from July 2005. This project has eight partners coming from different European countries (Italy: CNR-IREA, RSDE, POLIMI; Austria: TUW; Spain: ICC, UJI; Switzerland: SLF; Slovenia: ULFGG) and a big number of users interested on data and information produced (Web: <http://www.aware-eu.info>). The project is intended towards bridging the gap between the information providers about the state of water resources and the different stakeholders, including water policy makers, economic (hydropower companies, irrigation schemes, municipal water supply), and social (regional, basin and municipal authorities, citizens) stakeholders.

Calibration, validation and demonstration will be performed for representative catchments of different geogra-

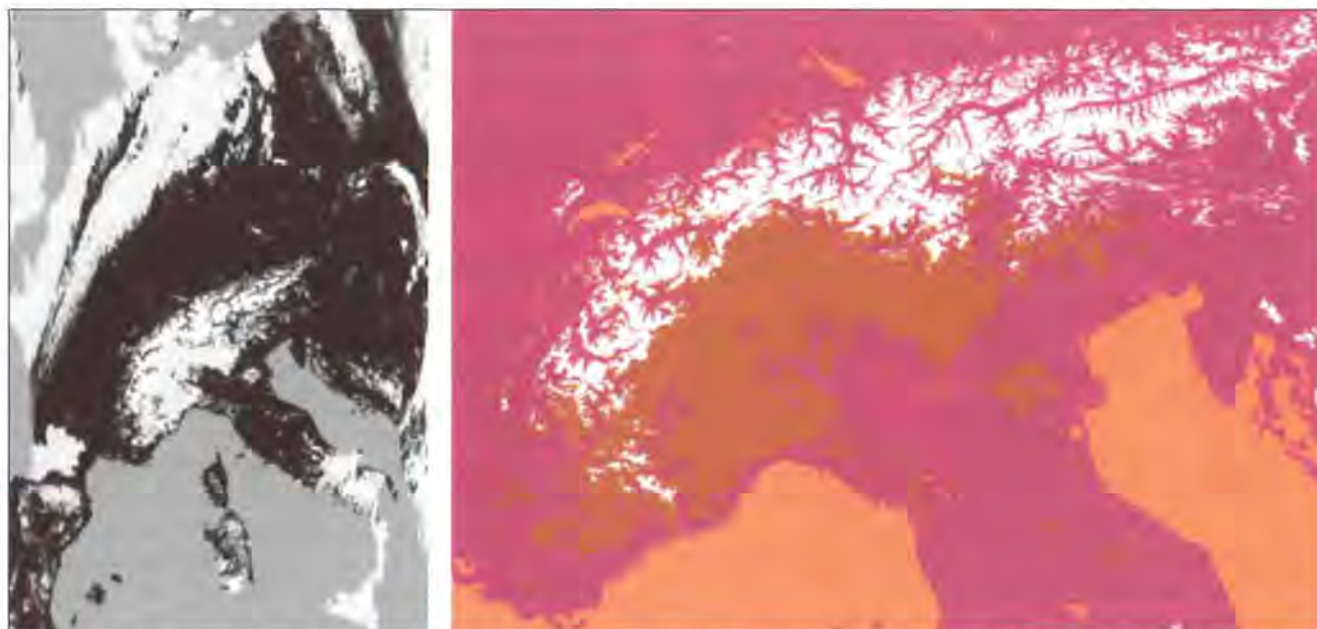


**Figure 1:** The MOD10 product for Europe and the product after the reprojection for the Alpine area. In white the snow coverage.

phic (climate, geology, etc.) conditions in the European Alps: this operation will include benchmarking of traditional models based on ground monitoring of the input-output control variables, and of innovative models assimilating ground and Earth Observation data under a spatially-distributed, physically-based approach.

Among the available sensors, MODIS has been chosen as the most suitable for producing the required parameters, according to factors identified in the analysis of requirements, such as temporal coverage and resolution, spectral and spatial resolution.

The dimensions of the considered Alpine basins do not allow the application of NASA MODIS mission elaboration methodology (HALL et al. 2001). A new approach tailored on Alpine basins has been settled.

A big amount of the project work, object of this paper, regards the elaboration of EO data to be used as inputs in the hydrological models. This data will be used for the extraction of parameters of hydrological models to be integrated with traditional measurements, however snow drifted and snow depth are not considered as inputs in the analysed models.

Due to the high number of images to be processed (for the high temporal resolution required by the hydrological models) some procedures have been set up and implemented to automatically identify, download, geocode and calibrate images as well as to extract snow parameters (ENGMAN AND GURNEY 1991).

As the main information used by all project models is the Snow Covered Area (SCA), different images classification procedures for producing snow cover maps have been compared in order to identify the most suitable for the purpose taking into account the need for repeatability and automation. The comparison resulted in a modification of the Normalised Difference Snow Index (NDSI) in order to customize it on the Alpine characteristics. While basins requiring a more detailed spatial resolution

and fractional cover information (Switzerland and Austrian ones), a set of classified images has also been planned by using the fuzzy statistical classifier. A set of procedures *ad hoc* will be implemented for the extraction of parameters from EO data. This information regards the distribution of snow-cover, the albedo and the temperature and could be an improvement of the data retrieved in situ.

The novelty of the presented approach consists in the tailoring of the NASA snow cover monitoring method changing the conventional steps of the procedure.

## 2. Methods

### 2.1. EO data acquisition

The selection of the suitable EO data depends on many factors:

- Historical and revisit times (temporal coverage and resolution) requirements;
- Spatial requirements;
- Spectral bands measured by the sensor (spectral resolution);
- Cost vs. value of the information;
- Data processing requirements.

Different kind of EO data has been taken into consideration: NOAA-AVHRR, MODIS, Landsat TM sensor and ASTER. The MODIS images are the selected one. The major advantages of MODIS are that it provides a sufficiently high repetition rate and cover an area as larger as the Alps.

The MODIS sensor is well suited for snow cover monitoring. Its repetition cycle of less one day allows to map the change of snow cover extent with a sufficiently high temporal resolution. The temporal resolution is the characteristics that not allow applying the Landsat TM sen-

sensor that has a repetition cycle of 15 days and may not all images available can be used due to the clouds cover. These kinds of images have a better spatial resolution respect to the NOAA-AVHRR (1.1 km<sup>2</sup>). RANGO et al. (1983) state that the NOAA's spatial resolution of 1.1 km is sufficient if large areas of more than 200-500 km<sup>2</sup> are targeted, however, an area of 500 -1000 km<sup>2</sup> and more seems to provide a better sound statistical data basis. Several basins in the Alps zone not allow the applicability of the NOAA sensors due to the smaller area.

The spectral bands measured by MODIS sensors have different spatial resolution from 250 m to 500 m. The electromagnetic spectrum is divided in 36 parts (bands) subdivided in visible, near infrared, medium infrared (only the visible and near infrared ones, bands 1 and 2, have a resolution of 250 m). Also from this point of view the selected sensor MODIS is better than other as NOAA that have not channels in the medium infrared that is a very useful to identify the snow cover area.

The last, but not less important characteristics of a sensor is the availability and the cost. In this case the MODIS images are free and very easily available on the NASA's Server. It is possible to order the images by internet and the day after you can pull down them.

The web site is:

<http://edcimswww.cr.usgs.gov/pub/imswelcome/>.

Two kind of MODIS data are available: the not classified ones (MOD02) and the processed ones (products). Among these products we can find maps regarding the cloud coverage (MOD35), surface temperature (MOD11), vegetation indexes (MOD13), snow coverage (MOD10) (<http://modis.gsfc.nasa.gov/>). As said before, these products are not generally suitable for each part of the world and it should be necessary a tuning phase to obtain correct information on the studied zones.

A variety of snow and ice products (see Figure 1) is produced from the MODIS sensors, and the products are available at a variety of spatial and temporal resolutions (MAURER et al. 2003).

The dimensions of the considered Alpine basins do not allow the application of NASA MODIS mission elaborati-

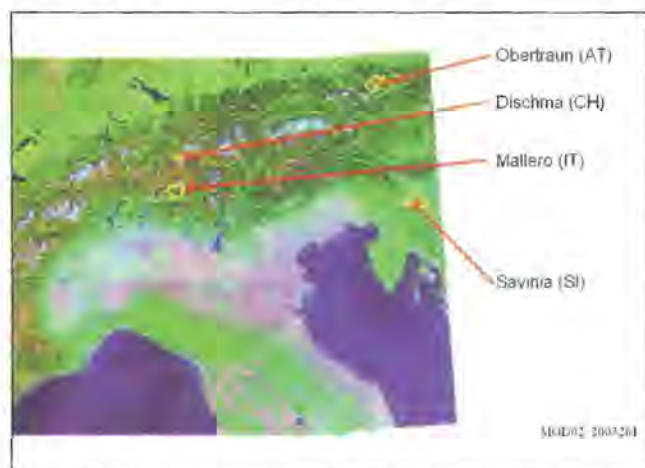


**Figure 2:** The Alpine range in a MODIS image (resolution of 500; R, G, B; 6, 2, 3). The selected basins as test areas are visible with a yellow colour boundary. The hydrological year selected as first test analysis is the 2002/2003.

on methodology. A new approach tailored on Alpine basins has been settled. For this initial phase, basins in the Countries of each partner of the project have been selected. These are: Mallero in Lombardy, Sava in Slovenia, Dischma in Switzerland and Obertraun in Austria, as shown in the Figure 2.

## 2.2. Analysis of the algorithm for the classification

When defined the images to be downloaded from the NASA server considering cloud coverage and geographical information, 12 images (one a month) has been selected for the production of the Snow Cover Area. In the following releases this number could increase and could be tuned for each basin. We have analysed which is the best procedure of classification to be applied to the images. Firstly it is necessary to underline that the results of the classification is different considering the whole Alpine range and the single basins. When the test sites have been decided, it is recommended to test different classification procedures to check the best one (easier and faster to be applied).

For this application only the first 7 bands of the MODIS images will be used, because of the spatial resolution required (not less than 500 meters). So, the spectral range of application changes from visible to near, medium, short wave infrared.

The procedure applied has been different on the basis of the spatial resolution of the EO data. We consider 500 meters and 250 meter MODIS imagery.

The first test to check the best classification has been applied on 04th January 2003 and 11th January 2003 images. This preliminary activity allows verifying the applicability of supervised or unsupervised classification for our purposes. Then, the date selected for testing classification has been the 91st Julian day of year 2003, corresponding to the 1st April and conventionally corresponding to the first day of the ablation season.

Different procedures have been considered. *Unsupervised* classification (*ISODATA e K-means*), where it is not necessary to train the classifier giving the information of ground truth. Methodologies of threshold and indexing (like NDVI and NDSI) can be also considered unsupervised and they have been tested.

Then *supervised* classification approach has been analysed where the contribution of the user is very high. Among these the *maximum likelihood* and the *fuzzy* classification.

After an analysis cost/benefits, considering the high number of images to be processed and to guarantee a service all over the entire Alpine range, the *Normalised Difference Snow Index* (NDSI) has been chosen as the more appropriated approach to be used in the project. However, the computing of this index has been modified in the consecutive releases for tuning it to the particular zones considered. Topography effects have not been considered in the snow mapping because of the spatial resolution of the product.

### 2.3. Procedure of elaboration of MODIS imagery

The procedure for the extraction of the Snow Cover Area has passed through a complex phase of improving. Different releases have been produced to reach the best SCA product.

The hydrological year selected as first test analysis was the 2002/2003.

Here the steps of the procedure of classification applied to MODIS data to produce the first release.

1. Choice of images
2. Filling the MetaData information
3. Geometrical correction of images
4. Reflectance conversion of the DNs
5. Water slicing
6. Computing of NDSI and its slicing
7. Cloud cover masking
8. SCA production
9. Exporting in GeoTiff format

#### 2.3.1. Choice of images

The choice of the images suitable for the project purposes starts from the downloading of cloud mask file from the NASA server (MOD35, Oct.2002 – Oct.2003). The reason is that these files are easier to be treated for their dimension. The images downloaded are 300 (for the year 2002) and 842 (for the year 2003), 2 to 6 a day, from MOD35 product (cloud mask, 1 km resolution).

Then, this procedure produces a selection of images

that guarantees a total coverage of the Alpine range and with a little cloud coverage. A spatial coverage analysis (panoramic corrections that guarantee a minimum distance of the external boundaries from the interest zone) has been finally conducted. Considering also cloud cover and geographical analysis, a total number of 140 images (Oct.2002 – Oct.2003) with a low percentage of clouds have been produced.

#### 2.3.2. MetaData information

During the acquisition and the choice of images to be used in the process, also information regarding images has been archived reading automatically the metafiles (in *xml* format). This allows the creation of a descriptive catalogue of the images and their characteristics according to the normative *INSPIRE* and *ISO9115*.

It has been possible to fill the table of METADATA (for all the images) using a program written in Access with the ancillary information for each image. In the scheme (Figure 3) are shown metadata information that have been associated to every image.

#### 2.3.3. Geometrical correction of Images

After the selection of the useful images using the MOD35 cloud mask, they have been georeferenced using the geolocation information available by the NASA. Geolocation files have been downloaded from the NASA server (MOD03, Oct.2002 – Oct.2003).

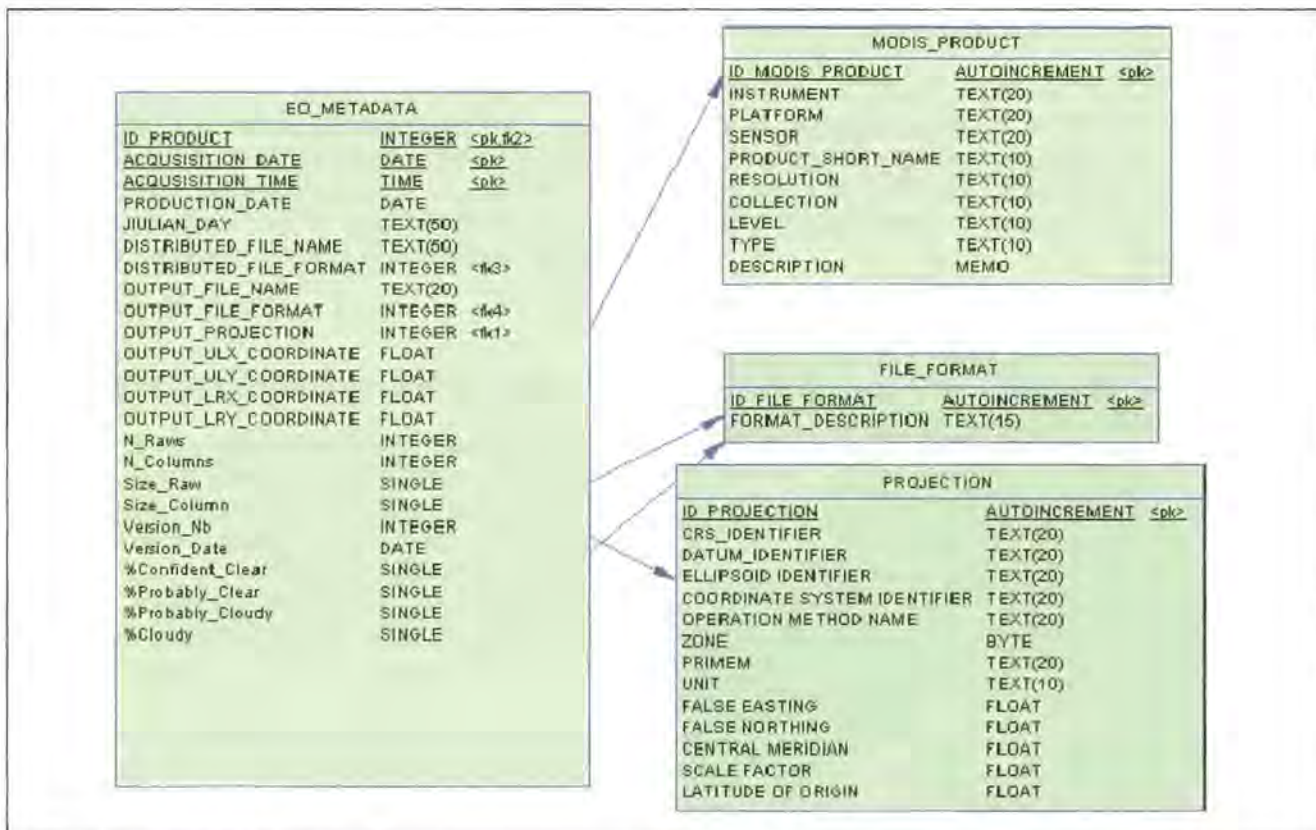


Figure 3: The METADATA scheme

Considering the position of the entire Alpine range (a big area), geographical considerations about different projection has been necessary.

All the information collected (choice of map projections in other EC projects, rules for choosing suitable map projection, recommendations of workshops...) have been analysed, but even the inner aspect of this project such as:

- extension of the area of interest
- data involved
- variety of Coordinate Reference System used by the partners

We arrived to choose an appropriate CRS based on the datum **WGS84**, while the coordinates system we decided to use is **UTM Universal Transverse Mercator**.

One of the recommendations of INSPIRE (The INfrastructure for SPatial InfoRmation in Europe) agrees the use of map projections in order to avoid the use of ellipsoidal coordinates as the mapping of ellipsoidal coordinates to planes ones, cannot be made without distortion. For scales larger than 1:500000 the map projection to use for conformal pan European mapping can be a Transverse Mercator.

AWARE involves the use of data connected to water basins collected at a scale larger than 1:500000 (sometimes even 1:10000): so the use of a conformal map projection such **UTM Universal Transverse Mercator** is suitable to the aim of the project.

The reason for this choice in AWARE project is also due to the wide use of it between the partners of the project, but even for the extreme facility of passing from another coordinate system to this, using a great variety of GIS Software.

The MODIS imagery for the hydrological year 2002-2003 have been treated in a different way because Alps are situated in two different zone of the Universal Transverse Mercator (UTM) projection. So, 12 images have been selected and reprojected in the two zones: UTM 32 N and UTM 33 N.



**Figure 4:** MODIS image 2002-299 georeferenced; zone UTM 132 + UTM 133.

The used projection is: UTM WGS84 but the images are subdivided in the two zones UTM32 and UTM33 (see Figure 4).

A quality check of the geocoding process has been provided using the images in the EU project CORINE2000, obtained by Joint Research Centre.

#### 2.3.4. Conversion in reflectance

The values of the pixels on the images (MOD02) available at NASA are Digital Numbers not atmospherically corrected. It has been decided to use a unique value of reflectance for each band (equal till the fourth places of decimals) to convert in reflectance value (see Table 1).

All the bands considered in the next elaborations are radiometrically corrected.

#### 2.3.5. NDSI index for snow identification

The Normalised Difference Snow Index (NDSI) has been performed and improved by D. HALL on 2001 (HALL et al. 2002). This index, similar to the well known NDVI for vegetation studies, from the MODIS bands 4 and 6 allows identifying snow cover area using an adequate threshold.

$$NDSI = \frac{SWIR - NIR}{SWIR + NIR} \Rightarrow NDSI = \frac{MODIS\ 4 - MODIS\ 6}{MODIS\ 4 + MODIS\ 6}$$

Snow detection is achieved through the use of two groups of grouped criteria tests for snow reflectance characteristics in the visible and near-infrared regions.

When computed this map of NDSI, to obtain the snow cover information it is necessary to consider values bigger than a threshold retrieved from literature or image analysis. The key phase is the decision of this threshold that should be representative for all the snow covered area in the images. It has been decided the fixed value 0.55. In the next releases it will be considered its dependence by seasons and zones (specification for test basins).

#### 2.3.6. Water slicing and masking procedure

As advised in the NASA approach (for providing MOD10 product) and as well known analysing images, it has been necessary to consider the water in the images analysed and find an innovative procedure to well distinguish this feature from snow and clouds.

The best information about water presence is suitable from near infrared bands, that in MOD02 corresponds to band 2.

So, it is normally necessary to establish a threshold over which the band is classified as water. From literature this threshold is 0.11 ( $W\ sr^{-1}\ m^{-2}$ ). In the first release of work, a threshold have been be tuned for sea and inland water separately.

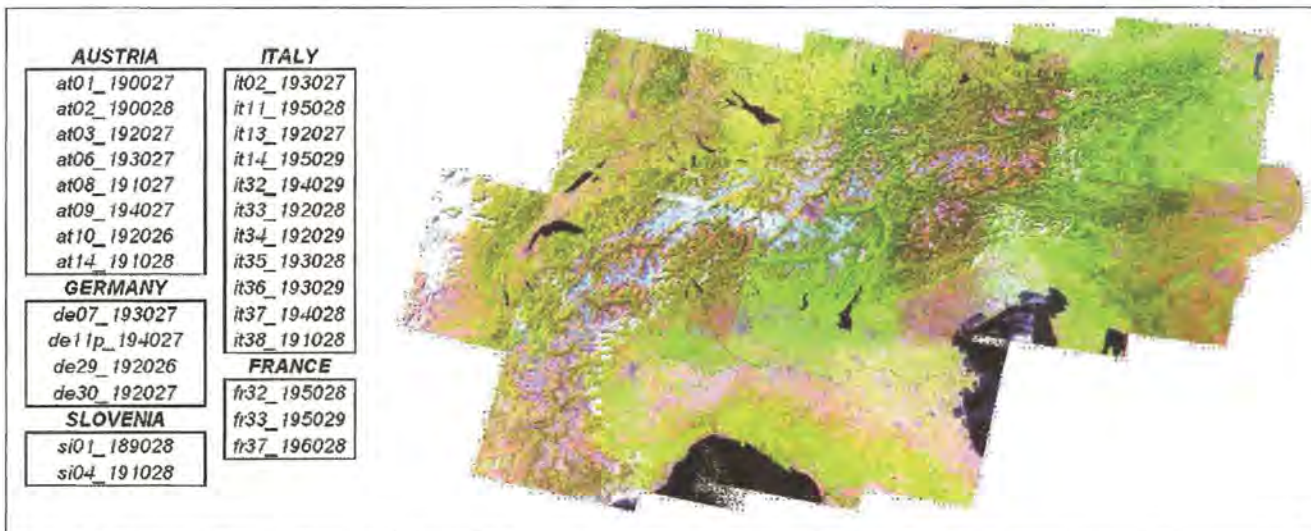


Figure 5: 28 Landsat TM images in the European countries and the mosaic for the Alpine range.

Therefore, this approach is incorrect because of misclassification of shadowed zones as water. So, the next releases of the SCA product have a water masking. Sea water and lakes have been masked using alternatively MOD02 and MOD10 images (tuning the slicing threshold for a clear sky image) and the mosaic of 28 Landsat TM images of years 2000-2002 (used to produce the CORINE land cover by EC: <http://image2000.jrc.it/>).

After the extraction of inland water and seawater they have been summed in a unique mask to be use once for every image at the beginning of the procedure. Here the procedure for calculation of the two masks.

### 2.3.6.1. Water masking from CORINE

28 Landsat images have been selected from the server of Joint Research Council (JRC: <http://image2000.jrc.it/>). The Corine Landsat images (25m of resolution) have been mosaicked using the projections UTM32 and

UTM33 WGS84. The procedure has been performed twice: one for each projection. Only a cut zone has been considered for every projection (see Figure 5). The mosaic has been classified with an unsupervised procedure (10 classes and 10 iterations).

Then, the vector obtained from the *unsupervised* classification need a procedure of "cleaning" because of the numerous shapes wrongly classified. This procedure had to be performed manually. However, not all the lakes classified have to be used in the water mask because they are not comparable with the pixel size of the MODIS image.

### 2.3.6.2. SEA masking from MOD02

The definition of sea water and coastal zones boundaries, to eliminate problems with classification of water as undetermined, has been performed using MOD02 band 2 of a dry image without clouds (with a threshold not from literature) with a resolution of 250m and using the MODIS product MOD10 at 500m (see Figure 6 and 7).

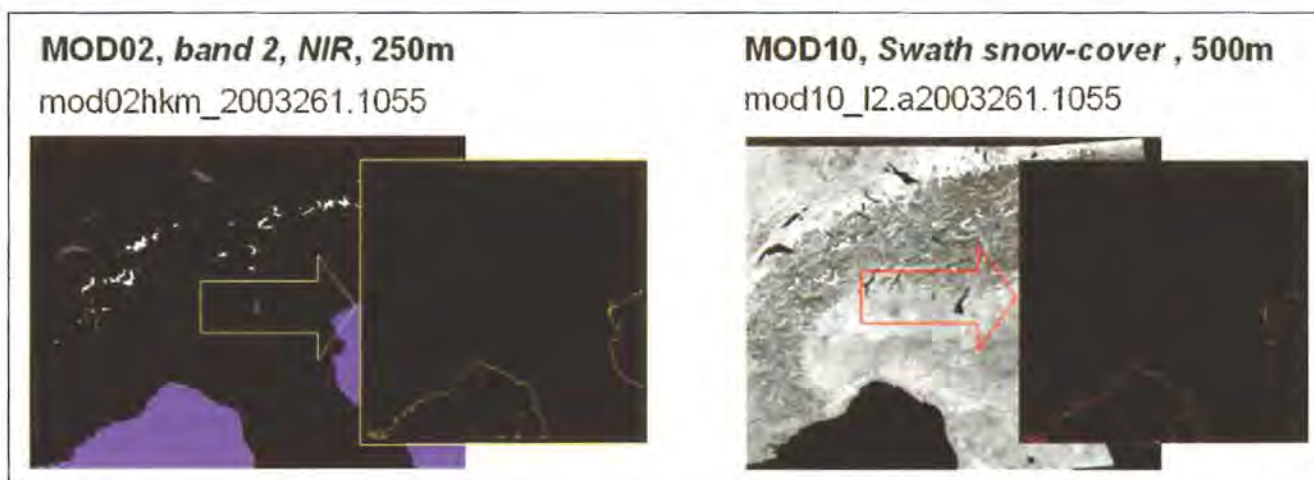
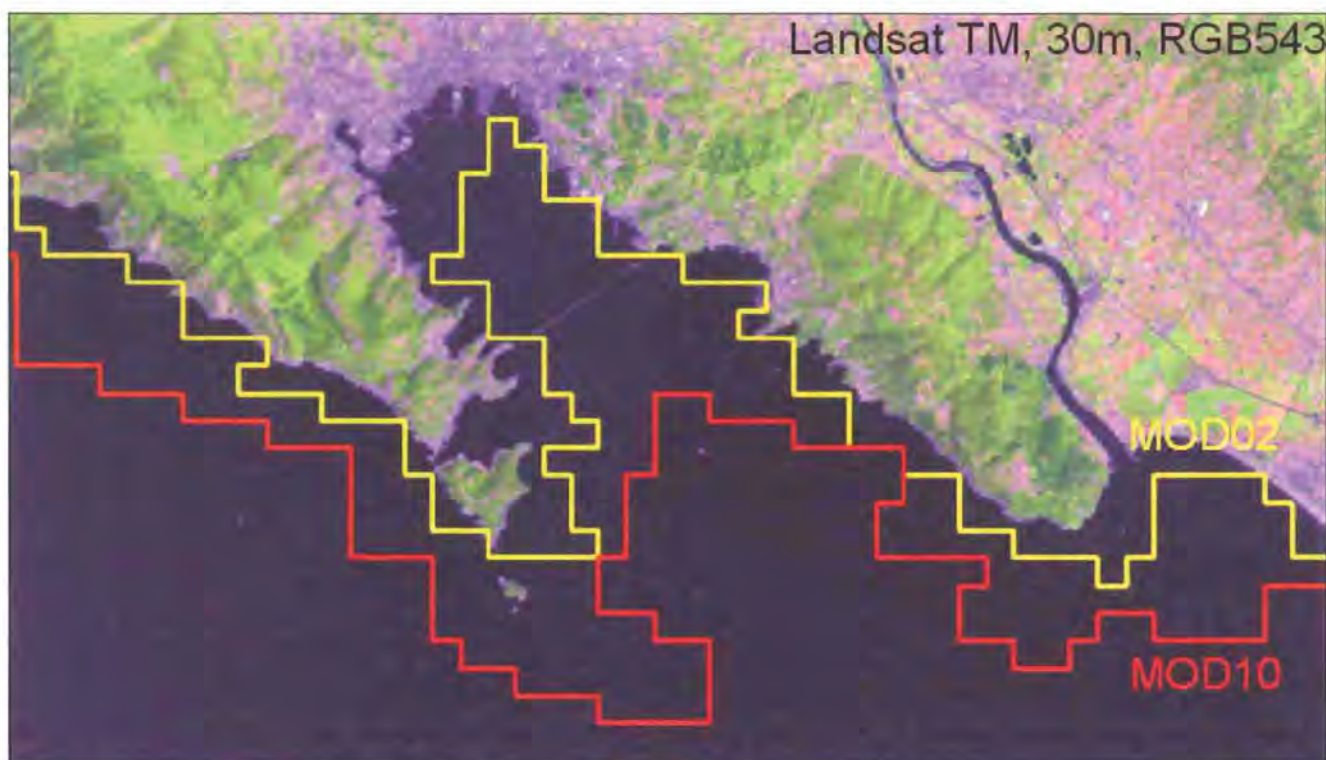
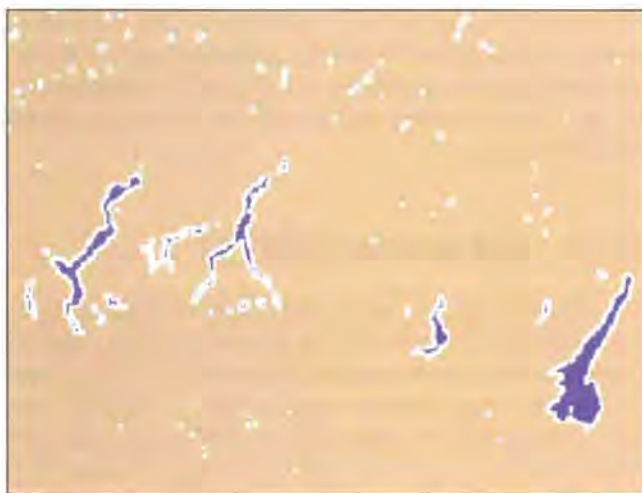


Figure 6: The sea coast derived from MOD02 and MOD10.



**Figure 7:** The Liguria (Italy) coast and the vectors of the classification of the sea coast. It is evident that the MOD10 boundary is less accurate than the MODO2 one.



**Figure 8:** The Lombardy lakes (blue colour) and the buffer (250/500/750 m) applied.

### 2.3.6.3. Buffering the water boundary zone

There is a zone of uncertainty around the lakes where pixel could be classified wrongly. So, a buffer has been applied in and out the lake boundaries. The buffer zone depends on the dimension of the object: if the lake is big it is possible to use a big buffer, if it is small, we consider a smaller buffer zone. This buffer is of 250m if the lake is small and 500/750m if it is big. For the sea boundary 500 and 750 buffers has been used. These buffered pixel will be use to create a quality flag in the next releases (see Figure 8).

### 2.3.7. Cloud cover masking

The cloud coverage of the images has been eliminated (masked) from the SCA result using MOD35 product (1000 m resolution). All the necessary images have been downloaded in the previous step. The procedure provides the creation of a cloud mask from the interpretation of the product. It is a *conservative* cloud mask that is independent by the kind of clouds. Maybe in a following realise will be considered to calculate a *liberal* cloud mask. This is the final step of the procedure and provides a mask that applied to the previous steps lets pass only feature that are not water or clouds and are snow. This kind of products allows to identify the percentage of cloud cover and the kind of clouds. Then, it has been possible to select 12 images (one a month) with the best (the minimum) cloud coverage. For every month 5 or 6 images has been excluded because of their dense cloud coverage. Images that pass the test are the clearest sky ones among those selected in a month (see figure 9).

## 3. Results: SCA production

The result of the first release of the SCA is a 2 classes product where *snow* and *no-snow* have been distinguished and classified as a mask. This is a problem for users that want to know if in a zone the class no-snow is due to the cloud coverage or to a bare soil. So, in the following releases, it has been decided to produce a 4 classes product where water (inland and sea water), clouds and undetermined (bare soil, vegetation, urban, etc.) are specified.

ACQUISITION DATE	%Confident Clear	%Probably Clear	%Probably_Cloudy	%Cloudy	TOTAL CLOUDY
29-Dec-02	46.75	3.49	3.26	46.5	49.76
13-Dec-02	27.30	4.23	5.22	63.25	The most free-cloud image wins
08-Dec-02	21.04	5.40	3.7	69.86	
06-Dec-02	9.64	2.87	1.95	85.53	
15-Dec-02	5.64	3.93	1.82	88.61	90.43
31-Dec-02	6.60	2.71	1.36	89.34	90.70
22-Dec-02	0.22	0.65	0.14	98.99	99.13

Figure 9: The choice of an image in a month is depending on the percentage of cloud coverage on all the Alpine region.

The SCA product is then exported in the format that users want. For instance \*.tif, \*.raw, \*.img, etc. format depending on the software is used. Obviously all the projections and geographic information are included. The image is classified initially in 8 classes resulting from combination of the previous steps, as explained before.

The final product is classified in 4 classes, merging, with an accurate interpretation (tuned for every single image), the 8 classes obtained before. The 8 classes are produced with an automatic procedure; the 4 classes with the interpretation (more subjective). The interpretation phase is necessary because of the presence of different type of clouds that have been wrongly classified as snow or water (see Figure 10).

In the figure 11, the raw images and the classified maps for the zone UTM32 are shown. One of the most evident problems in this classification result is the generalized overestimation of water, misclassified as shadowed zo-

nes. In winter/spring water is attributed to snow shadowed; in summer to slopes shadowed (undetermined class). The use of the water masking has solved this problem.

#### 4. Discussion: Future Improvements

The resulting SCA maps have been validated using the NASA product MOD10 (1000 m resolution) and comparing the snow information obtained from in situ measurements of weather stations: some discordances have been found. Because of interpretation and classification errors in the SCA product, that not allowed the partners to completely use the product, it will be necessary to improve the results with new steps in the procedure or changing the information retrieved by a single step. Here the next step to be performed to produce the new releases.

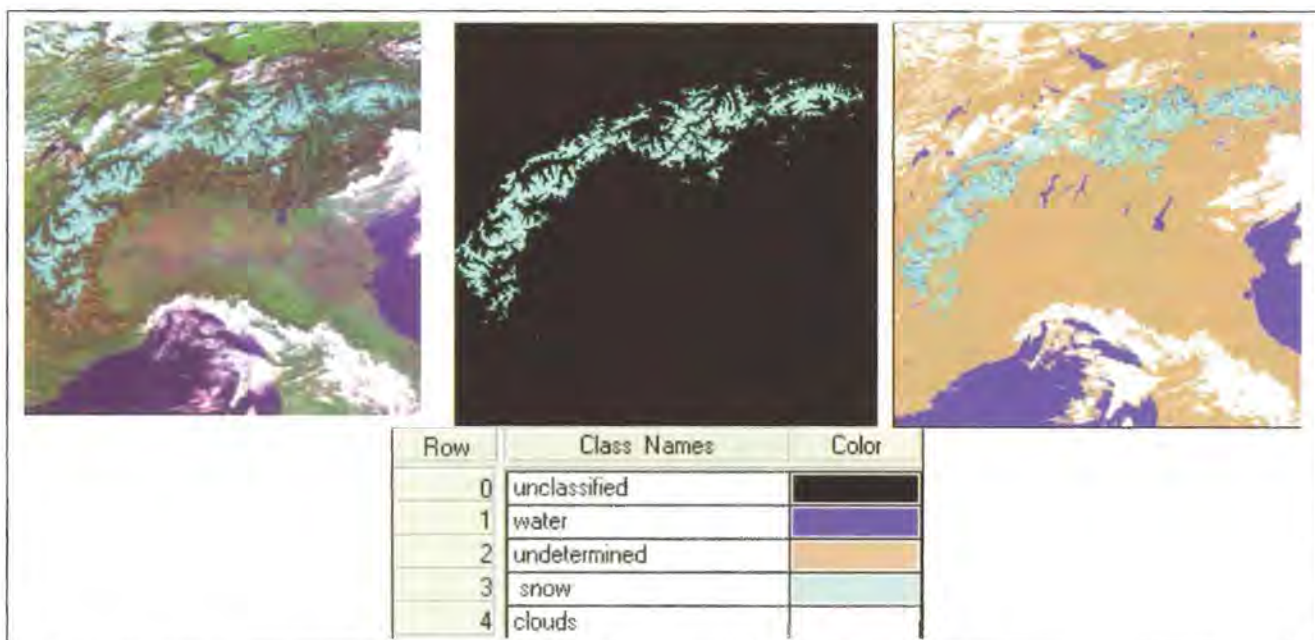
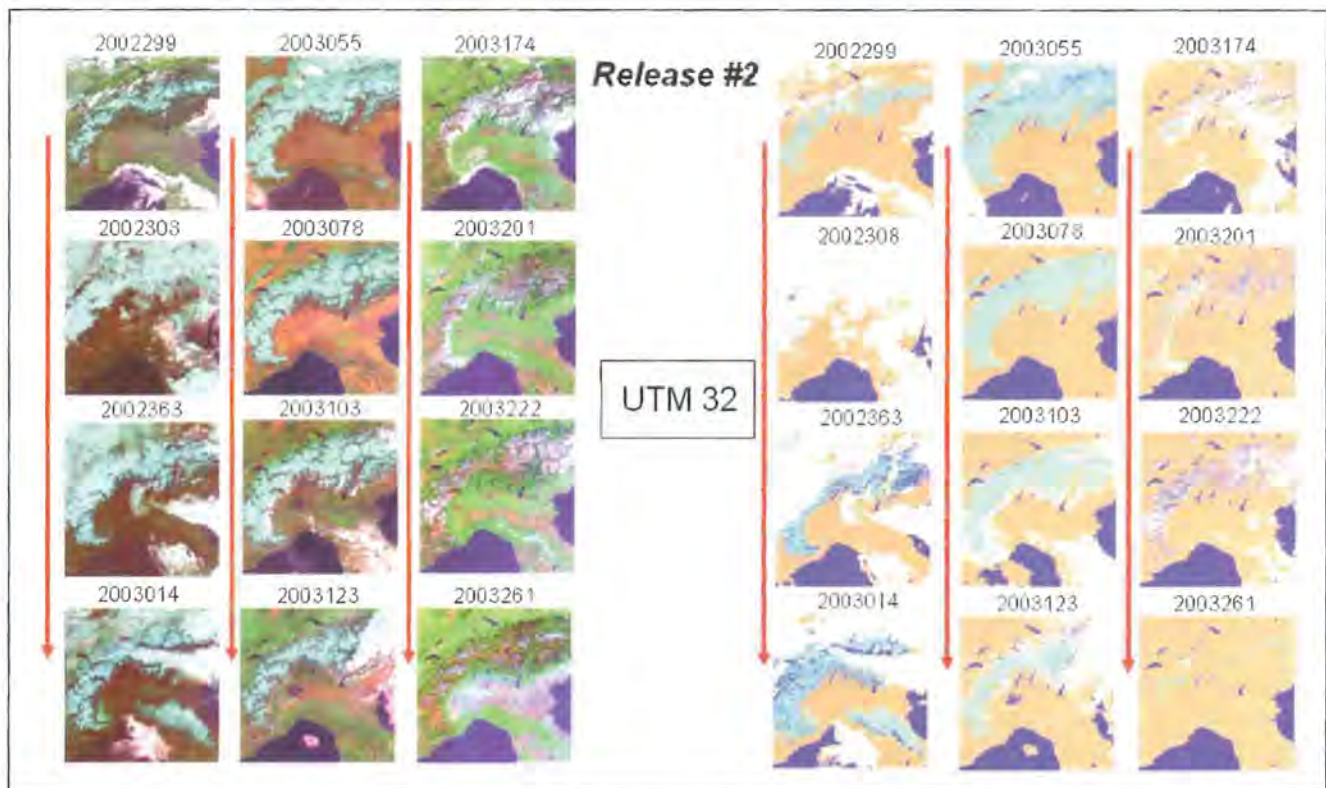


Figure 10: The 18th September 2002 MODIS image (RGB723) and the SCA map. releases 1 and 2.



**Figure 11:** The 12 raw images (RGB 723) and the 4 classes maps for the zone UTM32.

#### 4.1. Fuzzy classification

To increase the potentiality of the classification, considering the low resolution of the images analysed (from 250 to 500 and 1000 m) it is advised to use an unmixing classification methodology. This allows improving the accuracy of the mapping, because it is possible to distinguish features that are inside the pixel.

The resolution of the result is not the resolution of the pixel, but it is more accurate allowing to know about the mixture of classes. It is a supervised classification and it is necessary a good knowledge of the territory to selected samples. Starting from a training set of information about the content of a class in a pixel, the procedure produce an image for every class in which the value of the pixel are the percentage of membership to one of the selected class (see Figure 12).

A fuzzy classification approach will be applied to those basin that are not well visible with the available sensors (MODIS) and when others sensors are not acquired (*Obertraum Basin*, 334 km<sup>2</sup>; *Dischma Basin*, 43,3 km<sup>2</sup>). It is not excluded that this procedure will be tuned also for other selected basins. The procedure needs a very good knowledge of the landcover as a ground truth to select the training set. The partners and users will be necessary in this key phase.

#### 4.2. Reflectance conversion

In the next releases, the value of conversion in of Digital Number in Reflectance will be tuned considering the

(very low) variations of this parameter depending on seasonal variability. Moreover, the application of MOD09, that is a MODIS product already converted in reflectance, will be tested.

#### 4.3. Increasing of frequency of acquired images

It has been decided to produce other SCA product in order to obtain a major frequency of the coverage. The selection of new images is based on a check about the presence of clouds in a number of chosen basins for the project.

#### 4.4. Cloud masking improvement

Analysing the results has been possible to see that some images are very cloudy both on the selected basins and both in other regions. So, it is evident that the frequency of image acquisition is not enough to guarantee a complete coverage of the Alpine range for the project purpose (clear sky images). The analysis of the cloud coverage percentage of an image fails when clouds are concentrated only in a part of the image.

The cloud product used is a conservative mask that is independent by the type of clouds. In the following realises it will be considered a liberal cloud mask in which different kind of clouds (dense, fog, cirrus, etc.) are identified to improve the accuracy of the result because of the interaction of this feature and the landcover at the Earth surface.

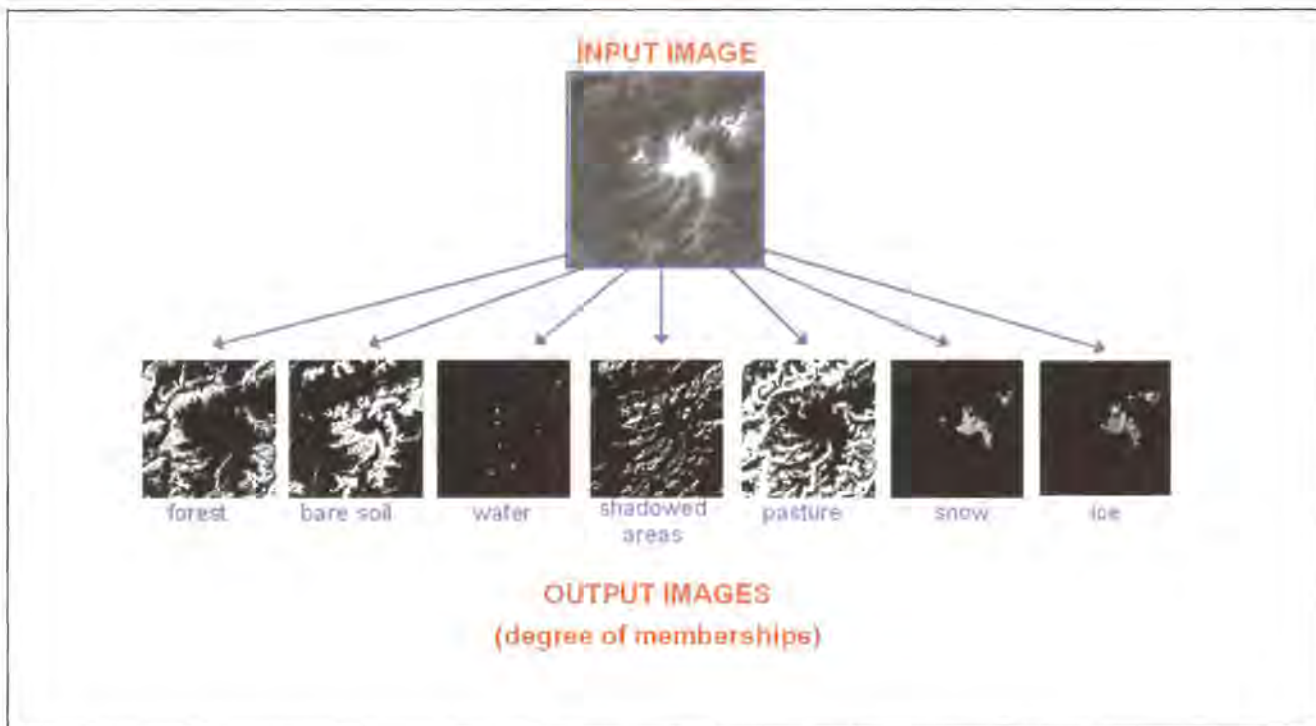


**Figure 12:** Fuzzy classification produces an image for each class in which we want the raw image classified.

#### 4.5. Pixels bad values analysis

In the next releases will be also analysed the problem regarding the bad values of the pixels. Errors in sensor acquisition produce pixels in the images with no-signal. It is possible to apply a filter to mask these holes.

#### 4.6. NDSI threshold values analysis

The NDSI threshold used to mask the snow cover varies with the images and the seasons. In the next works it will be considered a seasonal tuning to obtain a more accurate result. Then, pixel with a too low reflectance in band 4 will be also eliminated from the NDSI map ( $b4 > 0.10$ ).

#### 4.7. Quality flag definition

Due to the errors in the different steps of the analysed procedure, in the next releases will be produce a *quality flag* map. This is a matrix that allows to know for each pixel how is the quality of the process that produced it. For instance, the georeferencing methodology, using the NASA software *MRT Swath* produces some pixels with no information and in the water masking buffer zone indicates the uncertainty of the classification.

### 5. Conclusions

The AWARE project is an important test to define the potentiality of using medium resolution satellite data as input in hydrological model applied to the Alpine basin.

The main application of EO data is snow mapping because of the importance of the spatially distributed observations for snowmelt modelling.

Model innovation stems with the enhanced capability of Earth Observation data to provide continuous information on the state variables, that can be poorly accounted for, when using the traditional approach based on input-output control.

The EO data procedure applied has been tested over different Alpine basins and demonstrates the completely usefulness for the purposes proposed. Improvements and new releases will be performed during the whole period of the work project.

#### Acknowledgements

A particular thank to NASA who allowed the use of the data without limitations, to JRC who gave us the access to CORINE project, to the EC who funded the project and to CNR-IREA researchers who worked with us.

#### References

- ANDREADIS, K.M. AND LETTENMAIER, D.P. (2005): Assimilating Remotely Sensed Snow Observations into a Macroscale Hydrology Model. Preprint submitted to Advances in Water Resources.
- CARSEY, F. (1992): Remote sensing of ice and snow: review and status. *Int. Journal of Remote Sensing*, 13, 5-11.

- CHANG, A.C., FOSTER, J.L. AND HALL, D.K. (1987): Nimbus-7 SMMR derived global snow cover parameters, *Ann. Glaciol.*, **9**, 39-44.
- ENGMAN, E.T. AND GURNEY, R.J. (1991): *Remote Sensing in Hydrology* (London: Chapman and Hall).
- GRODY, N.C. AND BASIST A.N. (1996): Global identification of snowcover using SSM/I measurements, *IEEE Trans. Geosci. Remote Sensing*, **34** (1), 237-249.
- HALL, D.K., RIGGS, G.A., SALOMONSON, V.V., DIGIROLAMO, N.E. AND BAYR, K.J. (2002): MODIS snow-cover products, *Remote Sens. Environ.*, **83**, 181-194.
- HARRISON, A.R. & LUCAS, R.M. (1989): Multi-spectral classification of snow using NOAA AVHRR imagery. *International Journal of Remote Sensing*, **10** (5), pp. 907-916.
- KLEINDIENST, H., WUNDERLE, S., VOIGT, S. (2000): Snow Line Analysis in the Swiss Alps Based on NOAA-AVHRR satellite data. *Proceedings of EARSel-SIG-Workshop Land Ice and Snow, Dresden/FRG, June 16 – 17.*
- MATSON, M. (1991): NOAA satellite snow cover data, *Palaeogeography and Palaeoecology*, **90**, pp. 213-218.
- MAURER, E.P., RHOADS, J.D., DUBAYAH, R.O. AND LETTENMAIER, D.P. (2003): Evaluation of the snow-covered area data product from MODIS, *Hydrol. Processes*, **17**, 59-71.
- PEPE, M., BRIVIO, P.A., RAMPINI, A., ROTA NODARI, F. (2004): G. Snow cover monitoring in Alpine regions using ENVISAT optical data, *IEEE Trans. on Geoscience and Remote Sensing* (submitted).
- RAMSAY, B. (1998): The interactive multisensor snow and ice mapping system, *Hydrological Processes*, **12**, pp. 1537-1546.
- RANGO, A., MARTINEC, J., FOSTER, J. & MARKS, D. (1983): Resolution in operational remote sensing of snow cover. *IAHS Publ 145*: 371-381.
- ROBINSON, D.A., DEWEY, K.F. AND HEIM, R.R. (1993): Global snow cover monitoring: an update. *Bulletin of American Meteorological Society*, **74**, pp. 1689-1696.
- SCHMUGGE, T.J., KUSTAS, W.P., RITCHIE, J.C., JACKSON, T.J. AND RANGO, A. (2002): Remote sensing in hydrology. *Advances in Water Resources* (Elsevier); **25** (2002)1367-1385.
- SWAMY, A.N. AND BRIVIO, P.A. (1997): Modelling runoff using optical satellite remote sensing data in high mountainous alpine catchment of Italy. *Hydrological Processes*, VOL. 11, 1475-1491.
- WINTHER, J.G. & HALL, D.K. (1999): Satellite-derived snow coverage related to hydropower production in Norway: present and future. *International Journal of Remote Sensing*, **20** (15), 2991-3008.

WEBSITES:

- <http://www.aware-eu.info>  
<http://edcdaac.usgs.gov/main.asp>  
<http://modis.gsfc.nasa.gov/>  
<http://image2000.jrc.it/>  
<http://edcimswww.cr.usgs.gov/pub/imswelcome/>

# 13 The dilemma of resolution and seasonality of snow cover in alpine environments

SUSANNE SCHMIDT<sup>1</sup> AND BERNHARD WEBER<sup>2</sup>

<sup>1</sup> Department of Geography, University of Bonn, Germany,

<sup>2</sup> Institute of Geodesy & Geoinformatics, Department of Photogrammetry, University of Bonn, Germany

## Abstract

In this study the effect of topography on snow cover distribution was analysed using a new combined research approach using terrestrial images. With this approach the quality of semi-empirical models to describe the pattern of snow cover distribution as a function of the topography was estimated. Validation showed that the snow cover pattern is not only determined by major topography features but also by gravitative processes and heat fluxes. The differentiated snow cover pattern can be monitored using the new, advanced approach based on terrestrial images. This approach is characterized by data with high spatial (10 m) and temporal (daily) resolution. In this study the temporal resolution of images is restricted to approximately every fifth days due to bad weather conditions. Nevertheless this method attains a higher temporal resolution than remote sensing techniques and a higher spatial resolution than point measurements. The existing gap between high resolution needs for modelling and available data is closed with this use of terrestrial images and the developed semi-automatic analyses procedure. Snow cover modelling and analyses of hydrological, geomorphologic and ecological responses of snow cover in high mountains can be highly improved by the presented approach. The study were carried out from winter 2002 until 2004; the presented analyses consider only the winter 2003/04.

## 1. Introduction

Despite interannual variations of weather conditions, seasonal snow cover distribution in mountain regions are relatively persistent over the years (FRIEDEL 1961; GJAAREVOLL 1956: S. 16; HALL & MARTINEC 1985; YAMADA 1996). Such long-term patterns substantially control ecological (KÖRNER 1999; LÖFFLER 2005), geomorphological (KELLER 1994) and hydrological processes (BLÖSCHL & KIRNBAUER 1992). Topographical effects on the snow cover have been described in many studies, but there is lack of studies that are able to quantify this impact (BLÖSCHL & KIRNBAUER 1992; KÖLBEL 1984; KÖNIG & STURM 1998; TAPPEINER et al. 2001). Data with high spatial and temporal resolution are required, to quantify seasonal snow cover distribution on the meso-scale. In accordance with MCKAY & GRAY (1981) we define the meso-scale as a scale characterized by snow redistribution processes such as wind drift and avalanches. Conventional approaches of snow cover monitoring are based

on point measurements or remote sensing techniques (GOODISON et al. 1981; HALL & MARTINEC 1985; SEIDEL & MARTINEC 2004). The latter is limited by either coarse spatial and high temporal resolution or vice versa, and hence these are improper methods to monitor fine-scale and rapid snow cover changes at the meso-scale. Point measurements are locally very precise but not adequate to monitor larger areas. These conventional approaches are therefore not suitable for meso-scale spatial and temporal observations and for the analyses of meso-scale snow cover distribution (CHRISTIANSEN 2004; TAPPEINER et al. 2001).

The aim of this study is to test and apply a new high resolution technique based on terrestrial images for monitoring snow cover dynamics on steep slopes at the meso-scale. The results of this new technique serve as a basis for the quantification of topographical effects on the snow cover distribution. The study was carried out from October 2002 until September 2004; the presented analyses consider only the winter 2003/04.

## 2. Study area

The study area is situated in the Lötschental (Swiss Alps), a northern tributary of the Rhone-Valley (Fig. 1). The valley extends over 160 km<sup>2</sup> and has a main direction from NE to SW. The elevation ranges from 1375 m to 3200 m a. s. l. at the northern and 3400 m a. s. l. at the southern ridge. Highest mountain is the Bietschhorn (3953 m ü. M.) which overtops the southern ridge with approximately of 400 m. Due to its geological structure, the valley has an asymmetrical cross section resulting in an average inclination of the SW-facing slope of 30° and of 37° on NE-facing slope. Hence, the critical limit for avalanche release is exceeded in many parts. The slopes are forested up to 2200 m a.s.l. with larch (*Larix decidua*) and spruce (*Picea abies*). Measurements from the meteorological station Ried (1500 m a.s.l.) show a long-term average annual (measurement period: 1974–1998) temperature of 4.7 °C and an annual amplitude of -3.6 °C (January) to 13.9 °C (July). The importance of the seasonal snow cover for the Lötschental becomes obvious by looking at the annual distribution of precipitation. On average 50 % of the total annual precipitation (1112 mm) falls as snow in the valley floor and the proportion increases with altitude.

## 3. Methods

### Terrestrial Photogrammetric Image Acquisition and Analysis

To monitor and analyze the snow cover distribution at the meso-scale, two digital cameras were mounted on opposite slopes above the timberline. They monitored variations of snow cover distribution on NW- and SE-facing slopes on a daily basis. Due to unfavourable illumination conditions, the digital camera that monitored the snow cover distribution on the NW-facing slope, takes

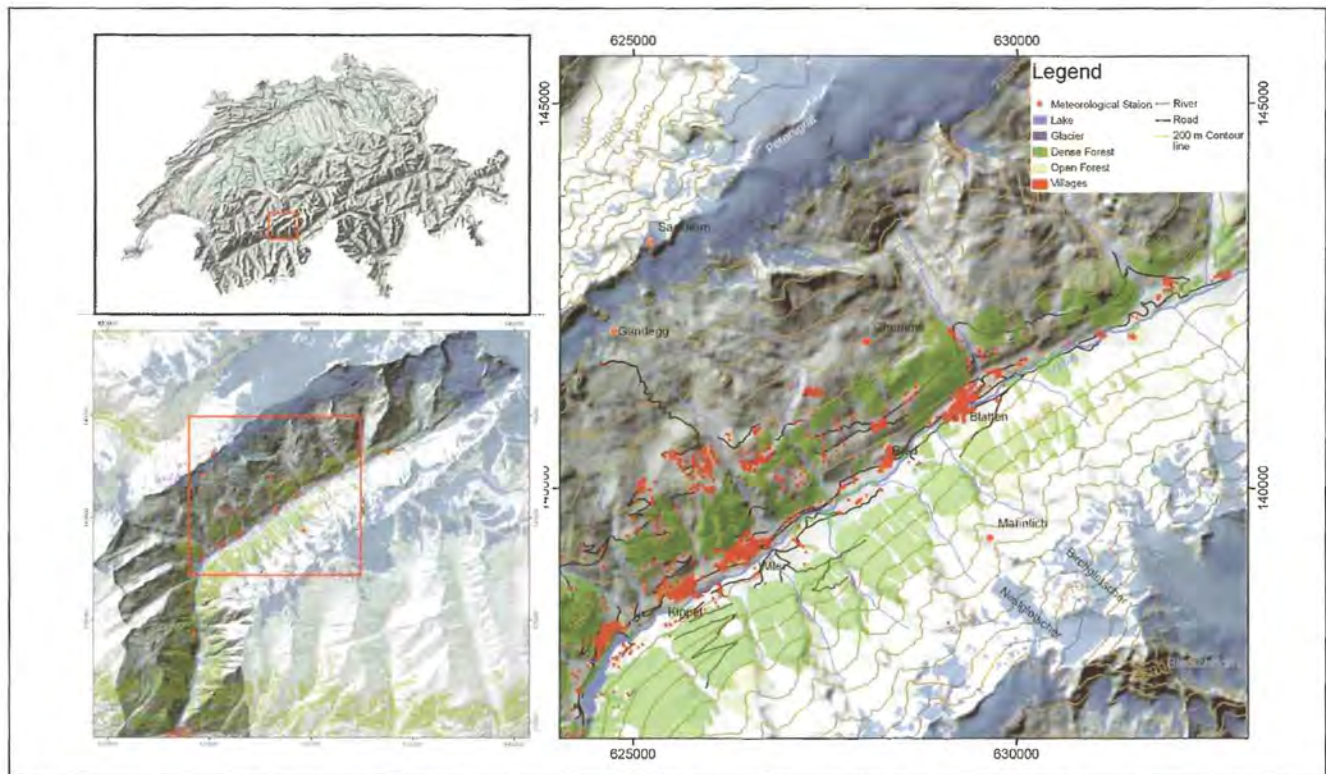


Figure 1: Location of the Lötschental and study area (reprinted with permission of swisstopo (BA071052)).

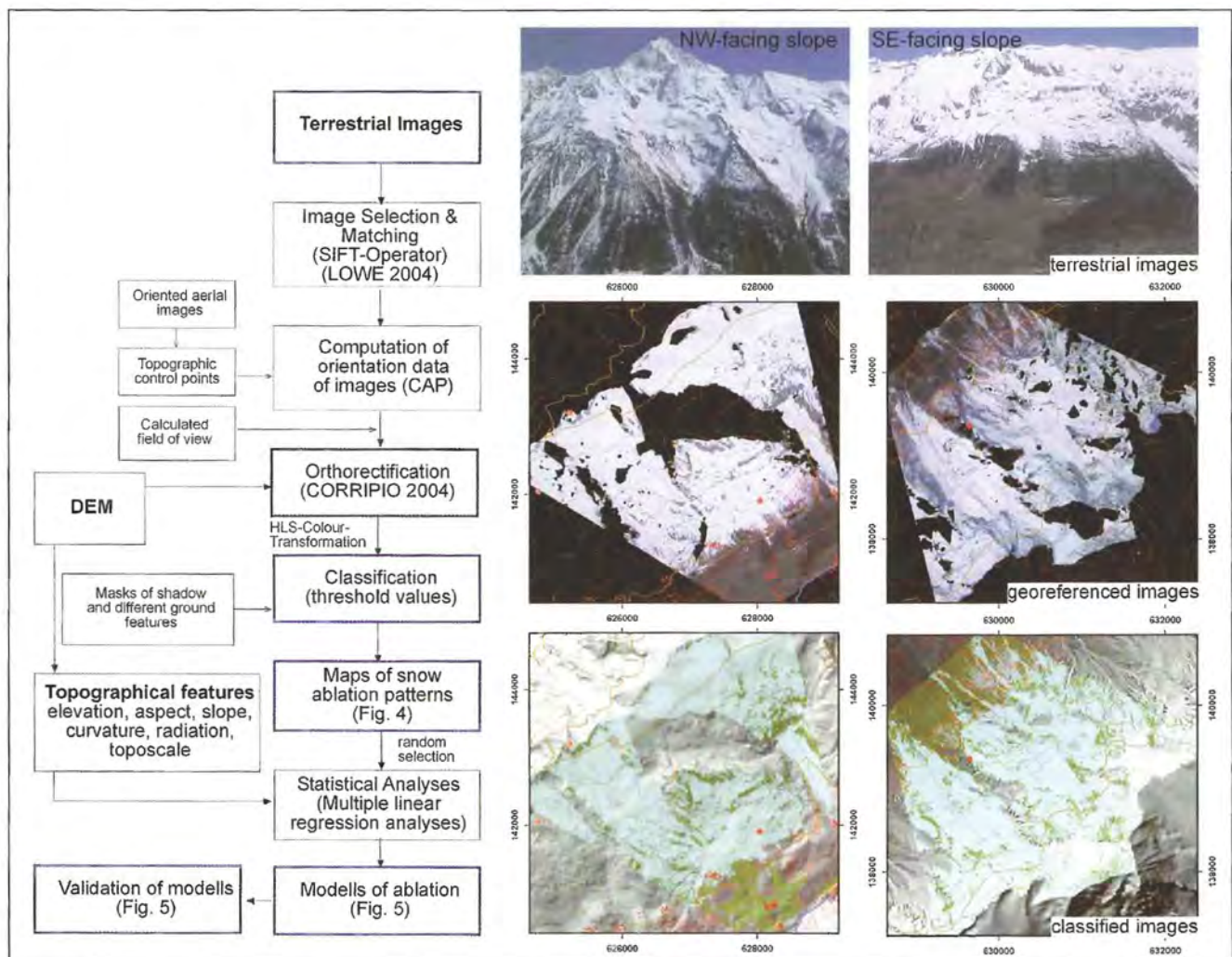


Figure 2: Flow chart of terrestrial image processing and analyses (left), examples from the SE-facing (middle) and NW-facing slope (right). (Pictures: Susanne Schmidt)

two images every day. To analyse the snow cover distribution in relation to topography it is necessary to georeference the terrestrial images (Fig. 2). These images are generated using the program "Georeferencing Terrestrial Photography" (CORRIPIO 2004). The input parameters for the computation of the georeferenced images are: a digital elevation model with a resolution of 10 x 10 m (SWISSTOPO 2004), the orientation data of the images, and the size of the CCD chip (camera manufacturer: KODAK).

To achieve a high accuracy of the topographical dependent analysis, a good consistency between the digital elevation model and the georeferenced images is necessary. To obtain the desired accuracy a calculation of the orientation data of every image has been carried out. Orientation parameters must be computed for each image individually, because the parameters may change from image to image due to climatic influences like wind, snow and temperature variation. The orientation data for every image consists of: (1) three rotation parameters for spatial rotations, (2) coordinates of the camera position in a ground control system (x, y, z), and (3) principle distance. The latter is approximately the focal length of the lens.

We use a spatial resection with a simultaneous estimation of the principle distance to calculate the orientation data. The program CAP (Combined Adjustment Program, HINSKEN & KOTOWSKI 1988-2003, vers. 2.29 (see HINSKEN 1989)) was used for that purpose. For this calculation well distributed control points in a ground control system are necessary. These points must be identified and measured in the images. But, at high altitudes only a small number of topographic control points are available from the Swiss survey department. Therefore, it was necessary to measure additional control points. This was performed with the help of oriented aerial images (image flight from the year 2000) with stereoscopic measurements in photogrammetric models.

The terrestrial images were taken at predefined times using an automatic control system. Temporally neighbouring images from the same position can therefore be called monoscopic image sequence. If the orientation of the images would have not been influenced by meteorological phenomena, one would have been able to overlay every image and every image detail would have been at the same image position. Then it would have been sufficient to calculate the orientation data of only one image and use this data for the whole image sequence. Because this is not possible, a strategy for the orientati-

on of a monoscopic image sequence has been developed:

- Measurement of control points and orientation of a reference image of the sequence in a ground control system: Due to a measurement of the control points the orientation of the reference image can be calculated using the spatial resection.
- Calculation of the orientation of all images in a local coordinate system: In this step differences between the orientations of the reference image and all other images are calculated. We use an automatic matching approach between corresponding points on the images for that purpose. In this project the SIFT-operator (LOWE 2004) is used for point extraction and matching.
- Calculation of all orientation data in the ground control coordinate system: If the orientation of the reference image and the differences to all other images are achieved, the orientation data of all images in the ground control coordinate system can be calculated by means of a 3D-transformation.

With this approach the manual measurement for the whole orientation of the monoscopic image sequence is reduced to the measurement of only one reference image. The number of images of one sequence is limited by the similarity of the images and by the amount of data. The size of one sequence was mostly 150 images and 260 at maximum. These numbers are our experiences with the current experimental software and may be increased by improving the implementation.

Using this semi-automated orientation strategy the time-consuming manual and error-prone process parts are calculated automatically. With the current implementation status it was possible to orientate all 1072 images of both cameras and both years in 15 image-sequences and provide the orientation data for further processing.

For the analyses of topographical influence on snow cover distribution it is necessary to classify the georeferenced images into snow free and snow covered areas. Due to variations in reflection properties of snow free and snow covered areas (DOZIER & PAINTER 2004) we used a process of thresholds. To improve the classification, masks of shadow and different ground features like geology and vegetation were applied. This was possible, because each image was georeferenced. Threshold values depend on variation of illumination like different weather or snow conditions and must be set for each image. Due to different weather conditions like clouds, fog, snow fall in the ablation period it was not possible to

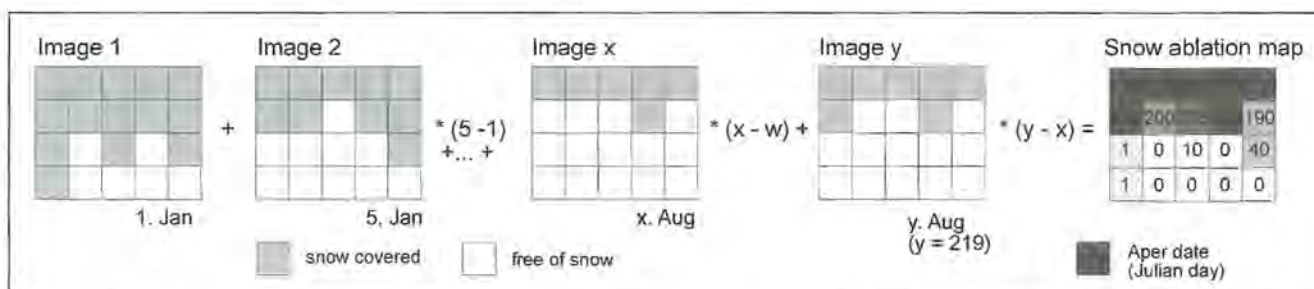


Figure 3: Procedure to calculate the ablation pattern of snow.

process each image. Therefore, approximately one image every five days was used from January until the end of ablation period. For further statistical analyses of snow cover patterns in relation to topography, it was necessary to generate a map of snow cover duration for the whole ablation period. For this map the snow cover duration was estimated for each pixel as a calendaric sum. The binary data (1 for snow covered 0 for snow free) were summed up regarding the temporal differences to the previous binary snow cover data (Fig. 3).

### Statistical Analyses

For the quantification of the topographical impacts on snow cover distribution we used multiple linear regression analyses (CHANG & LI 2000). The aim of these statistical analyses was to develop a semi-empirical model, which describes the snow cover patterns (dependent variable) in relation to topographical parameters (independent variable) in a simple form:

$$Y = \alpha + \beta_1 X_1 + \beta_2 X_2 + \dots + \beta_m X_m + \varepsilon$$

with:

- $Y$  = dependent variable: snow cover distribution
- $X_1 \dots X_m$  = independent variable: elevation, slope, aspect (cos, sin), curvature (i=1, ..., m)
- $\alpha$  = intercept
- $\beta_1 \dots \beta_m$  = regression coefficients (i=1, ..., m)
- $\varepsilon$  = RMS-Error (BAHRENBERG et al. 2003: S. 31)

The regression coefficients can be regarded as a measure of the weight of a single parameter on the dependent variable. All topographic features were standardized to enable comparability (BAHRENBERG et al. 2003: S. 33). All the used topographic parameters like elevation, slope, aspect, curvature (SCHMIDT & HEWITT 2004) and potential solar radiation (ZIMMERMANN 2000) were derived using a 10 m resolution DEM.

20 % of the snow cover duration map, which were generated from terrestrial images, was selected randomly for the regression analyses (HAWTH'S ANALYSIS TOOLS V. 3.21). The following areas were excluded beforehand:

- (1) areas free of snow: on the one hand this areas are characterized by micro-scale features and single trees, which are not detected in the digital elevation model, i.e. small boulders, trees; and on the other hand steep slopes (>44° and 60°, respectively) are free of snow the whole winter; in the further model we defined steep slopes as free of snow the whole winter, (2) forests, due to the fact that trees covered the view to the ground of forest, no information on the snow cover distribution in forested areas are available, this areas were excluded from calculations, (3) areas which were snow covered on the last image, we assumed that this snow is firn and no seasonal snow cover. Moreover, statistical analyses of terrestrial images were conducted for both slopes separately due to different snow cover conditions. Based on these multiple linear regressions, patterns of snow cover distribution were modelled for the Löt-schental.

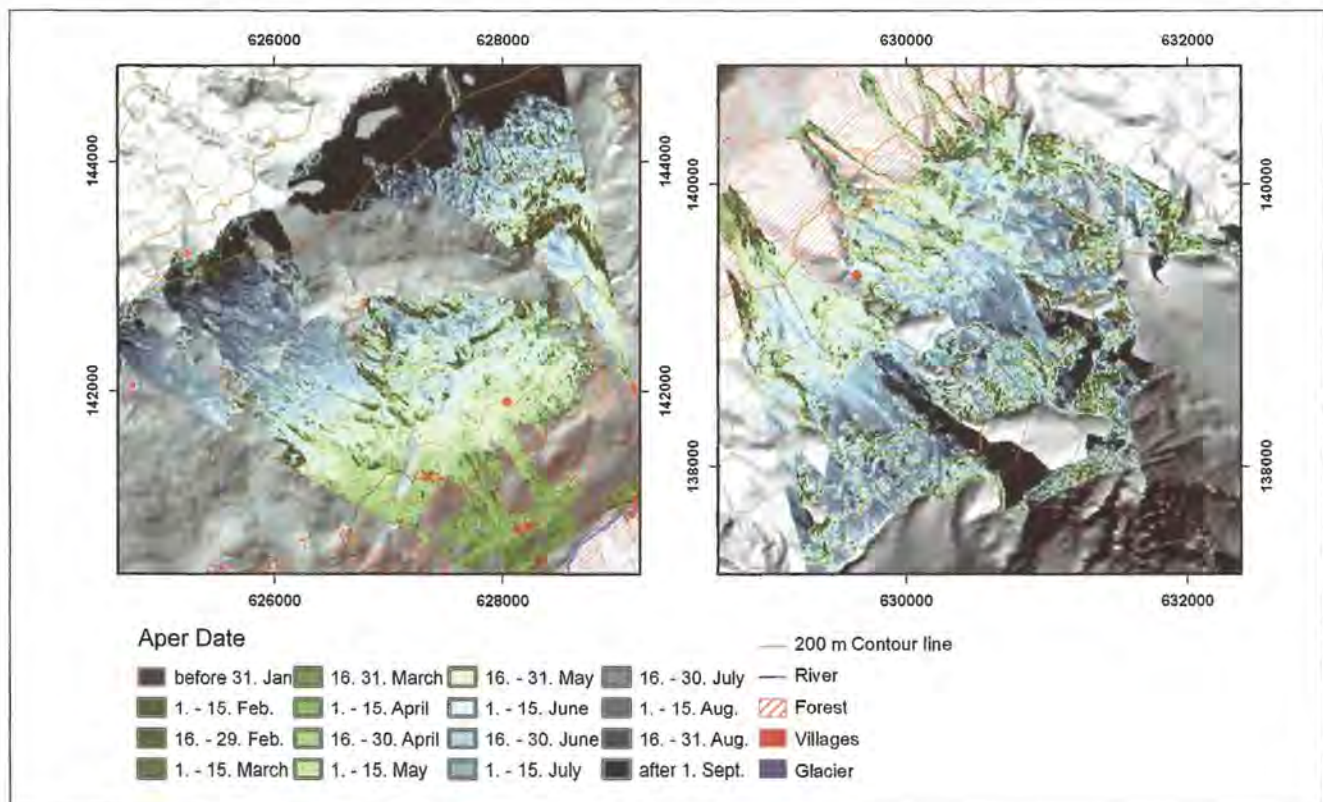


Figure 4: Maps of snow cover patterns based on terrestrial images.

#### 4. Results

The map (Fig. 4) shows the ablation pattern of snow on the NW- and SE-facing slope. During the whole winter steep slopes and ridges are snow free. On the NW-facing slope the ablation started approximately 14 days later than on the SE-facing slope at the same altitude. Therefore the elevation dependant temporary snow line is strongly alternated by slope angle, aspect and curvature. Rapid changes of ablation pattern as well as small-scale patterns of snow indicate the necessity of a high temporal and spatial resolution of monitoring data. Snow cover pattern on the NW-facing slope - characterised by slope angles exceeding 37° - is modified by gravitative processes; i.e. snow melt in accumulation zones of avalanches are retarded by more than 80 days, while the release zones are snow free much earlier.

a timeframe of ±10 days and 55 % within a timeframe of ±20 days. The greatest discrepancies occur in the run-out-zones of avalanches and snow gliding, on steep slopes, and on glacier tongues (Fig. 5 bottom).

#### 5. Discussion

The influence of topography on the persistent snow cover pattern has been described in several studies (EHRLER & SCHAPER 1997; GJAEREVOLL 1956: S. 16; HALL & MARTINEC 1985; KÖLBEL 1984; YAMADA 1996). With the presented method, it was possible to quantify the influence by using terrestrial images.

The snow cover pattern cannot be described by topographic features alone. The main structures of the pattern are expressed, indeed, but the temporal and spatial

**Table 1:** Regression analyses of snow cover patterns in relation to topographical parameters.

	Intercept	Elevation	Slope	Pot. Rad.	Topo scale	Min. Curv.	Max. Curv.	RMS	Adj. R <sup>2</sup>
<b>NW-facing slope</b>									
2003/04	96.0800	0.0627 <sup>4)</sup>	-2.0670 <sup>4)</sup>	-0.0004 <sup>4)</sup>	-0.0830 <sup>4)</sup>	927.90 <sup>4)</sup>	-758.1 <sup>4)</sup>	32.75	<b>36.02*</b>
z		0.6381	-0.4938	-0.1204	-0.2097	0.1376	-0.1335	0.7999	
<b>SE-facing slope</b>									
2003/04	-55.9500	0.1115 <sup>4)</sup>	-1.2460 <sup>4)</sup>	-0.0003 <sup>4)</sup>	-0.1308 <sup>4)</sup>	697.30 <sup>4)</sup>	-454.10 <sup>4)</sup>	24.51	<b>74.87*</b>
z		0.8655	-0.2186	-0.0449	-0.189	0.0635	-0.0542	0.5013	
<b>Both slopes</b>									
2003/04	-10.23	0.09331 <sup>4)</sup>	-1.5500 <sup>4)</sup>	-0.0001 <sup>4)</sup>	-0.1204 <sup>4)</sup>	67.52 <sup>4)</sup>	-47.82 <sup>4)</sup>	28.65	<b>60.84*</b>
z		0.7949	-0.3314	-0.0875	-0.0218	0.0758	-0.0674	0.6258	

upper number: regression coefficient

lower number: standardized regression coefficient

level of significance of partial regression coefficient <sup>1)</sup> 10 %, <sup>2)</sup> 5 %, <sup>3)</sup> 1 %, <sup>4)</sup> 0.1 %

\* significant on 5 %-level (F-distribution)

Due to the different snow cover conditions on both investigated slopes, statistical analyses were calculated separately for each slope (Tab. 1). The analyses show that on the SE-facing slope 75% of the snow cover pattern is explainable by topographic features, whereas the snow cover pattern on the NW-facing slope is explainable to a proportion of 36%. On the NW-facing slope, the standardized regression coefficients show the major effect of elevation and slope angle, while on the SE-facing slope elevation is the only superior factor controlling the snow cover pattern. All the other factors are of minor but significant effect on both slopes.

For the purpose of a quantitative validation of the semi-empirical model, the results of terrestrial images were compared with the modelled snow cover patterns. Using the semi-empirical model, which is based on statistical analyses of the terrestrial images (Fig. 5 top), 42 % of the area of the SE-facing slope is predicted correctly within a temporal bias of ±10 days, and 68 % of the area is correct within a timeframe of ±20 days. On the NW-facing slope only 15 % is calculated correctly within

variations are not covered. The terrestrial images show that gravitative processes like avalanches modify considerably the main structure already in the beginning of the depletion period. Avalanches effect consequently hydrological, geomorphological and ecological processes (DE JONG ET AL. 2005; PHILLIPS 2000; RYCHETNIK 1984). According to BLÖSCHL & KIRNBAUER (1991) and TAPPEINER et al. (2001) these gravitative processes can neither be described by first order topographic features like slope aspect, angle and elevation nor by secondary features like curvature and topographic position. Hence, complex topographic features have to be developed that are able to detect these gravitative processes. Methodological approaches are done by MAGGIONI et al. (2005) who use slope length besides primary parameters. Due to the steeper characteristic of the NW-facing slope in comparison to the SE-facing slope, gravitative processes are more dominant on the NW-facing slope. Due to the fact, that gravitative processes cannot be explained by first and second order topographic features, the explainable proportion of snow cover patterns is lower on

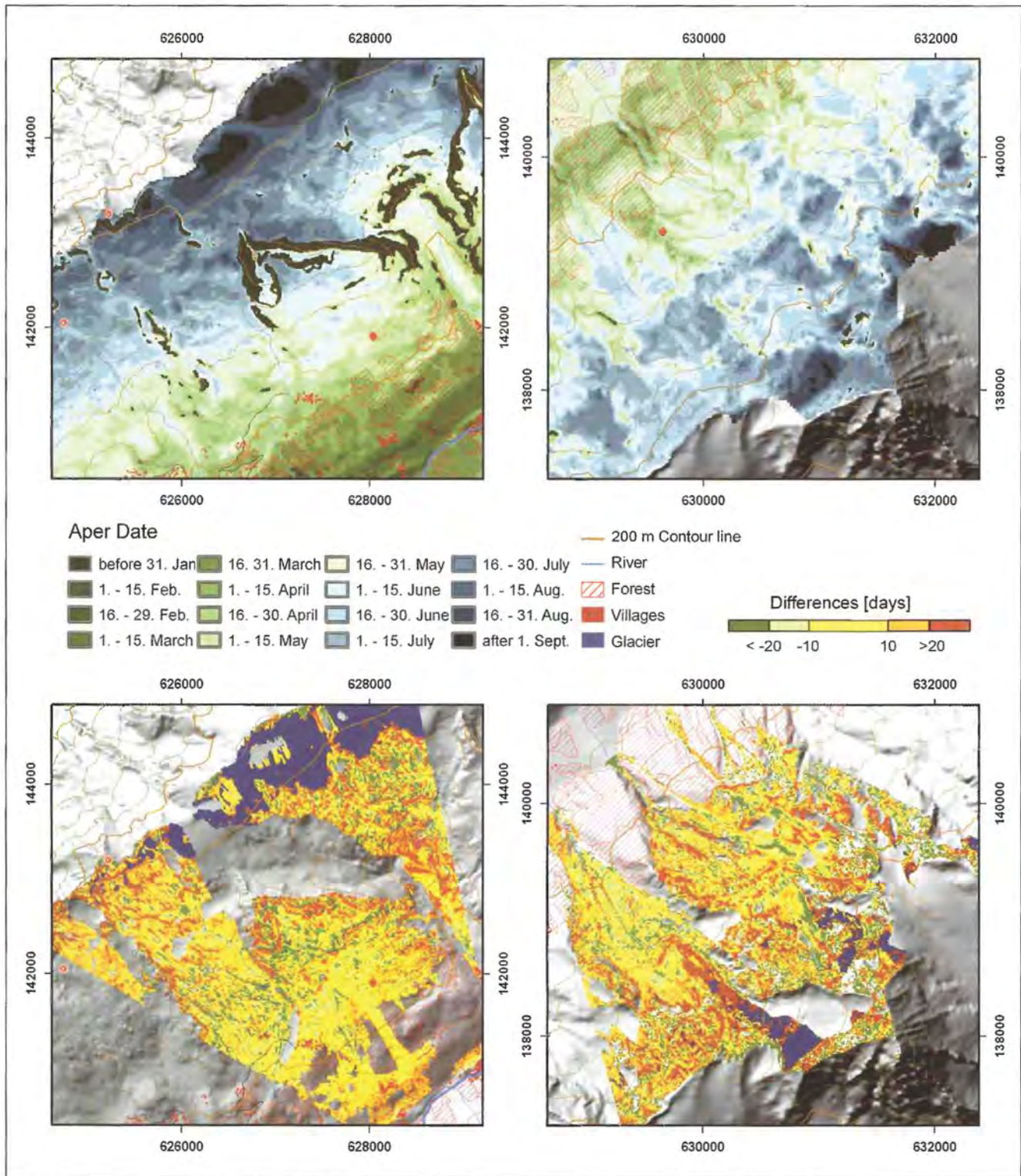


**Figure 5:** Modelled snow cover distribution (top) and validation of models (bottom).

the NW-facing slope than on the SE-facing slope. Moreover, on both slopes snow cover variations are influenced by turbulent and advective heat fluxes originating from snow free areas (STÄHLI & JANSSON 1998). These snow free areas provide a lower albedo compared to snow covered areas resulting in a higher energy budget for snowmelt. According to MARSH (1999) the difference between snow covered and snow free areas can be up to 42 °C. Depletion maps generated from terrestrial ima-

ges show that melting exceeds from snow free area, i.e. rocks, pikes, and release areas of avalanches. Additionally, the snow cover patterns are varied by other parameters like vegetations cover, glaciers and permafrost. Hence, these variations of snow cover pattern are mainly controlled by snow depth, which cannot be referred to topographical features alone (BARRY 1992; BERNHARD & WEIBEL 1999; HOLTMEIER & BROLL 1992; LÖFFLER 2005; LUCE et al. 1999; PHILLIPS 2000).

## 7. Conclusion

Due to the "topography-independent" variation, the snow cover pattern can only be partly explained by topographical features alone. Hence, the exact prediction of snow cover distribution will remain limited (BLÖSCHL et al. 1991).

With the use of spatial and temporal high resolution data these uncertainties can be recorded. The semi-automatic process developed in this study enables a high precision of geographical positions of the terrestrial images, which is a crucial prerequisite for topographical analyses. The orthorectification of each image enables the use of masks of shadow and ground features that lead to an improved classification procedure. These methods have not been applied to terrestrial images yet.

Digital terrestrial images can be used for a new method to monitor the meso-scale distribution of snow cover. This meso-scale method provides more accurate spatial results than conventional approaches of snow measurements. Additionally, the spatial validity of point measurements and physical based models can be verified with high temporal and spatial resolution data. The presented method solves the dilemma of resolution and seasonality.

## References:

- BAHRENBERG, G., GIESE, E. & NIPPER, J. (2003): Statistische Methoden in der Geographie 2. Multivariate Statistik. Teubner Studienbücher der Geographie, 2: Stuttgart, 415 S.
- BARRY, R.G. (1992): Mountain Weather and Climate: London, 313 S.
- BERNHARD, L. & WEIBEL, R. (1999): Modelling Snowmelt Using a Digital Terrain Model and Gis-Based Techniques. In: R. DIKAU & H. SAURER [Hrsg.]: GIS for Earth Surface Systems: Analysis and Modelling of the Natural Environment: Stuttgart, S. 25-47.
- BLÖSCHL, G. & KIRNBAUER, R. (1991): Point Snowmelt Models with Different Degrees of Complexity - Internal Processes. *Journal of Hydrology*, 129, S. 127-147.
- BLÖSCHL, G. & KIRNBAUER, R. (1992): An Analysis of Snow Cover Patterns in a Small Alpine Catchment. *Hydrological Processes*, 6, S. 99-109.
- BLÖSCHL, G., KIRNBAUER, R. & GUTKNECHT, D. (1991): A Spatially Distributed Snowmelt Model for Application in Alpine Terrain. In: BERGMANN, H., LANG, H., FREY, W., ISSLER, D. & SALM, B. [Hrsg.]: Snow, Hydrology and Forests in High Alpine Areas (Proceedings of the Vienna Symposium). IAHS Publ. No. 205, S. 51-60.
- CHANG, K.-T. & LI, Z. (2000): Modelling Snow Accumulation with a Geographic Information System. *Int. J. Geographical Information Science*, 14, S. 693-707.
- CHRISTIANSEN, H.H. (2004): Meteorological Control on Interannual Spatial and Temporal Variations in Snow Cover and Ground Thawing in Two Northeast Greenlandic Circumpolar-Active-Layer-Monitoring (Calm) Sites. *Permafrost and Periglacial Processes*, 15, S. 155-169.
- CORRIPIO, J. (2004): Snow Surface Albedo Estimation Using Terrestrial Photography. *International Journal of Remote Sensing*, 25, S. 5705-5729.
- DE JONG, C., ERGENZINGER, P., BORUFKA, M., KÖCHER, A. & DRESEN, M. (2005): Geomorphological Zoning: An Improvement to Coupling Alpine Hydrology and Meteorology? In: DE JONG, C., COLLINS, D. & RANZI, R. [Hrsg.]: Climate and Hydrology in Mountain Areas: London, S. 247-260.
- DOZIER, J. & PAINTER, T. (2004): Multispectral and Hyperspectral Remote Sensing of Alpine Snow Properties. *Annual Review of Earth and Planetary Sciences*, 32, S. 465-494.
- EHRLER, C. & SCHAPER, J. (1997): Analyse von Ausaperungsmustern der saisonalen Schneedecke mit Fernerkundungsmethoden. *Geographica Helvetica*, 1, S. 11-20.
- FRIEDEL, H. (1961): Schneedeckendauer und Vegetationsverteilung im Gelände. *Mitteilungen der forstlichen Bundes-Versuchsanstalt Mariabrunn*, 59, S. 317-369.
- GJAEREVOLL, O. (1956): The Plant Communities of the Scandinavian Alpine Snow-Beds. *Det. Kgl. Norske Vidensk. Selsk. Skrift*, 1, 1, 405 S.
- GOODISON, B.E., FERGUSON, H.L. & KAY, G.A. (1981): Measurement and Data Analysis. In: GRAY, D.M. & MALE, D.H. [Hrsg.]: Handbook of Snow. Principles, Processes, Management & Use., S. 194-274.
- HALL, D.K. & MARTINEC, J. (1985): Remote Sensing of Ice and Snow: London, 189 S.
- HINSKEN, L. (1989): CAP - Ein Programm zur kombinierten Bündelausgleichung auf Personal Computern. *BuL : Bildmessung und Luftbildwesen, Organ der Deutschen Gesellschaft für Photogrammetrie und Fernerkundung e.V. Zeitschrift für Photogrammetrie und Fernerkundung* 57, S. 92-95.
- HOLTMEIER, F.-K. & BROLL, G. (1992): The Influence of Tree Islands and Microtopography on Pedoecological Conditions in the Forest-Alpine Tundra Ecotone on Niwot Ridge, Colorado Front Range, U.S.A. *Arctic and Alpine Research*, 24, S. 216-228.
- KELLER, F. (1994): Interaktionen zwischen Schnee und Permafrost. *VAW Mitteilungen* 127, 145 S.
- KÖLBEL, H. (1984): Die Schnee-Ausaperung im Gurgler Tal (Ötztal/Tirol). *Salzburger Geographische Arbeiten*, Bd. 12: Salzburg, 214 S.
- KÖNIG, M. & STURM, M. (1998): Mapping Snow Distribution in the Alaskan Arctic Using Aerial Photography and Topographic Relationships. *Water Resources Research*, 34, S. 3471-3483.
- KÖRNER, C. (1999): Alpine Plant Life: Functional Plan Ecology of High Mountain Ecosystems: Heidelberg, 333 S.
- LÖFFLER, J. (2005): Snow Cover Dynamics, Soil Moisture Variability and Vegetation Ecology in High Mountain Catchments of Central Norway. *Hydrological Processes*, 19, S. 2385-2405.
- LOWE, D.G. (2004): Distinctive Image Features from Scale-Invariant Keypoints. *International Journal of Computer Vision*, 60, S. 91-110.

- LUCE, C.H., TARBOTON, D.G. & COOLEY, K.R. (1999): Subgrid Parameterization of Snow Distribution for an Energy and Mass Balance Snow Cover Mode. *Hydrological Processes*, 13, S. 1921-1933.
- MAGGIONI, M., GRUBER, U. & STOFFEL, A. (2005): Definition and Characterisation of Potential Avalanche Release Areas. <http://GIS.esri.com/library/userconf/proc02/pa1161/p11> (Letzter Aufruf: 05.08.2006).
- MARSH, P. (1999): Snowcover Formation and Melt: Recent Advances and Future Prospects. *Hydrological Processes*, 13, S. 2117-2134.
- McKAY, G.A. & GRAY, D.M. (1981): The Distribution of Snowcover. In: GRAY, D.M. & MALE, D.H. [Hrsg.]: *Handbook of Snow. Principles, Processes, Management & Use*, S. 153-190.
- PHILLIPS, M. (2000): Influence of Snow Supporting Structures on the Thermal Regime of the Ground in Alpine Permafrost Terrain. *Eidgenössisches Institut Für Schnee- Und Lawinenforschung: Davos*, 146 S.
- RYCHETNIK, J. (1984): Methoden der Erfassung und Auswertung der Ausaperung und Lawinenaktivität an einem Lawinenhang. In: BRECHTEL, H. M. [Hrsg.]: *Snow Hydrologic Research in Central Europe*, 162, S. 153-165.
- SCHMIDT, J. & HEWITT, A. (2004): Fuzzy Land Element Classification from DTMs Based on Geometry and Terrain Position. *Geoderma*, 121, S. 243-256.
- SEIDEL, K. & MARTINEC, J. (2004): Remote Sensing in Snow Hydrology. *Runoff Modelling, Effect of Climate Change: Heidelberg*, 150 S.
- STÄHLI, M. & JANSSON, P.-E. (1998): Test of Two SVAT Snow Submodels During Different Winter Conditions. *Agricultural and Forest Meteorology*, 92, S. 29-41.
- TAPPEINER, U., TAPPEINER, G., ASCHENWALD, J., TASSER, E. & OSTENDORF, B. (2001): GIS-Based Modelling of Spatial Pattern of Snow Cover Duration in an Alpine Area. *Ecological Modelling*, 138, S. 265-275.
- YAMADA, Y. (1996): On the Topographical Origin of Some Remaining Snow Patterns, "Yukigata". In: A.A. ASSOCIATION [Hrsg.]: *Proceedings of the International Snow Science Workshop 1996, Banff Canada.*, S. 75-80.
- Zimmermann, N.E. (2000): Shortwave. <http://www.wsl.ch/staff/niklaus.zimmermann/programs/ams/shortwavc.aml> (Letzter Aufruf: 5.03.2006).

## 14 Computational fluid dynamics simulation of snow drift in alpine environments for operational avalanche warning

SIMON SCHNEIDERBAUER, WALTER HINTERBERGER  
AND PETER FISCHER<sup>1</sup>

<sup>1</sup> dTech-Steyr, Dynamics & Technology Services GmbH,  
Steyrerweg 2, A-4400 Steyr, Austria

### Abstract

Due to increasing development of Alpine environments by transport and tourism the forecasting of avalanche danger becomes more and more important. The protection of civil facilities and human lives is one major aim of avalanche forecasting. Cornices and snow banks, which contribute most to the avalanche danger, are primarily formed by snow drift. If the boundary shear stress acting on the snow cover, which is induced by the wind, exceeds a certain threshold, snow will be entrained. On the contrary, if the flow does not exert enough shear stress, snow is deposited. Hence, erosion and deposition zones are built, whereby the geometry of the snow pack changes. These deformations of the shape of the snow pack couple to the wind field and thus the flow is changed by the new geometry. This coupling creates time dependent erosion and deposition zones.

The amount of snow grains, which can be transported by the flow, contributes additionally to snow drift occurrences. An increasing wind speed raises the amount of drifting snow. If a fence slows down the flow, snow will be deposited by a decreasing amount of drifting snow.

The numerical simulation of complex snow drift processes has to challenge with time dependent geometries of the snow cover and particle transport phenomena. Furthermore, snow erosion and accumulation are determined by boundary shear stress criteria leading to a deformation of the snow cover.

### 1. Introduction

Human civilization is affected by blowing and drifting snow in various ways. Primarily the influence on avalanche formation in Alpine regions has to be emphasized. The snow depth at mountainsides and the dead load of snow slabs are important factors that determine whether avalanches occur. In addition to fresh fallen snow, snow drift contributes a lot to the amount of snow at mountainsides. Mainly leeward the snow depth is determined by the strength of drifting snow. At mountainsides even with a slope angle of about nearly 30° avalanches may be released due to very high snow depths. Finally, drifting snow forms big snow cornices at mountain ridges (Figure 1). That is why snow cornices are a second important factor triggering avalanches. Wind deposited snow forms can cause an avalanche release.



**Figure 1:** Snow cornice on a leeward slope of a mountain ridge (copyright by WILHELM GAULHOFER).

Often human beings or important infrastructures are threatened by avalanches. In addition, because of the increasing touristic development of Alpine terrain, the knowledge about the actual avalanche situation becomes more and more important for shielding human lives. In Austria 28 people are killed on average by avalanche activities every year (GAYL AND BAUER 2000). For example, in 1999 a very strong avalanche buried the half of Galtür, an Austrian mountain village. Furthermore, avalanches were responsible for direct structural damages of the order of 287 million euros in Switzerland during winter 1998/99 (EIDGENÖSSISCHES INSTITUT FÜR SCHNEE- UND LAWINENFORSCHUNG 2000).

It is very difficult to predict avalanches. Meteorologists have to rely on selective measurements of the actual weather situation and selective snow profiles. From this sparse information avalanche risk is determined. The knowledge of zones where wind deposits snow and forms cornices as a function of the overall weather situation is of vital importance for avalanche warning.

Avalanche formation is only one consequence of blowing and drifting snow. Less hazardous but a still important economic aspect is the influence of snow drift on everyday life. Snow drift causes additional snow loads on structures. Several halls collapsed due to that additional weight in Central Europe in the winter of 2005/06. Furthermore, drifting snow causes additional road clearing and generates traffic snarls.

### 2. The Physical Concept

Since ANDERSON et al. (1991) it is common to distinguish between three different transport modes of drifting snow:

#### Surface creeping/Reptation:

The transport modes, that are located nearest to the ground up to a height of the order of the surface roughness, are referred to as surface creeping and reptation. The transport of the grains is not affected by the wind but depends on the impact of other particles if we take into account that snow is cohesive. Nevertheless, this transport mode makes a weak contribution to snow transport. Typical grain sizes are of the order of 1 mm.

### Saltation:

The grains are partially influenced by the turbulence of the wind. Saltating grains are capable of rebounding and ejecting other grains. The typical grain diameters in the saltation mode are between 0.05 and 0.5 mm. Most of the snow transport occurs in this transport mode, whereas the volume fraction of the snow particles is in the range of  $10^{-5}$  to  $10^{-3}$ . Furthermore, for high wind speeds the height of the saltation layer can reach about 0.1 m.

### Suspension:

In the suspension transport mode, which is located above the saltation layer, the snow particles are lifted up far away from the snow pack and are carried over large spatial distances without rebounding from the surface. They can reach a height of several hundred meters, whereas typical volume fractions are lower than  $10^{-4}$  and the grains are usually smaller than in the saltation layer.

The transport modes described above are illustrated in Figure 2. The figure points out the different volume fractions in the different transport modes. In addition, the white circles indicate grains bound on the snow pack and the grains in motion are designated by the filled circles.

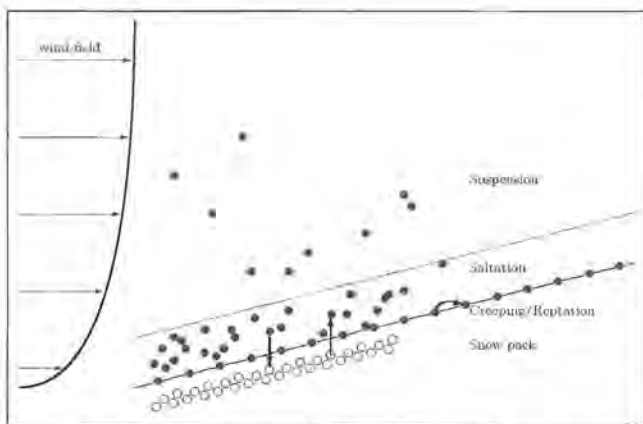


**Figure 2:** Transport modes of blowing and drifting snow: Creeping and Reptation, saltation and suspension. Snow pack indicates the structural snow cover.

GAUER (GAUER 1999) estimated that saltation starts at wind speeds at 10 m height of about 5 - 8 m/s, whereas the different transport modes contribute to the snow drift as follows:

S. C./Reptation	5 - 25 %
Saltation	50 - 75 %
Suspension	3 - 40 %

As previously mentioned, saltation contributes most to the mass transport but with increasing wind speed suspension increases, too.

Snow transport can be described as follows. If the wind shear exceeds a certain threshold grains will be entrained and set in motion. The so called *fluid threshold* (BAGNOLD 1941) is given by

$$\tau_{c_s} = (A_e)^2 (\rho_p - \rho_a) g d_p.$$

$\rho_p$  and  $\rho_a$  are the densities of the snow particles and air. Furthermore  $g$  denotes the standard acceleration due to gravity,  $d_p$  the snow particle diameter and  $A_e$  a dimensionless empirical parameter, which is a function of the particle shape and particle cohesion. The exact underlying mechanism which is responsible for the initiation of the snow drift process is not completely known. Following BAGNOLD, ANDERSON AND HAFF (ANDERSON AND HAFF 1991) estimated that the number of entrained grains per unit time and unit area depends linearly on the excess shear stress

$$\frac{\partial N_e}{\partial t} = \xi (\tau_a - \tau_{c_s}),$$

where  $\tau_a$  denotes the air induced shear stress.  $\xi$  is an empirical constant with the dimensions of (force times time) $^{-1}$ . The entrained particles are easily accelerated by the wind because of their small mass and diameter. Already entrained grains contribute to the wind shear, i.e. they reduce the threshold. In addition, the wind influences the heights of the transport modes, whereas the saltation layer height increases with increasing wind speed (OWEN 1964). Therefore, a higher amount of snow can be transported and more grains are entrained per unit of time. Due to the interaction between grains and wind the wind field is modified. However, if the wind shear is below a second *threshold*, the *impact threshold*, snow will be accumulated

$$\tau_{c_i} = (A_i)^2 (\rho_p - \rho_a) g d_p,$$

where  $A_i$  is again a dimensionless empirical parameter. Grains, whose motion is directed towards the snow pack, are deposited. The mass flux to the snow pack can be obtained by the change of volume fraction of the snow in an arbitrary control volume. In especially the change of mass inside the control volume has to be equal to the mass flux through the faces of the control volume by the principle of mass conservation.

Finally, it should be mentioned that only a certain amount of grains can be transported by the wind. This leads to deposition where the volume fraction exceeds a third *threshold*, the *saturation volume fraction*. In all cases, gravity acts as a body force. Due to the slope angle of the snow pack the snow grains are affected by a downhill-slope force. Since the shear stress thresholds mentioned above are only valid for flat plains a modification, which additionally incorporates the slope angle, is applied.

The transport processes discussed above cause a deformation of the snow pack. In deposition zones the snow cover is growing and thus the new shape influences the local velocity field. In addition, in erosion zones a reversed process takes place. Hence, due to the modification of the wind field the zones change with time and depend on the shape of the snow pack.

### 3. A mixture Model Approach

The mixture model approach is based on the balance equations of a mixture for interpenetrating phases, where the phases are allowed to move with different velocities (FLUENT Inc. 2005). In the model we consider three different phases:

- Air
- Drifting snow
- Precipitation.

Air acts as carrier phase and is observed as a wind field or primary phase. The transported grains are modeled by the secondary phases, which are observed as drifting snow. The saltation and the suspension layers are not separated, but they are given by the behavior of the snow phase due to the flow field of air and due to the influence of gravity. This snow drift model is fundamentally based on BAGNOLDS impact and erosion criteria (BAGNOLD 1941), which distinguish between zones of erosion and zones of deposition. Additional empirical relationships, which are obtained from several measurements (e.g. NAAIM-BOUVET et al. 2001), such as the height of the saltation layer, which influences the saturation volume fractions in the finite control volumes, are of vital importance for computational calculations.

Precipitation is included by an additional secondary phase to incorporate the different physical properties of precipitating snow and drifting snow. In especially different grain sizes, densities and particle shapes are placed in the snow drift simulation.

### 4. The Numerical Model

In our mixture model approach the saltation and suspension layer are not treated separately in different calculation domains as in GAUER 1999 and DOORSCHOT 2002. The saltation layer is rather modeled by volume fractions of the snow phase in the volume cells adjacent to the snow cover. The mass fluxes are obtained from the flow field of the snow phase. BAGNOLDS "stick-slip" criteria are used to distinguish between zones of deposition and aerodynamic entrainment. To avoid unphysical effects in the flow field we introduced a saturation volume fraction. The deformations of the snow cover are predefined by the mass fluxes and the unit surface normals. A dynamic mesh model will remesh the domain if yield criteria are exceeded. In addition, precipitation can be considered.

The numerical modeling of snow drift using a mixture model approach can be divided into two segregated calculations for each time step:

1. Calculation of the flow field by the commercial computational fluid dynamics software FLUENT.
2. Computation of the mass fluxes between snow pack and saltation transport mode in order to use our modification of the BAGNOLDS erosion and deposition criteria, respectively.

The computation of the mass fluxes is hooked into FLUENT by using *User Defined Functions* (UDFs). Using UDFs can increase and individualize the solver capabilities. The user is able to manipulate or access solver variables at different points of the solution process by UDFs. These functions have to be implemented in the "C" programming language.

Both calculation steps mentioned above are simultaneous processes in nature. For a more exact computation the snow drift calculation should be performed within every non linear flow field iteration. Because of small time steps the snow drift effects are only tiny contributions. Therefore, the calculation can be performed in a segregated way. As we compute the snow drift only once for each time step computational time is reduced significantly. In Figure 3 the flow chart of our snow drift calculation is shown.

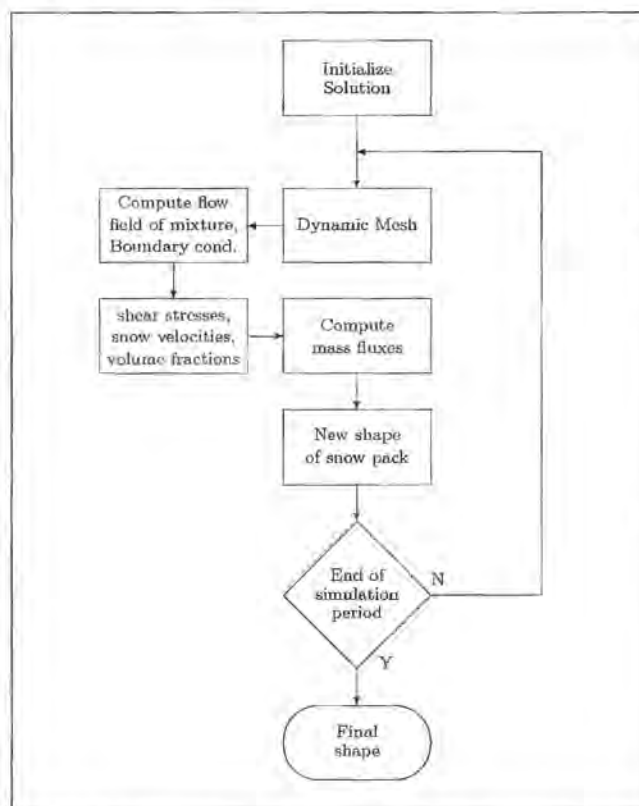


Figure 3: Flow chart of the numerical snow drift model.

### 5. Results

#### 5.1. Snow Drift around a 3D Fence with Bottom Gap

The deposition patterns around obstacles such as buildings or the effects of a snow fence are typical problems of significant practical interest. Several research teams studied fences at full scale or in wind tunnel, e.g., the experiments of NAAIM-BOUVET et al. 2001.

We investigated a three dimensional snow fence with a height of  $H=0.5$  m and with a bottom gap of  $0.2H$ . The dimensions of the computation domain were chosen  $10H$  in upwind and  $30H$  in downwind direction. The side boundaries of the grid are allocated approximately  $10H$  away from the lateral edges of the fence.

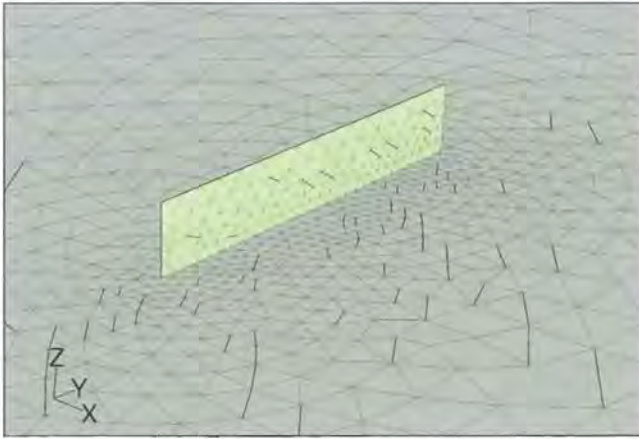


**Figure 4:** Sketch of the mesh of the snow cover around the three dimensional fence with a bottom gap of 0.2 H

The mesh of the snow cover consists of 932 nodes and 1812 faces and is depicted in Figure 4. Based on the inequality estimate for the mesh resolution we were led to a time step size of 0.01 s.

At the bottom a 0.1 m deep erodible layer of cohesionless snow with a maximum packing limit of 0.5 was assumed. The typical particle diameter was set to 300  $\mu\text{m}$  and the density of the snow grains was set to 400  $\text{kg m}^{-3}$ . The critical wall shear stresses were set to (e.g. GAUER 1999):

Fluid threshold	0.0247 Pa
Impact threshold	0.01984 Pa

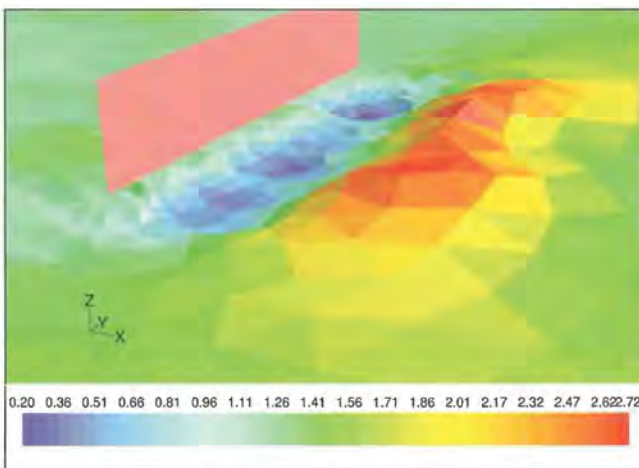


**Figure 5:** Snow drift around a three dimensional fence with a bottom gap of 0.2 H and a height of  $H = 0.5$  m at real time 5000 s. The color bar corresponds to the snow depth  $h/h_{\text{ref}}$  with  $h/h_{\text{ref}} = 0.1$  m

In Figure 5 the resulting deposition pattern, which seems to be quite reasonable around the snow fence is shown. In addition, the velocity field vectors at the vertical symmetry plane are plotted in Figure 6. In Figure 7 the velocity vectors are drawn around the fence at a constant height  $h/h_{\text{ref}} = 0.4$ , which illustrates the three dimensional effects at the side edges of the fence. Hence, one would expect a slightly different deposition pat-

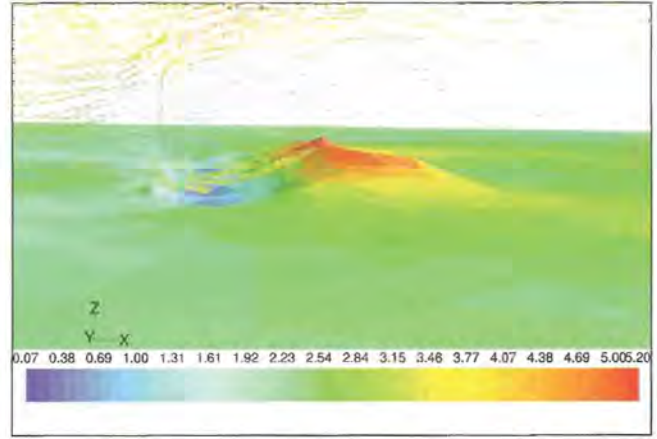


**Figure 6:** Velocity vectors at the middle plane in  $\text{m s}^{-1}$  at 5000 s

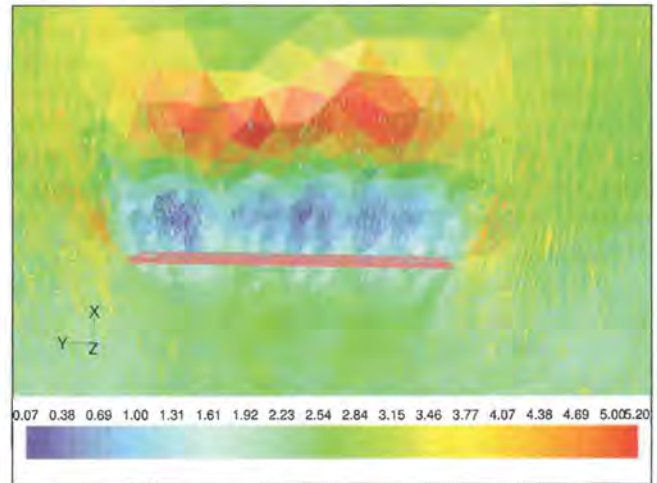


**Figure 7:** Velocity vectors at constant height  $h = 0.4$  in  $\text{m s}^{-1}$  at 5000 s

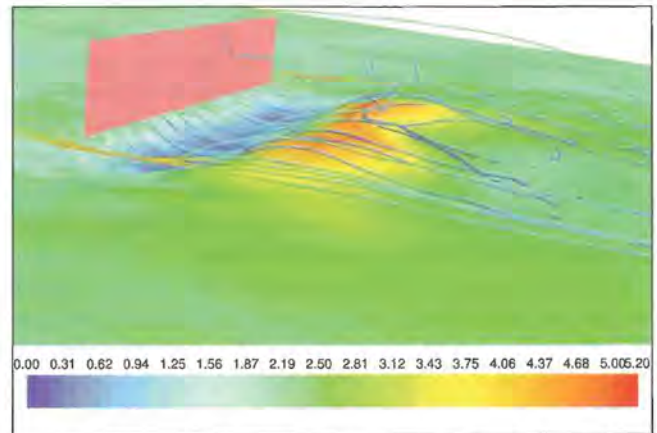


**Figure 8:** Pathlines of massless particles around the fence at 5000 s. The colorbar corresponds to the velocity of the particles.

tern in three dimensions. In Figure 8 the pathlines of massless particles around the snow fence are plotted to point out the effect of turbulent flows on snow drift.

## 5.2. Snow Drift over a 3D Mountain Ridge

Snow drift distributions of fracture zones are very important for operational avalanche warning. In practice the



**Figure 9:** Snow drift pattern at the upwind side of the mountain ridge. The color bar corresponds to the snow depth in m

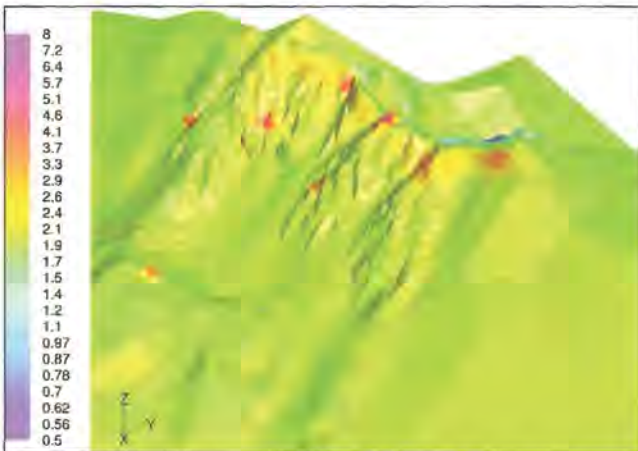


**Figure 10:** Snow drift pattern at the downwind side of the mountain ridge. The color bar corresponds to the snow depth in m

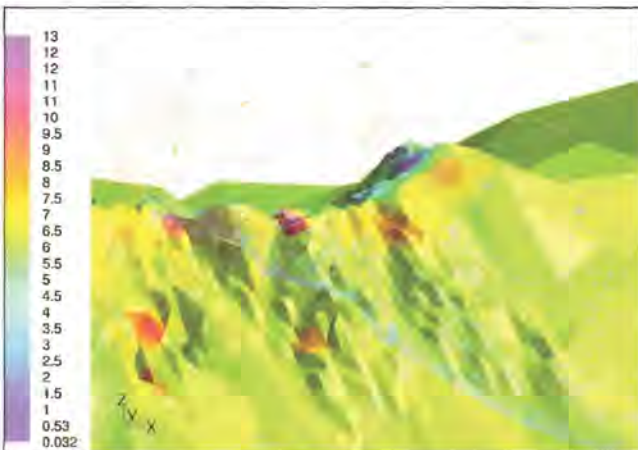


**Figure 11:** Velocity vectors at a vertical plane across the mountain ridge in  $\text{m s}^{-1}$

assessment of those zones is a major problem for the present avalanche warning systems. Computer simulations can be used to determine snow drift patterns in those zones.

We determined a snow drift distribution across a two-dimensional mountain ridge, the "Innsbrucker Nordkette". We assumed the same physical properties as used in the snow drift simulation of the 3D fence. These values are very reasonable for snow drift in Alpine terrain. At the

bottom a 2 m deep erodible layer of cohesionless snow was assumed and the undisturbed wind field was set to  $6 \text{ m s}^{-1}$ .

In Figure 9 the snowdepth upwind of the mountain ridge after a drifting period of three days is shown. Most of the initial snow layer is eroded due to high wind speeds near the ridge and is freighted downwind. The downwind deposition pattern is shown in Figure 10. Downwind beyond the crest line at the beginning of the chutes the wind forms up to 8 m high snow cornices. Additional huge snow drift patterns arise at the cleft areas downwind of the ridge. Figure 11 indicates the big vortex, which are obvious behind obstacles, downwind of the ridge.

## 6. Conclusions

Blowing and drifting snow are one of the key factors in formation of avalanches, but there is a lack of knowledge about the influence of different weather situations on deposition patterns. Hence, great interest exists in the prediction of snow drift occurrences as additional information for avalanche forecasting. Nowadays, avalanche forecasters are restricted to punctual measurements of the snow depths and snow property values. The simulation of snow drift provides an exhaustive profile of the snow depth and the prediction of the formation of snow slabs, respectively. As an additional feature the snow drift model can be used for the simulation of snow drift patterns around obstacles, such as snow fences and buildings. The additional snow loads on buildings due to snow drift are of major importance for structural damages.

However, the simulations performed also exhibit restrictions connected to snow drift modeling such as:

- The computational effort increases nonlinearly with the increase of the area of interest and spatial resolution of the area. The major problem here is caused by the restriction of the dynamic mesh model to use a tetrahedral mesh.
- The three degrees of freedom grid update algorithm may show unstable behavior, if snow drift around obstacles is considered. Additional geometric smoothing methods (the Umbrella operator, e.g. KOBELT et al. 1998) had to be included to stabilize the update (for further investigations see SCHNEIDERBAUER 2006).
- The maximum possible computational time step decreases with increasing spatial resolution.
- The physical simulation of snow drift in a complex terrain is difficult to realize because of the poor information about boundary conditions. In future activities weather models will be used to obtain more realistic boundary conditions.

Snow drift simulations can help assessing avalanche danger due to better knowledge about the potential fracture volume and the distribution of fracture areas. The three dimensional simulations are in good agreement with observations in nature. Finally, our fully three dimensional model is well applicable for simulating snow

drift over full scale mountain ridges. Calculated snow distributions can be used to provide boundary conditions for simulations in avalanche hazard mapping.

### Acknowledgements

Thanks go to WLV Tirol for providing the laser scan data of the "Innsbrucker Nordkette" and to ZAMG Graz for their feedback about wind conditions and snow drift patterns.

### References

- ANDERSON, R.S. AND HAFF, P.K. (1991): Wind modifications and bed response during saltation of sand and air. *Acta Mechanica (Supplementum)*, vol 1:21-51.
- ANDERSON, R.S., SORENSON, M. AND WILLETS, B.B. (1991): A review of recent progress in our understanding of aeolian sediment transport *Acta Mechanica (Supplementum)*, vol 1:1-19.
- BAGNOLD, R.A. (1941): *The physics of blown sand and desert dunes*. London: Methuen.
- DOORSCHOT, J. (2002): *Mass Transport of Drifting Snow in High Alpine Environments*. PhD Thesis, Swiss Federal Institute of Technology Zurich.
- Eidgenössisches Institut für Schnee- und Lawinenforschung (2000): *Der Lawinenwinter 1999 – Ergebnisanalyse*. Davos.
- GAUER, P. (1999): *Blowing and Drifting Snow in Alpine Terrain: A Physically-Based Numerical Model and Related Field Measurements*. PhD thesis, SLF Davos.
- GAYL, A. AND BAUER, H. (2000): *Jahrbücher des Konsortiums für Alpine Sicherheit / Lawinenhandbuch 2000*. Institut für Lawinen- und Wildbachforschung.
- FLUENT Inc. (2005): *FLUENT 6.2 USER'S GUIDE*.
- KOBBELT, L., CAMPAGNA, S., VORSATZ, J. AND SEIDEL, H.P. (1998): Interactive multiresolution modeling on arbitrary meshes. In *SIGGRAPH Conference Proceedings 1998*, pages 105-114. Addison Wesley Publishing Company.
- NAAIM-BOUVET, F., NAAIM, M. AND MICHAUX, J.L. (2001): Final scale snowdrift processes: major outcomes from col du lac blanc and related experiments in wind-tunnel. *Proceedings of the International Seminar on Snow and Avalanches Test Sites – Grenoble*.
- OWEN, P.R. (1964): Saltation of uniform grains in air. *Journal of Fluid Mechanics*, vol 20(2):225-242.
- SCHNEIDERBAUER, S. (2006): *Computational Fluid Dynamics Simulation of Snow Drift in Alpine Environments*. Johannes Kepler Universität Linz. Institute for Theoretical Physics.

## 15 Distributed modelling of snow processes in the Berchtesgaden National Park (Germany)

ULRICH STRASSER<sup>1</sup>, HELMUT FRANZ<sup>2</sup>  
AND WOLFRAM MAUSER<sup>1</sup>

<sup>1</sup> Department of Geography, Ludwigs-Maximilians University, Luisenstraße 37, D-80333 Munich, Germany

<sup>2</sup> Berchtesgaden National Park, Doktorberg 6, D-83471 Berchtesgaden, Germany

### Abstract

An automatic network of meteorological stations has been assembled in the Berchtesgaden National Park. From these stations, continuous records of 10 minutes to half-hourly measurements are collected via wireless GSM transmission and stored in a central database, starting in August 1998. The spatial arrangement of the stations, their range in altitude between 617 m and 2445 m a.s.l. and the temporal duration of the measurements generated a unique data set enabling a continuous modelling of a wide range of environmental processes. This paper describes the application of the spatially distributed snow processes model AMUNDSEN which includes (a) spatial interpolation of the meteorological variables considering topography, (b) a sophisticated scheme to compute short- and longwave radiative fluxes with shadows and cloudiness, (c) parameterization of snow albedo based on its age and temperature and (d) simulation of the snow surface energy balance by iteratively adopting its temperature. Finally, snow interception, sublimation and melt unload in forest canopies are simulated with a physically based scheme considering effective leaf area index and tree height for the prevailing mixed forest, larch, spruce and mountain pine stands in the National Park area. The simulation results for the ground snow cover are compared to point measurements. By applying a built-in stochastic weather generator, synthetic future time series of meteorological input data according to a given temperature trend can be produced and used for estimating climate change effects on the snow cover evolution. This modelling system represents the basis for including further distributed eco-physical models, e.g. for the simulation of hydrological, climatological or biological processes under changing climatic conditions.

### 1. Introduction

In terms of water availability for mankind, snow dominated regions are important in their function of collecting, storing and releasing water resources: more than one-sixth of the Earth's population is relying on glaciers and seasonal snow packs for their water supply (BARNETT et al. 2005). Most parts of these regions are mountains

with their respective forelands. People depend on the mountains for food, hydroelectricity, timber or mineral resources. 50 % of the world's population rely on the supply from mountain watersheds for fresh water (MOUNTAIN AGENDA 1998). In mountain regions, water resources are accumulated and stored during winter, and released into rivers and streams during the ablation season in late spring and summer. Therefore, e.g. the European Alps are often referred to as a "water tower" for Europe (VIRIOLI et al. 2003); the Rhine, the Danube, the Rhone and the Po are fed by water originating from the headwatersheds in the Alps. Beneficial effects of the nival and glacial runoff regimes for the downstream population include the increased collection of precipitation amount due to the topographical structure of mountain ridges. Secondly, evaporation rates are lower in the mountain regions due to the colder temperatures (which also reduces transpiration rates), and such runoff coefficients, i.e. the fraction of rainfall which contributes to discharge does increase. And, most important, the temporary storage of rainfall as snow and ice enables a time-delayed release of the melt water, generally coinciding with periods of low precipitation rates (i.e., high temperature and radiation periods in summer). Thus, a mountain snow cover represents a natural storage system of significant importance in terms of availability and distribution of the resource water in the forelands (ZIERL AND BUGMANN 2005). Quantitative measures and predictions of the resources are subject to notable uncertainties due to the large variability of mountain snow cover in space and time (KLEMES 1990). Phase and amount of precipitation varies largely in rugged terrain, shading can locally reduce the available energy for melt, and the processes of the snow-vegetation interactions further modify the distribution of the seasonal snow cover in the mountains. In this paper, these aspects are addressed by means of a distributed modelling system to enhance our knowledge and understanding of the effects governing the uneven distribution of the snow resources and thus enabling us to improve our capability in predicting their release, availability and quality.

### 2. Methods

#### 2.1 Site description

The Berchtesgaden National Park is located in southeast Germany in Bavaria, at the southern corner of the administrative district "Berchtesgadener Land" (figure 1). The park was founded in 1978 and comprises an area of approximately 208 km<sup>2</sup> (<http://www.national-park-berchtesgaden.de/>). For the most part, the border of the National Park is represented by the national boundary to Austria. Only in the north, the National Park adjoins the settlement areas of the communities Berchtesgaden, Schönau at the Königssee as well as Ramsau, all of them in the borderland of the National Park. The forests are subordinated to the National Park authority since 1987. The moderate to high alpine area of the National Park includes the massifs Watzmann (2713 m



**Figure 1:** Location of the Berchtesgaden National Park (Germany).

a.s.l.) and Hochkalter (2606 m a.s.l.) as well as parts of the massifs Hoher Göll, Hagengebirge, Steinernes Meer and Reiter Alm, which are situated at the national boundary to Austria. The mountain massifs are separated by the deep valleys stretching from south to north of the Königssee (water level 603 m a.s.l.), the Wimbach and the Klausbach. The valley areas are characterized by extensive forests (KONNERT 2004). The relief reaches up to the nival zone with the Blaueisgletscher, the most northern glacier of the Alps, shaded by the surrounding steep rock walls and fed by avalanches sliding down from them. However, the Blaueis has significantly retreated in the past years and is at risk to completely disappear in the next decades (WINKLER 2005). The climate of the National Park area is subject to significant spatial variability, conditional to the relief gradient of more than 2000 m. Small scale local differences are caused by the general position in the mountainous landscape, the windwards or lee position to the prevailing winds, the exposition to the sun and other factors. Mean measured annual rainfall in the valleys is approximately 1500 mm with a maximum in July which is also the warmest month; the coldest month is January.

## 2.2 Data

### 2.2.1 Meteorological data

The automatic network of the meteorological stations which are located within the area of the National Park

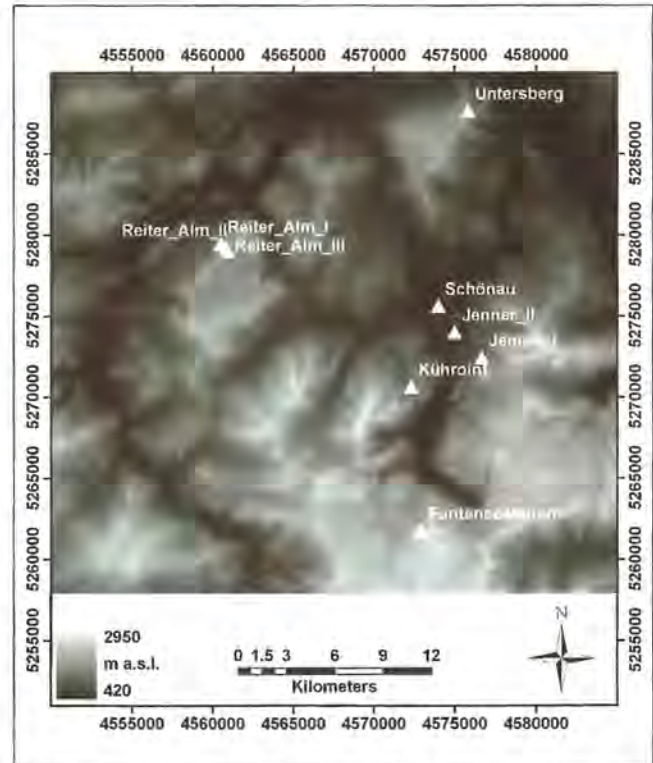


**Figure 2:** Digital elevation model (DEM) for the National Park area and its surrounding, original resolution 10 m. The circles represent the locations of the meteorological stations which comprise the automatic network.

are part of the operational infrastructure from three different institutions: the stations at Jenner, Reiter Alm, Kühroint and Funtenseetauern are part of the Bavarian avalanche warning service (LWZ) of the State Office for Environment, the Untersberg station is maintained by the Administration of Salzburg and the Schönau station belongs to the network of the German Weather Service (DWD). The spatial arrangement of the automatic stations and the range of altitudes they cover (617 m to 2445 m a.s.l.) allow to derive a relatively detailed picture of the spatial and temporal variability of the meteorological variables in this high alpine area. Figure 2 shows the locations of the stations within the area of the National Park, and the relief character for which the locations are representative, e.g. the summits of Untersberg and Funtenseetauern (1776 m and 2445 m a.s.l., respectively). By connecting these automatic stations via wireless GSM transmission with a central database we made a unique data pool available which allows to run continuous distributed models making use of these data in an operational mode with high temporal resolution. The time period between the data pollings is daily, but can be set to higher temporal resolution if required. Table 1 gives an overview of the parameters which are recorded at each station. All data are aggregated to hourly means (i.e., average for temperature, humidity, wind speed, radiation and air pressure; sum for precipitation; maximum for maximum wind speed) and checked for plausibility. Missing values due to periods in which a sensor was out of operation are characterized as such. Continuous records of the meteorological parameters start in 1998.

**Table 1:** Altitude, location and set of recorded parameters with temporal resolution for the stations comprising the automatic network in the Berchtesgaden National Park. Coordinate system is UTM.

Station	Altitude [a.s.l.]	Easting [m]	Northing [m]	Parameters	Resolution
Reiter Alm I	1755 m	4560494	5279436	WS, WS <sub>max</sub> , WD	10 min.
Reiter Alm II	1670 m	4560835	5279235	T, T <sub>S0</sub> , T <sub>S20</sub> , T <sub>S40</sub> , T <sub>S60</sub> , T <sub>SS</sub> , H, SH	10 min.
Reiter Alm III	1615 m	4560950	5278982	T, H, GR, RR, P, SH	10 min.
Kühroint	1407 m	4572314	5270625	T, H, GR, RR, WS, WD, P, SH	10 min.
Funtenseetauern	2445 m	4572939	5251755	T, H, WS, WD	10 min.
Jenner I	1200 m	4576659	5272417	T, T <sub>S0</sub> , T <sub>S20</sub> , T <sub>S40</sub> , T <sub>SS</sub> , H, SH	10 min.
Jenner II	660 m	4575786	5275825	T, H, P	10 min.
Schönau	617 m	4573987	5275597	T <sub>005</sub> , T, H, GR, DR, SS, WS, WD, P, AP	10 min.
Untersberg	1776 m	4575822	5287649	T, H, WS, WS <sub>max</sub> , WD, P	30 min.

WS	= wind speed	T <sub>S20</sub>	= snow temperature (0.2 m)	SS	= sunshine duration
WS <sub>max</sub>	= maximum wind speed	T <sub>S40</sub>	= snow temperature (0.4 m)	GR	= global radiation
WD	= wind direction	T <sub>S60</sub>	= snow temperature (0.6 m)	DR	= direct radiation
T	= temperature	T <sub>SS</sub>	= snow temperature (snow surface)	RR	= reflected radiation
T <sub>005</sub>	= temperature (0.05 m)	H	= humidity	P	= precipitation
T <sub>S0</sub>	= snow temperature (0.0 m)	SH	= snow height	AP	= air pressure at sea level

### 2.2.2 Forest canopy data

For the simulation of canopy interception processes, data fields of leaf area index (*LAI*) and canopy height are required for the model as additional input. In the National Park area, these datasets have been derived from the forest inventory data, a color infrared aerial photograph interpretation and by application of the relations by HAMMEL AND KENNEL (2001). However, for snow cover modelling an effective *LAI* for the winter is required, a period in which vegetation is not active; minimum *LAI* values for the winter season have therefore been derived by multiplying the values for spruce with a factor of 0.8, and the one for pine with 0.6; for the mountain pine shrubs (*pinus mungo*), *LAI* is assumed to be 3.2 (KONNERT 2006). To account for the stems and branches, dis-

tributed values for the cortex area index are added in the modelling. For continuous applications, effective *LAI* is assumed to linearly increase between minimum and maximum during May, and to linearly decrease during October and November. Results of effective winter *LAI* and canopy height for the National Park area are given in figure 3.

### 2.3 Models

The *Alpine MULTIscale Numerical Distributed Simulation ENGINE AMUNDSEN* (STRASSER et al. 2004) is a model shell which dynamically provides distributed fields of a variety of meteorological variables, input-output data processing capabilities, real time visualization of the

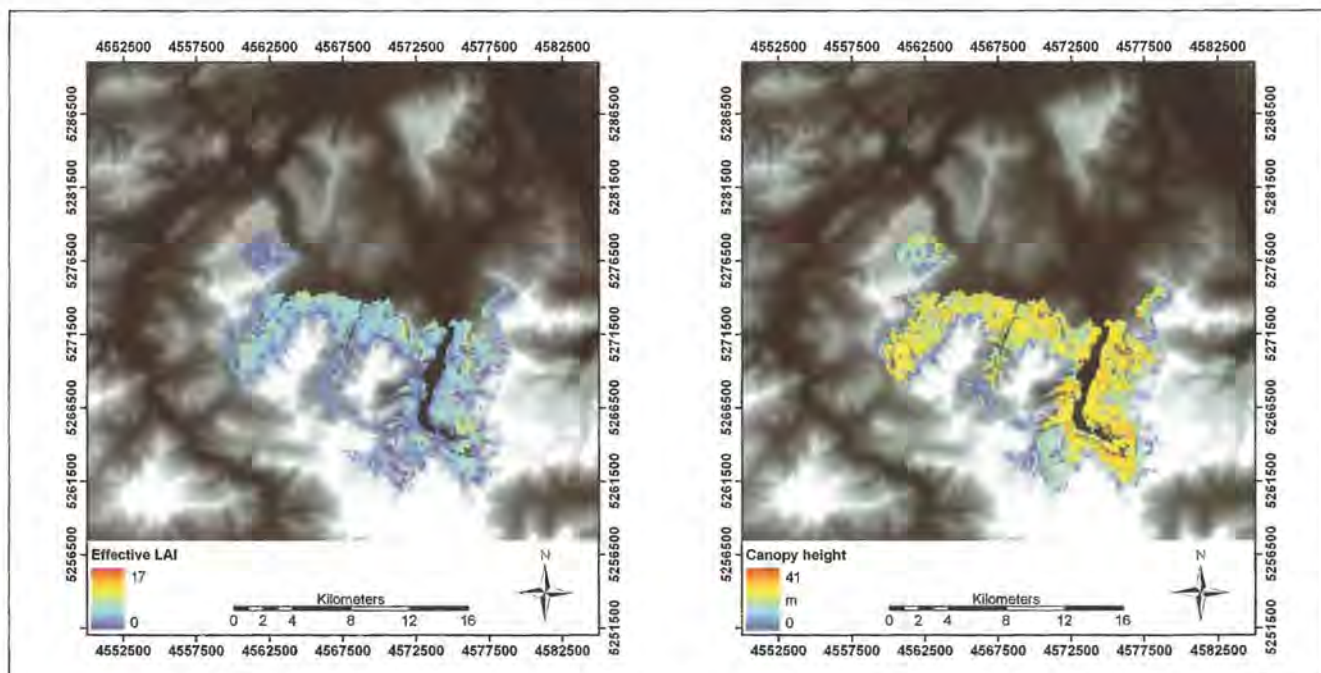


**Figure 3:** Effective winter leaf area index and canopy height (right) for the forest canopies within the National Park area.

computed fields and a modular interface to plug in existing point models. In the current version, the functionality of AMUNDSEN includes several interpolation routines for scattered meteorological measurements, rapid computation of topographic parameters from a digital elevation model, sophisticated simulation of short- and longwave radiative fluxes including consideration of shadows and cloudiness, parameterization of snow albedo, modelling of snow- or icemelt with either an energy balance model or an enhanced temperature index model considering radiation and albedo, modelling of forest snow processes and a built-in stochastic weather generator to produce synthetic future meteorological data for climate change scenario simulations. All generated fields are visualized dynamically during the simulation (figure 4). The functionality of the system including examples is further described in the following sections.

### 2.3.1 Interpolation of meteorological variables

For spatially distributed model applications, fields of temperature or any other meteorological variable must be provided in appropriate temporal resolution. In AMUNDSEN we apply the following procedure (STRASSER AND MAUSER 2001): first, a so called *gradient field* is

derived by linear regression of the meteorological observations with altitude; this regression is then applied for the DEM area. Then, the residuals (i.e., the differences between the measurements and the *gradient field* at the station locations) are spatially interpolated applying an inverse distance weighting (IDW) approach, resulting in the so called *residual field* representing the local deviations from the *gradient field*. The weights are the inverse cubic distances from a DEM pixel to the stations around. In a last step, gradient and residual field are added up. This algorithm is applied for each time step. It ensures that the station observations are reproduced, and it can be applied irrespective of whether a relation of the meteorological variable with altitude or local deviations exists. However, extrapolations beyond the station locations or out their range of altitudes should be interpreted with caution. As an example for the results of the spatial interpolation of the station recordings, figure 5 shows interpolated and cumulated (ground) precipitation for the National Park area (August 1, 1999 to July 31, 2000): Accordingly, liquid precipitation (rainfall) decreases with altitude, whereas solid precipitation (snowfall) increases with altitude. The canopy areas, visible as edges around the mountain massifs, are characterized by distinctly less solid precipitation due to wintery snow sublimation losses of snow from the trees, but more li-

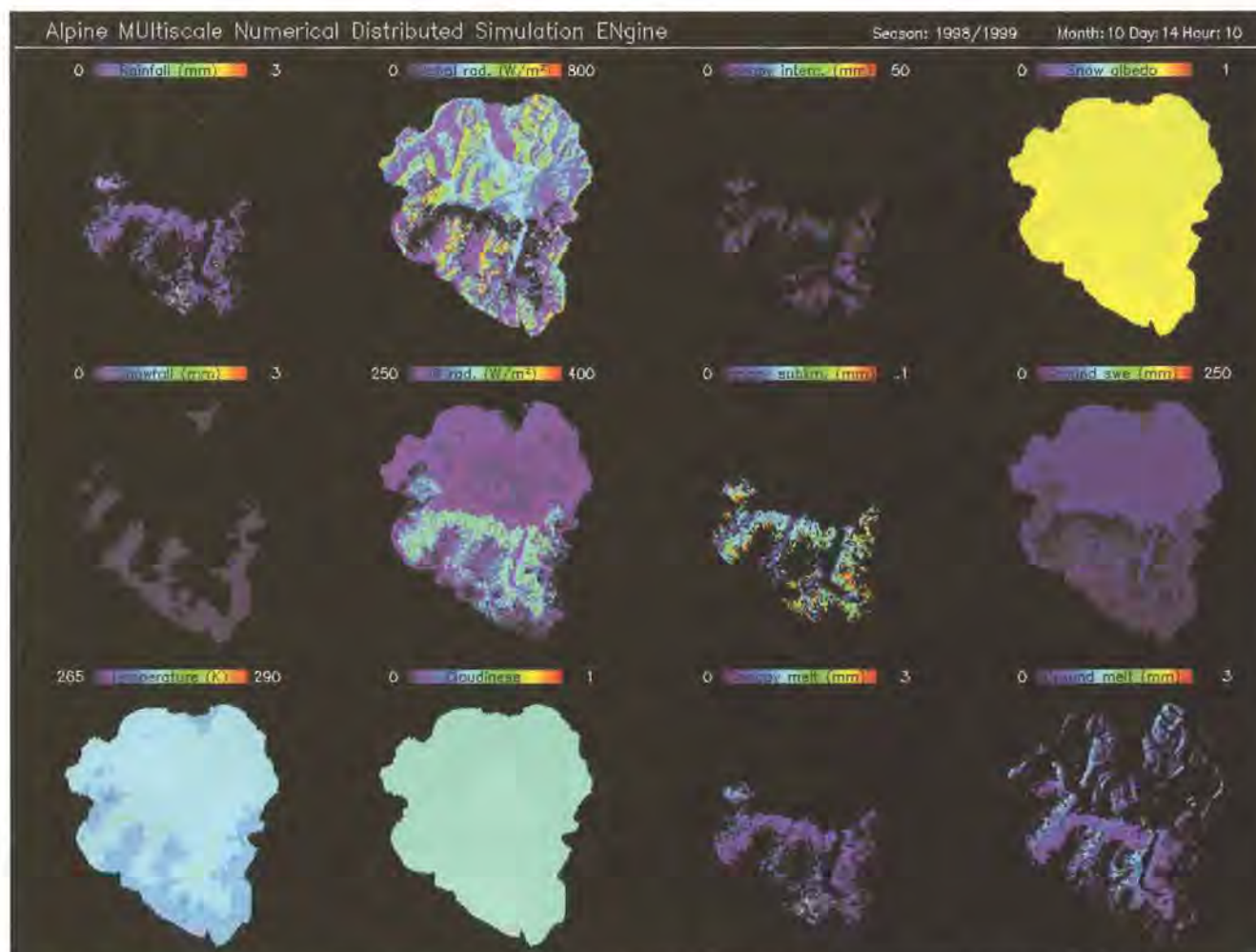
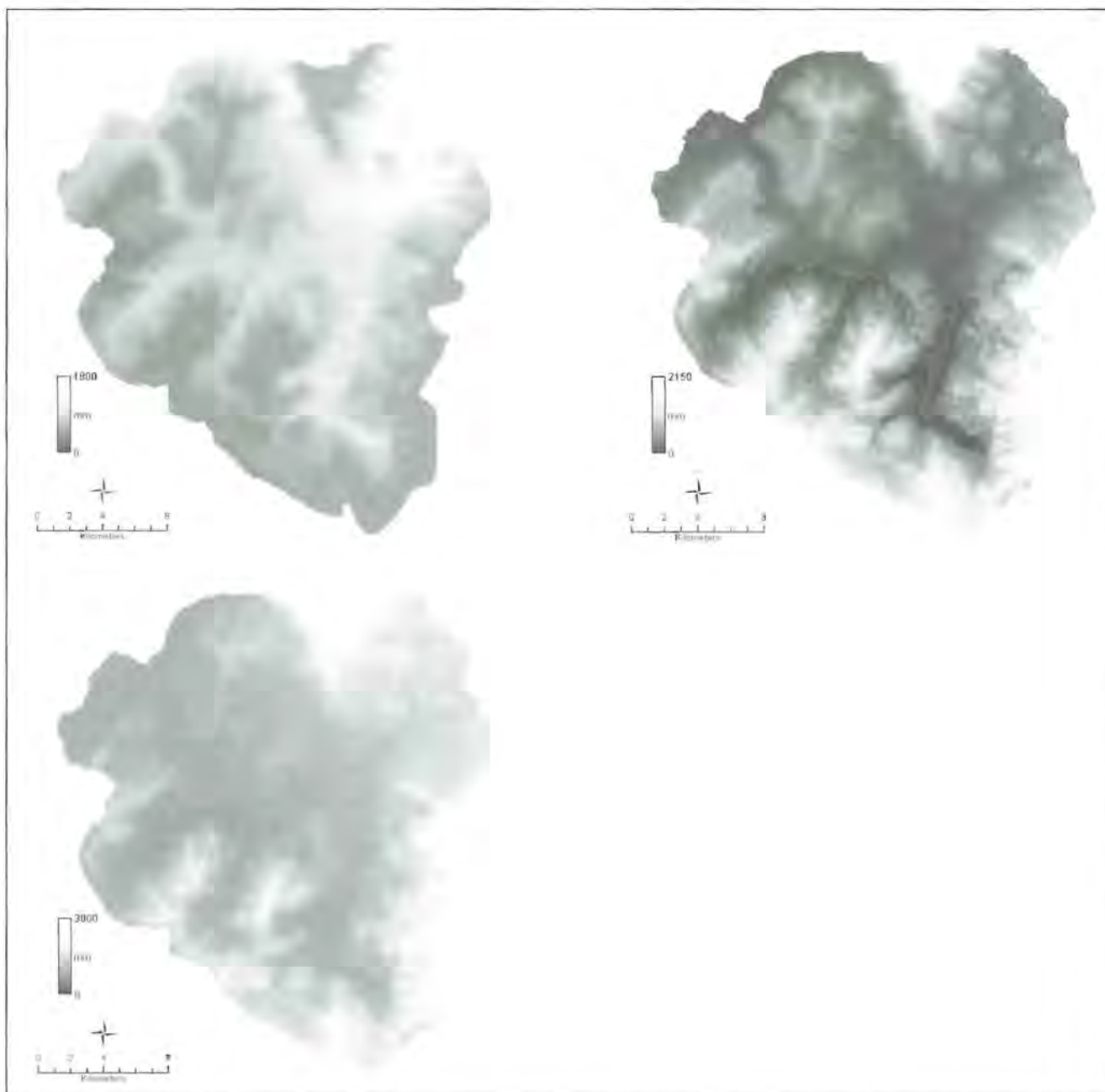


Figure 4: Visualization of computed fields during simulation in AMUNDSEN for the time step October 14, 1998, 10 am and the area of the Berchtesgaden National Park.



**Figure 5:** Liquid (top left) and solid (snowfall, top right) and total precipitation (left) for the National Park area, August 1, 1999 to July 31, 2000.

liquid precipitation due to the melt from the trees during winter. Maximum total precipitation is reached in the Untersberg region, the most prominent barrier for the prevailing wind direction which brings moist air to the Alps.

### 2.3.2 Simulation of radiative fluxes

On the ground, local differences in the shortwave radiative fluxes are caused by several elevation dependent atmospheric processes and the effect of topography: (1) loss due to Rayleigh and aerosol scattering and absorption by water vapour, ozone and other trace gases, (2) gain due to multiple reflections between the atmosphere and the ground and reflections from the surrounding ter-

rain, as well as loss due to obstruction of the horizon and (3) loss due to absorption and scattering by clouds. The effects of these processes which cannot be spatially distributed by simple interpolation are quantified by means of a parameterization scheme which derives all factors from local terrain characteristics as well as physical and empirical relations. It computes the effects of hills-hading, decrease of atmospheric transmittance due to the individual processes of scattering, and considers multiple reflections between the atmosphere and the ground as well as reflections from surrounding terrain. Direct and diffuse shortwave radiative fluxes for each grid cell are parameterized after a rigorous evaluation of the DEM of the area using efficient vectorial algebra algorithms, the principles of which are described in detail in CORRIPIO (2003).

Hillshading is computed by scanning the projection of cells onto a solar illumination plane perpendicular to the sun direction. By checking the projection of a grid cell over this plane, following the direction of the sun, it is determined whether a point is in the sun or in the shade of another cell. To increase computational efficiency of the algorithm, an array of cells is defined for every cell on the sun side of the grid border; the length of this array is given by the nearest intersection of a line along the vector opposite to the sun and the DEM boundaries.

The sky view factor is an important parameter for the computation of incoming diffuse and multiple scattered shortwave radiation, especially in areas of high albedo like snow covered mountains, and for the net balance of longwave radiation. Horizon angles are calculated using a more economical algorithm than a rigorous evaluation of all the angles subtended by every grid cell to each other (CORRIPIO 2003); Following IQBALS (1983) unit sphere method, the sky view factor is computed as the ratio of the projected surface of visible sky onto the projected surface of a sphere of unit radius (NUNEZ 1980). For the computation of the horizon zenith angles for selected azimuths a modification of CORRIPIOS (2003) shading algorithm is used. To save computation time, the sky view factors for all grid cells are stored in a separate file which is read in at the beginning of a simulation run.

For the estimation of the area fraction of the different surface types we apply a temperature index snowmelt model for melting conditions, considering simulated global radiation  $Q_{s\downarrow}$  and parameterized albedo  $\alpha$ ,  $M$  being the hourly melt rate in mm (PELLICCIOTTI et al. 2005):

$$M = tf \cdot T_o + af \cdot Q_{s\downarrow} \cdot (1 - \alpha) \quad (1)$$

$tf$  and  $af$  are empirical coefficients, called temperature and albedo factor, expressed in  $\text{mm} \cdot \text{h}^{-1} \cdot \text{°C}^{-1}$  and  $\text{m}^2 \cdot \text{mm} \cdot \text{h}^{-1} \cdot \text{W}^{-1}$ , respectively. Since simulations run continuously over the year, no initial snow water equivalent distribution is considered as model input; the few remaining glaciers in the area (Blauveis, Watzmannletscher and Eiskapelle) are small and not considered here.

Finally, the sum of the direct and diffuse radiative fluxes is corrected for the visible portion of the hemisphere by multiplying their sum with the sky view factor for each pixel. In a last step, direct reflections from the surrounding terrain are added by considering the shortwave radiation, the ground view factor and the fraction as well as albedo of the reflecting surfaces.

The presented solar radiation model is parametric and not truly physical. Nevertheless, it gives good estimates of the individual atmospheric transmittances (NIEMELÄ et al. 2001, STRASSER et al. 2004) and can be applied for any area if an appropriate DEM is available.

Longwave radiative fluxes are computed using the formula of GREUELL et al. (1997) considering cloudiness derived from recordings of global radiation which is also used to correct global radiation. Finally, incoming longwave radiation is composed of a fraction coming from the atmosphere, and one from the surrounding slopes. Thereby it is considered whether these slopes are snow covered or not.

### 2.3.3 Parameterization of albedo

The albedo of a snow cover depends on many factors: whether the surface is frozen or not, the amount of debris cover, water, and impurity content of snow; the main driving variable is the grain size. The reflectivity of snow is also dependent on wavelength, normally decreasing from the visible to the near infrared. Standard parameterizations for albedo employ the age of the snow surface as a surrogate for the processes which have an effect on it. We model the snow albedo  $\alpha$  using the ageing curve approach (ROHRER 1992, U.S. ARMY CORPS OF ENGINEERS 1956):

$$\alpha = a_{min} + a_{add} \cdot e^{-kn} \quad (2)$$

where  $k$  is a recession factor, depending on air temperature (see table 2) and therewith snow surface properties, and  $n$  the number of days since the last considerable snowfall which caused an increase of the snow albedo to its maximum value. This function integrates

**Table 2:** Parameter values used in the snow model in AMUNDSEN.

Parameter	Symbol	Value	Unit
Soil heat flux	$B$	2.0	$\text{W} \cdot \text{m}^2$
Minimum snow albedo	$a_{min}$	0.5	—
Maximum snow albedo	$(a_{min} + a_{add})$	0.9	—
Recession factor ( $T > 273.16 \text{ K}$ )	$k$	0.4	$\text{d}^{-1}$
Recession factor ( $T \leq 273.16 \text{ K}$ )	$\tilde{k}$	0.3	$\text{d}^{-1}$
Specific heat of snow	$c_{ss}$	$2.1 \cdot 10^3$	$\text{J} \cdot \text{kg}^{-1} \cdot \text{K}^{-1}$
Specific heat of water	$c_{sw}$	$4.18 \cdot 10^3$	$\text{J} \cdot \text{kg}^{-1} \cdot \text{K}^{-1}$
Melting heat of ice	$c_i$	$3.375 \cdot 10^5$	$\text{J} \cdot \text{kg}^{-1}$
Sublimation/resublimation heat of snow	$l_s$	$2.8355 \cdot 10^6$	$\text{J} \cdot \text{kg}^{-1}$
Emissivity of snow	$\varepsilon$	1.0	—
Hourly threshold snowfall for albedo reset		$0.5 \cdot 10^{-3}$	m
Threshold temperature for phase detection		273.16	K
Stefan-Boltzmann constant	$\sigma$	$5.67 \cdot 10^{-8}$	$\text{W} \cdot \text{m}^{-2} \cdot \text{K}^{-4}$

the evolution of the physical properties of the surface grain and has proven its reliability in many applications at various scales (e.g. STRASSER et al. 2004, STRASSER AND MAUSER 2001, SCHULLA 1997, PLÜSS AND MAZZONI 1994). With equation (2), albedo is simulated on an hourly basis, using the independent variables time and air temperature which correlate well with long term changes to the reflectance properties of the snow surface associated with metamorphism and the build up of light absorbing impurities. An hourly snowfall of more than 0.5 mm water equivalent is interpreted as significant, i.e. then albedo is reset to its maximum value of 0.9. A temperature of 1°C proved to be a robust threshold for the phase change between snow and rain (STRASSER 1998).

### 2.3.4 Snow-canopy interaction

A forest canopy can lead to both less snow water equivalent (swe) and shorter duration, or more swe and longer duration of the snow cover beneath the trees, depending on many factors such as stand properties, geographic location, size of clearings and their distribution and meteorological conditions (POMEROY et al. 1998, MARSH 1999, POMEROY et al. 2002). The latter vary distinctly from those in the open. Main phenomena affecting the climatic conditions inside a forest comprise: shadowing effect of the trees for solar radiation, longwave radiation of the trees, increase of humidity, reduction of temperature fluctuation amplitudes and reduction of wind speed. The albedo of the forest itself, usually between 0.1 and 0.3, changes considerably with the presence of snow under the trees. The moderation of the turbulent exchanges inside the canopy diminishes the sensible and latent heat fluxes, thus making the net radiation fluxes the principal energy sources for snowmelt. Here, we apply a scheme to (a) reduce solar radiation, (b) consider thermal emission of the trees, (c) reduce wind speed, (d) modify humidity and (e) moderate temperature for the snow surface beneath the canopy based on the approaches of DUROT (1999) and LISTON AND ELDER (2006). Required input parameters are effective LAI and tree height.

On the other hand, a certain amount of precipitation is kept back in the interception storage. From there, it can melt, fall down, or sublimate back into the atmosphere. This latter process leads to a reduction of precipitation which is accumulated in the ground snow pack.

We apply a snow interception model for forest canopies which has been developed on the basis of the approach developed by LISTON AND ELDER (2006). It considers interception, sublimation and melt unload of the snow falling onto the trees. Resulting unloaded mass is added to the precipitation reaching the ground beneath the trees (see figure 5). There, the energy balance is computed as described in 2.3.5, but with meteorological parameters modified for the canopy ground.

Validation of the snow interception model has been conducted by LISTON AND ELDER (2006) with MONTESI et al.'s (2004) observations from the USDA Fraser Experimental Forest near Fraser, Colorado, U.S.A. They conclude that

while for an individual simulation hour, the model result can misrepresent the measurement, where as for entire events the coupled atmosphere-biosphere system is adequately simulated.

### 2.3.5 Snow cover mass and energy balance

The snow cover module in AMUNDSEN is designed as a physically based model for the simulation of the energy balance, the water equivalent and the melt rate of a snow cover. For the simulation of the energy balance the short- and longwave radiation, the sensible and latent heat fluxes, the energy conducted by solid or liquid precipitation as well as condensation/sublimation and a constant soil heat flux are taken into account. The snow albedo is modelled using the above described function considering the age and the surface temperature of the snow pack. For each time step the following scheme is followed: first, it is distinguished between melting conditions (air temperature > 273.16 K) and no melt (air temperature ≤ 273.16 K). In the first case, the computations include: (a) calculation of the energy balance, (b) decision whether eventual precipitation is solid or liquid (if not measured), (c) calculation of the water mass and energy budget based on the hypothesis of no snowmelt at the current time step, (d) comparison of the total available energy with that sustained as snow by the total available mass of the snow pack at 273.16 K, (e) calculation of the snowmelt produced by the available excess energy and (f) update of the mass and energy budgets. In the other case (air temperature ≤ 273.16 K), an iterative procedure to adopt the snow surface temperature is applied. Parameters used in the snow model are given in table 2. Generally, the energy balance for a snow surface can be expressed in (in W · m<sup>-2</sup>) as:

$$Q + H + V + A + B = \Delta E \quad (3)$$

where  $Q$  is the radiation balance,  $H$  the sensible heat flux,  $V$  the latent heat flux,  $A$  the advective energy supplied by solid or liquid precipitation,  $B$  the soil heat flux and  $\Delta E$  the change of the internal energy status of the snow pack for the current time step. The radiation balance  $Q$  is composed of the net balances of short- and longwave radiation (fluxes towards the surface having a positive sign):

$$Q = Q_{s\downarrow} + Q_{s\uparrow} + Q_{l\downarrow} + Q_{l\uparrow} \quad (4)$$

The longwave emission  $Q_{l\uparrow}$  is calculated with an emissivity  $\varepsilon = 1.0$  and the Stefan-Boltzmann constant  $\sigma$ :

$$Q_{l\uparrow} = -\sigma \cdot \varepsilon \cdot T_s^4 \quad (5)$$

with  $T_s$  being the snow surface temperature. For physical descriptions of the turbulent fluxes detailed measurements of the snow surface properties are required. Therefore, in AMUNDSEN they are replaced by simple empirical descriptions which are valid for medium roughness and a wide range of wind speeds. In areas where the contribution of the turbulent fluxes to the energy ba-

lance of the snow pack is small, the such induced loss of accuracy is negligible. The sensible heat flux  $H$  in  $\text{W} \cdot \text{m}^{-2}$  is expressed as:

$$H = \alpha \cdot (T - T_s) \quad (6)$$

where  $T$  is the measured air temperature and  $\alpha$  the heat transfer index in  $\text{W} \cdot \text{m}^{-2} \cdot \text{K}^{-1}$ .  $\alpha$  is determined using a function which approximates various wind speed measurements over a snow surface (ESCHER-VETTER 1980):

$$\alpha = 5.7 \cdot \sqrt{W} \quad (7)$$

where  $W$  is the measured wind speed. The latent heat flux  $V$  in  $\text{W} \cdot \text{m}^{-2}$  is calculated using a formula as proposed by KUCHMENT AND GELFAN (1996), assuming adiabatic stratification in the boundary layer:

$$V = 32.82 \cdot (0.18 + 0.098 \cdot W) \cdot (e_1 - e_s) \quad (8)$$

where  $e_1$  is the water vapour partial pressure at measurement level and  $e_s$  the water vapour saturation pressure directly above the snow surface, with both water vapour pressures being calculated using the Magnus formula. The small mass changes  $\delta e$  (in mm) generated by sublimation or resublimation are simulated with

$$\delta e = \frac{V \cdot t}{l_s} \quad (9)$$

Where  $t$  is the model time step in seconds and  $l_s$  is the sublimation/resublimation heat of snow.

The advective energy  $A$  supplied by precipitation depends on its phase. If measured, both components of precipitation are considered in the model. If not measured, a threshold temperature is assumed for the distinction between snow and rain. The energy advected by precipitation  $P$  is calculated for rain in  $\text{W} \cdot \text{m}^{-2}$  with

$$A = P \cdot (c_i + c_{sw} \cdot (T - 273.16)) \quad (10)$$

and, accordingly, for snow:

$$A = P \cdot ((T - T_s) \cdot c_{ss}) \quad (11)$$

where  $c_i$  is the melting heat of ice,  $c_{ss}$  the specific heat of snow and  $c_{sw}$  the specific heat of water. In the first case (rainfall), precipitation is added to melt, in the second (snowfall) to the existing swe.

For the case of melting conditions (air temperature  $> 273.16 \text{ K}$ ), a tentative energy status of the snow pack is calculated with equations (3) to (11) since it does not yet account for the melt in the current time step. Therefore, the excess energy available for melt generation is calculated in the next step. The minimum energy status  $E_s$  required for the initialisation of the melting process in the snow pack is expressed as:

$$E_s = 273.16 \cdot c_{ss} \cdot Z \quad (12)$$

where  $Z$  is the snow water equivalent of the snow pack. This energy represents an isothermal state of the entire snow pack at  $273.16 \text{ K}$ , the snow cover is "ready for melt". If the energy status of the snow pack  $E$  extends

$E_s$ , the energy surplus is consumed for the melting process. Thereby the melt water equivalent  $M$  in mm is calculated as

$$M = \frac{E - E_s}{c_i} \quad (13)$$

After exhaustion of the energy surplus due to snow melt the energy status and water equivalent of the snow pack are updated for the current time step.

For the case of no melting condition (air temperature  $\leq 273.16 \text{ K}$ ), an iterative procedure to adopt the snow surface temperature is applied with re-calculation of the energy balance in each iteration. Thereby snow surface emission and turbulent fluxes are updated. This procedure makes sure that the snow surface temperature is properly adopted such that the energy balance is closed in each time step; for the case that (a) the procedure does not converge, (b) melt occurs due to extreme radiation (in high mountain or polar areas) or (c) the snow surface cools unrealistically too much a correction is applied.

Validation of the model has been conducted at many alpine sites (ZAPPA et al. 2003, ETCHEVERS et al. 2003, STRASSER et al. 2002, STRASSER 1998). At the catchment scale, results have been compared with satellite data derived snow cover (STRASSER AND MAUSER 2001, TASCHNER et al. 1998). An overview of the model's application and its validation is given in PRASCH et al. (2007).

### 2.3.6 Climate generator

The climate generator we propose here belongs to the type of stochastic, non-parametric nearest-neighbour resamplers (YOUNG 1994, BUIHAND AND BRASMA 2001, YATES et al. 2003), and is directly integrated into AMUNDSEN (STRASSER AND MAUSER 2006). It produces data with the same temporal resolution as the input data, i.e. as is required by the snow model, and does not alter the physical relations between the meteorological parameters. Basic assumption of the method is that a climate storyline can be divided into time periods which are characterized by a certain temperature and precipitation, and these two variables are not independent from each other:

$$\bar{P} = f(\bar{T}) \quad (14)$$

with  $\bar{P}$  being the mean precipitation of a certain time period,  $\bar{T}$  its mean temperature and  $f$  their functional dependency. In our application the periods are weeks.

In a first step, a typical annual course of the meteorological variables is constructed by computing mean temperature and total precipitation for the periods using all years of the measured historical dataset. The result is a mean annual climate course for the region in which the meteorological stations are located, built up of 52 weeks with specific  $T/P$  relations.

This mean annual climate course is used to construct the future data period by period: first, the according temperature is modified with a random variation and the given trend. Then a corresponding precipitation is derived, considering the  $T/P$  relation and again a random

**Table 3:** Features of the simulated climate in 100 years and the IPCC B2 temperature trend shift of 2.7 K

Variable	Annual	Summer only	Winter only
Temperature	+2.7 K	+2.7 K	+2.7 K
Precipitation	-551 mm	-283 mm	-269 mm
Global radiation	+16.1 W · m <sup>-2</sup>	+20.0 W · m <sup>-2</sup>	+11.8 W · m <sup>-2</sup>
Humidity	-5.8 %	-4.9 %	-6.7 %
Wind speed	+0 m · s <sup>-1</sup>	-0.2 m · s <sup>-1</sup>	+0.1 m · s <sup>-1</sup>

variation. As a result, the week to construct is defined by a certain temperature and precipitation. In a last step, the period from the historical periods with the most similar  $T$  and  $P$  is selected applying the nearest neighbour criterion. Measured data of this period is then added to the future time series to be constructed. This procedure is repeated for all 52 weeks of the year, and all years of the future time series. By modifying the random variation, a change in variability can be simulated. However, no other extremes can be reproduced than have been recorded in the historical data. To allow for more flexibility in the construction of the periods, the basic population from which the measured week is chosen (= the number of years for which observational data is available) can be synthetically extended by allowing for one or more periods before and after the one to be constructed. The principles of the climate generator are illustrated in figure 6.

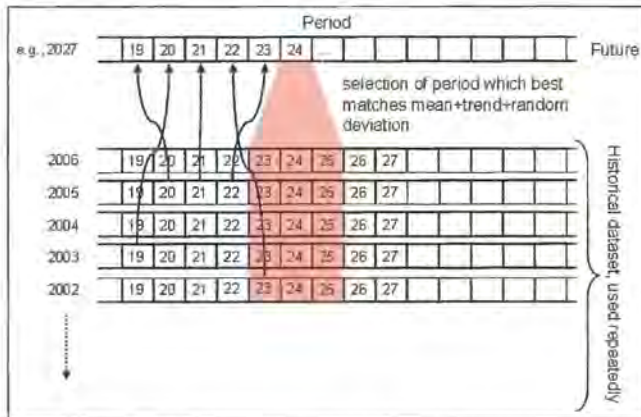


**Figure 6:** Principle of selecting periods of measured data to build up a future data time series with a certain temperature trend and random deviation.

The described procedure has a number of specific features. The advantages include its very efficient applicability: computation for 100 years of future climate for the 11 stations in the region only takes several minutes on a standard PC. The meteorological input into the climate generator is physically consistent, since all measured, and in the validated range for the hydrological modelling. A synthetic baseline scenario can easily be constructed by assuming a Null trend of temperature. Finally, the spatial resolution of the data is preserved; it is exactly valid for the locations of the stations. However, one significant drawback of the method is that auto-correlation between the single periods is lost, and the con-

sideration of changes in the variability of the meteorological variables is limited; together with the fact that changes in extreme values are not considered it becomes clear that the data resulting from the method cannot be used for modelling variations of probability and extent of hydrological extremes.

Consecutive application of the climate generator produces different climates due to the random deviation which is considered.

### 3. Results and discussion

#### 3.1 Snow-canopy interaction

In this section, results of the modelling of the canopy-snow interaction and the effect on the seasonal course of the ground swe, as well as the water balance, are discussed. We simulated the seasonal evolution of the snow cover for the winters 1998/1999 to 2004/2005. For most canopy stands in the National Park area, annual snow sublimation amounts to 100 to 150 mm, approximately (figure 7). Highest sublimation losses can be expected for the forest stands with the largest canopy height/ $LAI$  values, which is a location in the Königsbach valley at 1200 m a.s.l. (28 m high firs with an effective  $LAI$  of 17.15). There, total annual snow sublimation is more than 300 mm in 1999/2000, a very snow-rich winter with frequent snowfall events. Sublimation of snow strongly varied between the seasons: in 2000/2001, a winter with only a shallow snow cover, the maximum total sublimation of snow from the canopy (in the Königsbach valley) not even amounts to 200 mm. However, this still represents a remarkable amount of precipitation which is removed from the local water cycle and redirected back into the atmosphere: if one assumes a mean sublimation loss of 100 mm and a forest coverage of 50 % in the area of the National Park, these losses add up to a seasonal total of 10 Mio. m<sup>3</sup> water! Without the forest, this amount would be stored in the ground snow cover and released into runoff when melting.

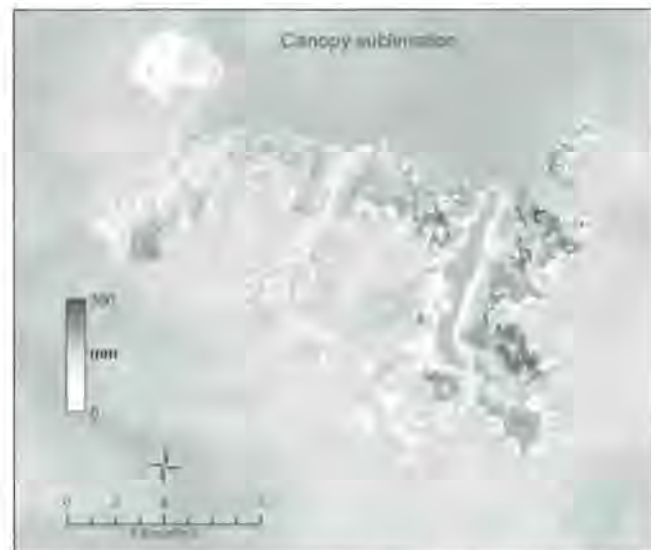


**Figure 7:** Modelled total wintery snow sublimation from the canopies in the Berchtesgaden National Park (1999/2000).

### 3.2 Snow cover evolution

In the following section, we first discuss the validation of the snow model by comparison with measured swe at the location of a meteorological station (3.2.1). Then we apply it for the historical seasons 1998 to 2005 for an alpine site at 1776 m a.s.l. (Untersberg); and we compare the results with those found for a typical valley bottom site at 617 m a.s.l. (Schönau) (3.2.2); the historical seasons serve as a reference for the future climate simulations for the seasons 2093 to 2100 which were produced by application of the climate generator. We discuss the consequences of a temperature change of 2.7 K until 2100 (IPCC 2001) on the course of the seasonal evolution of the snow cover and runoff generation (3.2.2). For all simulations, we applied the model with a 50 m resolution digital elevation model and with an hourly time step.

#### 3.2.1 Validation

To validate the model, the snow model was applied at the location of the Kühroint station (1407 m a.s.l.). There, manually recorded swe pit measurements are available, and recordings from automatic sensors since December 2004. The comparison (figure 8, right) between modelled and measured swe shows that the model results are reasonable if locally recorded data is used (mean deviation 31 mm). To test how model accuracy changes if interpolated input data is used we made an experiment and compared simulated swe with the measurements for 1999/2000 (before the sensors were installed).

In figure 8 (left) one can see that model accuracy is still in a reasonable range, and the duration of the snow period is well captured (mean deviation 117 mm). However, in other winter seasons with less snow accumulation and intermediate melting periods the model results can also be less reliable (not shown here).

#### 3.2.2 Historical seasons

In this section, we discuss the snow cover evolution for the seven available historical seasons for the locations Untersberg (1776 m a.s.l.) and Schönau (617 m a.s.l.). Generally, both duration as well as maximum water equivalent vary largely over the seven winter seasons (figure 9, top left for the Untersberg). In April 2000, the simulated snow water equivalent (almost 2000 mm) is more than four times as much as in April 2003 (450 mm). This variation between winters with high and long lasting snow cover and winters with very shallow and temporally limited snow cover is typical for temperate mountain sites in the mid latitudes. First snowfalls can occur as early as September (1998, 2001), but later melting can lead to complete disappearance of snow in December (2000, 2003). In the snow-rich seasons the ground is covered from November until mid of June (1998/1999, 1999/2000), e.g. more than half of the year. In contrast, in 2002/2003 snow cover duration lasts only from December until early May. Nevertheless, all winters of the reference seasons are characterized with a distinct and continuous snow coverage from January, with a maximum swe towards the end of the accumulation phase in April, a typical feature of the seasonal Alpine snow cover. In figure 9 (bottom left), the mean course of the snow cover evolution for the historical seasons 1998 to 2005 is shown.

At the valley location in Schönau (617 m a.s.l.), both swe of the snow cover is much less and its duration shorter. The mean of the seven historical winter seasons 1998 to 2005 represents a typical course (figure 9 top right). The maximum appears much earlier (January), and the melting season ends by the beginning of April.

#### 3.2.3 Future scenarios

We applied the climate generator as described in 2.3.6 and produced a time series of hourly temperature, pre-

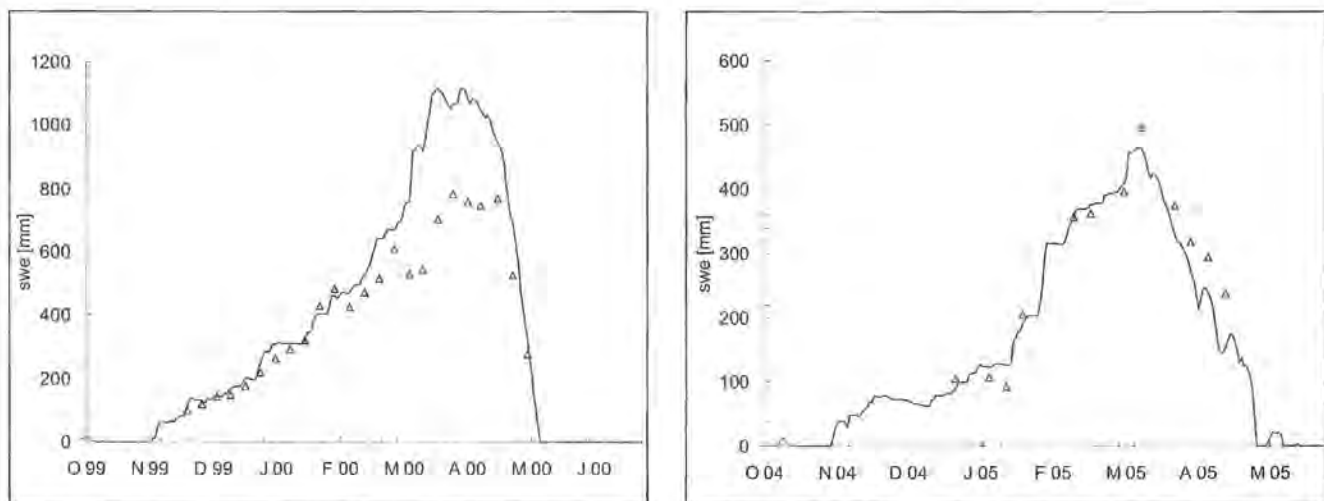


**Figure 8:** Validation (triangles) of the snow model simulations (solid line): In 1999 to 2000 (left), no meteorological measurements have been recorded at the Kühroint location (1407 m a.s.l.); the model is driven with interpolated fields of the meteorological parameters; mean deviation = 117 mm. In 2004 (right), station recordings started on December 26, and the model is driven with measurements; mean deviation = 31 mm.

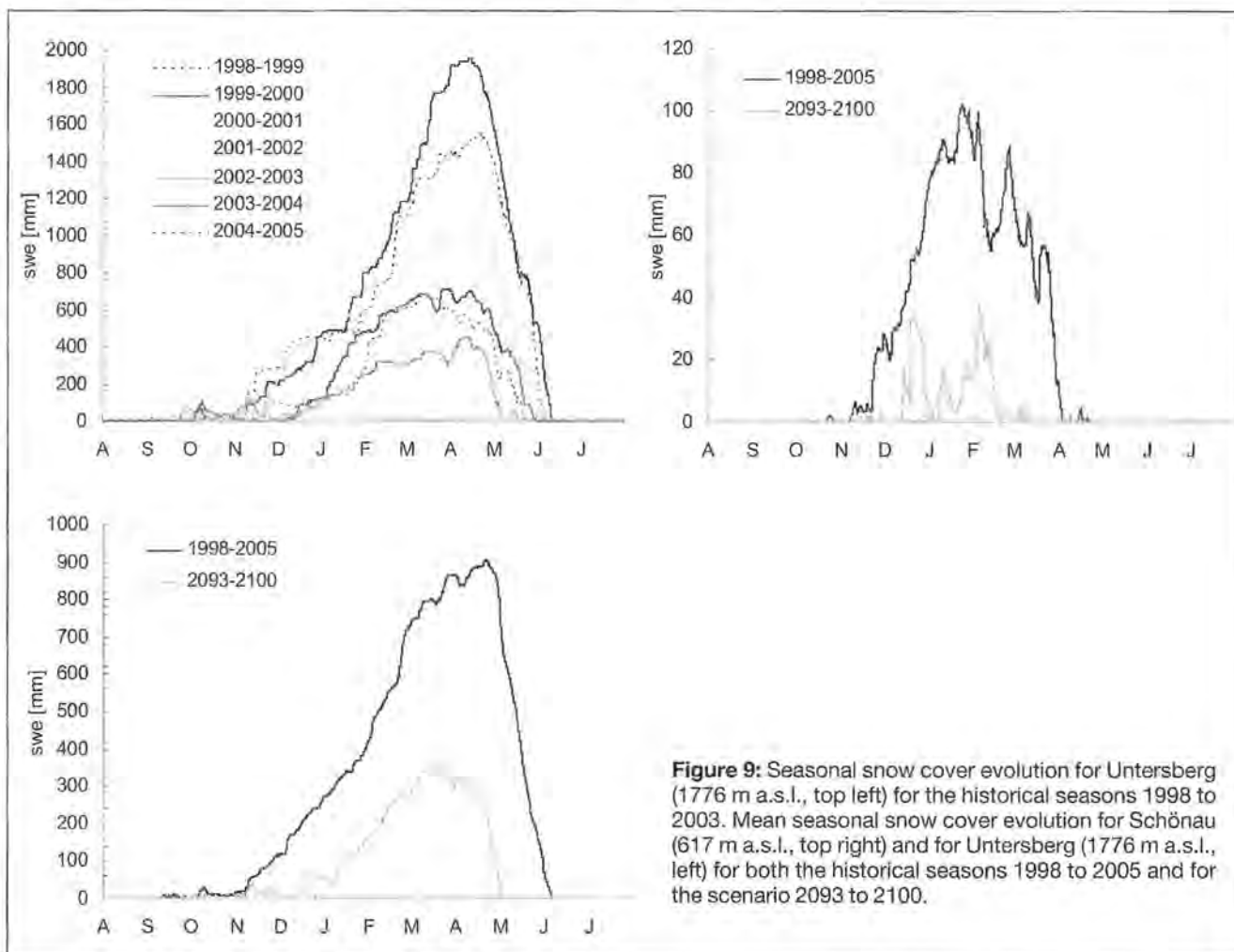


**Figure 9:** Seasonal snow cover evolution for Untersberg (1776 m a.s.l., top left) for the historical seasons 1998 to 2003. Mean seasonal snow cover evolution for Schönau (617 m a.s.l., top right) and for Untersberg (1776 m a.s.l., left) for both the historical seasons 1998 to 2005 and for the scenario 2093 to 2100.

precipitation, global radiation, humidity and wind speed for 2005 to 2100 (table 3). The simulated temperature increase for this scenario results in the 2.7 K as predicted by the IPCC B2 scenario. Since interseasonal variability of the snow cover is significant in our area, we compare the mean of seven years (2093 to 2100) with the historical evolution. The effects on the simulated mean annual snow cover on Untersberg are significant (figure 9, bottom left). A first shallow, but continuous snow cover exists from November, but it almost disappears again in December. Significant accumulation starts in January. Maximum swe is in March, and below 400 mm. Still, continuous snow coverage exists until end of April. In general, a typical alpine snow cover with accumulation and ablation exists on Untersberg even in this moderate future scenario, but both its swe and temporal duration is reduced.

For Schönau, in a flat and open valley situation, mean snow coverage in 100 years is not even continuous anymore, but a sequence of snow-covered and snow-free episodes without a single maximum of swe for the winter period. Compared to the mountain site, reduction of swe is more pronounced, since climatic conditions are more often closer to melting.

What are the consequences in the snowmelt-driven runoff generation dynamics? Not much changes in the valley until end of December. During January, more runoff

will be generated due to the intermediate melting events – despite reduced precipitation. The most remarkable effect, however, is the earlier end of snowmelt runoff due to disappearance of the snow cover: in 100 years, the valleys will be snow free one month earlier than today. On the mountain, snowmelt generated runoff will be reduced until end of November (but precipitation will fall as rain), but from December it will be more than today, with comparably little change in the second half of the scenario period. Then, melt efficiency is stronger, but there is less snow to melt. Main difference is the end of the snowmelt runoff due to disappearance of the snow cover: on the mountain, snowmelt will also stop one month earlier than today.

#### 4. Conclusions

We applied a physically based snow cover mass and energy balance model including effects of canopy interception for the Berchtesgaden National Park area. Simulated sublimation losses of snow from the trees into the atmosphere vary from season to season but represent a significant amount of water which is not stored as snow on the ground (and later released as runoff during snowmelt) but directly redirected into the atmosphere. This effect is most effective in stands which are charac-

terized by very high trees with large LAI values, and seasons with frequent snowfall events. The order of magnitude of these sublimation losses will have to be validated with water balance simulations.

After validation at the location of a meteorological station we apply the snow model using a synthetic time series of future meteorological input data for the IPCC B2 temperature increase of 2.7 K until 2100. The future meteorological data not only represents the preset temperature trend, but also a decrease in precipitation and humidity, and an increase in global radiation (wind speed does not change). Modelled snow cover dynamics are compared for both a mountain and a valley site which are representative for the area.

Generally we draw the conclusion that during the next 100 years the mountain snow cover *swe* will be reduced by more than its half, and snow cover duration will be shorter by about one month at the start in autumn, and again one month in the end in spring. The effect will be stronger in valley locations than further up in the mountains. In 100 years a typical winter snow period will last only from January to April, and is disrupted by snow-free episodes in the valleys. These conclusions apply for the climatic conditions as in the Berchtesgaden National Park area, and assuming IPCC B2 conditions.

The consequences of this future development are manifold, from hydrological, ecological, economical and other perspectives. Winter runoff will increase, while the available water resources decrease in summer as a result of the smaller building-up of the snow pack, having direct consequences for the storage and release mechanisms of hydropower plants and in-stream hydraulic plants. Especially sensitive to changes in climate are Alpine and pre-Alpine regions due to their heterogeneous runoff generation, and processes like accumulation and melt of snow. The changes in hydrology to be expected due to climate change, and their effect on land and water resources design and management practices are topic of current research (e.g., BRONSTERT et al. 2002, MENZEL AND BÜRGER 2002, MIDDLEKOOP et al. 2001). Hydropower generation, use of river water for cooling in power plants and irrigation practices will most likely have to adopt.

The habitat of many plants and animals depend on climate parameters: changing temperature, precipitation or radiation will lead to migration and extinction of species, threatening biodiversity in high alpine areas. Vegetation zones will geographically shift due to change of ecological factors, the composition of the mixed mountain forests will alter, and the carbon cycle change.

From an economical point of view, recreational activities are deeply rooted in the cultural identity of the Alpine region, and much of winter tourism focuses on snow-dependent Alpine and cross-country skiing. Even now, snow conditions have already been deteriorating as the result of higher winter temperatures, and the number of days with sufficient snow for cross-country and Alpine skiing is declining. Changes are also expected for the current winter traffic patterns – some ski resorts might lose their profitability in certain periods, and others

might benefit from their higher altitude and attract even more guests. Long-term survival of ski resorts can be assumed if at least 70 % of the ski seasons (December 1 until April 15) have at least 100 days with good snow condition, i.e. at least 30 to 50 cm of snow depth (BÜRKI et al. 2003). In the Swiss Alps, an upward-shift of approximately 500 m for the long-term survival of ski resorts (according to snow conditions) has been determined for a variety of IPCC scenarios with a 100 year horizon (VERBUNT AND GURTZ 2004). The retreat of the Alpine glaciers also effects mountain hydrology considerably, and can increase the risk of floods and of natural hazards due to thawing of permafrost, loss of slope stability and lake outburst events.

This work is part of an ongoing research in the framework of the GLOWA-Danube project which addresses the effects of global change on the water cycle in the upper Danube catchment, in which the Berchtesgaden National Park area represents a test site for model development and validation (<http://www.glowa-danube.de/>). Further snow-related research in this project will therefore include the issues snow-vegetation interaction (see also <http://users.aber.ac.uk/rie/snowmip2.html>), wind-induced snow transport, avalanches, and the interaction between the natural resources in ski resorts and vehicular traffic flow (see related papers in this issue). The changing climate makes these research efforts a challenge.

## Acknowledgements

We are thankful to all who provided their help and assistance for writing the manuscript of this paper, in particular Volkmar Konnert and Michael Vogel from the National Park authority (Berchtesgaden) for data processing and subsidizing our activities. Hugo Vogt (Inzell) provided validation data and manifold advices. We also acknowledge the contributions of the team of Park rangers for their technical support for the field campaigns as well as valuable expertise for the field work. We profited from fruitful discussions and collaboration with Markus Weber (Munich) regarding the modelling of the snow processes. Stefanie Mayer (Munich) processed the meteorological data; these were generously supplied by the Administration of Salzburg (Untersberg), the Administration Union of the Berchtesgaden-Königssee region (Schönau) and the Bavarian Avalanche Warning Center of the State Office for Environment in Munich (Jenner, Reiter Alm, Kühroint and Funtenseetauern). Michael Warscher (Munich) set up the database for automatically collecting and distributing the meteorological records. Matthias Bernhardt (Munich) helped in the field and contributed many ideas in our discussions. Monika Prasch (Munich) read and improved the manuscript of this paper. Two anonymous reviewers who are authors of other contributions in this volume provided valuable improvements for the manuscript of this paper. The grants with which this work was facilitated were provided by the GLOWA-Danube project (<http://www.glowa-danube.de/>).

## References

- BARNETT, T.B., ADAM, J.C. AND LETTENMAIER, D.P. (2005): Potential impacts of a warming climate on water availability in snow-dominated regions. In: *Nature*, Vol. 438/17, doi:10.1038/nature04141, 303-309.
- BRONSTERT, A., NIEHOFF, D. AND BÜRGER, G. (2002): Effects of climate and land-use change on storm runoff generation: present knowledge and modelling capabilities. In: *Hydrol. Process.*, 16, 509-529.
- BÜRKI, R., ELSASSER, H. AND ABEGG, B. (2003): Climate change – Impacts on Tourism Industry in Mountain Areas. 1st Conference on Climate Change and Tourism. Djerba, April 2003.
- BUISHAND, T.A. AND BRANDSMA, T. (2001): Multisite simulation of daily precipitation and temperature in the Rhine Basin by nearest-neighbour resampling. In: *Water Resour. Res.*, 37 (11), 2761-2776.
- CORRIPIO, J. (2003): Vectorial algebra algorithms for calculating terrain parameters from DEMs and solar radiation modelling in mountainous terrain. In: *Int. J. Geogr. Inf. Sci.*, 17(1), 1-23.
- DUROT, K. (1999): Modélisation hydrologique distribuée du bassin versant nivo-pluvial de Sarennes. Validation des données d'entrée et développement d'un module de fonte nivale sous forêt. PhD thesis, LTHE, Grenoble.
- ESCHER, VETTER, H. (1980): Der Strahlungshaushalt des Vergnügertourismus als Basis der Energiehaushaltsberechnung zur Bestimmung der Schmelzwasserproduktion eines Alpengletschers. *Met. Inst. Wiss. Mitt.*, Nr. 39, 115 p. Münchner Universitäts-Schriften, Fachbereich Physik, Universität München.
- ETCHEVERS, P., MARTIN, E., BROWN, R., FIERZ, C., LEJEUNE, Y., BAZILE, E., BOONE, A., DAI, Y.-J., ESSERY, R., FERNANDEZ, A., GUSEV, Y., JORDAN, R., KOREN, V., KOWALCZYK, E., NASONOVA, N.O., PYLES, R.D., SCHLOSSER, A., SHMAKIN, A.B., SMIRNOVA, T.G., STRASSER, U., VERSEGHY, D., YAMAZAKI, T. AND YANG Z.-L. (2004): Validation of the surface energy budget simulated by several snow models (SnowMIP project). Papers from the International Symposium on Snow and Avalanches, June 2003, Davos, Switzerland. In: *Ann. Glaciol.*, Vol. 38, 150-158.
- GREUELL, W., KNAP, W. AND SMEETS, P. (1997): Elevational changes in meteorological variables along a midlatitude glacier during summer. In: *J. Geophys. Res.*, 102(D22), 25941-25954.
- HAMMEL, K. AND KENNEL, M. (2001): Charakterisierung und Analyse der Wasserverfügbarkeit und des Wasserhaushaltes von Waldstandorten in Bayern mit dem Simulationsmodell BROOK90. *Forstliche Forschungsberichte München* 185, 148 p.
- IPCC (2001): *Climate Change 2001: The Scientific Basis* (eds Houghtoun, J.T. et al.). The Intergovernmental Panel on Climate Change, Cambridge Univ. Press, Cambridge, UK.
- IQBAL, M. (1983): *An introduction to solar radiation*. Academic Press, London, 390 p.
- KLEMES, V. (1990): *Hydrology of Mountainous Areas*. IAHS, No. 190, 29-43.
- KONNERT, V. (2004): Standortkarte Nationalpark Berchtesgaden. *Forschungsbericht 49*, Nationalpark Berchtesgaden.
- KONNERT, V. (2006): pers. comm.
- KUCHMENTS, L.S. AND GELFAN, A.N. (1996): The determination of the snowmelt rate and the meltwater outflow from a snowpack for modelling river runoff generation. In: *J. Hydrol.*, 179, 23-36.
- LISTON, G.E. AND ELDER, K. (2006): A Distributed Snow-Evolution Modeling System (SnowModel). In: *J. Hydrometeorol.*, Vol. 7, No. 2, 217-234.
- MARSH, P. (1999): Snowcover formation and melt: recent advances and future prospects. In: *Hydrol. Process.*, 13, 2117-2134.
- MENZEL, L. AND BÜRGER, G. (2002): Climate change scenarios and runoff response in the Mulde catchment (Southern Elbe, Germany). In: *J. Hydrol.*, 267, 53-64.
- MIDDLEKOOP, H., DAAMEN, K., GELLENS, D., GRABS, W., KWADIJK, J.C.J., LANG, H., PARMET, B.W. A.H., SCHÄDLER, B., SCHULLA, J. AND WILKE, K. (2001): Impact of climate change on hydrological regimes and water resources management in the Rhine basin. In: *Clim. Change*, 62, 105-128.
- MONTESI, J., ELDER, K., SCHMIDT, R.A. AND DAVIS, R.E. (2004): Sublimation of intercepted snow within a subalpine forest canopy at two elevations. In: *J. Hydrometeorol.*, 5, 763-773.
- MOUNTAIN AGENDA (1998): *Mountains of the World: Water Towers for the 21st Century*. 32 p, Paul Haupt AG, Bern (Switzerland).
- NIEMELÄ, S., RÄISÄNEN, P. AND SAVIJÄRVI, H. (2001): Comparison of surface radiative flux parameterizations. Part II: Shortwave radiation. In: *Atmos. Res.*, 58, 141-154.
- NUNEZ, M. (1980): The calculation of solar and net radiation in mountainous terrain (Risdon, Tasmania). In: *J. Biogeogr.*, 7(2), 173-186.
- PELLICCIOTTI, F., BROCK, B., STRASSER, U., BURLANDO, P., FUNK, M. AND CORRIPIO, J. (2005): An enhanced temperature-index glacier melt model including shortwave radiation balance: development and testing for Haut Glacier d'Arolla, Switzerland. In: *J. Glaciol.*, V. 51, Nr. 175, 573-587.
- PLÜSS, C. AND MAZZONI, R. (1994): The Role of Turbulent Heat Fluxes in Energy Balance of High Alpine Snow Cover. In: *Nordic Hydrol.*, 25, 25-28.
- POMEROY, J.W., GRAY, D.M., HEDSTROM, N. AND JANOWICZ, J.R. (2002): Prediction of seasonal snow accumulation in cold climate forests. In: *Hydrol. Process.* 16, 3543-3558.
- POMEROY, J.W., GRAY, D.M., SHOOK, K.R., TOTH, B., ESSERY, R.L.H., PIETRONIERO, A. AND HEDSTROM, N. (1998): An evaluation of snow accumulation and ablation for land surface modelling. In: *Hydrol. Process.* 12, 2339-2367.
- PRASCH, M., STRASSER, U. AND MAUSER, W. (2007): Application of a physically based model for the simulation of accumulation and ablation of snow (ESCIMO). In: *Research reports, National Park Berchtesgaden* (this issue).
- ROHRER, M.B. (1992): Die Schneedecke im Schweizer Alpenraum und ihre Modellierung. *Zuer. Geogr. Schriften*, H. 49, 178 p, Zürich.
- SCHULLA, J. (1997): Hydrologische Modellierung von Flussgebieten zur Abschätzung der Folgen von Klimaänderungen. *Zürcher Geographische Schriften*, H. 69, 161 S., Zürich.

- STRASSER, U. AND MAUSER, W. (2006): Using a stochastic climate generator for simulating global warming effects on the water resources in a mountain basin. In: Geophysical Research Abstracts, abstracts of the European Geosciences Union General Assembly 2006, Vienna, Austria.
- STRASSER, U. AND MAUSER, W. (2001): Modelling the Spatial and Temporal Variations of the Water Balance for the Weser Catchment 1965-1994. In: *J. Hydrol.*, Vol. 254/1-4, 199-214.
- STRASSER, U., CORRIPIO, J., BROCK, B., PELLICCIOTTI, F., BURLANDO, P. AND FUNK, M. (2004): Spatial and Temporal Variability of Meteorological Variables at Haut Glacier d'Arolla (Switzerland) During the Ablation Season 2001: Measurements and Simulations. In: *J. Geophys. Res.*, Vol. 109 (3), doi:10.1029/2003JD003973.
- STRASSER, U., ETCHEVERS, P. AND LEJEUNE, Y. (2002): Intercomparison of two Snow Models with Different Complexity Using Data from an Alpine Site. In: *Nordic Hydrol.*, 33 (1), 15-26.
- STRASSER, U. (1998): Regionalisierung des Wasserkreislaufs mit einem SVAT-Modell am Beispiel des Weser-Einzugsgebiets. Münchener Geographische Abhandlungen, Reihe B, Band 28, 146 p, ISBN 3 925 308 88 1.
- TASCHNER, S., STRASSER, U. AND MAUSER, W. (1998): Modelling the Spatial Snow Water Equivalent Using NOAA-AVHRR Data for Mesoscale Catchments. In: SPIE Proc. Series, Proceedings of the EUROPTO 1998 Conference, Barcelona.
- U.S. ARMY CORPS OF ENGINEERS (1956): Snow Hydrology, U.S. Army Corps of Engineers, North Pacific Division, Portland, Oregon, USA, 437 p.
- VERBUNT, M. AND GURTZ, J. (2004): The use of hydrological models for socio-economic decisions in view of climate change. In: HERRMANN, A. AND SCHRÖDER, U. (eds.): Studies in Mountain Hydrology, IHB/HWRP-reports, H 2, Koblenz.
- VIVIROLI, D., WEINGARTNER, R. AND MESSERLI, B. (2003): Assessing the hydrological significance of the world's mountains. In: *Mt. Res. Dev.*, 23, 32-40.
- WINKLER, D. (2005): Der Blaueisgletscher in Not. Berchtesgadener Heimatkalender 2006, 45-48.
- YATES, D., GANGOPADHAY, S., RAJAGOPALAN, B. AND STRZEPEK, K. (2003): A technique for generating regional climate scenarios using a nearest neighbour algorithm. In: *Water Resour. Res.*, 39 (7), SWC 7-1 - 7-14.
- YOUNG, K.C. (1994): A multivariate chain model for simulating climatic parameters with daily data. In: *J. Appl. Meteor.*, 33, 661-671.
- ZAPPA, M., POS. F., STRASSER, U., WARMERDAM, P. AND GURTZ, J. (2003): Seasonal water balance of an Alpine catchment as evaluated by different methods for spatially distributed snowmelt modelling. In: *Nordic Hydrol.*, 34 (3), 179-202.
- ZIERL, B. AND BUGMANN, H. (2005): Global change impacts on hydrological processes in Alpine catchments. In: *Water Resour. Res.*, Vol. 41, W02028, doi:10.1029/2004WR003447.

**Internet links (last access: August 5, 2007)**

Berchtesgaden National Park:  
<http://www.nationalpark-berchtesgaden.de/>  
 GLOWA-Danube: <http://www.glowa-danube.de/>  
 SnowMIP2: <http://users.aber.ac.uk/rie/snowmip2.html>

## 16 Climate change and the competition among ski areas for day tourists

MONIKA TEPFENHART, WOLFRAM MAUSER  
AND FLORIAN SIEBEL

Department of Geography, Ludwig-Maximilians  
University (LMU), Luisenstr. 37, D-80333 Munich,  
Germany

### Abstract

We analyse the competition dynamics of ski resorts when exposed to climate change. To this aim, we propose a model for day tourism which takes into account the displacement of the level of the snow-reliability, the attractiveness due to the existing infrastructure and the travel times between the places of residence of day tourists and the ski areas. We apply our model to simulate the competition dynamics of ski resorts in the Bavarian Alps and Tyrol. Whereas in the long run only the ski resorts located high enough are expected to survive, ski resorts at medium altitudes may also profit in the nearer future due to a redistribution of the day tourists. Our results show that it is important to work with realistic travel times.

### 1. Introduction

Climate change is expected to play a major role in the adaptation process of ski resorts. There are several studies from different countries (e.g. BREILING et al. 1997, ELSASSER AND BÜRKI 2002, KÖNIG AND ABEGG 1997) where the impact of climate change on winter tourism was examined. According to these studies (BÜRKI 2000, ELSASSER AND BÜRKI 2002) a ski resort can be considered as snow-reliable, if in 7 out of 10 winters a sufficient snow covering of at least 30 to 50 cm is available for ski sport on at least 100 days between December 1 and April 15. Applying this rule, the percentage of snow-reliable ski resorts in Switzerland will drop from 85% to 44% if the level of snow-reliability increases from 1200 m a.s.l to 1800 m a.s.l. Similar changes are expected for other European countries as it can be seen in Fig. 1. The figure depicts the maximum and minimum altitude distribution of 495 ski resorts located in Austria, Germany, Switzerland and Italy. A ski resort is expected to be endangered by climate change, when its maximum altitude is beneath the level of snow-reliability.

Including the possibility of snowmaking technology the situation is less dramatic, as it was shown for the skiing industry in southern Ontario (Canada) (SCOTT et al. 2003). However, snow making facilities have their limitations, too, as for temperatures above  $-3^{\circ}\text{C}$  they are not economic. Moreover snow guns rely on an enormous amount of available water and energy (HAHN 2004).

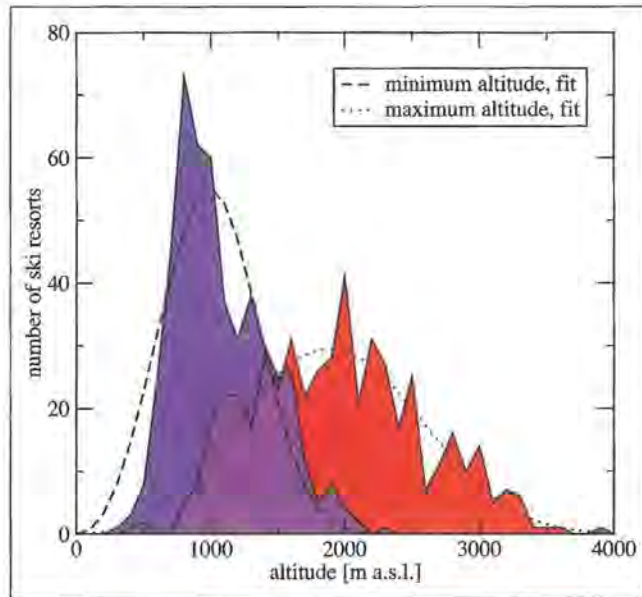


**Figure 1:** Distribution of the maximum and minimum altitudes of 495 ski resorts in Austria, Germany, Switzerland and Italy (Bergfex.at 2006). The altitudes were divided into elevation classes with a width of 100 m. The distribution of the maximum (minimum) altitudes is shown in red (blue). The curves were fitted with the Weibull distribution.

In the current work we are interested in the competition of ski areas for day tourists. For day tourists, the travel time between their place of residence and a ski resort is a decisive factor for the selection of a particular ski resort. Thus, in order to attract day tourists, ski resorts need not only be snow-reliable but must be located within the reach of day tourists.

This paper is structured as follows: Section II describes the model for day tourism. In section III an overview on the input data is presented, which have been used throughout the calculations. Sections IV, V and VI deal with the results.

### 2. Ski resort dynamics: The model

The ski resorts  $S_j$  are characterized by their maximum altitude above sea level  $h_j$  and the lift capacity  $k_j$ , i.e. the potential number of persons which can be transported by the available lift facilities per hour. For our minimal model, the attractiveness of a ski area  $S_j$  is given by

$$A_j = k_j H(h_j - h_0), \quad (1)$$

where  $H(\dots)$  is the Heaviside function, i.e.

$$H(h_j - h_0) = \begin{cases} 0 & \text{for } h_j < h_0, \\ 1 & \text{for } h_j \geq h_0. \end{cases} \quad (2)$$

In our model, ski resorts are only attractive, if they are located at altitudes which ensure snow-reliability, i.e. their maximum altitude  $h_j$  is above the *level of snow-reliability*  $h_0$ . As a consequence of climate change the level of snow-reliability is expected to increase by about 150 m

per 1°C (KÖNIG AND ABECC 1997). Snowmaking facilities lead to a technical level of snow-reliability  $\tilde{h}_0$  which is beneath the level of snow-reliability (SEIGER 2004). Local effects can also lead to snow-reliable ski areas below or above the level of snow-reliability. In our model we do not take snow making facilities and local effects into account. We distribute the area under investigation into a regular grid with cell centers

$$x_m = x_0 + m\Delta x, \quad (3)$$

$$y_n = y_0 + n\Delta y. \quad (4)$$

At each cell center  $x_i = (x_m, y_n)$  we prescribe the total population of that cell,  $e_i$ , as well as the percentage  $p_i$  of people who are going on a day trip to one of the ski resorts. The preference for ski tourists living in cell with cell centre  $x_i = (x_m, y_n)$  to visit ski resort  $S_j$  is defined by

$$\pi_{ij} = A_j T_{ij}. \quad (5)$$

The quantity  $T_{ij}$  depends on the travel time between cell  $x_i$  and the location of the ski resort  $S_j$ . For more information about  $T_{ij}$  refer to section III of this paper.

We can calculate the number of day tickets sold in each ski resort, prescribing the climate impact at the level of snow-reliability  $h_0$ . The number of day tickets  $\sigma_{ij}$ , which is sold in ski area  $S_j$  to people in cell  $x_i$  can be calculated from

$$\sigma_{ij} = \frac{\pi_{ij}}{\sum_j \pi_{ij}} e_i p_i. \quad (6)$$

Note that for  $(\pi_{ij} > 0)$  the above model is equivalent to the multinomial logit model (TRAIN 2003). This can be seen after introducing utility functions

$$U_{ij} = \ln(\pi_{ij}). \quad (7)$$

Assuming Gumbel distributions of the unobserved part of utility the multinomial logit model results in the logit choice probability

$$P_{ij} = \frac{\exp(U_{ij})}{\sum_j \exp(U_{ij})}. \quad (8)$$

Here we choose the form (6) to enforce that for vanishing preference, i.e.  $\pi_{ij} = 0$  no tickets will be sold.

The total number of day tickets sold to people with place of residence in  $x_i$  is

$$\sigma_i = \sum_j \sigma_{ij} = e_i p_i. \quad (9)$$

The total number of day tickets sold in ski area  $S_j$  is

$$\sigma_j = \sum_i \sigma_{ij}. \quad (10)$$

Note that in this simple model the number of day tickets sold in all ski areas is constant

$$\sum_j \sigma_j = \sum_{i,j} \sigma_{ij} = \sum_i e_i p_i. \quad (11)$$

### 3. Data

We work on a grid of dimensions 425 km x 430 km and with an individual cell area of 1 km<sup>2</sup>, i.e.  $\Delta x = \Delta y = 1$  km, and  $x_0 = y_0 = 0$  km. Our area under investigation is shown in Fig. 2 and corresponds the hydrological catchment of the Upper Danube (LUDWIG et al. 2003). Table 1 shows the values for the maximum altitude and the capacity of

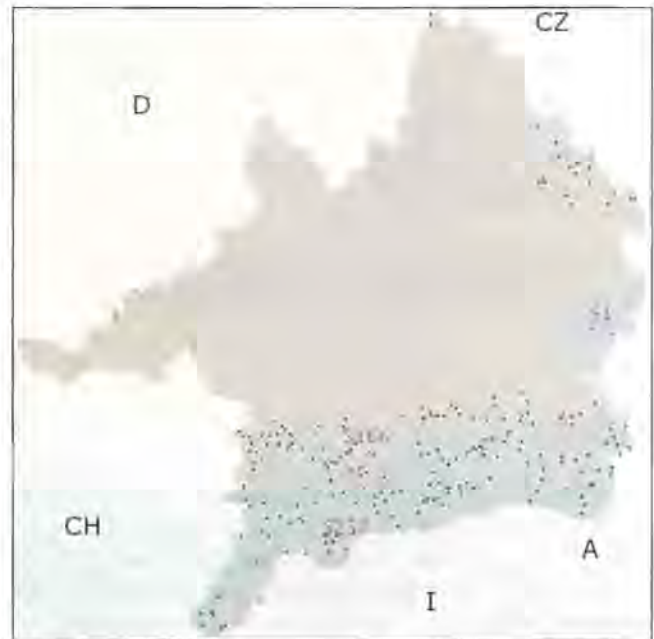


**Figure 2:** Distribution of ski resort (black dots) in the Upper Danube catchment (gray area). The lowest and highest situated ski resorts ( $S_1$  und  $S_{237}$ ) as well as the ski resort  $S_{166}$  (Garmisch Partenkirchen) are labeled.

**Table 1:** Parameter of three selected ski resorts  $S_1$ ,  $S_{166}$  and  $S_{237}$ . The parameters of the ski resorts in our model are their maximum altitude and capacity.

ski resort $S_j$	altitude $h_j$ [m a.s.l.]	capacity $k_j$ [person/h]
$S_1$	557	500
$S_{166}$	2050	17000
$S_{237}$	3440	76000

three selected ski resorts, which are also labeled in Fig. 2 by their identifier. The ski resorts are numbered in ascending order according to their maximum altitude. Ski resort  $S_1$  is therefore the ski resort with the lowest maximum altitude and the ski area  $S_{237}$  is the ski resort with the highest maximum altitude. In Fig. 3 the minimum and maximum altitudes of the ski resorts are plotted.

The quantity  $T_{ij}$  in Eq. (5) is part of the preference  $\pi_{ij}$  which depends on the travel time between cell  $x_i$  and the location of the ski resort  $S_j$ . We used three different setups for  $T_{ij}$ :

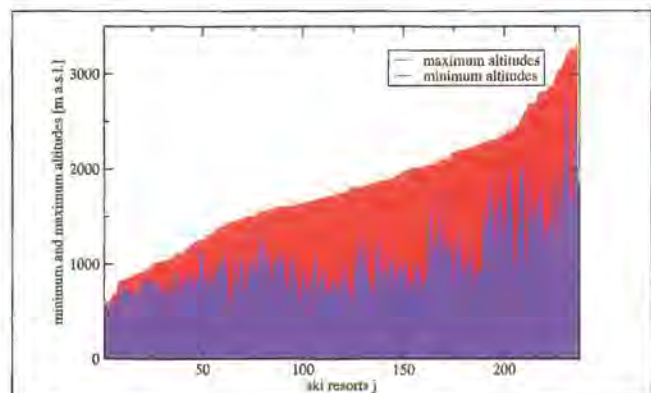


**Figure 3:** The maximum and minimum altitudes of the examined ski resorts, which we labeled on the horizontal axis.

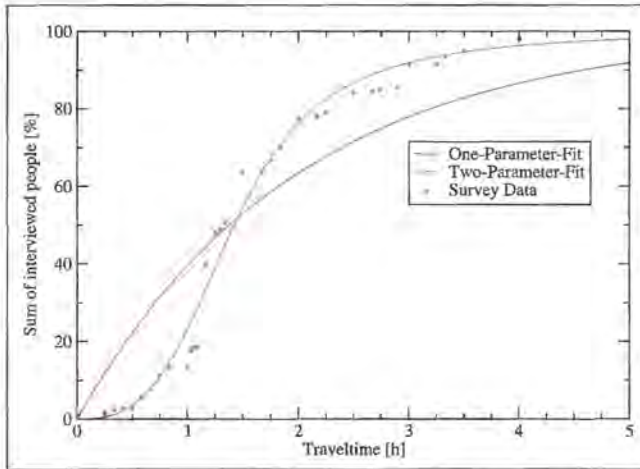


**Figure 4:** Percentage distribution of the travel times for day tourists (KLASSEN 2001). The survey data is shown in violet. The distribution was fitted with a one-parameter-fit (two-parameter-fit), which is shown in red (blue).

The first setup is the result of a one-parameter-fit of the survey data (see Fig. 4).

The function used for  $T_{ij}$  is

$$T_{ij} = \exp\left(-\frac{\tau(i,j)}{\tau_0}\right), \quad (12)$$

where  $\tau(i,j)$  is a metric which describes the travel time between cell  $x_i$  and the location of the ski resort  $S_j$ . We took for  $\tau(i,j)$  travel times determined by the traffic model DaTraM (SIEBEL AND MAUSER 2007). The constant  $\tau_0$ , for the optimal fit to the empirical data (KLASSEN 2001) is given by

$$\tau_0 = (1.99 \pm 0.17)h. \quad (13)$$

To the empirical data KLASSEN (2001) has determined the percentage distribution of the travel times of day tourists in the skiing area  $S_{166}$  Garmisch-Partenkirchen on two weekends in March 2000 (see Fig. 4).

The second setup is based on a two-parameter-fit of the survey data (see Fig. 4).  $T_{ij}$  is given by

$$T_{ij} = 1 - \frac{2}{\pi} \operatorname{atan}\left(a_0 \tau(i,j)^{a_1}\right) \quad (14)$$

Inserting the travel times  $\tau(i,j)$  in hours, the constants  $a_0$  and  $a_1$  are given by

$$a_0 = (4.91 \pm 3.46) 10^{-6} \quad (15)$$

$$a_1 = 2.75 \pm 0.16. \quad (16)$$

The third setup is also based on a two-parameter-fit of the survey data (see Fig. 4).  $T_{ij}$  is given by

$$T_{ij} = 1 - \frac{2}{\pi} \operatorname{atan}\left(a_0 \left(\frac{d(i,j)}{\hat{v}}\right)^{a_1}\right), \quad (17)$$

where the travel time  $\tau(i,j)$  is determined by the Euclidean distance function  $d(i,j)$  and an average speed of travel  $\hat{v}$  of 80 km/h.

The population is heterogeneously distributed in the study area (EGERER 2001). 9115 of the 70000 cells in the study area are inhabited. According to HARRER (1995), we assume a homogeneous percentage of ski tourists of  $p_i = 0.05$ .

#### 4. The importance of realistic travel times

We examined the importance of using realistic travel times. Therefore we used the three different setups of our model, described by the Eq. (12), (14) and (17), in order to determine the number of sold tickets under ideal conditions, where all ski resorts are considered as snow-reliable.

In order to quantify the difference in sold day tickets we introduce the percent deviation  $P_j$  for each ski resort.  $P_j$  is given by

$$P_j = \frac{\sigma_j(c) - \sigma_j(c_r)}{\sigma_j(c_r)}, \quad (18)$$

where  $\sigma_j(c)$  is the number of sold tickets in ski resort  $S_j$  calculated for one of the setups, denoted with  $c$  for a specific definition of  $T_{ij}$  and  $\sigma_j(c_r)$  is the number of sold tickets in ski resort  $S_j$  for the reference setup  $c_r$ . For the reference setup  $T_{ij}$  is calculated with the two-parameter-fit and modelled travel times Eq. (14). Fig. 5 shows the results for two cases: For case 1 we took the Euclidean distances for the travel times and a two-parameter-fit Eq. (17). For case 2 we considered DaTraM travel times and the one-parameter-fit Eq. (12).

The standard deviation of the difference between the two setups amounts to about 45% and 25% for case 1 and case 2, with maximum deviations of 153% and 92.45%.

We realize for case 1 a systematic growth in the deviations towards higher situated ski areas, which means that the number of sold day tickets calculated with Euclidean distances are overestimated for ski resorts of high altitu-

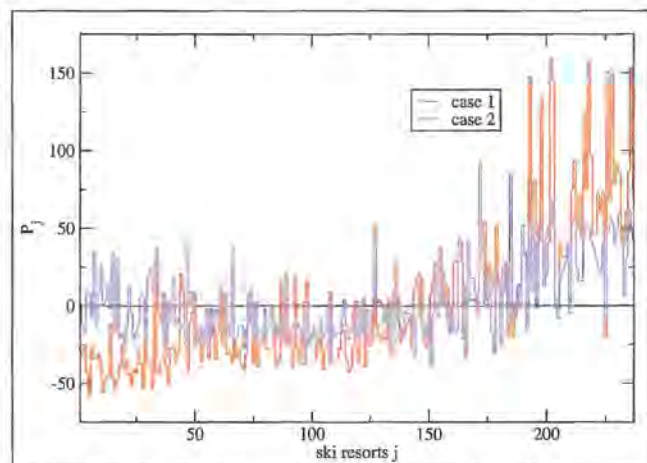


**Figure 5:** The graphic shows the percent deviation between the setups described by Eq. (17) for case 1 and by Eq. (12) for case 2 versus the reference setup described by Eq. (14).

des. This is partly due to a lower road density in mountain regions. Moreover the adaptation to the topography leads to steeper gradients and therefore to longer travel times. In contrast Euclidean distances represent the shortest distances between the corresponding cells and lead therefore to an underestimation of the travel times. With an increasing deviation of the level of snow-reliability towards higher altitudes the use of realistic travel times becomes more and more important in the model. We realize for case 2 a systematic decline in the deviations for lower situated ski areas and a systematic growth in the deviations towards higher situated ski areas. The deviations are caused through the smaller gradient of the one-parameter-fit. Therefore the results throughout this paper are determined by using realistic travel times and a two-parameter-fit.

### 5. The utilization of the ski resorts

Fig. 6 illustrates the number of sold day tickets under ideal conditions. The number of tickets varies strongly between 46 in ski resort  $S_2$  with a capacity of 500 persons/h and 8091 in ski resort  $S_{157}$  with a capacity of 77500 persons/h. Other peaks of the distribution, are caused by large ski resorts with high capacities.

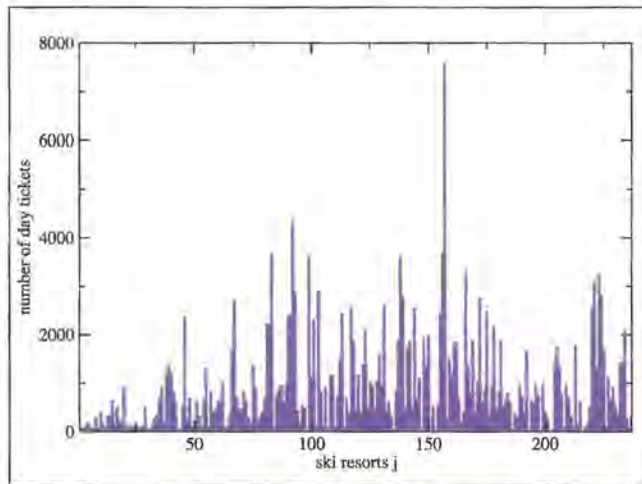


Figure 6: Number of sold tickets when all ski resorts are considered as snow-reliable.

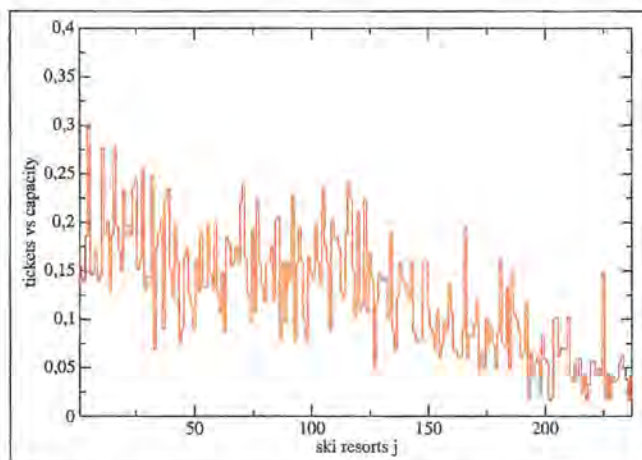


Figure 7: Utilization of ski resort when all ski resorts are considered as snow-reliable.

To demonstrate the utilization of the ski resorts under investigation we examined the ratio of the number of sold tickets in a ski resort and the capacity of the ski area, i.e.  $U_j = \sigma_j / k_j$ . Fig. 7 illustrates this ratio for all ski areas under ideal assumptions. The values for the utilization vary strongly between 0.016 and 0.299. We observe a systematic decline in the utilizations towards higher located ski areas. Under ideal conditions highly situated ski resorts are not attractive for local recreation due to the long travel times.

### 6. Climate change effects on the competition dynamics of ski resorts

The increase of the level of snow-reliability leads to the closure of ski-resorts in lower regions. Table 2 demonstrates how the number of closed ski areas increases while the level of snow-reliability increases.

Table 2: Number of closed ski areas at different levels of snow-reliability.

$h_0$ [m a.s.l.]	Closed ski areas	Closed ski areas [%]
555	0	0
1200	45	19
1500	76	32
1800	129	54.4
2100	172	71.7

We examined the geographic distribution of the ski resorts. Fig. 8 shows the remaining ski resorts at the levels of snow-reliability 1200 m a.s.l., 1500 m a.s.l., 1800 m a.s.l. and 2100 m a.s.l.. A comparison of the distribution of the ski areas at the level of snow-reliability 1200 m a.s.l. with the total distribution of the skiing areas presented in Fig. 2 shows a strong decline in the number of ski resorts in the Bavarian Forest. A further shift of the level of snow-reliability causes a reduction of the ski resorts in Bavarian Prealps. At the level of snow-reliability at 2100 m a.s.l. we realize that only ski resorts in the Alps have survived.

With the model described in section II we determined the number of sold tickets for different levels of snow-reliability  $h_0$ , Eq. (10). At each replacement of the level of the snow-reliability towards higher altitudes the reduced number of ski areas comes up for all ski tourists. Therefore we realize an increase in the number of sold tickets at each level in the remaining ski resorts. Fig. 9 shows the quantitative growth in the number of sold tickets, caused by the climate impact, for each ski resort.

For an additional description of the mentioned growth we examined the relative increments in the number of sold tickets for each ski area and that is we examined the ratio  $R_j = \sigma_j(srl) / \sigma_j(555)$ , where  $\sigma_j(srl)$  is the number of sold tickets in ski area  $S_j$  at the corresponding level of snow-reliability  $srl$ . Fig. 10 shows the relative increments in the number of sold tickets for each ski resort.

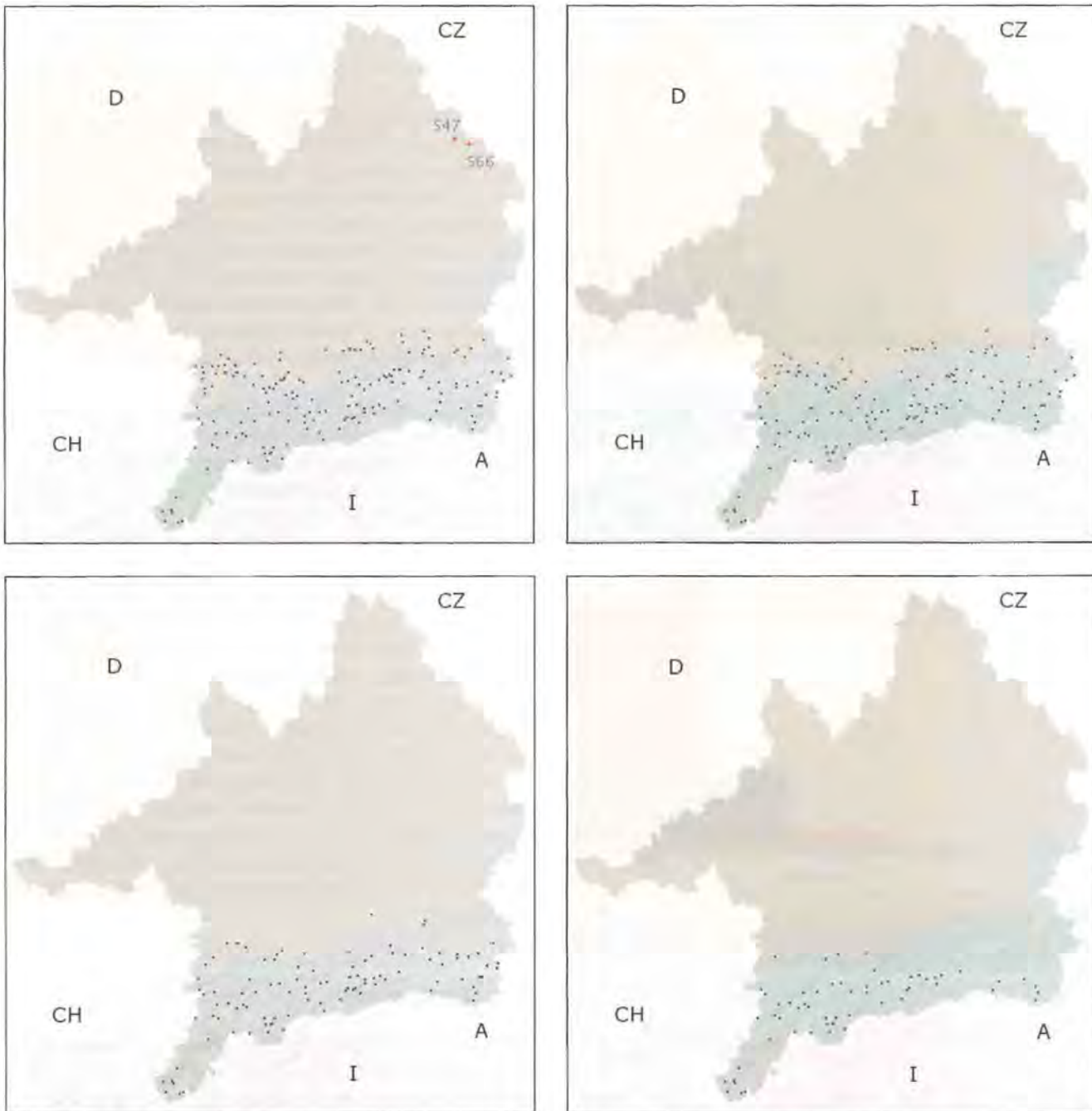


**Figure 8:** Ski areas which survive the rise of the level of snow-reliability to 1200 m a.s.l., 1500 m a.s.l., 1800 m a.s.l. and 2100 m a.s.l., depicted in the top left, top right, down left and down right panel.

**Table 3:** Mean values of the relative increments in the number of sold tickets at different levels of snow-reliability.

$h_0$ [m a.s.l.]	Mean value $P_i$ [%]
555	0
1200	7
1500	20
1800	83
2100	283

The relative growth rates caused by the shifts to 1200, 1500 and 1800 m a.s.l. are almost constant, with the exception of a few peaks in the curves. The constancy is due to the large number of ski areas, the large choice of the ski resorts provides balanced travel times. The curve

for 1200 m a.s.l. in Fig. 10 shows two peaks. These peaks represent the ski resorts  $S_{47}$  and  $S_{66}$  located in the Bavarian Forest, see Fig. 8. As the maximum altitudes of the other ski areas in Bavarian Forest are below 1200 m a.s.l., the two ski resorts come up for many other ski visitors in the area and are therefore for a short period the winner of the situation. The relative growth rates in the number of sold tickets for the ski resorts  $S_{47}$  and  $S_{66}$  are approx. 18%, whereas for all other ski resorts the relative growth rates are just around 7%. The constancy of the relative growth rates vanishes with the decrease of the number of ski resorts. The location of the ski resorts becomes more important when the number of ski resorts decreases.

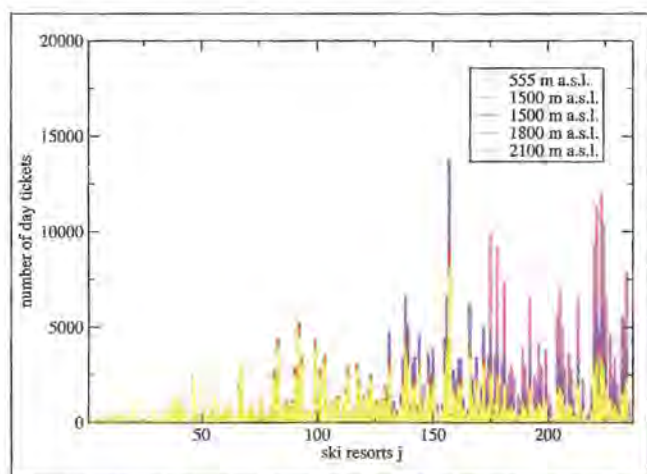


**Figure 9:** Number of sold tickets for each ski resort at the levels of snow-reliability 555 m a.s.l., 1200 m a.s.l., 1500 m a.s.l., 1800 m a.s.l., and 2100 m a.s.l.

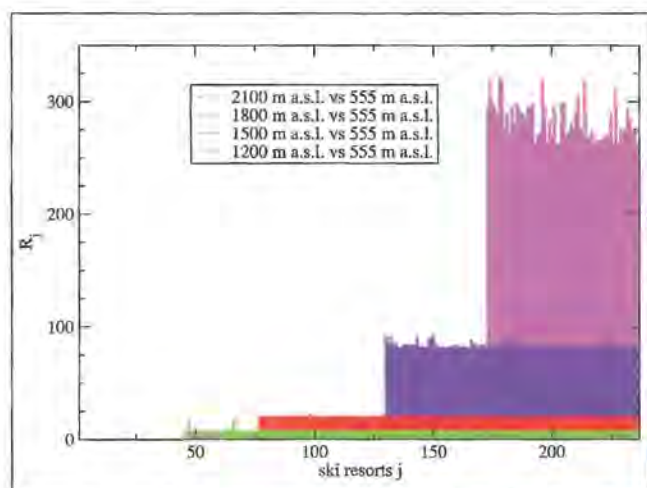


**Figure 10:** Relative increments in the number of sold tickets at the levels of snow-reliability at 555 m a.s.l., 1200 m a.s.l., 1500 m a.s.l., 1800 m a.s.l., and 2100 m a.s.l.

## 7. Conclusion and outlook

We presented a general model for day tourism to ski resorts which calculates the number of sold tickets. The model takes into account the displacement of the level of snow-reliability, the attractiveness due to the existing infrastructure and the travel times between the places of residence of day tourists and the ski areas. We applied the model to the Upper Danube catchment.

Our results show the necessity to use realistic travel times, the number of sold tickets for ski resorts at high altitudes is strongly overestimated when calculated with Euclidean distances. We examined the impact of climate change on the snow-reliability of ski resorts. Currently 81% of the ski resorts in the Upper Danube catchment can be considered as snow-reliable. Hereby we assume that the level of snow-reliability is at 1200 m a.s.l.. According to recent works (STEIGER 2004) this level of snow-reliability can be applied to the Bavarian-Alps.

It is expected that the level of snow-reliability will shift towards higher altitudes in the next decades. In our work we have examined the number of sold tickets for the ski resorts in our area under examination for several predicted shifts of the level of snow-reliability towards higher altitudes. The movement of the level of the snow-reliability to 1500 m a.s.l. causes 32% of the ski resorts to close, for a shift to 1800 m a.s.l. and 2100 m a.s.l. the values are 54.4% and 71.7%, respectively. We realize a strong decline in the number of ski resorts in the Bavarian Forest at the level of snow-reliability 1200 m a.s.l.. A further shift of the level of snow-reliability will lead to a strong decrease of the ski resorts in the Bavarian Prealps. Finally, only ski resorts in the Alps will survive.

The model presented in this paper can be extended in several ways: Currently the total number of ski tourists is considered to be constant. More realistically, the number of ski tourists should depend on the number and attractiveness of the ski resorts close to their place of residence. As socio-economic differences do effect the decision of individuals, we plan to extend the model in such a way that differences between humans will be considered. The number of sold tickets in our model currently depends on the level of snow-reliability. A more sophisticated model should work with measured snow data or data from climate models, which can describe local climatic effects. Moreover, it should be remarked that the travel times which have been used by the model, have been calculated under ideal conditions. Therefore we plan to consider feedback effects when determining the travel times of the tourists between their place of residence and the ski resorts. Finally, the relation between day tourists and overnight guests should be worked out.

## Acknowledgements

This work is supported by the GLOWA-Danube project sponsored by the German Federal Ministry of Education and Research. We would like to thank Mario Sax from the University of Regensburg, Institute of Geography for providing us the data about the ski resorts.

## References

- Bergfex.at (2006): url: <http://www.bergfex.at>
- BREILLING, M., CHARAMZA, P. AND SKAGE (1997): Klimasensibilität Österreichischer Bezirke mit besonderer Berücksichtigung des Wintertourismus. Report 97:1, Institute for Landscape Planning, Alnarp.
- BÜRKI, R. (2000): Klimaänderung und Anpassungsprozesse im Tourismus – dargestellt am Beispiel des Wintertourismus. Publikation der ostschweizerischen Geographischen Gesellschaft NF H6, St Gallen.

- EGERER, M. (2001): GLOWA-Danube Jahresbericht 2001: GLOWA-Danube, Integrative Techniken, Szenarien und Strategien zur Zukunft des Wassers im Einzugsgebiet der Oberen Donau, Teilprojekt Ökonomie: Ein regionalökonomisches, sektoral disaggregiertes Modell der Wassernutzung im Einzugsgebiet der Oberen Donau.
- ELSASSER, H. AND BÜRKI, R. (2002): Climate change as a threat to tourism in the Alps. *Climate Research*, vol. 20, 253-257.
- HAHN, F. 2004: Künstliche Beschneigung im Alpenraum. *CLIPRA International Report*.
- HARRER, B. (1995): Tagesreisen der Deutschen. Schriftenreihe des Deutschen Wirtschaftswissenschaftlichen Instituts für Fremdenverkehr an der Universität München, 46, München.
- KLASSEN, N. (2001): Einfluss der Information auf die individuelle Freizeitmobilität. Ph. D. Thesis, Technische Universität München.
- KOENIG, U. AND ABEGG, B. (1997): Impacts of Climate Change on Winter Tourism in the Swiss Alps. *Journal of Sustainable Tourism*, vol. 5, 46-58.
- LUDWIG, R., MAUSER, W., NIEMEYER, S., COLGAN, A., STOLZ, R., ESCHER-VETTER, H., KUHN, M., REICHSTEIN, M., TENHUNEN, J., KRAUS, A., LUDWIG, M., BARTH, M. AND HENNICKER, R. (2003): Web-based Modeling of Water, Energy and Matter Fluxes to Support Decision Making in Mesoscale Catchments - the Integrative Perspective of GLOWA-Danube. *Physics and Chemistry of the Earth*, vol. 28, 621-634.
- SCOTT, D., McBOYLE, G. AND MILLS, B. (2003): Climate change and the skiing industry in southern Ontario (Canada): exploring the importance of snowmaking as a technical adaptation. *Climate Research*, vol. 23, 171-181.
- SIEBEL, F. AND MAUSER, W. (2007): Simulating vehicular traffic in a network using dynamic routing. *Mathematical and Computer Modelling of Dynamical Systems*, vol. 13, 83-97.
- STEIGER, R. (2004): Klimaänderung und Skigebiete im bayerischen Alpenraum. Master's Thesis, Institut für Geographie, Naturwissenschaftliche Fakultät, Leopold-Franzens-Universität Innsbruck, St Gallen.
- TRAIN, K.F. (2003): *Discrete Choice Models with Simulation*. Cambridge University Press, Cambridge.

# 17 A parameterization for the turbulent fluxes over melting surfaces derived from eddy correlation measurements

MARKUS WEBER

Commission for Glaciology of the Bavarian Academy of Sciences and Humanities, Alfons-Goppel-Str. 11, D-80539 Munich, Germany

## Abstract

The temperature of a melting surface of snow or ice should never exceed 0°C even if the layer of air above is much warmer. Hence the thermal layering mostly is characterized by a stable state. Under such conditions the exchange of heat and moisture is severely limited because of depauperate turbulence.

During a clear day between 80 and 90 percent of the energy available for melt is delivered by the radiation budget. Almost the complete residual of the surface energy balance is distributed on the turbulent fluxes of sensible and latent heat. Over a period of time with overcast and windy weather the relevance of the turbulent fluxes may rise from 10 to 30 percent and more. Thus the accurate calculation of the turbulent heat fluxes is very important for the melt modelling of water production.

To parameterize turbulent transport processes within the stable stratified surface layer using the *Monin-Obukhov*-similarity theory is inaccurate in contrast to unstable conditions. Catabatic flows generated at inclined areas may raise the efficiency of mixing by forcing mechanical turbulence. Under such conditions, e.g. the presumed invariance of the fluxes with height is definitely violated and therefore the common known scheme is inapplicable.

The analysis of data from *Eddy-Correlation*-measurements over an inclined surface gives an insight to the structure of turbulence within the surface layer. The experiments were carried out in August 1998 (HyMEX98) and August 2000 (HyMEX 2000) at Vernagtferner (Oetztal Alps, Austria). The results presented in this paper show that the integral to the cospectra and thus the kinematic fluxes can be well calculated using the so called "flux-variance relationship". Therefore an approach like a bulk formula can be proved the best fit for parameterization. The amazing analogy of the turbulent structure of the enthalpy distribution, in contrast to that of moisture, suggests that the latent heat flux can be calculated using a similar algorithm.

This contribution shows a workable bulk parameterization scheme to calculate the turbulent fluxes in case of a stable stratified surface layer.

## 1. Introduction

A layer of accumulated snow or ice can basically be ablated by mechanical erosion and by transformation from the solid to the liquid or gaseous state. The latter processes of melting or sublimation require a lot of thermal energy: to melt 1 kg of ice at 0°C an amount of 0.334 MJ of energy is required. To evaporate it, an additional 2.5 MJ is needed. Potential sources of energy are the absorption of long-wave and short-wave radiation and the turbulent fluxes from the atmosphere. Over snow, the energy sinks are the reflection of the short-wave radiation and the emission of long-wave radiation at the surface. Advection of very cold or very dry air may result in important losses of energy by turbulent fluxes directed into the atmospheric surface layer. The available energy flux **SE** for phase transformation is determined by the well known surface energy balance equation

$$SE = RB + H + LE + G \quad [Wm^{-2}] \quad [1.1]$$

where **RB** is the radiation balance, **H** the turbulent flux of sensible heat, **LE** that of the latent heat and **G** the heat conduction into or out of the snow pack. During melt conditions it is justified to consider **G** as negligibly small. The term **RB** balances the incoming and outgoing radiative fluxes in the short wave (**S**) and long wave (**L**) range using the commonly known equation

[1.2]

$$RB = (S \downarrow - S \uparrow) + (L \downarrow - L \uparrow) [T_s] \quad [Wm^{-2}]$$

A flux directed from the atmosphere towards the surface is considered positive. Snow- or icemelt, the transition from the solid to the liquid state, occurs only under the condition that the surface temperature rises up to 0°C and the residual **SE** is positive. These conditions are usually associated with positive values of the air temperature above the surface and with a positive radiation balance. In that case each term of the right side of eq. [1.1] is a potential source for melt. In contrast, if the air temperature drops below zero, sublimation represented by the latent heat flux **LE** is the exclusive process, which leads to a mass loss of the snow pack (apart from mechanical erosion, which is not considered here).

Since the consumption of energy to sublimate 1 kg of solid water is more than eight times higher than melt, the latter is the most efficient process to ablate the snow cover in any case. The temperature of a melting surface of snow or ice will never exceed 0°C even if the layer of air above is much warmer. This boundary conditions lead to some interesting implications:

- Unlike other surface types, the very important upper boundary value of the surface temperature is a well known constant without any variation in time.
- The long wave emitted radiation flux  $L \uparrow$  is an important sink for the energy balance and directly dependent on the surface temperature. It never exceeds an upper threshold of approx.  $315 Wm^{-2}$ . The incoming long-wave radiation, however, is dependent on air temperature and humidity (KUZMIN 1961). Advection of

warmer and more humid air will always increase the energy available for melt.

- Thermal layering near the surface is mostly characterized by extreme stable stratification, i.e. air temperature increases with height above ground. Very strong vertical temperature gradients can be found in the magnitude of some K/m. Under such conditions exchange of heat and moisture should be severely limited because of suppressed thermal turbulence. But if turbulent motion is generated mechanically by windshear, friction and so on, the resulting flux of sensible heat is always directed to the surface and therefore an enhancement to the surface energy budget.
- The kind of the contribution – increasing or reducing – of the latent heat flux to the energy balance depends on the humidity conditions. A partial pressure of water vapour below 6.15 hPa is leading to losses by evaporation, while a higher content provides additional energy from condensation.
- A deep snow cover smoothes the bumpiness of the underlying surface of an area and therefore decreases its aerodynamic roughness.

The individual contribution of each energy balance component varies in a wide range, which depends on the local conditions. For example the partitioning of energy which is delivered by the short-wave radiation balance is primarily controlled by the albedo, which covers a range of values between 0.9 for fresh fallen snow and 0.3 for firn or even 0.15 for bare ice. At a high mountain site, the contribution of the radiation balance during a clear day in the summer may rise up from 80 to 90 percent of the energy available for melt, which amounts to more than 600 Wm<sup>-2</sup> (WEBER 2005). Almost the complete carryover of the right side of the energy balance equation is distributed to the turbulent fluxes of sensible and latent heat.

Due to the fact that fresh fallen snow reflects up to 90% of the incoming short wave radiation, the fraction of the absorbed energy is comparable to the magnitude of the turbulent fluxes, i.e. within a range of approx. 50 - 150 Wm<sup>-2</sup>. For this reason a correct determination of both the sensible and the latent heatflux should be achieved. This is especially important since, under conditions of large radiation input and simultaneous presence of cold and dry air, ablation is mainly caused by sublimation. However, the question remains how the turbulent fluxes can take on the high values despite of the very stable stratification of the near surface layer.

Over inclined terrain the development of a typical catabatic flow can be frequently observed. It is characterized by a low level jet near the surface which is incompatible with the assumption of a constant flux layer, but the latter represents one of the most stringent assumptions for the application of the similarity theory (MONIN & Obukhov 1958; STULL 1988).

Furthermore, one can learn by observation that the catabatic flow shows an intensive turbulent motion, as long as the mean wind speed does not exceed critical values which depends on the local conditions (WEBER 2005). With increasing speed the character of the flow

becomes more and more laminar, and the efficiency of the turbulent transport is reduced. A sophisticated parameterization scheme should consider this process.

This paper shows a practical approach, based on results of experimental investigations HyMEX98 and HyMEX 2000, which were carried out on an alpine glacier in 1998 and 2000 (WEBER 2005, BRAUN et al. 2004, ESCHER-VETTER & WEBER 2000).

## 2. Common methods to determine the turbulent fluxes

In contrast to the radiative fluxes the turbulent fluxes cannot really be directly determined by a physical method. However formulas are well established which result from the hydrodynamic model known as the set of the primitive equations. Thus the sensible heat flux  $H$  and the latent heat flux  $LE$  can be calculated by

$$H = -\bar{\rho} \cdot c_p \overline{w'T'} \quad [2.1] \quad \text{and} \quad LE = -\bar{\rho} \cdot l_v \overline{w'q'} \quad [2.2]$$

with mean density  $\bar{\rho}$ , heat capacity of air  $c_p$ , vertical wind speed  $w$ , air temperature  $T$ , latent heat of vaporisation  $l_v$  and specific humidity  $q$ . The overbar symbol indicates an instruction for averaging the argument over an adequate time period, which depends simultaneously on the scale of the largest element of the turbulent motion and the mean speed of the flow. It intuitively follows from an idea of G.I. TAYLOR (1938), the so-called *Taylor's Hypothesis of Frozen Turbulence* which is a transformation of the attributes of the elements of the turbulent motion to a time series of a measured quantity, and vice versa. In this sense *frozen* is a synonym for *stationary*. This concept of a model of near surface turbulence establishes the general basis for the *Eddy Correlation Method* (ECM) which will be discussed later.

The primes denote the actual deviation of a quantity from the average over the period mentioned above. The mean value is equivalent to the well known variance. Multiplication and averaging the timeseries of the deviation of two quantities, e.g. the vertical wind speed component  $w$  and the air temperature  $T$  finally leads to the covariance, which is defined as the so-called *kinematic flux* of sensible heat. Finally, the multiplication by the mean density  $\bar{\rho}$  and the heat capacity of air  $c_p$  delivers the heat flux in Wm<sup>-2</sup>. The moisture flux can be accordingly determined, using the quantities  $w$  and the specific humidity  $q$  to get the kinematic flux, and the latent heat of vaporisation  $l_v$  instead of  $c_p$  to calculate the latent heat flux  $LE$ .

Equations 2.1 and 2.2 are valid at any location, time and level above the surface, but in practice, they are not easily applicable. It requires enormous data recordings of very high accuracy and resolution in time. Hence, the following approach is commonly used, based on the analogy to molecular heat conduction:

$$H = \bar{\rho} \cdot c_p \cdot K_H \frac{\partial \bar{T}}{\partial z} \quad [2.3] \quad \text{and} \quad LE = \bar{\rho} \cdot l_v \cdot K_{LE} \frac{\partial \bar{q}}{\partial z} \quad [2.4]$$

As the kinematic flux is replaced by the vertical gradient of the mean temperature  $T$  or the specific humidity  $q$  multiplied by a turbulent exchange coefficient  $K$ , the approach is well known as *profile method* or *K-approach*. The overbar symbol indicates the identical procedure for aggregation as defined in eq. [2.1/2]. The potentially differing coefficients  $K_H$  (sensible heat) and  $K_{LE}$  (latent heat) can be determined by comparison of eq. [2.3/4] with eq. [2.1/2], but the validity of the result would be local.

If the fluxes are constant with height, the profile can be integrated and the turbulent efficiency of the exchange coefficient may be calculated depending on properties of the profile of wind speed and the thermal stability of the surface layer (STULL 1988). Using the *similarity theory* (MONIN & Obukhov 1958) the interrelation is described by *universal stability functions*, which were determined empirically (e.g. BUSINGER et al. 1971, DYER 1974). The validity of this function is now well proven for neutral and unstable layering but it fails under the conditions of a stable surface layer and especially within catabatic flows. What remains is only the fact that the calculation of the turbulent fluxes depends on a variable, which characterizes the state of the flow, and on the vertical profiles of temperature, humidity and wind speed. Among others, e.g. OERLEMANS (2001) introduced further simplifications of eq. [2.3/4]:

$$H = \rho \cdot c_p \cdot C_H \cdot U \cdot (T - T_0) \quad [2.5]$$

and respectively

$$LE = \rho \cdot l_v \cdot C_{LE} \cdot U \cdot (q - q_0) \quad [2.6]$$

whereas  $U$ ,  $T$  and  $q$  now represent the time-aggregated horizontal wind speed, air temperature and specific humidity at a well defined level (in general at 2 m above the surface). Variables provided with a zero-Index denote the values directly on the snow surface. Equations of this type are frequently called *bulk formulae*.  $C_H$  and  $C_{LE}$  are not equal to  $K_H$  and  $K_{LE}$  in eq. [2.3/4], but are simple functions or constants derived from experimental results and adapted to the location where they are applied.

In spite of the strong simplifications, the bulk formulas of eq. [2.1/2] and [2.3/4] still consider the essential interrelations of turbulent transport: the dependency on air density, wind speed and stability.

Parameterizations of this type are widely and successfully used in melt water production models. At larger scales, even simpler models are used to calculate the sensible heat flux (e.g. ESCHER-VETTER 2000, STRASSER et al. 2002, STRASSER et al. 2007 (this volume)):

$$H = 5.7 \cdot \sqrt{U} \cdot (T - T_0) \quad [2.7]$$

Eq. [2.7] is normally used to approximate the sensible heat flux in catchments situated in mountainous regions. Compared to eq. [2.5] it has evident failings. The first three variables on the right side of eq. [2.5] were condensed to one single constant, which was derived using data measured at an elevation of approx. 2800 m a.s.l. (Weissfluhjoch). Hence the formula shows no more explicit dependency of the flux on altitude, but only indi-

rect through the temperature decrease with height. The formula may be applicable in small areas with a limited elevation range. For areas with an elevation range of more than 2000 m, methodical errors in the determination of the sensible heat flux of up to 30% have to be accepted due to the decrease of air density.

Using eq. [2.7] an increasing wind speed results in larger sensible heat fluxes following the idea that higher wind speed leads to a higher intensity of the turbulence. However, above a critical threshold the flow becomes more and more laminar and therefore the turbulent transport becomes less efficient. This effect is taken into account by reduction of the influence of the wind speed with the square root function.

The knowledge of accurate values of surface temperature and humidity during melting conditions can be seen as an important advantage, in contrast to only knowing the values 2 m above the ground which are tuned by the local processes of energy exchange. Temperature above a melting snow field is strongly reduced compared to the one above bare ground at the same elevation. Therefore one has to take care in the modelling if a field of temperature and humidity is interpolated using gradients between a few stations. This procedure may cause methodical errors, if there are significant subscale deviations of the resulting temperature field. But as further discussed in the following paragraphs, the calculated fluxes are not valid at a local point, but represent a mean value averaged over an upstream area (fetch) of a minimum of  $10^4 \text{ m}^2$  up to more than  $1 \text{ km}^2$ . Therefore it may be better for the accuracy of model results to use as input for the equations similar "representative mean values" instead of local measurements.

### 3. Eddy Correlation measurements and time series analysis

To prove the validity of the methods described in paragraph 2, a reference value of the kinematic flux is needed. An approach to determine it directly is given by the well known *Eddy Correlation Method*. It is based on the idea to translate the information about the spacial structure of turbulence to a function of time using the mean wind speed. The theoretical background was given early by TAYLORS hypothesis. The postulate of stationarity of the flow means: an isolated element of turbulent motion (eddy) has to evolve and to persist while passing the sensor. A simplified illustration of the principle is shown in Fig. 1. A more detailed description of the basics can be found in STULL (1988), FÖKEN (2003) or WEBER (2005). Thus, the method delivers information only along a cross-section, which is in line with the upstream medium wind direction. The extension of the result from the line to an area requires the additional assumption of lateral homogeneity.

The determination of the fluxes of sensible and latent heat requires technically highly developed sensors. A 3-dimensional ultrasonic anemometer is required to measure the fluctuations of each component of the wind vector with sufficient precision and frequency. The sa-

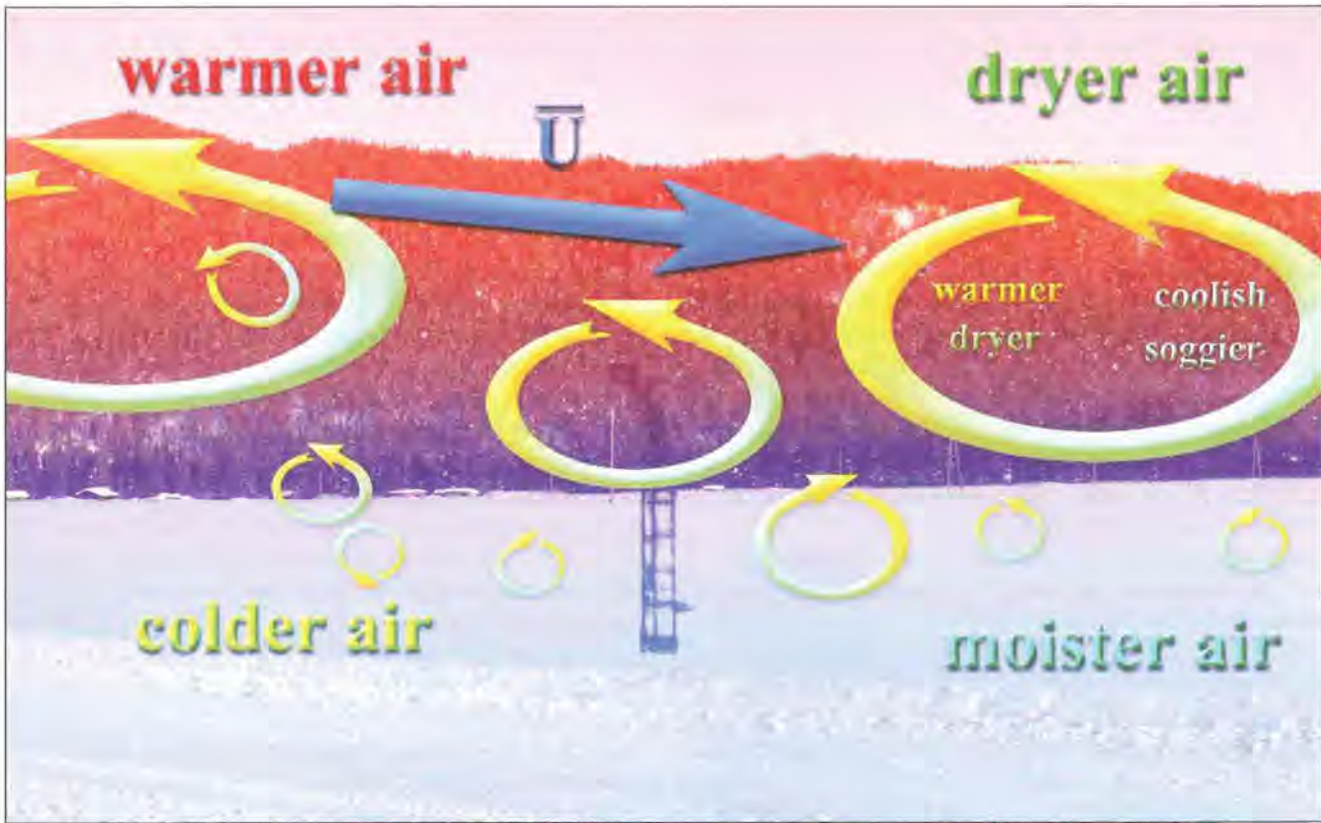


**Figure 1:** The principle of the eddy correlation method: elements of turbulent motion (so-called eddies), which are embedded in a turbulent flow with a mean wind speed  $\bar{U}$ , are passing a fixed sensor. An isolated element has to evolve and to persist while passing the instrument. The attributes of the air within the domain of influence of the eddy were translated to measured time series of the quantities.

me instrument is able to measure the fluctuations of the (virtual) temperature which has to be corrected due to the influence of the fluctuations of water vapour to get the (potential) air temperature. Measurement of the fluctuation of the specific or absolute humidity requires a separate sensor, e.g. an instrument working on the principle of absorption of monochrome light by water vapour. Especially the spectral line of Krypton or Lyman- $\alpha$  can be used successfully.

Required frequency for the measurements of a discrete time series of the wind vector components, the air temperature and humidity are in the range of 30 to 100 samples per second (Hz). As a first approximation the kinematic flux can be calculated using

[3.1] for sensible heat

$$\overline{w'T'} = \frac{1}{N-1} \left[ \sum_{k=0}^{N-1} w_k \cdot T_k - \frac{1}{N} \left( \sum_{k=0}^{N-1} w_k \sum_{k=0}^{N-1} T_k \right) \right]$$

[3.2] and for latent heat

$$\overline{w'q'} = \frac{1}{N-1} \left[ \sum_{k=0}^{N-1} w_k \cdot q_k - \frac{1}{N} \left( \sum_{k=0}^{N-1} w_k \sum_{k=0}^{N-1} q_k \right) \right]$$

The variable  $N$  denotes the count of numbers of the time series, which covers the required period for averaging. E.g., using a sampling rate of 20 Hz, it may range from

36.000 to 72.000. From the horizontal components of the wind speed the friction velocity  $u_*$  can be calculated by substitution of the scalars in eq. [3.1] by the horizontal cartesian wind vector components  $u$  (W – E) and  $v$  (N – S) and

$$u_*^2 = \sqrt{u'w'^2 + v'w'^2} \quad [3.3].$$

$u_*$  is an informative parameter to consider the influence of the aerodynamical roughness of the surface and the fraction of the mechanically induced turbulence.

From the theoretical point of view the eddy correlation method seems to be speciously simple. The sums in eq. [3.1 – 3.3] can be easily calculated in real time during data acquisition and after  $N$  measurements are captured. So values for the turbulent fluxes are immediately available. But that is only half the truth. First of all the algorithm listed above is based on strong simplifications and the experimental data has to fit to the special requirements of the spectral model of turbulence. This will be discussed in the next section. Secondly the instruments have a lot of malfunction sources. Therefore in practice it is an exhausting procedure to get usable data sets and results. This is especially the case for the measurements over melting surfaces under cold and wet weather conditions.

Because of the difficulty to align the sensor in a fixed position there is an imperative need for an additional pro-

be, which records the inclination of the instrument setup continuously. Frost-covered sensors are the main reason for frequent break downs of the instruments and gaps in data series. An unfavourable signal-to-noise ratio leads to a reduction of the quality and of the high temporal resolution of the measurement signal. Additional difficulties are wind shadowing effects by the probe itself and errors due to an inevitable displacement of different instruments. To minimize these errors e.g. a special rotor system was developed which automatically adjusts the probe to the best position with respect to the direction of the incoming air flow. A suitable equipment to measure covariances is shown in Fig. 2. It was used during the HyMEX98 experiment on Vernagtferner. More details concerning the experimental experiences, description of technical problems and possible solutions can be found in WEBER (2005).

Eddy correlation measurements were carried out not only to determine the fluxes, but also to investigate the physical nature of the turbulent exchange processes. The internal conditions within the atmospheric surface layer over a melting snow or ice surface differ distinctly from those over a bare ground surface. In the latter case layering is unstable, the location of the source for heat is well defined, but the location of the heat sink is situated above but it extends to the entire boundary layer. Besides the mechanically generated turbulence by friction

forces additional turbulent motion is well developed by buoyancy forcing. The eddy size increases with height. Under strong convective condition there is a disposition to form large coherent organized structures (e. g. "plumes", STULL 1988), which are embedded within the flow and make the heat transport very efficient.

In the case of a melting surface the situation is contrary: the location with sources for heat within the atmospheric boundary layer is not exactly locatable and may be in the upper part of the surface layer or in some cases above it. Even a complete decoupling of the surface layer from the upper layers can be observed. However, for the sink of heat the bottom is a clearly defined location. Thermal layering is extremely stable, and as a result, vertical movement is strongly constrained. Stimulation of turbulence by buoyancy forces is nearly impossible and is generated only mechanically by shear stress. The required kinetic energy of the turbulent motion has to be extracted from that of the mean flow, which will be reduced in speed. Hence catabatic down flow is an important source for turbulence within the stable surface layer.

Nevertheless, similarly organized structures can be detected within the stable layer over a melting surface as under convective conditions. They can be found as mainly three types of patterns in the high resolution time series of temperature or humidity as shown in Fig. 3: *ramp structures*, *waves* and *spikes*. The ramp structure is similar to that of a convective plume (KAIMAL & BUSINGER 1970), but its temperature record seems to be mirrored on the time axis (WEBER 2005). It illustrates the event of the special mixing process by entrainment of warmer air from layers above. Within a period of 30 to 60 seconds the layer becomes colder because of the continuous extraction of heat at the snow or ice surface and mixing of air upwards by the turbulence. At the sharp edge the cold air mass will suddenly be replaced by new warm air from above, and the process is repeated. Therefore the main effect of the catabatic plumes is to destruct the stable stratification. The function of the *spikes* is similar; they transport cold air from the bottom upwards. Wave patterns can be particularly found within the transition period around sunrise and sunset: The stable stratified air mass is initiated to oscillate. But as there is no correlation to vertical movements, no forcing enhancement of the turbulent transport can be expected.

#### 4. Spectral analysis and flux calculations

Present understanding of the turbulent transport is strongly affected by the applied modelling concepts. To avoid misinterpretation, the conformity of the results with the model used should be proven. The model of atmospheric turbulence used for that purpose here is based on VAN DER HOVEN'S energy (variance) spectrum (VAN DER HOVEN 1957). As shown in Fig. 4, this spectrum of periodical motion can be divided in 4 well defined ranges with selected types of turbulence which each has typical properties with respect to life time and dimension.



**Figure 2:** System for eddy correlation measurements, which is mounted on a 2 m tower and run continuously during 5 day periods in August 1998 and 2000, respectively, at Vernagtferner (Oetztal Alps, Austria) at an elevation of 3000 m a.s.l. The glaciologist is Markus Weber, the author. (Picture by Jan Greune)

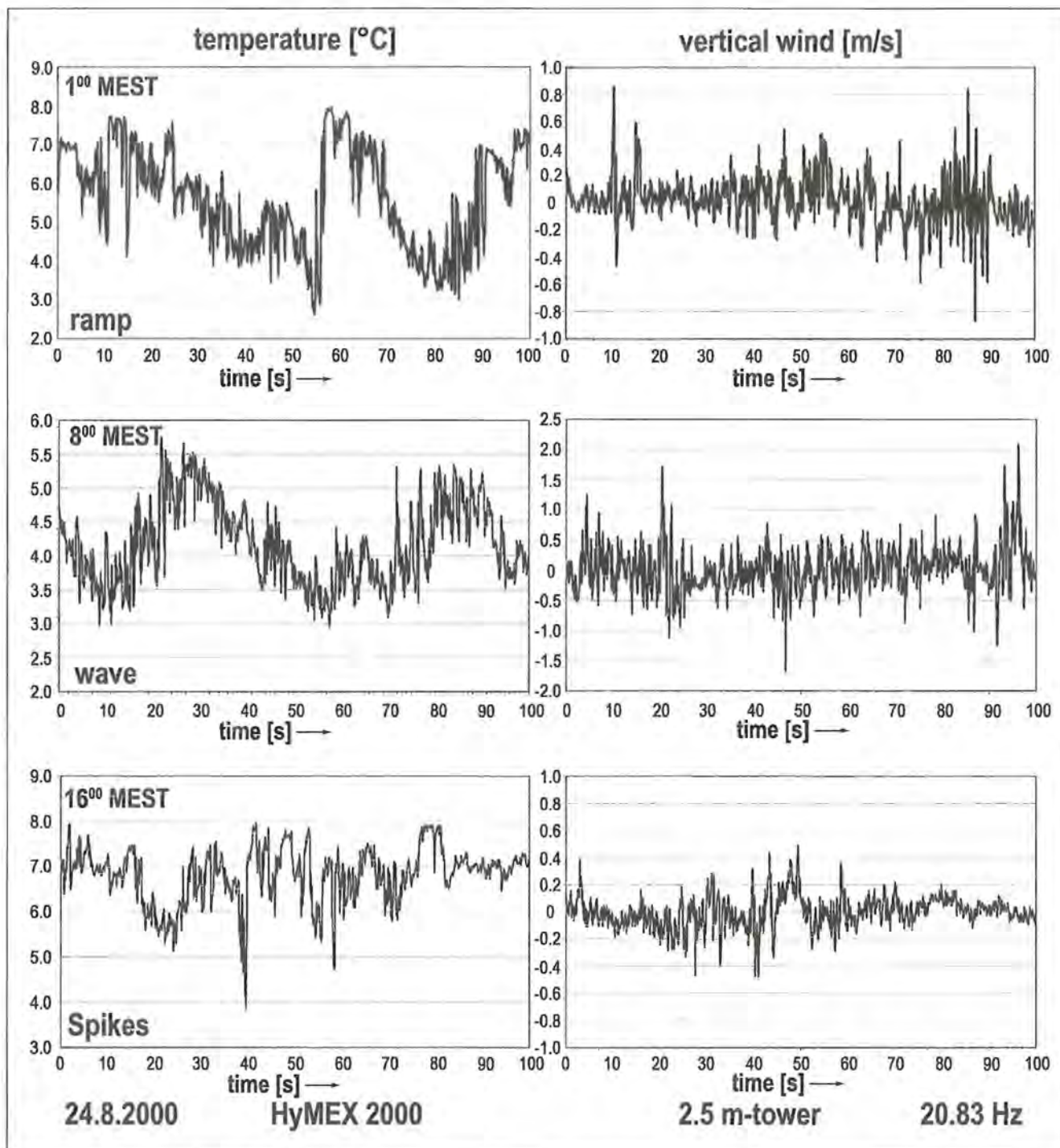


**Figure 3:** Examples of simultaneous 20.83Hz time series of air temperature and vertical wind speed, measured over a melting surface (Vernagtferner, Austria). Positive values for the vertical wind are directed upwards. The temperature data show examples of characteristic pattern within a stable layer (adapted from WEBER 2005).

The vertical transport occurs within the range of the micro-scale turbulence. It can be divided into a section where energy is generated and another where energy is dissipated, according to the denotations “buoyancy forced” and “mechanically generated” used in paragraph 3. The resulting value of the covariance respectively, which is determined using the statistical procedure described above, needs an additional analysis of the data to be interpreted properly as a turbulent heat flux. Therefore the result of the spectral analysis used here has to

show satisfactory agreement to this model of the micro scale turbulence.

In addition it is a useful tool

- to test the raw data series for signal errors and noise; a closer look on the decline within the inertial subrange of the variance spectra reveals whether the sampling frequency and the data accuracy of the sensors are sufficient;

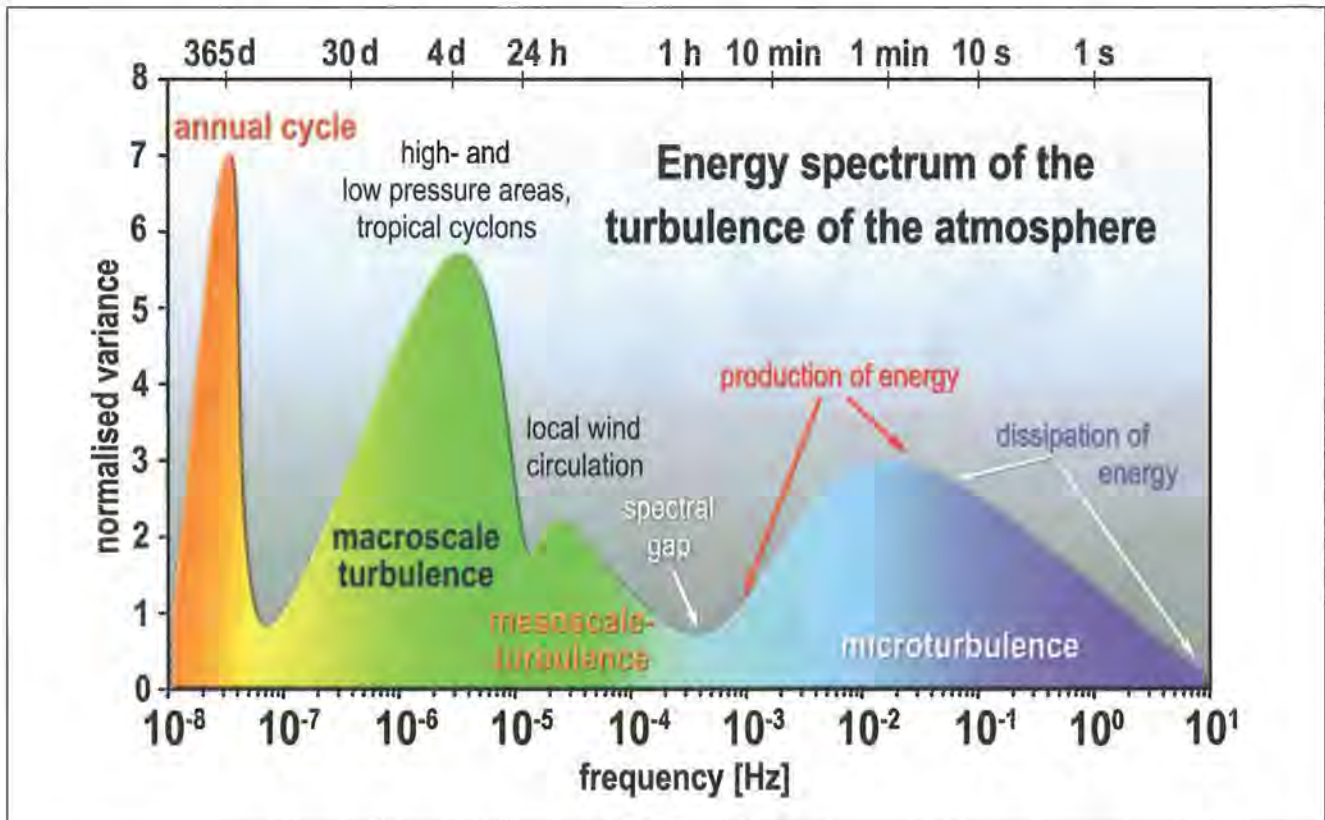


**Figure 4:** Schematic illustration of a 3-year atmospheric turbulence variance spectrum of the horizontal wind speed. The processes of turbulent heat exchange cover the blue colored frequency range of the microturbulence, separated from large scale circulations by a distinctive minimum (spectral gap). The figure is based on VAN DER HOVEN (1957) and ROEDEL (2000).

- to determine essential corrections to the obtained variance and covariance;
- to analyse the structure of the turbulent flow and the transport processes by comparing the spectra among each other and to the well known standard spectra.

The coefficients  $S(n)$  of the variance spectra (sometimes denoted also as power spectrum) from a discrete time series  $f(k)$  with  $N$  numbers of equidistant and successive values (now gaps are admitted) can be determined by the common Fourier Transformation

$$S(n) = \sum_{k=0}^{N-1} \frac{f(k)}{N} \exp(-i2\pi nk / n) \quad [4.1]$$

Summation over all the coefficients of the power spectrum results in the total variance  $\sigma^2$  of the time series

$$\sigma^2 = \sum_{n=1}^{N-1} S(n) \quad [4.2]$$

To computationally transform the time series to the variance spectra the common FFT-algorithm (*Fast-Fourier-Transformation*) is used, which is highly efficient, but normally this restricts the length of the data sets of  $N=2^m$  values, where  $m$  is an integer.

To analyse and compare the spectra they can be graphically presented in an appropriate way. Standardisation and normalisation can be performed by multiplication of

the spectral coefficients with the frequency  $f$  and subsequent scaling with the total variance. Plotting of such spectral curves using a semi-log axis has the advantage that the fraction of the area below the curve is proportional to its contribution to variance. An example is shown in Fig. 5, where the variance spectra of the fluctuation of temperature, humidity, vertical and horizontal wind speed are compared. Clear differences within the high frequency range of the scalar quantities and the horizontal wind speed are errors in the signal. The horizontal course of the humidity spectrum at the end of the inertial subrange indicates random noise at frequencies above 0.3 Hz.

Using a log-log axis for plotting, all normalised spectra should merge together. KAIMAL AND FINNIGAN (1972) and KAIMAL et al. (1994) have prepared standardised spectra adapted to the condition of a stable surface layer on homogeneous terrain. The example in Fig. 6 shows very good agreement of the spectra, measured at different locations and times at Vernagtferner (Austria). At frequencies higher than  $10^{-2}$  Hz the spectra also fits very well with the standard spectra. That means the basic turbulence theory might be fulfilled. But the range of energy production shows characteristic deviations which can be related to the special entrainment processes mentioned above. In addition, the maximum size of the eddy seems to be limited to the dimension of the melting surface.

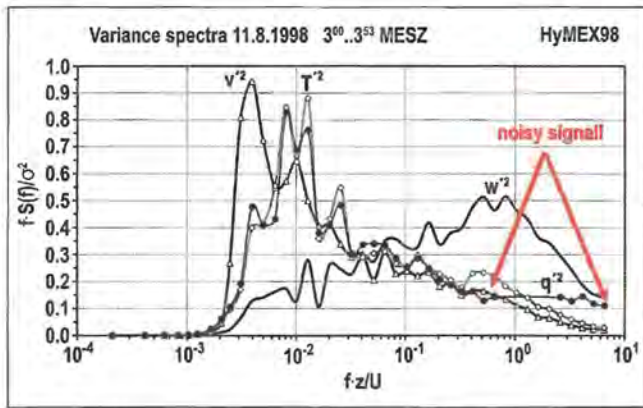


**Figure 5:** Normalised variance spectra of air temperature (T), specific humidity (q), horizontal wind speed (v) and vertical wind speed (w). The labeled section within the inertial subrange of the spectra of q clearly indicates some noise, which is superimposing the signal

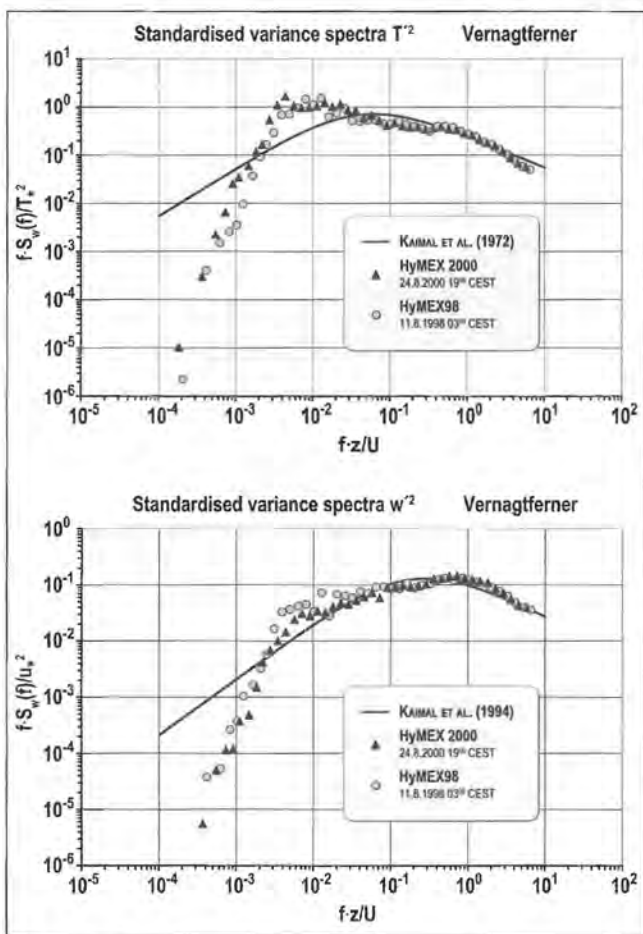


**Figure 6:** Standardised variance spectra of air temperature (top) and vertical wind speed (bottom) in comparison with standard spectra according to KAIMAL et al. (1972) and KAIMAL AND FINNEGAN (1994).

The kinematic flux is defined by the covariance and therefore by the integral of the cospectrum. It can be discretely calculated using the real part (Re) and the imaginary part (Im) of the concerned quantities:

$$Co_{ab} = \text{Re}(S_a) \cdot \text{Re}(S_b) + \text{Im}(S_a) \cdot \text{Im}(S_b) \quad [4.3].$$

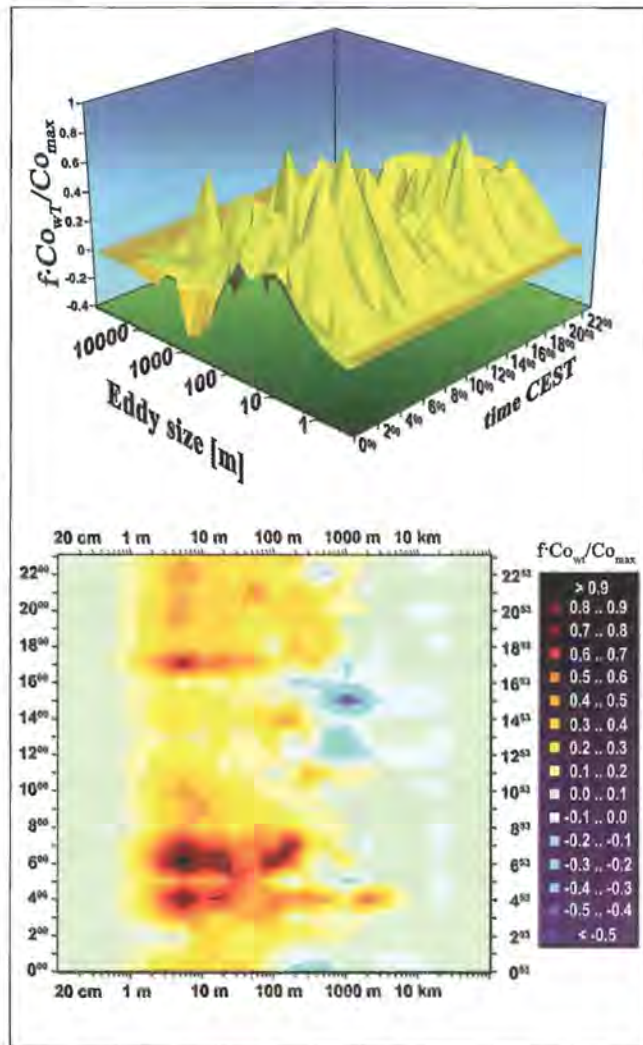


**Figure 7:** Diurnal variation of normalised cospectra of the sensible heat flux (Vernagtferner, Austria).

Standardisation of the cospectra using the mean wind speed as a scaling factor enables the illustration of the footprint and the detection of the source area of the flux. Fig. 7 shows the distribution of the flux intensity of sensible heat versus the characteristic eddy size and time. Mapping the result clearly shows that the fetch for the main fraction of the flux is within a distance of 500 m upwind. The maximum of the sensible heat flux occurs in the period at the second part of the night when the catabatic forcing becomes maximal. At noon one can detect bands where the contribution of the flux becomes negative. These have their source at limited snow free areas in the summit regions, where a hot rock surface enables ascending air masses forced by convection. This contribution has to be removed from the total covariance as it is not related to the melting surface. The amazing analogy between the turbulent structure of the enthalpy distribution and that of moisture suggests that the area below the standardised cospectrum of sensible heat has to be congruent with that of latent heat. If not, this may be an indicator of technical errors or an inadequate response time of the probe. As shown in Fig. 8, the close correlation between the fluctuation of air temperature and humidity justifies the application of

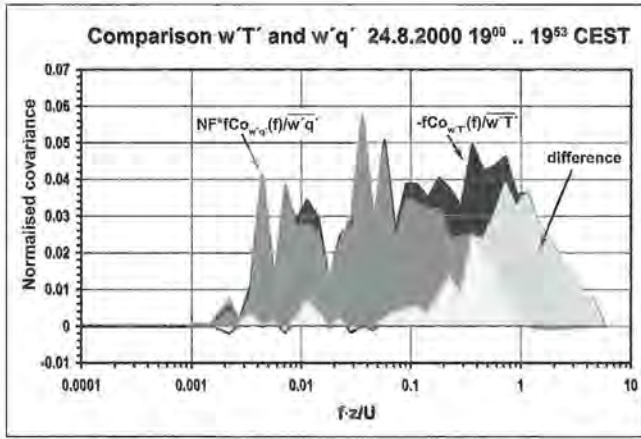


Figure 8: Comparison between the normalised cospectra of sensible and latent heat (Vernagtferner, Austria).

the following procedure based on the *Bowen ratio* (Bowen 1926) to estimate the covariances of the latent heat flux proportional to that of the sensible heat flux:

$$\overline{w'q'} = \overline{w'T'} \frac{\sigma_q}{\sigma_T} \quad [4.4]$$

Since there are much more difficulties to measure humidity fluctuations than these of temperature or wind speed, eq. 4.4 seems to be a suitable approach to fill inevitable gaps in the data recordings.

## 5. A bulk-parameterization approach of the turbulent fluxes

Extensive analysis of experimental data leads to the conclusion, that the concept to model the turbulent transport presented here may be suitable (WEBER 2005). In the following, the parameterizations are tested and improved.

First it is a fact that the covariance can be split into the product of a correlation coefficient  $\mathbf{R}$  and the variances of each component:

$$\overline{a'b'} = \sum_{k=0}^{N-1} Co_{ab}(f_k) = R_{ab} \cdot \sigma_a \cdot \sigma_b \quad [5.1]$$

This approach is better known as the “flux-variance-relationship” (FOKEN 2003). It is assumed that a satisfying relationship of the following type can be found:

$$\sigma_T \approx T - T_S \quad \text{and} \quad \sigma_w \approx \sigma_u \approx \bar{U} \quad [5.2]$$

Then the following simple bulk-equation can be derived:

$$H = \rho \cdot c_p \cdot R_{wT} \cdot f(U) \cdot f(T - T_0) \quad [5.3]$$

Eq. 5.3 has a similar structure to the one of eq. 2.5. The main difference is the unknown correlation coefficient  $\mathbf{R}$  which must have a close relation to the exchange coefficient  $\mathbf{C}$  of eq. [2.5].

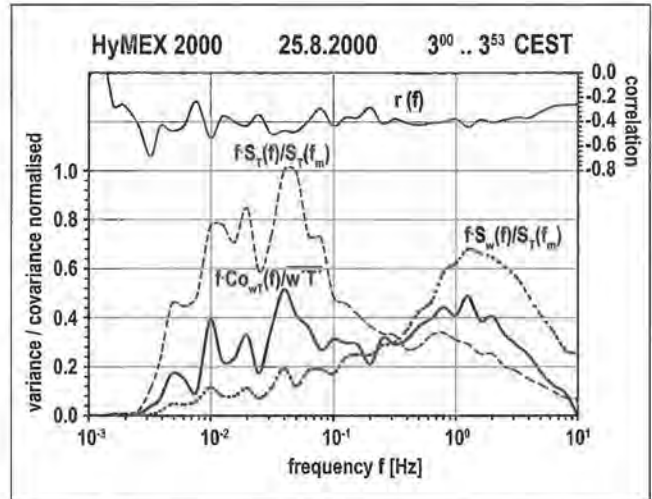


Figure 9: Combination of the cospectra  $w'T'$  derived from the variance spectra of  $T$  and  $w$ . On top: the resulting coefficient of correlation (Vernagtferner, Austria).

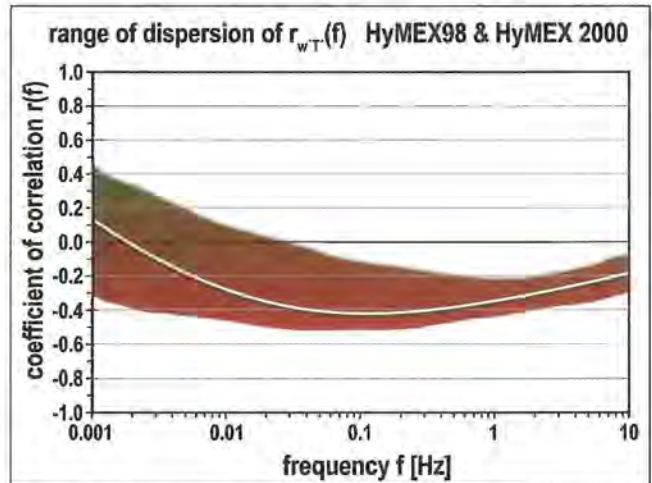


Figure 10: Range of dispersion of the correlation coefficient between the variances of temperature and vertical wind speed based on 240 samples (Vernagtferner, Austria).

Fig. 9 shows that  $\mathbf{R}$  is not a significant function of frequency. It can be seen that it is almost constant over the entire frequency range. But there may exist an important dependency on the intensity of turbulence and therefore on atmospheric stability. The observed range of dispersion of the correlation coefficient based on the entire dataset of the experiments HyMEX98 and HyMEX2000 (240 values) is depicted in Fig. 10. The maximal variation can be found at the range of frequencies which equals that for production of energy. Thus a simple linear function must be sufficient to approximate the influence of the stability to the mean correlation coefficient.

The necessary functions can be determined by a simple linear regression analysis (Fig. 11). Equations [5.5] to [5.6] are simple bulk functions to calculate sensible and latent heat fluxes, the constants are empirical. The correlation coefficient can be replaced either by a constant value estimated  $\mathbf{R}_{wT} = -0.35$ , or better by the result of eq. [5.4] which considers the observed influence of the relationship between stability, wind speed and turbulence evolution.

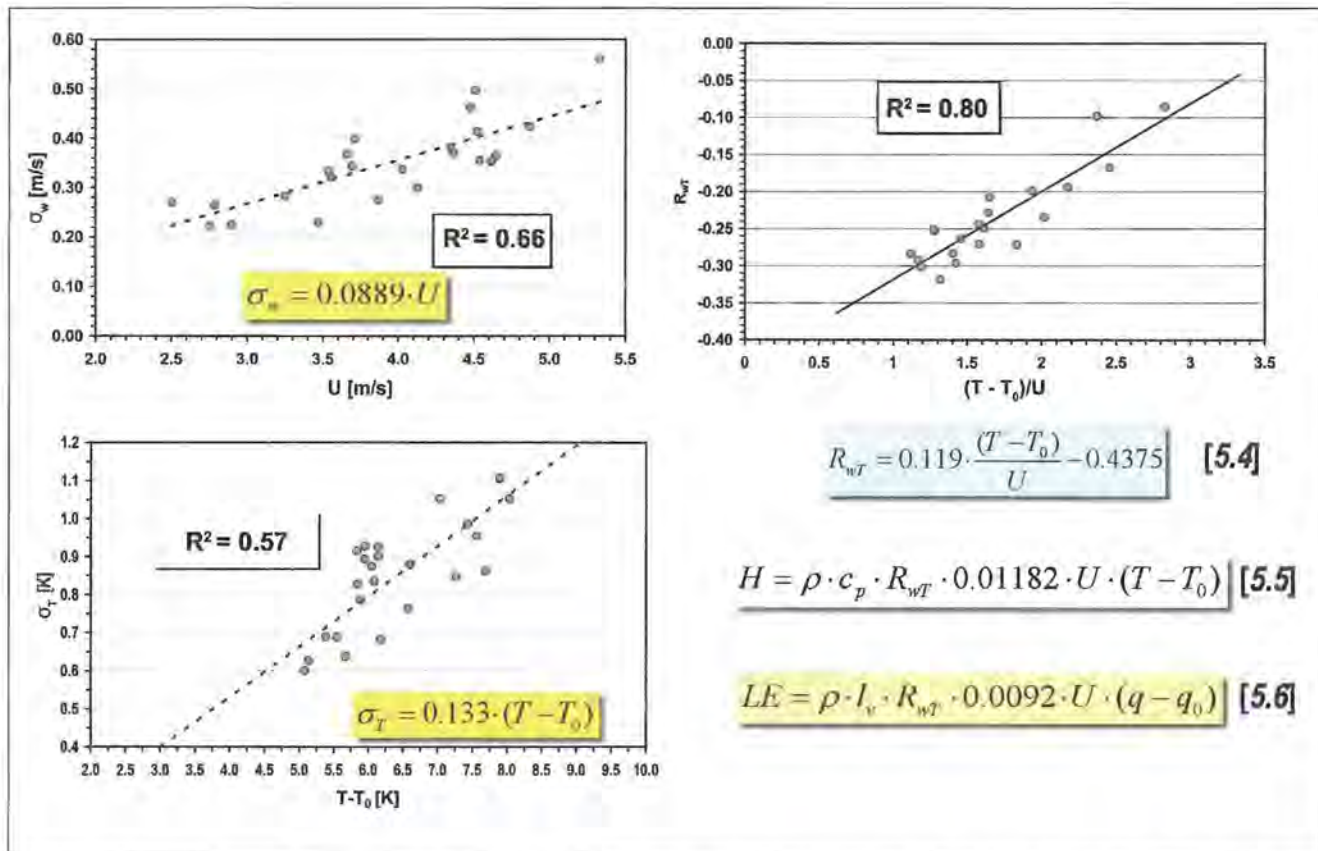


Figure 11: Regression analysis to derive bulk formulas for the sensible and latent heat fluxes (data from Vernagtferner, Austria).

Table 1: Daily mean values of the sensible heat flux  $H$  [ $W/m^2$ ] at two different locations 2.5 m a.g. at Vernagtferner determined by different methods. 1): reference flux directly calculated from eddy correlation measurements ( $\pm$  estimated range of error); 2) flux calculated using eq. [2.7] and hourly means of air temperature, surface temperature and wind speed at 2.5 m a.g.; 3) application of the parameterization eq. [5.5] and a constant value  $-0.35$  for the correlation coefficient,  $R$ ; 4) utilization of eq. [5.5] and additionally of the parameterization of the correlation coefficient  $R$  using eq. [5.4]. (Excerpt from WEBER 2005).

Date	9.8.1998	10.8.1998	11.8.1998	24.8.2000	25.8.2000	26.8.2000
ECM flux <sup>1)</sup>	27.5 $\pm$ 15	34.7 $\pm$ 15	41.0 $\pm$ 15	61.7 $\pm$ 10	60.0 $\pm$ 10	45.8 $\pm$ 15
Eq. [2.7] <sup>2)</sup>	77.93	82.95	82.41	71.40	62.50	63.50
$R_{wT} = 0.35$ <sup>3)</sup>	49.96	83.02	54.80	79.69	71.26	54.80
Eq. [5.5] + [5.4] <sup>4)</sup>	29.64	36.89	48.63	67.40	68.07	55.37

Table 1 gives criteria of assessment to the performance of the different parameterizations by comparing daily means of the fluxes to the directly measured reference. The methods neglecting the influence of the turbulence efficiency, the simple approach eq. [2.7] and eq. [5.5] using a constant correlation coefficient tend toward overestimate the real sensible heat flux. Introduction of the square root of the horizontal wind speed is not sufficient to correct the effect of the flow to get more and more laminar with increasing speed.

Additional sources of error result from not considering the local influence of the air density using eq. [2.7]. It can be seen by comparing the values of 1998 to that of 2000, which are archived at different locations and elevations. The more sophisticated parameterization [5.5] and [5.4] matches up best to the measurements.

An example of the application of the three different approaches to calculate the hourly diurnal variation of the fluxes of sensible and of latent heat is shown in Fig. 12. Comparison with the result from direct measurements shows the best fit by using the sophisticated parameterization. This is valid as well for the flux of sensible heat as for the flux of latent heat, despite of some overestimation of the magnitude of flux near its maximum. Especially periods characterized by weak turbulence are not very well represented using algorithms, where the variation of the correlation coefficient is not considered. But overall all approaches used here are applicable for modelling the turbulent fluxes while accurate input data at 2 – 2.5m a.g. is available. To validate the approaches presented here, very accurate direct measurements have been used. This must be considered if the performance of the parameterization is estimated.

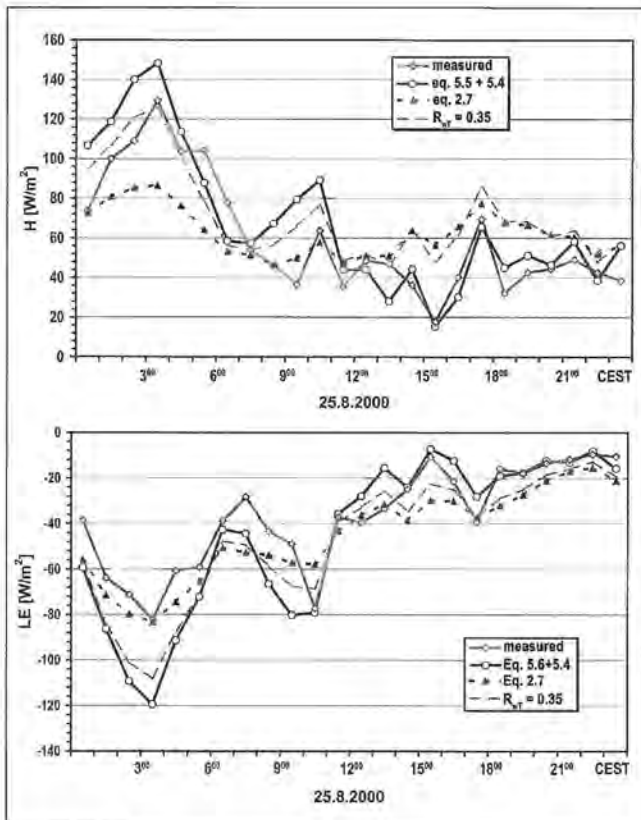


**Figure 12:** Application of the bulk approaches to calculate the sensible (top) and latent heat fluxes (bottom) using eq. 5.5, 5.4, 5.6, 5.4, 2.7, 5.5 and 5.6 with a constant  $R_s$ . Comparison with values measured by eddy correlation (Vernagtferner, Austria).

## 6. Conclusions

For distributed, physically based modelling of snow- or icemelt robust and accurate algorithms to calculate the energy balance terms are required. The formula to determine the turbulent fluxes presented here is now implemented into the snow model component of the Danubia decision support system developed in the GLOWA-Danube project (MAUSER & STRASSER 2005) where it seems to work successfully. It fulfils requirements like representing the dependence of the fluxes on altitude. Further it gives a better fit with the measurements than common approaches used so far.

The approach claims **not to be** "universal". Probably it is only applicable to the area where it was derived. Additional measurements may be expensive but could confirm the results found in this study.

## Acknowledgments

The author would like to thank all colleagues who contributed to this study and assisted during the field experiments. Financial support was provided by the German Research Foundation and Federal Ministry of Education and Research **bmb+f** as part of the GLOWA-Danube project.

## References

- BOWEN, I.S. (1926): The ratio of heat losses by conduction and by evaporation from any water surface. *Physical review*, 27, 779 – 787.
- BRAUN, L.N., ESCHER-VETTER, H., HEUCKE, E., SIEBERS, M & WEBER, M. (2004): Experiences with the new "Vernagtferner" hydro-meteorological station. In: OERLEMANS & TIJM-REIJMER: Book of extended abstracts of presentation at the Workshop "Automatic Weather Stations on Glaciers", Pontresina, 28 to 31 March 2004, IMAU, 38 - 44.
- BUSINGER, J.A., WYNGAARD, J.C., IZUMI, Y. & BRADLEY, E.F. (1971): Flux-profile relationships in the atmospheric surface layer. *J. Atm. Sci* 28: 181 – 189.
- DYER, A.J. (1974): A Review of Flux-Profile-Relationships, *Boundary Layer Meteorology*, 7, 363-372.
- ESCHER-VETTER, H. (1980): Der Strahlungshaushalt des Vernagtferners als Basis der Energiehaushaltsberechnung zur Bestimmung der Schmelzwasserproduktion eines Alpengletschers. *Münchener Universitäts-Schriften, Fachbereich Physik - Univ. München Met. Inst., Wiss. Mitt. Nr. 39*, 117 S.
- ESCHER-VETTER, H. (2000): Modelling meltwater production with a distributed energy balance method and runoff using a linear reservoir approach - results from Vernagtferner, Oetztal Alps, for the ablation seasons 1992 to 1995. *Zeitschr. f. Gletscherkunde und Glazialgeologie*, 36, 119-150.
- ESCHER-VETTER, H. & WEBER, M. (2000): Measuring and modelling the Vernagtferner energy balance components: results from HYMEX98 and the PEV model. *Snow and ice. Österreichische Beiträge zu Meteorologie und Geophysik 23* (2000) preprints, 111.
- FOKEN, T. (2003): *Angewandte Meteorologie – Mikrometeorologische Methoden*. Springer Verlag, Berlin, ISBN 3 540 00322 3, 289 S.
- KAIMAL, J.C. & BUSINGER, J.A. (1970): Case studies of a convective plume and a dust devil. *J. Appl. Meteorol.*, 9, 612-620.
- KAIMAL, J.C., WYNGAARD, J.C., IZUMI, Y & COTÉ, O.R. (1972): Spectral characteristics of surface-layer turbulence. *Quart. J. Royal Meteorol. Soc.*, 98, 563-589.
- KAIMAL, J.C. & FINNIGAN, J.J. (1994): *Atmospheric Boundary Layer Flows*. Oxford University Press, New York, 289S.
- KUZMIN, P.P. (1961): *Melting of snow cover*. Translated from Russian by Israel Program for scientific Translation, 1972, 290 S.
- MONIN, A.S. & OBUKHOV, A.M. (1958): Fundamentale Gesetzmäßigkeiten der turbulenten Vermischung in der bodennahen Schicht der Atmosphäre. In: GOERING, H. (Hrsg): *Sammelband zur statistischen Theorie der Turbulenz*. Akademie-Verlag, Berlin, 199-224.
- OERLEMANS, J. (2001): *Glaciers and Climate Change*. A.A. Balkema Publishers, Lisse/Abingdon/ Exton/ Tokyo, ISBN 90 265 1813 7, 148 S.
- OHATA, T. (1991): The effect of glacier wind on local climate, turbulent heat fluxes and ablation. *Zeitschr. f. Gletscherkunde und Glazialgeologie*, 25 (1), 49-68.

- STRASSER, U., ETCHEVERS, P. & LEJEUNE, Y. (2002): Intercomparison of two Snow Models with Different Complexity Using Data from an Alpine Site. In: *Nordic Hydrol.*, 33 (1), 15-26.
- ROEDEL, W. (2000): *Physik unserer Umwelt – die Atmosphäre*. Springer Verlag, Berlin, Heidelberg, 498S.
- STULL, R.B. (1988): *An Introduction to Boundary Layer Meteorology*. Kluwer Academic Publishers, Dordrecht, ISBN 90 277 2769 4, 666p.
- TAYLOR, G.I. (1938): The spectrum of turbulence. *Proc. Royal. Soc. London*, A164, 476-490.
- VAN DER HOVEN, I. (1957): Power spectrum of horizontal wind-speed in the frequency range from 0.0007 to 900 cycles per hour. *J. of Meteorol.*, 14, 160 - 164.
- WEBER, M. (2005): Mikrometeorologische Prozesse bei der Ablation eines Alpengletschers. Dissertation, Institut für Meteorologie und Geophysik der Universität Innsbruck, 319p (<http://www.glaziologie.de/publikat/klima.html>)
- WEBER, M. AND KUHN, M. (2005): Glowa-Danube: Modelling snow cover and glaciers within the catchment area of Passau-Achleiten gauge. In: *GLOWA-Danube status report phase II, 2004 – 2005*, ([http://www.glowa-danube.de/PDF/reports/statusreport\\_phase2.pdf](http://www.glowa-danube.de/PDF/reports/statusreport_phase2.pdf))

## 18 Measurement network in the Berchtesgaden National Park: the example of Kühroint Measurement Station

BENNO WIESENBERGER, WOLFRAM SOMMER

Sommer GmbH & Co KG, Straßenhäuser 27, A-6842 Koblach, Austria

### Overview

Extending over 210 km<sup>2</sup>, the Berchtesgaden National Park is located in south-eastern Bavaria, not far from the German-Austrian frontier. Research projects and the development of geographic information systems require the acquisition of environmental data there. As far as possible, data collection is to continue throughout the entire year in a fail-safe manner.

So, modern measurement stations were installed in Berchtesgaden National Park in December, 2004. These installations consist of an anemometry station on Stuhljochgrat (Stuhljoch Ridge) at 2520 m a.s.l. and a main measuring field with snow sensory technology on the edge of an alpine meadow on Kühroint at 1420 m a.s.l. Data from both measuring stations are collected at the main measuring field and retrieved over GSM modem by the Avalanche Alert Service of the Bavarian Environmental Protection Agency (Bayerisches Landesamt für Umwelt LfU, Augsburg) on an hourly basis.

### Sensors and measurements

#### „Stuhljochgrat“ anemometry station - 2520 m a.s.l.

The installation is operated all the year round with the help of a 60W solar panel.



Picture: Lawinenwarnzentrale Bayern

Sensors	Measurement
Air temperature / humidity	Air temperature [°C]
	Air humidity [%]
Wind direction / speed	Wind direction [degree]
	Wind speed [m/s]
	Squall [m/s]
Electric power supply	Battery voltage [V]

#### „Kühroint“ Main Measuring Field - 1420 m a.s.l.

Power is supplied over a 230 VAC mains supply.

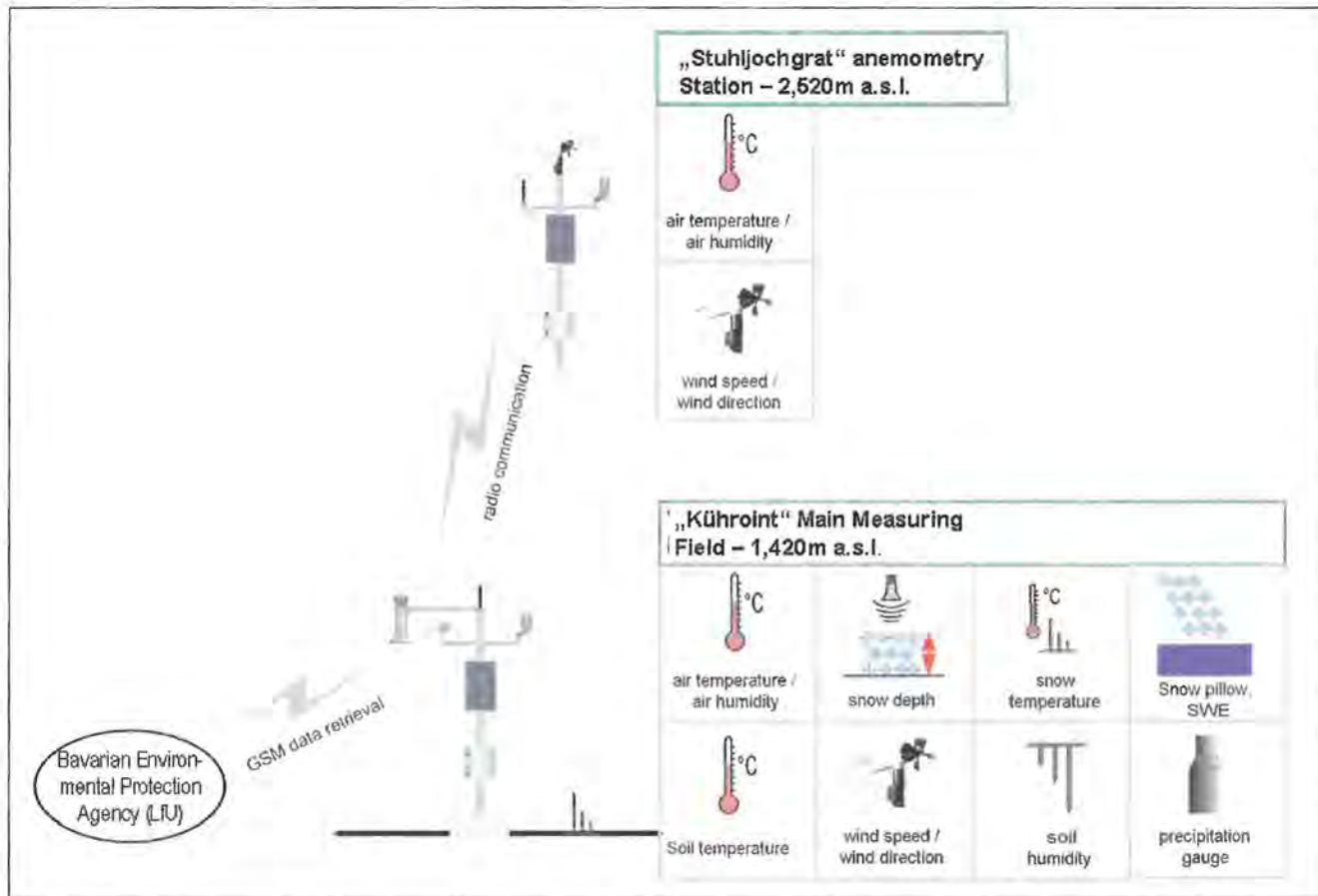
Sensors	Measurement
Air temperature / humidity	Air temperature [°C]
	Air humidity [%]
Wind direction / speed	Wind direction [degree]
	Wind speed [m/s]
	Squall [m/s]
Precipitation gauge with heating and wind protection	Precipitation [mm]
Global radiation	Direct radiation [W/m <sup>2</sup> ]
	Reflect radiation [W/m <sup>2</sup> ]
Snow pillow	Snow-water-Equivalent [mbar]
Ultra sonic snow depth sensor	Snow depth [cm]
Soil temperature	Temperature 2 cm [°C]
	Temperature 5 cm [°C]
	Temperature 10 cm [°C]
	Temperature 20 cm [°C]
	Temperature 50 cm [°C]
Snow temperature	Snow temperature 0 cm [°C]
	Snow temperature 20 cm [°C]
	Snow temperature 40 cm [°C]
	Snow temperature 60 cm [°C]
	Snow temperature 80 cm [°C]
Soil humidity	Measurement 5 cm [Vol.-% water content]
	Measurement 20 cm [Vol.-% water content]
	Measurement 50 cm [Vol.-% water content]



Picture: Helmut Franz

## Data acquisition and transmission

Data from the Stuhljochgrat anemometry station are transmitted by radio to the central data acquisition station at the Kühroint measuring field and stored there. The central acquisition stations data queries are performed automatically over GSM modem.



## Future prospects

In the future, new technology will decrease the operating expenses of the online measuring network while allowing data query intervals to be reduced. Query intervals in the minute range are possible using GPRS solutions combined with radio networks for areas outside the GPRS network coverage area. By taking advantage of

data flat-rates, GPRS query costs can be considerably reduced in comparison to GSM query costs. Starting in the autumn of 2007, Sommer will be offering complete solutions based on this technology, covering the station on to data transmission and data analysis.



The „Kühroint“ Main Measuring Field 1420 m a.s.l. in spring 2007

(Foto by © Peter Neusser)

## 19 Field trip to the Ice Chapel in the National Park Berchtesgaden

Saturday, Oktober 7, 2006

HELMUT FRANZ, MATTHIAS BERNHARDT,  
MONIKA PRASCH, VOLKMAR KONNERT AND  
ULRICH STRASSER

### 1. Climate, Hydrology and Geology

The Berchtesgaden National Park is located in southeast Germany in the Free State of Bavaria. The park was founded in 1978 and comprises an area of approximately 208 km<sup>2</sup>. The montane to high alpine area of the National Park and of the associated biosphere reserve includes the massifs *Watzmann* (2713 m a.s.l.) and

*Hochkalter* (2606 m a.s.l.) as well as parts of the massifs *Hoher Göll*, *Hagengebirge*, *Steinernes Meer* and *Reiteralm*. These massifs are separated by deep valleys characterized by extensive forests. The area reaches up to the nival zone, the *Blaueisgletscher* being the northernmost glacier of the Alps.

The climate of the National Park area is subject to significant spatial variability, strongly influenced by the relief gradient of more than 2000 m. Small scale local differences are caused by the specific location in the mountainous landscape, the position to windward or lee of the prevailing winds, and solar incidence angles. The observed mean annual temperature is 8°C, precipitation amounts to 1650 mm in the valley areas.

The bedrocks of the *Berchtesgadener Alps* mainly are of triassic origin, the *Dachstein* limestone being dominant. It forms the largest parts of the summit regions, the high plateau areas and the steep walls like the famous east face of the *Watzmann*. Karst is common and leads to expanded cave systems in the underground.



**Figure 1:** Aerial infrared-photograph of *Eisbachtal* with the breakpoints of the field trip in the National Park Berchtesgaden: *Königssee* (1), Peninsula of *St. Bartholomä* (2), Mountain forest (3), view to the ice chapel (4) and ice chapel (5).



Figure 2: The peninsula of St. Bartholomä with the Watzmann mountain massif.

Archiv Nationalparkverwaltung

## 2.1 Tourism in the Königssee region

The most important factors for local tourism are: the *Königssee*, the church of *St. Bartholomä* and the mountain massifs *Watzmann* and *Steinerenes Meer*. A fleet of 21 electrical boats cross the *Königssee*. Most popular outdoor activities comprise walking, hiking and mountain climbing. The hiking path network of more than 200 km is supported and marked by the National Park Administration. In 2006, the National Park was visited by about 1.1 million guests. 24.000 inhabitants are living in the five municipalities of the region. Most of the income is obtained by tourism, approximately 80% during the summer season. A regional-economical analysis showed that the National Park oriented tourism generates an annual income of 4.6 Mio Euros, associated with approximately 200 full time jobs in the region.

## 3. Habitat levels and forestry

Rock and debris cover approximately 20 % of the total Park area. In the alpine and sub alpine zone expansive grasslands and dwarf pines dominate. The altitudinal belt between forest and timber line widened mainly through grazing. On carbonate rock, dwarf pines dominate as replacement for forest companies.

44% of the protected area of the National Park is covered by forests. In the sub alpine belt between 1400 and 2000 m a.s.l., spruces as well as a mixture of spruces and larches are common. Larches mixed with Swiss

stone pines cover some smaller areas. In the montane level between 700 and 1400 m a.s.l. a mixture of deciduous and coniferous forests prevails. The dominating species are red beech (*Fagus sylvatica*), white fir (*Abies alba*), spruce (*Picea abies*) and sycamore (*Acer montanus*). This belt is characterized by the significant anthropogenic use in former decades. Use of wood for the saline in Berchtesgaden, hunting for trophies as well as agriculture and forestry by the mountain farmers caused this change. Currently the unnatural spruce mono cultures are actively developed into mountain mixed woodlands by the National Park Administration.

All animal species typical for the northern limestone Alps can be found in the National Park. Up to now approximately 55 kinds of mammal, over 100 breeding birds and 40 kinds of migratory bird, 15 types of fish (mainly in the *Königssee*) as well as 8 amphibians and 7 kinds of reptile are proven. Among them are typically alpine breeds such as the chamois and the capricorn, the groundhog, the mountain hare, the snow vole, the alpine snow grouse and many more. The formerly typical predators bear, lynx and wolf were eradicated in the middle of the 19th century. By contrast, the density of doe, deer and chamois has been highly increased by intense preserving measures since this time.

The systematic change of the spruce mono cultures into natural mountain mixed forests with domestic species is an aim of the National Park Authority. To assure a sufficient natural regeneration doe, chamois and deer are hunted. It is planned to continue this development within the next decades.

#### 4. Alpine farming

At the beginning of the 19th century, 91 alps were located in the area of the National Park. Presently, 35 alps are still managed, the others were given up for economic reasons. Causes for this were poor soils, short vegetation times, difficult accessibility, increasing water scarceness and karst formation. Proprietor of these faces is the Free State of Bavaria, represented by the National Park Administration. The usage rights of the alpine farmers are several hundred years old and entitle them to use the mountain pastures. The alp areas are now attracting people for recovery. Besides, they accommodate a high number of animal and plant species. Therefore the preservation of the alps is highly desired for both the protection of species and for the conservation of the natural scenery, if it is geared to the principles of the traditional mountain pasture.



Figure 3: On the way to the ice chapel (Picture: Markus Weber).

#### 5. The Ice Chapel

The destination of the field trip, the famous ice chapel, can be reached from *St. Bartholomä*. It is located at an altitude of 880 to 960 m a.s.l. and its existence traces back to the supply of large masses of avalanche snow from the 1900 m high east face of the *Watzmann* mountain. Huge masses of snow are blown over the summit ridge, which reaches perpendicular to the prevailing wind directions, and deposited leeward in this rock face which acts like a funnel for the frequent avalanches. The respective accumulation amounts to a multiple of the actual local precipitation and takes place in winter and spring. In summer, the entire ice chapel is ablation area, but the body remains all over summer and does not significantly change its size. The ice chapel has glacier-like features like a glacier ice structure or crevasses, however the latter are due to shear stresses. Bedrock motion has not been observed. At the outlet, a church-like hall develops during summer due to melt water and warm air masses which flow through the ice body. It is dangerous, yet possible, to enter this hall and follow it up until the back rock wall where the main melt-water stream comes down. The ice chapel is a unique local snow feature, and it is supposed to better resist climate change induced retreat than most of the small glaciers in the region, albeit its very low position and small extent.

#### Acknowledgements

All field trip participants want to thank Ruth Weidinger for the organisation of the bus trip.



Figure 4: View to and outwards of the ice chapel. (Picture inside the ice chapel: Dr. Max Wisshak).

# Glossar

## Englisch

ablation  
advection  
albedo  
anemometer  
atmospheric circulation patterns  
avalanche  
avalanche risk  
backscatter  
blast  
bulk formula  
Empirical formula for calculating energy exchange which depends on meteorological parameters.  
The bulk-formula describes the energy exchange between an ice or water surface and the surrounding atmosphere.  
It is based on the assumption of a uniform (linear) gradient within the layer considered.  
buoyancy  
canonical correlation analysis (CCA)  
CCA is a way of measuring the linear relationship between two multidimensional variables by finding linear combinations of each set of variables that yields the highest possible correlation.  
capillary rise  
catchment  
circulation pattern  
cohesion  
cohesive  
conductivity  
convection  
cornice  
cospectrum (pl. cospectra)  
crest  
crevasse  
cross section  
debris  
depletion period  
depth hoar  
depth hoar crystal  
discharge  
discharge rate  
downstream  
drag force  
drainage  
eigenanalysis  
elevation  
emissivity  
empirical orthogonal function (EOF)  
The method of empirical orthogonal function (EOF) analysis is a decomposition of a data set in terms of orthogonal basis functions which are determined from the data. The method is the same as performing a principal components analysis on the data, except that the EOF method finds both time series and spatial patterns.

## Deutsch

Ablation  
Advektion  
Albedo, Rückstrahlvermögen  
Windmesser  
atmosphärische Zirkulationsmuster  
Lawine  
Lawinenrisiko  
Rückstreuung  
Böe, Luftstoß, Druckwelle  
Bulk-Formel  
Bei der Berechnung des Energieaustausches zwischen Eis- oder Wasseroberflächen und der angrenzenden Atmosphäre werden die Austauschkoefizienten der Energiebilanzgleichung durch empirisch ermittelte Funktionen in Abhängigkeit von meteorologischen Grundgrößen berechnet.  
Die Berechnung basiert auf der Annahme eines linearen Gradienten innerhalb der untersuchten Schicht.  
Auftrieb, Spannkraft  
kanonische Korrelationsanalyse  
Mit dem Verfahren der kanonischen Korrelationsanalyse lässt sich die Beziehung zwischen zwei Mengen von jeweils metrisch skalierten Variablen untersuchen. Dabei werden zwei Sets von Variablen jeweils linear kombiniert, so dass die Korrelation maximal wird.  
kapillarer Aufstieg  
Einzugsgebiet  
Zirkulationsmuster  
Kohäsion (Zusammenhang)  
zusammenhängend  
Leitfähigkeit  
Konvektion  
Wechte  
Co-Spektrum  
Grat  
Gletscherspalte  
Querschnitt, Wirkungsquerschnitt; Profil  
Geröll, Schutt  
Ablationsperiode  
Tiefenreif  
Becherkristall  
Abfluss, Ablauf  
Abflussrate  
flussabwärts  
Zugkraft  
Entwässerung; Abfluss  
Eigenwertanalyse  
Höhe  
Emissionsvermögen  
empirische Orthogonalfunktion  
Statistische Methode der zeitlichen und räumlichen Datenanalyse, die es ermöglicht, von einem Regressionsmodell mit korrelierten Einflussgrößen zu einem unkorrelierten Modell mit möglichst wenigen Einflussgrößen und möglichst hoher erklärter Varianz überzugehen. Sie entspricht der Methode der Hauptkomponentenanalyse.

equinoctial seasons  
evaporation  
excess energy  
face  
fence  
flood wave propagation  
fracture  
freeze  
gauging station  
glacial cirque area  
glacier tongue  
global radiation  
Gumbel distribution

The Gumbel distribution is a special type of the Generalized Extreme Value distribution.

It's a distribution of an extreme order statistic for a distribution of elements.

gust  
headwater  
heat flux  
impermeable  
impurity  
inclination  
inclined  
inflow  
interception  
interflow  
irrigation scheme  
jet stream  
laminar  
lapse rate  
large-scale  
leaf area index  
matter  
mesh  
mountainside  
multinomial logit model

The generalisation of the logit model to more than one alternative is referred to as multinomial logit model. A logit model describes the choice probability of a given individual to choose a certain alternative. The model is a discrete choice model which assumes utility-maximizing behaviour, and the error terms of the utility functions are independent and identically Gumbel distributed (s. Gumbel distribution).

#### NAO North Atlantic Oscillation

The North Atlantic Oscillation (NAO) is a climatic phenomenon in the North Atlantic Ocean of fluctuations in the difference of sea-level pressure between the Icelandic Low and the Azores High. It controls the strength and direction of westerly winds and storm tracks across the North Atlantic.

#### NAOI North Atlantic Oscillation index

To measure the difference in the pressure (between Ponta Delgada (Azoren) und Reykjavík (Island)) the NAO-Index (positive/negative) is established. It measures westerly winds on the North Atlantic, which are important for the European climate, especially in winter.

Äquinoktialjahreszeiten; Übergangsjahreszeiten  
Verdunstung  
Energieüberschuss  
Wand (eines Berges)  
Zaun  
Hochwasserwellenausbreitung  
Bruch  
frieren  
Messstation  
Karbereich  
Gletscherzunge  
Globalstrahlung  
Gumbel Verteilung

Die Gumbel-Verteilung stellt einen Fall der Extremwertverteilung dar (z.B. berechnet sie den in einem Zeitraum T zu erwartenden höchsten Messwert).

Böe, Windstoß  
Oberlauf  
Wärmefluss  
undurchlässig  
Fremdstoff, Verunreinigung  
Neigung  
schräg, geneigt  
Zufluss  
Interzeption  
Zwischenabfluss; unterirdischer Abfluss  
Bewässerungsplan, Bewässerungsmaßnahme  
Jetstream; Strahlstrom  
laminar, ohne Durchmischung  
Temperaturgefälle  
großmaßstäbig  
Blattflächenindex  
Material  
Messnetz, Maschenweite, Masche  
Berghang  
Multinomiales Logit Modell

Das Multinomiale Logit Modell stellt eine Erweiterung des Verfahrens der binären logistischen Regression mit mehr als zwei Ausprägungen dar. Das Modell beschreibt die Wahrscheinlichkeit eines Entscheidungsträgers für eine Handlungsalternative bei zwei Alternativen. Dabei wird angenommen, dass der Entscheidungsträger einen maximalen Nutzen anstrebt und dass die Fehler Gumbel verteilt sind (s. Gumbel Verteilung)

#### Nordatlantische Oszillation

Unter der Nordatlantischen Oszillation (NAO) versteht man die Schwankung des Druckverhältnisses zwischen dem Islandtief im Norden und dem Azorenhoch im Süden des Nordatlantiks. Sie beeinflusst Stärke und Richtung von Westwinden und Tiefdruckgebieten über den Nordatlantik.

#### Nord Atlantik Oszillation Index

Als Maßeinheit für die Differenz der standardisierten Druckanomalien (zwischen Ponta Delgada (Azoren) und Reykjavik (Island)) hat man den so genannten NAO-Index (positiv/negativ) eingeführt. Er misst die Westwinddrift auf dem Nordatlantik, welche für das Klima in Europa, besonders im Winter, entscheidend ist.

nivo...  
 outflow  
 out-of-phase  
 overcast  
 Penman-Monteith equation  
   Method for determining the actual  
   evapotranspiration  
 percolation  
 permeability  
 perturbation  
 plume, convective plume  
   Convective plumes are coherent vertical structures  
   of warm rising air having diameters and depths  
   on the order of the surface layer  
   depth ~100m.  
 pluvio...  
 polling  
 power plant  
 radiation budget  
 radiative flux  
 rawinsonde  
   special kind of a radiosonde  
 reptation  
 ridge  
 rime  
 riparian area  
 routing delay  
 rugged  
 runoff  
 run-of-river power plant  
 saltation  
   Snow particles are lifted from the bed by eddies.  
   If they are airborne they are following ballistic  
   trajectories.  
 shear stress  
 slab (avalanche)  
 sleet  
 slope  
 snow  
 snow course  
 snow covered area  
 snow drift  
 snow grain  
 snow gun  
 snow pack  
 snow pillow  
 snow pit  
 snow pole  
 snow water equivalent  
   snow water equivalent (swe) is the amount of water contain-  
   ed within the snow pack by melting the snow pack with  
   known height and density  
 snowmelt  
 squall  
 stress  
 sublimation  
 summit  
 surface creeping  
   Motion of Snow grains which are still in contact  
   with the bed  
 surface flow

schnee..  
 Abfluss  
 phasenverschoben  
 bewölkt  
 Penman-Monteith Gleichung  
   Ansatz zur Bestimmung der aktuellen  
   Evapotranspiration  
 Perkolation  
 Durchlässigkeit  
 Störung  
 Thermikblase  
   Eine Thermikblase entsteht durch eine lokal stark  
   überhitzte bodennahe Luftschicht, die vom Boden  
   abhebt und aufsteigt (thermische Konvektion).  
   Sie haben in etwa einen Durchmesser von 100 m.  
 niederschlags....  
 Abfragen (von Daten)  
 Kraftwerk  
 Strahlungsbilanz  
 Strahlungsfluss  
 Rawinsonde  
   spezielle Radiosonde  
 Siehe surface creeping  
 Gebirgskamm  
 Raueis, Raureif, Reif  
 Ufergebiet  
 Ablaufverzögerung  
 rau  
 Abfluss  
 Laufwasserkraftwerk  
 Saltation  
   Schneepartikel werden durch bodennahe Turbulenzen vom  
   Untergrund aufgehoben und folgen daraufhin ballistischen  
   Trajektorien  
 Scherbeanspruchung  
 Schneebrett (Lawine)  
 Graupel, Schneeregen  
 Hang, Gefälle, Neigung  
 Schnee  
 Schneeprofil (horizontal)  
 schneebedeckte Fläche  
 Schneedrift, Schneeverfrachtung  
 Schneekorn  
 Schneekanone  
 Schneedecke  
 Schneekissen  
 Schnee-Messstelle (vertikal)  
 Schneestange  
 Schneewasseräquivalent  
   Das Schneewasseräquivalent (swe) ist die Wassermenge in  
   mm, die man erhalten würde, wenn man eine Schneedecke  
   mit bekannter Höhe und Dichte schmelzen würde  
 Schneeschmelze  
 Böe, Windstoß  
 Spannung  
 Sublimation, Sublimierung  
 Gipfel  
 Oberflächenkriechbewegung  
   Bewegung von Schneekörnern mit Kontakt  
   zum Untergrund  
 Oberflächenfluss

suspension  
synoptic patterns  
tetrahedral  
thawing  
timber line  
torrential  
transmittance  
transpiration  
tributary  
turbulent suspended snow  
undulated  
unsaturated zone  
upper-level airflow  
utility function  
    The basic assumption of the concept is, that the actor  
    selects from a set of available alternatives the mostly  
    preferential one to him.  
volume fraction  
vortex  
vulnerability  
  
water equivalent  
    (s. snow water equivalent)  
water level  
water supply  
water vapour partial pressure  
water vapour saturation pressure  
watershed  
wind field  
wind shear

Suspension  
Synoptische Muster  
vierflächig  
Tauen  
Baumgrenze  
reißend  
Durchlässigkeit (atmosphärische)  
Transpiration  
Nebenfluss; Zufluss  
turbulent aufgewirbelter Schnee  
wellig, gewellt  
ungesättigter Bereich  
Luftstrom höherer Schichten  
Nutzen-Funktion  
    Grundlegende Annahme des Konzepts ist, dass der Akteur da-  
    nach strebt, aus der Menge ihm zur Verfügung stehender Al-  
    ternativen die von ihm am meisten bevorzugte auszuwählen.  
Volumenanteil  
Turbulenz; Wirbel  
Verletzbarkeit, Verwundbarkeit, Schadenanfälligkeit,  
Schwachstelle, Vulnerabilität  
Wasseräquivalent  
    (s. Schneewasseräquivalent)  
Wasserstand, Pegelstand  
Wasserangebot, Wasserversorgung  
Wasserdampfpartialdruck  
Wasserdampfsättigungsdruck  
Einzugsgebiet  
Windfeld  
Scherwind

## Corresponding authors

JUDIT ASZTALOS

Institute for Hydraulic and Water Resources Engineering, Water Resources Engineering Department, Vienna University of Technology, Karlsplatz 13/222, A-1040 Vienna, Austria  
E-mail: asztalos@hydro.tuwien.ac.at

DR. HEIKE BACH

VISTA Remote Sensing in Geosciences, Gabelsbergerstr. 51, D-80333 Munich, Germany  
E-mail: Bach@vista-geo.de

MATTHIAS BERNHARDT

Department of Geography, Ludwig-Maximilians University (LMU), Luisenstr. 37, D-80333 Munich, Germany  
E-mail: m.bernhardt@iggf.geo.uni-muenchen.de

DR. ROXANA BOJARIU

National Meteorological Administration, Sos. Bucuresti-Ploiesti 97, 013686 Bucharest, Romania  
E-mail: bojariu@clicknet.ro

ANGELO COLOMBI

IREA-CNR Institute for Electromagnetic Sensing of the Environment - National Research Council, Via Bassini 15, 20133 Milano, Italy, E-mail: colombi.a@irea.cnr.it

PERE ESTEBAN

CENMA/IEA - Snow and mountain research center, Institut d' Estudis Andorrans, Av. Rocafort, 21-23. Edifici Molí, AD 600 Sant Julià de Lòria, Andorra  
E-mail: pesteban.cenma@iea.ad

HELMUT FRANZ

Nationalpark Berchtesgaden, Nationalparkverwaltung, Doktorberg 6, D-83471 Berchtesgaden, Germany  
E-mail: h.franz@nationalpark-berchtesgaden.de

CARLES GARCÍA SELLÉS

Institut Geològic de Catalunya, C/Balmes 209-211, 08006 Barcelona, Spain  
E-mail: cgarcia@igc.cat

DR. ELENA GUSEVA-LOZINSKI

Immenhoferstr. 38, D-70180 Stuttgart, Germany  
E-mail: elena.gusewa@gmx.de

DR. LINGMEI JIANG

Center for Remote Sensing and GIS, Beijing Normal University, No.19 Xijiekouwai Street, 100875 Beijing, P.R. China,  
E-mail: jiang@bnu.edu.cn

GLÒRIA MARTÍ I DOMÈNECH

Institut Geològic de Catalunya, C/Balmes 209-211, 08006 Barcelona, Spain  
E-mail: gmarti@igc.cat

LAURENT MERINDOL

Météo-France, Centre national de recherches météorologiques (CNRM/CEN), 1441, rue de la piscine, 38400 St. Martin d'Hères, France  
E-mail : laurent.merindol@meteo.fr

MONIKA PRASCH

Department of Geography, Ludwig-Maximilians University (LMU), Luisenstr. 37, D-80333 Munich, Germany  
E-mail: m.prasch@iggf.geo.uni-muenchen.de

FRANCESCO ROTA NODARI

Remote Sensing Data Engineering (RSDE), Via Washington 78, 20146 Milano, Italy  
E-mail: ronofran@hotmail.com

SUSANNE SCHMIDT

Department of Geography, University of Bonn, Meckenheimer Allee 166, D-53115 Bonn, Germany  
E-mail: s.schmidt@giub.uni-bonn.de

SIMON SCHNEIDERBAUER

dTech-Steyr, Dynamics & Technology Services GmbH, Steyrerweg 2, A-4400 Steyr, Austria  
E-mail: simon.schneiderbauer@dttech-steyr.com

DR. ULRICH STRASSER

Department of Geography, Ludwigs-Maximilians-University (LMU), Luisenstraße 37, D-80333 Munich, Germany  
E-mail: u.strasser@iggf.geo.uni-muenchen.de

MONIKA TEPFENHART

Department of Geography, Ludwigs-Maximilians-University (LMU), Luisenstraße 37, D-80333 Munich, Germany  
E-mail: m.tepfenhart@iggf.geo.uni-muenchen.de

DR. MARKUS WEBER

Commission for Glaciology of the Bavarian Academy of Sciences and Humanities, Alfons-Goppel-Str. 11, D-80539 Munich, Germany  
E-mail: Wasti.weber@kfg.badw.de

BENNO WIESENBERGER

Sommer GmbH & Co KG, Straßenhäuser 27, A-6842 Koblach, Austria  
E-mail: wiesenberger@sommer.at

## Participants

Name	Institution	Country	E-Mail address
Asztalos, J.	Vienna University of Technology	Austria	asztalos@hydro.tuwien.ac.at
Bach, H.	VISTA	Germany	bach@vista-geo.de
Bernhardt, M.	University of Munich	Germany	m.bernhardt@iggf.geo.uni-muenchen.de
Bojariu, R.	National Meteorological Administration	Romania	bojariu@b.astral.ro
Boyle, D.	Desert Research Institute	USA	dboyle@dri.edu
Brandlhuber, T.	University of Munich	Germany	teresa.brandlhuber@campus.lmu.de
Braun, L.	Bavarian Academy of Sciences	Germany	Ludwig.braun@lrz.badw-muenchen.de
Busetto, L.	University of Milano-Bicocca	Italy	lorenzo.busetto@unimib.it
Colombi, A.	National Institute of Research	Italy	colombi.a@irea.cnr.it
Corripio, J.	Federal Institute of Technology (ETH)	Switzerland	corripio@ifu.baug.ethz.ch
Cremonese, E.	ARPA Valle d'Aosta	Italy	e.cremonese@arpa.vda.it
Dadic, R.	Federal Institute of Technology (ETH)	Switzerland	dadac@ifu.baug.ethz.ch
Dedieu, J.-P.	University of Savoie	France	dedieu@lgge.obs.ujf-grenoble.fr
Dinu, M.	Romanian-American University	Romania	mihaeladinu2003@yahoo.com
Ellehaug, J.	Svalbard University Center	Norway	jonas.ellehaug@unis.no
Essery, R.	University of Wales	England	rie@aber.ac.uk
Esteban, P.	Meteorological Service of Catalunya	Spain	pere.esteban@meteocat.com
Ferber, F.	University of Munich	Germany	frank.ferber@gmx.net
Fischer, P.	dTech-Steyr	Austria	peter.fischer@dtech-steyr.com
Fleischmann, M.	University of Munich	Germany	markus.fleischmann@gmx.net
Foppa, N.	University of Bern	Switzerland	foppa@giub.unibe.ch
Franz, H.	Berchtesgaden National Park	Germany	h.franz@nationalpark-berchtesgaden.de
Gabellani, S.	CIMA	Italy	simone.g@cima.unige.it
Garcia, C.	Institut Geològic de Catalunya	Spain	cgarcia@igc.cat
Gitti, A.	University of Brescia	Italy	alessandro.gitti@ing.unibs.it
Gottardi, F.	EDF - DTG	France	frederic.gottardi@edf.fr
Guseva-Lozinsky, E.		Germany	elena.gusewa@gmx.de
Haarpaintner, J.	Norut IT	Norway	joerg.haarpaintner@itek.norut.no
Hinterberger, W.	dTech-Steyr	Austria	walter.hinterberger@dtech-steyr.com
Holzmann, H.	University of Vienna	Austria	hubert.holzmann@boku.ac.at
Jiang, L.	University of Beijing	China	jlinmei@263.net
Jonas, T.	Federal Institute for Snow and Avalanche Research	Switzerland	jonas@slf.ch
Koch, F.	University of Munich	Germany	franziska.koch83@gmx.de
Krause, P.	University of Jena	Germany	p.krause@uni-jena.de
Kuchment, L.S.	Academy of Sciences	Russia	kuchment@mail.ru
Kühnlein, M.	University of Marburg	Germany	meike@kuehnlein.org
Landl, B.	Federal Institute for Snow and Avalanche Research	Switzerland	landl@slf.ch
Liston, G.E.	Colorado State University	USA	liston@cira.colostate.edu
Macchiavella, G.	CIMA	Italy	giorgia.macchiavella@cima.unige.it
Marigo, G.	ARPAV Avalanche Center of Arabba	Italy	gmarigo@arpa.veneto.it
Marty, C.	Federal Institute for Snow and Avalanche Research	Switzerland	marty@slf.ch
Mausser, W.	University of Munich	Germany	w.mausser@iggf.geo.uni-muenchen.de
Mayer, S.	University of Munich	Germany	steffi_m23@gmx.de
Merindol, L.	CEN/Météo-France	France	laurent.merindol@meteo.fr
Nagler, T.	ENVEO IT	Austria	thomas.nagler@enveo.at
Nolin, A.	Oregon State University	USA	nolina@geo.oregonstate.edu
Obled, Ch.	LTHE / ENSHMG	France	charles.obled@hmg.inpg.fr
Osenstetter, S.	University of Munich	Germany	sebastian.osenstetter@campus.lmu.de
Petkova, N.	National Institute of Meteorology and Hydrology	Bulgaria	nadejda.petkova@meteo.bg
Pinzer, B.	Federal Institute for Snow and Avalanche Research	Switzerland	pinzer@slf.ch

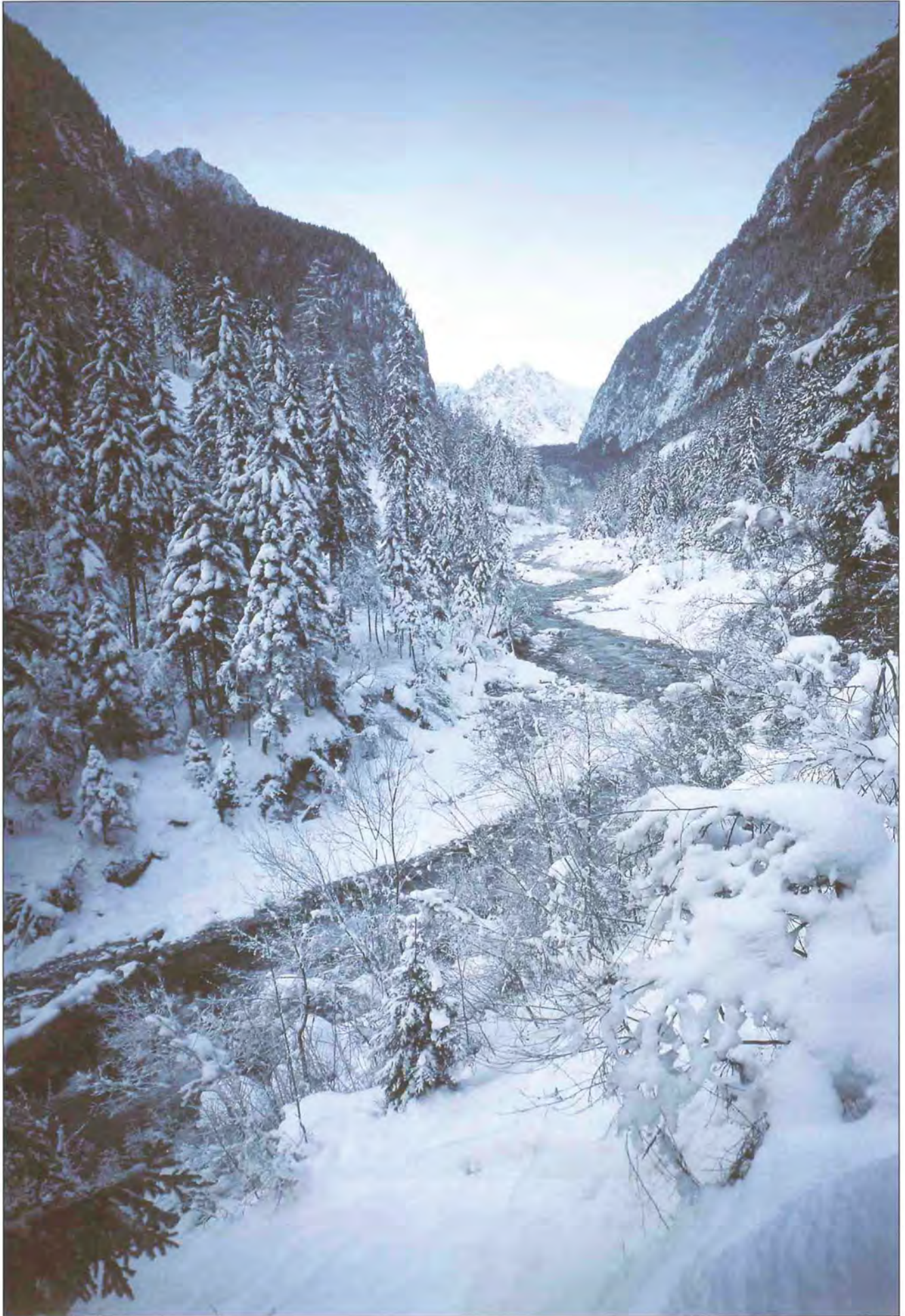
Pomeroy, J.	University of Saskatchewan	Canada	pomeroy@usask.ca
Röger, C.	University of Munich	Germany	
Rota Nodari, F.	Remote Sensing Data Engineering	Italy	ronofran@hotmail.com
Rothbart, M.	University of Munich	Germany	m.rothbart@iggf.geo.uni-muenchen.de
Rott, H.	ENVEO IT	Austria	helmut.rott@enveo.at
Rutter, N.	University of Wales	England	nick.rutter@aber.ac.uk
Saunders, I.	University of British Columbia	Canada	ian.saunders@ubc.ca
Schirmer, M.	Federal Institute for Snow and Avalanche Research	Switzerland	schirmer@slf.ch
Schmidt, S.	University of Bonn	Germany	s.schmidt@giub.uni-bonn.de
Schneiderbauer, S.	dTech-Steyr	Austria	simon.schneiderbauer@dtech-steyr.com
Schönbein, J.	University of Freiburg	Germany	johannes.schoenbein@ geographie.uni-freiburg.de
Schuster, G.	University of Freiburg	Germany	grit.schuster@geographie.uni-freiburg.de
Shi, J.	University of California	USA	shi@icess.ucsb.edu
Siljamo, N.	Finnish Meteorological Institute	Finland	niilo.siljamo@fmi.fi
Sommer, W.	Fa. Sommer Mess-Systemtechnik	Austria	office@sommer.at
Strasser, U.	University of Munich	Germany	u.strasser@iggf.geo.uni-muenchen.de
Studeregger, A.	ZAMG	Austria	arnold.studeregger@zamg.ac.at
Sturm, M.	CRREL	USA	msturm@crrel.usace.army.mil
Taschner, S.	Green City e.V. Munich	Germany	stefan.taschner@greencity.de
Tepfenhart, M.	University of Munich	Germany	m.tepfenhart@iggf.geo.uni-muenchen.de
Valt, M.	ARPAV Avalanche Center of Arabba	Italy	mvalt@arpa.veneto.it
Vogel, M.	Berchtesgaden National Park	Germany	m.vogel@nationalpark-berchtesgaden.de
Weber, B.	University of Göttingen	Germany	schwedenbjoern@yahoo.de
Weber, C.	Technical University of Dresden	Germany	cu706852@rcs.urz.tu-dresden.de
Weber, M.	Bavarian Academy of Sciences	Germany	wasti.weber@kfg.badw.de
Wiesenberger, B.	Fa. Sommer Mess-Systemtechnik	Austria	wiesenberger@sommer.at

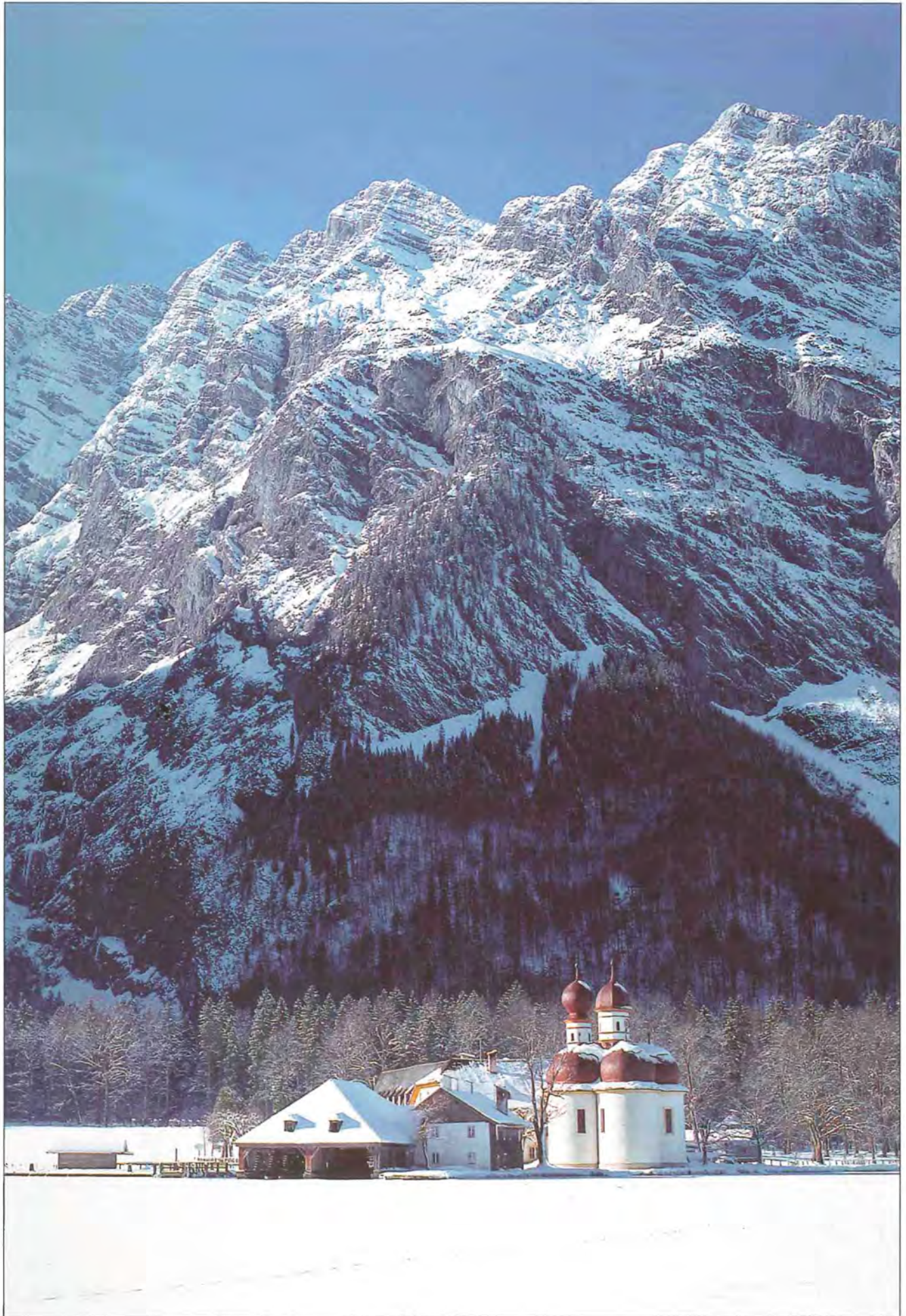












In der Reihe der Forschungsberichte sind erschienen:

- Nr. 1 G. Enders  
**Theoretische Topoklimatologie**
- Nr. 2 R. Bochter, W. Neuerburg, W. Zech  
**Humus und Humusschwund im Gebirge**
- Nr. 3 Herausgeber Nationalparkverwaltung  
**Zur Situation der Greifvögel in den Alpen**
- Nr. 4 G. Enders  
**Kartenteil: Theoretische Topoklimatologie**
- Nr. 5 O. Siebeck  
**Der Königssee - Eine limnologische Projektstudie**
- Nr. 6 R. Bochter  
**Böden naturnaher Bergwaldstandorte auf carbonatreichen Substraten**
- Nr. 7 Herausgeber Nationalparkverwaltung  
**Der Funtensee**
- Nr. 8 H. Schmid-Heckel  
**Zur Kenntnis der Pilze in den Nördlichen Kalkalpen**
- Nr. 9 R. Boller  
**Diplopoden als Streuzersetzer in einem Lärchenwald**
- Nr. 10 E. Langenscheidt  
**Höhlen und ihre Sedimente in den Berchtesgadener Alpen**
- Nr. 11 Herausgeber Nationalparkverwaltung  
**Das Bärenseminar**
- Nr. 12 H. Knott  
**Geschichte der Salinenwälder von Berchtesgaden**
- Nr. 13 A. Manghabati  
**Einfluß des Tourismus auf die Hochgebirgslandschaft**
- Nr. 14 A. Spiegel-Schmidt  
**Alte Forschungs- und Reiseberichte aus dem Berchtesgadener Land**
- Nr. 15 H. Schmid-Heckel  
**Pilze in den Berchtesgadener Alpen**
- Nr. 16 L. Spandau  
**Angewandte Ökosystemforschung im Nationalpark Berchtesgaden**
- Nr. 17 W. Berberich  
**Das Raum-Zeit-System des Rotfuchses**
- Nr. 18 U. Mäck, R. Bögel  
**Untersuchungen zur Ethologie und Raumnutzung von Gänse- und Bartgeier**
- Nr. 19 B. Ditttrich, U. Hermsdorf  
**Biomonitoring in Waldökosystemen**
- Nr. 20 F. Kral, H. Rall  
**Wälder - Geschichte, Zustand, Planung**
- Nr. 21 M. Klein, R.-D. Negele, E. Leuner, E. Bohl, R. Leyerer  
**Fischbiologie des Königssees: Fischereibiologie und Parasitologie**
- Nr. 22 W. Traunspurger  
**Fischbiologie des Königssees: Nahrungsangebot und Nahrungswahl, Bd. I**
- Nr. 23 R. Gerstmeier  
**Fischbiologie des Königssees: Nahrungsangebot und Nahrungswahl, Bd. II**
- Nr. 24 W. Hecht, M. Förster, F. Pirchner, R. Hoffmann, P. Scheinert, H. Rettenbeck  
**Fischbiologie des Königssees: Ökologisch-genetische Untersuchungen am Seesaibling und Gesundheitsstatus der Fische**
- Nr. 25 G. Hofmann  
**Klimatologie des Alpenparks**
- Nr. 26 K. Rösch  
**Einfluß der Beweidung auf die Vegetation des Bergwaldes**
- Nr. 27 H. Remmert, P. G. Rey, W. R. Siegfried, W. Scherzinger, S. Klaus  
**Kleinstmögliche Populationen bei Tieren**
- Nr. 28 B. Müller, W. Berberich, A. David  
**Schalenwild**
- Nr. 29 J. Köppel  
**Beitrag der Vegetation zum Wasserhaushalt**
- Nr. 30 H. Zierl et al.  
**Die Wallfahrt über das Steinerne Meer**
- Nr. 31 P. Pechacek  
**Spechte im Nationalpark Berchtesgaden**
- Nr. 32 Chr. Dommermuth  
**Beschleunigte Massenabtragung im Jennergebiet**
- Nr. 33 R. Bögel  
**Untersuchungen zur Flugbiologie und Habitatnutzung von Gänsegeiern**
- Nr. 34 A. Schuster  
**Singvögel im Biosphärenreservat Berchtesgaden**
- Nr. 35 M. Höper  
**Moose - Arten, Bioindikation, Ökologie**
- Nr. 36 T. Barthelmeß  
**Die saisonale Planktonsuccession im Königssee**
- Nr. 37 W. Lippert, S. Springer, H. Wunder  
**Die Farn- und Blütenpflanzen des Nationalparks**
- Nr. 38 G. Gödde  
**Die Holzbringung um den Königssee**
- Nr. 39 A. Stahr  
**Bodenkundliche Aspekte der Blaiktenbildung auf Almen**
- Nr. 40 R. Braun  
**Die Geologie des Hohen Gölls**
- Nr. 41 F. Gloßner, R. Türk  
**Die Flechtengesellschaften im Nationalpark Berchtesgaden und dessen Vorfeld**
- Nr. 42 R. Türk, H. Wunder  
**Die Flechten des Nationalparks Berchtesgaden und angrenzender Gebiete**
- Nr. 43 V. Konnerth, J. Siegrist  
**Waldentwicklung im Nationalpark Berchtesgaden von 1983 bis 1997**
- Nr. 44 S. Schmidlein  
**Aufnahme von Vegetationsmustern auf Landschaftsebene**
- Nr. 45 U. Brendel, R. Eberhardt, K. Wiesmann-Eberhardt, W. d'Oleire-Oltmanns  
**Der Leitfaden zum Schutz des Steinadlers in den Alpen**
- Nr. 46 Herausgeber Nationalparkverwaltung  
**Forschung im Nationalpark Berchtesgaden von 1978 bis 2001**
- Nr. 47 Th. Rettelbach  
**Die Antagonisten des Buchdruckers im Nationalpark Berchtesgaden**
- Nr. 48 P. Pechacek, W. d'Oleire-Oltmanns  
**International Woodpecker Symposium**
- Nr. 49 V. Konnerth  
**Standortkarte Nationalpark Berchtesgaden**
- Nr. 50 K. Fischer  
**Geomorphologie der Berchtesgadener Alpen**
- Nr. 51 Reinhard Gerecke, Helmut Franz  
**Quellen im Nationalpark Berchtesgaden**
- Nr. 52 Thomas Kudernatsch  
**Auswirkungen des Klimawandels auf alpine Pflanzengesellschaften im Nationalpark Berchtesgaden**

Zu beziehen über die Nationalparkverwaltung Berchtesgaden, Doktorberg 6, D-83471 Berchtesgaden



